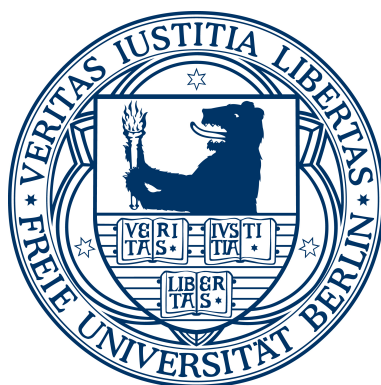


# Identification of selected small molecule targets in living cells using Capture Compounds™ through a bio-orthogonal chemical ligation method

Inaugural Dissertation  
to obtain the Academic Degree  
*Doctor rerum naturalium* (Dr. rer. nat.)

Submitted to the Department of Biology, Chemistry and Pharmacy  
of the Freie Universität Berlin



by

**João André Banha Oliveira**

from Lisbon, Portugal

November, 2015

The following experimental work was developed between December 2010 and August 2014 at caprotec bioanalytics GmbH under the supervision of Prof. Dr. Hubert Köster

**1<sup>st</sup> Reviewer:** Prof. Dr. Hubert Köster

**2<sup>nd</sup> Reviewer:** Prof. Dr. Markus Wahl

**Date of defense:** 11 April 2016

# Acknowledgments

---

I would like to express my appreciation to Prof. Hubert Köster, Founder and Managing Director of caprotec bioanalytics GmbH, for recruiting me and giving me this challenging but exciting opportunity to work in a start-up environment. Thank you for your support and positive feedback during our project discussions.

I would also like to acknowledge Prof. Markus Wahl at the Freie Universität Berlin for his acceptance to co-supervise my research project and aid me in navigating the bureaucracy.

A special thank you is dedicated to Dr. Mathias Dreger, Head of the Biochemistry Department at caprotec that guided me throughout this bumpy road. I deeply appreciate you always having your door open for discussion and giving your best to motivate me to move forward. I also need to thank you for your commitment in reviewing this dissertation and sharing your thoughts.

To all my colleagues at caprotec bioanalytics, some that were there from the beginning and others that came and went, thank you for the support around the lab and meetings but especially thank you for the funny moments. Laughter always makes the job easier. You made me feel less of an outsider addressing me in English but still teaching me some German. I will never forget *Luftfeuchtigkeit* and *Streichholzschächtelchen*.

There are a few colleagues I need to single out in my acknowledgements. Lisa von Kleist for the very helpful brainstorming sessions but most of all for your personality and work ethics. Yan Luo for getting me started in the lab and later collaborating in the phenobarbital project. The guys at the Medicinal Chemistry Lab, Simon Michaelis, Frank Polster and Daniel Ohlendorf, as well as Henrik Dieks for synthesizing all compounds I used in this work. Matthias Hakelberg and Christian Dalhoff from the Analytics Department for the continuous support in confirming the stability and quality of my compounds. Kathrin Bartho for taking good care of my mass spectrometry samples and analyzing them as quickly as possible as well as the friendly discussions around Excel tables on how to extract the information from the MS data. Finally, Michael Sefkow for the support and enthusiasm in this whole project. Thank you all.

This work was supported by the Initial Training Network, Bio-Orthogonal Chemo-Specific Ligation (BioChemLig), funded by the FP7 Marie Curie Actions of the European Commission (FP7-PEOPLE-2008-ITN-238434). Within this consortium I had the opportunity to establish great connections to my fellow colleagues, who I would like to salute for the friendship created during the meetings and putting up with the one biologist in the midst of all chemists. To Marco and Valentina, who chose to come to Berlin for their secondments, thank you for letting me teach you around a biochemistry lab. I truly enjoyed it. Also, to the P.I.s of the groups, thank you for your comments and guidance in the progress reports meetings.

A warm appreciation goes out to my family who have supported me in my journey across borders and away from home. Always concerned but also motivating me to keep on going and aim for happiness.

[REDACTED]

[REDACTED]

[REDACTED]

[REDACTED]

# Preface

---

The overall aim of this study was the introduction of a novel approach for the identification of small-molecule targets from living cells using capture compound mass spectrometry. To achieve this goal, the research was performed in a step-wise comprehensive manner that is reflected in the structure of this dissertation.

A general introduction covers the subjects underlying all the work that was developed, followed by three chapters of specific research, each containing an explanatory introduction, the obtained results and the specific methods used for those experiments.

The first specific chapter describes the establishment of the new methodology and necessary optimization steps, which were done in a simple system containing the small molecule capture compound and a purified recombinant protein that are known in the literature to interact, in this case the cyclic AMP and protein kinase A. The following chapter advances the established protocol to be used with a clinically relevant drug, dasatinib, in order to identify targets in more complex samples, such as cell lysates, and implement the initial parameters for capturing in living cells. The last of the experimental chapters explains how this novel workflow can shed some light on the hepatotoxic side-effect of phenobarbital, an old anti-epileptic drug. Finally, a summary of the complete research is outlined, where the achievements are discussed and future prospects presented.

This research project was integrated in a European Union Marie Curie Actions Initial Training Network – BioChemLig. Within this consortium we had regular meetings where progress reports were presented and several scientific and soft-skills seminars were offered. I presented a total of 6 communications in the 3-year period of the project. Additionally, I had the privilege to collaborate closer and host at caprotec two fellow members of BioChemLig: Valentina Bevilacqua, from the group of Frédéric Taran at the CEA Saclay in Paris, who synthesized new copper-chelating molecules that were introduced in some of the capture compounds I used for my research; and Marco Bartoloni, from the group of Jean-Louis Reymond at the University of Bern, whom I taught and aided in the capture of targets from cell lysates using his bicyclic peptides.

The collaboration with the University of Bern resulted in a publication that I co-authored: Bartoloni, M., Jin, X., Marcaida, M.J., [Banha, J.](#) *et al.* (2015) Bridged bicyclic peptides as potential drug scaffolds: synthesis, structure, protein binding and stability. *Chemical Science* 6 (10): 5473-5490.

During the course of this research project I was able to participate in an EMBO Practical Course in Chemical Biology from 27 March to 2 April 2011 at the EMBL in Heidelberg, Germany and attend the 3<sup>rd</sup> European Chemical Biology Symposium that took place 1-3 July 2012, in Vienna, Austria.

*You see things; and you say "Why?"  
But I dream things that never were; and I say "Why not?"*  
George Bernard Shaw

# Contents

---

<b>List of Tables</b> .....	<b>7</b>
<b>List of Figures</b> .....	<b>8</b>
<b>Abbreviations</b> .....	<b>10</b>
<b>Summary</b> .....	<b>11</b>
<b>Zusammenfassung</b> .....	<b>12</b>
<b>1. General Introduction</b> .....	<b>13</b>
1.1. Challenges in Drug Discovery .....	13
1.2. Drug target deconvolution .....	15
1.2.1. <i>In silico</i> approach.....	16
1.2.2. Affinity Chromatography.....	16
1.2.3. Activity-based protein profiling (ABPP) .....	17
1.2.4. Capture compound mass spectrometry (CCMS) .....	18
1.3. Click chemistry and bio-orthogonal ligations.....	21
1.3.1. Staudinger ligation .....	22
1.3.2. Copper-catalyzed azido-alkyne cycloaddition (CuAAC) .....	23
1.3.3. Metal-free click cycloadditions .....	25
<b>2. Labeling a protein using click chemistry</b> .....	<b>28</b>
2.1. Introduction.....	28
2.2. Results.....	31
2.2.1. Establishing and optimizing click-capture of PKARI using a cAMP CC.....	31
2.2.2. Mass Spectrometry analysis of captured proteins from HEK293 and HepG2 lysates using a classical and clickable cAMP capture compound .....	42
2.3. Specific Methods for the cAMP/PKARI system .....	48
2.3.1. Structures of used compounds .....	48
2.3.2. Establishing and optimizing click-capture of PKARI using a cAMP CC.....	50
2.3.3. Preparation of HEK293 lysates .....	50
2.3.4. Click capture of cAMP-binding proteins from cell lysates.....	53
<b>3. Identifying Dasatinib targets in cells</b> .....	<b>54</b>
3.1. Introduction.....	54
3.2. Results.....	58
3.2.1. Introducing a new copper-chelating azide in the CuAAC reaction.....	58
3.2.2. Capturing dasatinib targets in K562 cell lysate using CuAAC .....	60
3.2.3. Cell viability assay for dasatinib compounds in K562 cells .....	68
3.2.4. Capturing in living K562 cells.....	70
3.3. Specific methods for the dasatinib system.....	77
3.3.1. Structures of used compounds .....	77
3.3.2. Optimizing CuAAC reaction parameters with new copper-chelating azide .....	78
3.3.3. Capturing dasatinib targets in K562 cell lysate using CuAAC .....	79
3.3.4. Cell viability assay for dasatinib compounds in K562 cells .....	79
3.3.5. Capture of dasatinib targets in living K562 cells using CuAAC .....	80

<b>4. Phenobarbital: new binders for an old drug .....</b>	<b>81</b>
4.1. Introduction.....	81
4.2. Results.....	84
4.2.1. Determining permeability of phenobarbital-alkyne capture compounds.....	84
4.2.2. Developing a phenotypic assay to evaluate phenobarbital effect.....	85
4.2.3. Capturing phenobarbital targets in MH <sub>1</sub> C <sub>1</sub> cell lysate.....	97
4.2.4. Capture of phenobarbital targets in living MH <sub>1</sub> C <sub>1</sub> cells.....	101
4.2.5. Capturing phenobarbital targets in tissue with high EGFR expression.....	103
4.3. Specific methods for the phenobarbital system .....	105
4.3.1. Structures of used compounds .....	105
4.3.2. Treatment of MH <sub>1</sub> C <sub>1</sub> cells with phenobarbital.....	106
4.3.3. Subcellular fractionation of MH <sub>1</sub> C <sub>1</sub> cells.....	106
4.3.4. Treatment of MH <sub>1</sub> C <sub>1</sub> cells with high concentration of phenobarbital.....	106
4.3.5. Treatment of rat primary hepatocytes with phenobarbital .....	107
4.3.6. RT-PCR.....	107
4.3.7. Capture of phenobarbital targets in MH <sub>1</sub> C <sub>1</sub> cell lysate.....	109
4.3.8. Capture of phenobarbital targets in living MH <sub>1</sub> C <sub>1</sub> cells .....	110
4.3.9. Capture of phenobarbital targets in human placenta lysate.....	111
<b>5. Conclusions and Outlook.....</b>	<b>112</b>
<b>6. General Methods and Materials .....</b>	<b>116</b>
6.1. Cell Culture.....	116
6.1.1. HEK293 cell culture.....	116
6.1.2. K562 cell culture .....	116
6.1.3. MH <sub>1</sub> C <sub>1</sub> cell culture.....	117
6.1.4. Rat primary hepatocytes culture .....	117
6.2. Biochemistry General Methods.....	118
6.2.1. Protein concentration determination .....	118
6.2.2. SDS-PAGE.....	118
6.2.3. Polyacrylamide Gel Staining .....	119
6.2.4. Western Blotting .....	120
6.3. Mass Spectrometry .....	121
6.3.1. Sample acquisition and database match identification .....	121
6.4. Molecular Structures of Compounds .....	122
6.4.1. Capture compounds .....	122
6.4.2. Competitors.....	125
6.4.3. Ligands .....	125
6.5. Materials .....	126
6.5.1. Chemical reagents.....	126
6.5.2. Kits and Consumables.....	127
6.5.3. Buffers, media and solutions.....	128
6.5.4. Equipment .....	129
<b>References .....</b>	<b>130</b>

# List of Tables

---

Table 2–1: Summary of identifications from cAMP capture experiments in HEK293 and HepG2 lysates. ....	42
Table 2–2: Proteins identified as specifically competed with cAMP across the different capture methods in each type of cellular lysate.....	43
Table 2–3: Number of proteins identified as competed by cAMP in common between the different samples...44	
Table 2–4: Calculated intensity fold-changes (assay vs. competition) and MS counts for identified PKA subunits in each sample.....	45
Table 2–5: Summary of identifications from cAMP capture experiments in HEK293 lysates. ....	46
Table 2–6: Calculated intensity fold-changes (assay vs. competition) and corresponding significance value for identified PKA subunits from capture experiments using full and clickable cAMP capture compounds.....	47
Table 2–7: Summary of parameters utilized in PKARI labeling and capturing with a cAMP capture compound via a CuAAC reaction.....	52
Table 3–1: Summary of identifications from dasatinib capture experiments in K562 lysate.....	60
Table 3–2: List of competed and significant hits in dasatinib capture experiments in K562 lysate using a pre-clicked workflow.....	61
Table 3–3: List of competed and significant hits in Dasatinib capture experiments in K562 lysate using a click workflow.....	64
Table 3–4: Values for expected targets of Dasatinib in K562 lysate using a click workflow. ....	65
Table 3–5: Gene Ontology term enrichment from significantly competed proteins in Dasatinib capture experiment in K562 lysate using a click workflow. ....	66
Table 3–6: Effect of dasatinib or clickable dasatinib-alkyne capture compound on K562 cell viability. ....	69
Table 3–7: Summary of identifications from dasatinib capture experiments in K562 living cells in nine separate experiments.....	70
Table 3–8: Excerpt of potential hits for dasatinib in K562 living cell capture using a click workflow from 9 individual experiments.....	72
Table 3–9: Top20 list (sorted by increasing p value) of dasatinib-competed proteins when calculating values for all runs from all experiments.....	73
Table 3–10: Gene Ontology term enrichment from significantly competed proteins in dasatinib capture experiment in K562 living cells using a click workflow. ....	75
Table 4–1: PAMPA results of phenobarbital alkyne capture compounds.....	84
Table 4–2: Summary of identifications from phenobarbital capture experiments in MH <sub>1</sub> C <sub>1</sub> cell lysate.....	98
Table 4–3: Potential hits for phenobarbital in a rat hepatoma cell line (MH <sub>1</sub> C <sub>1</sub> ) from 3 individual experiments using a MS-based analysis.....	100
Table 4–4: Summary of identifications from phenobarbital capture experiments in MH <sub>1</sub> C <sub>1</sub> living cells. ....	101
Table 4–5: List of competed and significant hits in phenobarbital capture experiments in MH <sub>1</sub> C <sub>1</sub> living cells. .	102
Table 4–6: Summary of identifications from phenobarbital capture experiment in human placenta lysate. ....	103
Table 4–7: List of competed and significant hits in phenobarbital capture experiments in human placenta lysate. ....	103

# List of Figures

---

Figure 1-1: Drug Research and Development timeline. ....	13
Figure 1-2: Schematic representation of an affinity chromatography pull-down probe. ....	16
Figure 1-3: Schematic representation of an activity-based protein profiling (ABPP) probe. ....	17
Figure 1-4: Schematic representation of a capture compound. ....	18
Figure 1-5: Schematic workflows for three different target deconvolution techniques.....	19
Figure 1-6: Workflow for identification of small-molecule targets in living cells. ....	20
Figure 1-7: Illustration of bio-orthogonal ligation. ....	21
Figure 1-8: Classical (A) and traceless (B) Staudinger ligation.....	22
Figure 1-9: Mechanism of the copper-catalyzed azido-alkyne cycloaddition (CuAAC) .....	23
Figure 1-10: CuAAC-accelerating ligands of choice. ....	25
Figure 1-11: Strain-promoted azido-alkyne cycloaddition. Example reaction between DIFO and an azide. ....	26
Figure 1-12: Tetrazine ligation. ....	27
Figure 2-1: cAMP production and activation of PKA. ....	29
Figure 2-2: Labeling of recombinant PKARI using CuAAC in a serial dilution of cAMP-alkyne capture compound. ....	32
Figure 2-3: Labeling of recombinant PKARI using CuAAC in a serial dilution of cAMP-alkyne capture compound with corresponding competition samples. ....	32
Figure 2-4: Effect of copper sulfate concentration on the click labeling of recombinant PKARI using a cAMP-alkyne capture compound. ....	33
Figure 2-5: Effect of copper ligand TBTA on the click labeling of recombinant PKARI using a cAMP-alkyne capture compound. ....	34
Figure 2-6: Labeling of recombinant PKARI using a cAMP-alkyne capture compound at different CuAAC reaction times. ....	35
Figure 2-7: Labeling of recombinant PKARI using CuAAC with different biotin-azide concentrations.....	37
Figure 2-8: Click-capture of PKARI using a cAMP alkyne capture compound. ....	38
Figure 2-9: Labeling of PKARI with a cAMP-alkyne capture compound clicked to a biotin-azide using CuAAC with BTTE as copper ligand.....	40
Figure 2-10: Effect of time of CuAAC reaction on the labeling of PKARI with a cAMP-alkyne capture compound and a TAMRA-azide. ....	41
Figure 3-1: Schematic representation of the modular domains of the ABL kinases. ....	55
Figure 3-2: Representation of auto-inhibited (closed) and active (open) ABL kinases. ....	55
Figure 3-3: Proteins inhibited by kinase inhibitors with an affinity of less than 30 nM for ABL1 and ABL2. ....	56
Figure 3-4: Labeling of recombinant SRC and K562 cell lysate with a clickable dasatinib-alkyne capture compound using a new copper-chelating azide with a TAMRA label.....	58
Figure 3-5: CCMS chart of significantly competed hits in Dasatinib capture experiment in K562 lysate using a pre-clicked workflow. ....	61
Figure 3-6: STRING protein interaction analysis of significantly competed proteins in dasatinib capture experiment in K562 lysate using the pre-clicked workflow. ....	62
Figure 3-7: STRING protein interaction analysis of significantly competed kinases in Dasatinib capture experiment in K562 lysate using the click workflow.....	64

Figure 3-8: CCMS chart of significantly competed kinases in Dasatinib capture in K562 lysate using CuAAC. ....	65
Figure 3-9: STRING protein interaction analysis of significantly competed proteins in dasatinib capture experiment in K562 lysate using the click workflow.....	67
Figure 3-10: Scheme of multi-well plate for cell viability assay of dasatinib (Dasa) and dasatinib clickable compound (CPT392) in K562 cells. ....	68
Figure 3-11: Luminescence detection of cell viability assay of dasatinib and clickable dasatinib-alkyne capture compound in K562 cells.....	69
Figure 3-12: CCMS charts of CSK, ALDOC, ABL and BCR proteins in Dasatinib capture experiment in K562 living cells using a click workflow.....	74
Figure 3-13: STRING protein interaction analysis of significantly competed proteins in dasatinib capture experiment in K562 lysate using the click workflow.....	75
Figure 4-1: Luminal (phenobarbital) as it was packaged in 1940/1945. ....	81
Figure 4-2: Phenobarbital induces CYP2B expression via EGFR inhibition .....	83
Figure 4-3: Synthesized phenobarbital-alkyne capture compounds.....	84
Figure 4-4: Western Blot analysis of CAR in isolated nuclei and cytosol from MH <sub>1</sub> C <sub>1</sub> cells.....	85
Figure 4-5: Effect of phenobarbital on CAR translocation from cytosol to nucleus in MH <sub>1</sub> C <sub>1</sub> cells.....	86
Figure 4-6: Effect of phenobarbital on AMPK phosphorylation (pAMPK) in MH <sub>1</sub> C <sub>1</sub> cells treated in serum-free medium. ....	88
Figure 4-7: Comparative analysis of the effect of phenobarbital on AMPK phosphorylation for each time incubation point in MH <sub>1</sub> C <sub>1</sub> cells treated in serum-free DMEM.....	88
Figure 4-8: Effect of serum supplementation in AMPK phosphorylation (pAMPK) from non-treated (0 μM phenobarbital) MH <sub>1</sub> C <sub>1</sub> cells. ....	89
Figure 4-9: Effect of phenobarbital on AMP activated protein kinase (AMPK) phosphorylation (pAMPK) in a rat hepatoma cell line treated in complete medium. ....	90
Figure 4-10: Comparative analysis of the effect of phenobarbital on AMPK phosphorylation for each time incubation point in MH <sub>1</sub> C <sub>1</sub> cells treated in FBS-supplemented DMEM. ....	90
Figure 4-11: Effect of phenobarbital in CYP2B1/2 detection in a rat hepatoma cell line.....	91
Figure 4-12: Effect of high concentration phenobarbital on the detection of CYP2B1/2 in MH <sub>1</sub> C <sub>1</sub> cells using rat liver mitochondria matrix fraction as positive control for antibody reaction quality. ....	92
Figure 4-13: Effect of high concentration phenobarbital on the detection of CYP2B1/2 and AMPK phosphorylation in a rat hepatoma cell line.....	92
Figure 4-14: Detection of D-amino acid oxidase (DAO) in purified fractions and MH <sub>1</sub> C <sub>1</sub> lysate. ....	93
Figure 4-15: Effect of phenobarbital in the detection of D-amino acid oxidase (DAO), CYP2B1/2 and AMPK phosphorylation (pAMPK) from rat primary hepatocytes.....	94
Figure 4-16: Agarose gel electrophoresis of RNA, cDNA and PCR products.....	95
Figure 4-17: Effect of phenobarbital on CYP2B1 mRNA expression in a rat hepatoma cell line.....	96
Figure 4-18: Effect of phenobarbital on CYP2B1 mRNA expression in rat primary hepatocytes. ....	96
Figure 4-19: STRING protein interaction analysis of significantly competed proteins in phenobarbital capture experiments in MH <sub>1</sub> C <sub>1</sub> lysate .....	99
Figure 4-20: STRING protein interaction analysis of significantly competed proteins in phenobarbital capture experiments in human placenta lysate.....	104

# Abbreviations

---

<b>(p)AMPK</b>	(phosphorylated) AMP-activated kinase	<b>IR</b>	Infrared
<b>AKAP</b>	A-kinase anchoring protein	<b>LC</b>	Liquid chromatography
<b>ATP</b>	Adenosine tri-phosphate	<b>LTQ</b>	Linear trap quadrupole
<b>BCA</b>	Bicinchoninic acid	<b>MS</b>	Mass spectrometry
<b>BSA</b>	Bovine serum albumin	<b>nLC</b>	Nanoflow liquid chromatography
<b>BTTE</b>	Bis(tert-butyltriazoly)ethanol	<b>PAGE</b>	Polyacrylamide gel electrophoresis
<b>cAMP</b>	Cyclic adenosine mono-phosphate	<b>PB</b>	Phenobarbital
<b>CAR</b>	Constitutive androstrane receptor	<b>PBREM</b>	Phenobarbital responsive enhancer module
<b>CC</b>	Capture compound	<b>PBS</b>	Phosphate-buffered saline
<b>CCMS</b>	Capture compound mass spectrometry	<b>PCR</b>	Polymerase chain reaction
<b>CID</b>	Collision-induced dissociation	<b>PI</b>	Protease inhibitor cocktail
<b>CuAAC</b>	Copper-catalyzed azido-alkyne cycloaddition	<b>PKA</b>	Protein kinase A
<b>CYP</b>	Cytochrome P450	<b>RNA</b>	Ribonucleic acid
<b>DDM</b>	n-Dodecyl $\beta$ -D-maltoside	<b>RP</b>	Reverse phase
<b>DMEM</b>	Dulbecco's modified Eagle medium	<b>SA-MB</b>	Streptavidin-coated magnetic beads
<b>DMSO</b>	Dimethyl sulfoxide	<b>SDS</b>	Sodium dodecyl sulfate
<b>DNA</b>	Deoxyribonucleic acid	<b>TAMRA</b>	Tetramethylrodamine
<b>DTT</b>	Dithiotreitol	<b>TBS</b>	Tris-buffered saline
<b>ECL</b>	Enhanced chemiluminescence	<b>TBS-T</b>	Tris-buffered saline with 0.1% (v/v) Tween
<b>EDTA</b>	Ethylene-diamine-tetra-acetic acid	<b>TBTA</b>	Tris(benzyltriazolymethyl)amine
<b>EGFR</b>	Epidermal growth factor receptor	<b>THPTA</b>	Tris(3-hydroxypropyltriazolymethyl)amine
<b>FBS</b>	Fetal bovine serum	<b>UV</b>	Ultraviolet
<b>HEPES</b>	4-(2-Hydroxyethyl)piperazine-1-ethanesulfonic acid	<b>v/v</b>	Volume per volume
<b>HRP</b>	Horseradish peroxidase	<b>w/v</b>	Weight per volume

---

# Summary

---

The development of novel drug target deconvolution methodologies is a growing need in the pharmaceutical industry. The increased regulatory scrutiny demands that better and safer medicines reach the consumer market and, for that, a comprehensive characterization of the multiple targets and off-targets of the drug early in the development process is a key success factor.

Chemical proteomics advances have provided the tools to study drug mechanisms of action in a more direct and unbiased way than target-based screening strategies, by analyzing the effects in the context of the full proteome from the target cell or tissue of interest.

Capture compound mass spectrometry (CCMS) is a robust and versatile chemical proteomics technique due to the original design of the probes. Capture compounds are trifunctional molecules that traditionally carry a selectivity function, consisting of the small molecule under study, attached to a scaffold bearing a tag, such as a fluorophore or biotin, and a UV-reactive moiety protruding from the central core that covalently binds the probe to the target protein. Although capture compounds are very efficient and specific in targeting of even low affinity and low abundant targets, their use has been limited so far to working with cellular lysates or targeting cell-surface proteins.

The main objective of this work was to advance CCMS to implement and optimize workflows for the use of newly designed permeable capture compounds to profile small molecule drugs in living cells, where the targets are in their unaltered natural environment. Bio-orthogonal “click” chemistry provides the prerequisite for the use of permeable capture compounds bearing only the selectivity and reactivity functions, and a small “clickable” chemical handle to bind and cross-link the targets in living cells and afterwards specifically attach the sorting/detection function by a controlled chemical click reaction such as the copper-assisted azide-alkyne cycloaddition (CuAAC).

Initial reaction parameters for the click reaction were tested using a clickable cAMP capture compound in a solution of recombinant PKARI. The optimization efforts in copper ion concentration, ligand nature, duration and pH of the reaction, azide and alkyne concentrations yielded substantial improvements from the starting point. Capturing PKA subunits from cell lysates with the optimized parameters proved to be possible to use this workflow but the results were not fully satisfactory.

A capture compound with a non-natural selectivity function was used to further develop target identification in cell lysates and living cells using the new click reaction. The kinase inhibitor dasatinib was profiled using this strategy and *bona fide* targets were successfully identified using the clickable compound. ABL, BCR and SRC were specifically identified in lysates and CSK, a known dasatinib binder, was positively identified for the first time by chemical proteomics in living cells.

The newly established click workflow allowed to better characterize phenobarbital, a drug that was developed as an anti-epileptic but elicits unexplained hepatocarcinogenic effects in some species. The results of capture experiments suggest that this small molecule interacts with several proteins in the epidermal growth factor receptor signaling pathway and that the primary target could be the transcription factor YBX1, and not the receptor itself as it was suggested recently. A cell-based assay was developed to validate this finding but was not further explored due to time constraints.

In summary, the strategy to identify small molecule targets in living cells using capture compounds and bio-orthogonal chemo-selective ligation methods was successfully established. This method provides the tools for a better characterization of the target profiles of drugs and still has potential to be further innovated.

# Zusammenfassung

---

Die Entwicklung neuer Methoden zur Dekonvolution der Profile von Zielproteinen für pharmazeutische Wirkstoffe ist von wachsender Bedeutung für die Pharmaindustrie. Eine umfassende Charakterisierung der Zielproteine einschließlich sogenannter „Off-targets“ ist ein Schlüsselfaktor um bessere und sicherere Medikamente auf den Markt zu bringen.

Fortschritte in der Chemischen Proteomanalyse bieten Werkzeuge für die direktere und bezüglich der Zielproteine hypothese-freie Untersuchung der Wirkungsmechanismen von Medikamenten, bei der die Bindung im Kontext des vollständigen Proteoms der Zielzelle oder des Zielgewebes untersucht wird.

Die Capture Compound Massenspektrometrie (CCMS)-Technologie ist eine robuste und sehr flexibel einsetzbare Technik in der chemischen Proteomanalyse. Capture Compounds sind trifunktionelle Moleküle, die in ihrer klassischen Version eine Selektivitätsfunktion tragen, die dem zu untersuchenden Kleinmolekül-Wirkstoff entspricht, die mit einer Gerüststruktur verbunden ist, welche außerdem eine Isolierungsfunktion sowie eine UV-aktivierbare Reaktivitätsfunktion für die kovalente Verbrückung zum gebundenen Zielprotein enthält. Obwohl Capture Compounds sehr effizient und spezifisch Zielproteine bindet, war ihr Einsatz bislang wegen fehlender Permeabilität auf Zell-Lysate bzw. auf Oberflächenproteine lebender Zellen beschränkt.

Ziel der vorliegenden Arbeit war die Weiterentwicklung der CCMS-Technologie durch Implementierung und Optimierung des Einsatzes permeabler Capture Compounds neuartigen Designs zur Profilierung von Kleinmolekül-Wirkstoffen in lebenden Zellen, in denen die Zielproteine in ihrer natürlichen Umgebung vorliegen. Bio-orthogonale „Click“-Chemie bietet die Voraussetzung für den Einsatz permeabler Capture Compounds, die lediglich die Selektivitätsfunktion, die Reaktivitätsfunktion sowie eine kleine, „Click“-fähige chemische Gruppe enthalten. Bindung und Verbrückung zu den Zielproteinen kann in den lebenden Zellen erfolgen, und erst danach die Sortier-/Detektionsfunktion in einer kontrollierten chemischen „Click“-Reaktion (wie z.B. die Kupfer-katalysierte Azid-Alkin-Cycloaddition, CuAAC) angebracht werden.

Initiale Reaktionsbedingungen für die „Click“-Reaktion wurden mit einer Capture Compound mit cAMP als Selektivitätsfunktion in einer Lösung einer rekombinanten PKARI getestet. Die Optimierung der Reaktion brachten substantielle Verbesserungen in der Reaktionsausbeute im Vergleich zu den Startbedingungen.

Um die Identifizierung von Zielproteinen in Zell-Lysaten und lebenden Zellen unter Verwendung der „Click“-Reaktion weiter zu entwickeln, wurde eine Capture Compound mit einer anderen Selektivitätsfunktion verwendet. Das Kinaseinhibitor-Medikament Dasatinib wurde mit dieser Strategie profiliert. Die *bona fide* Zielproteine ABL, BCR, und SRC wurden spezifisch in Zell-Lysaten und zum ersten Mal CSK mit chemischer Proteomanalyse in lebenden Zellen identifiziert.

Der neu etablierte methodische Arbeitsablauf ermöglichte es, Phenobarbital besser zu charakterisieren, weil es in einigen Spezies hepatocarcinogen wirkt. Die Ergebnisse der Capture-Experimente legen nahe, dass der primäre Binder der Transkriptionsfaktor YBX1 sein könnte.

Insgesamt konnte die Strategie, Zielproteine von Kleinmolekül-Wirkstoffen in lebenden Zellen mit Hilfe neuartiger Capture Compounds und bio-orthogonaler chemo-selektiver Ligation erfolgreich etabliert werden. Diese Methode bietet ein Werkzeug für die bessere Charakterisierung der Zielprotein-Profile von Medikamenten und hat das Potential, noch weiter verbessert zu werden.

# 1. General Introduction

## 1.1. CHALLENGES IN DRUG DISCOVERY

The pharmaceutical industry is facing unprecedented challenges to its business model. Over the past decade, concerns about the industry's integrity and transparency regarding drug safety and efficacy have been raised, and lead to an increased regulatory scrutiny<sup>1</sup>.

The traditional drug development timeline (Figure 1-1) consists of a discovery phase, which includes the target-to-hit, screening, hit-to-lead, and lead optimization stages that provide a clinical candidate for the development phase consisting of pre-clinical, phases I, II and III clinical trials, culminating in a submission to the competent authorities for a drug launch.

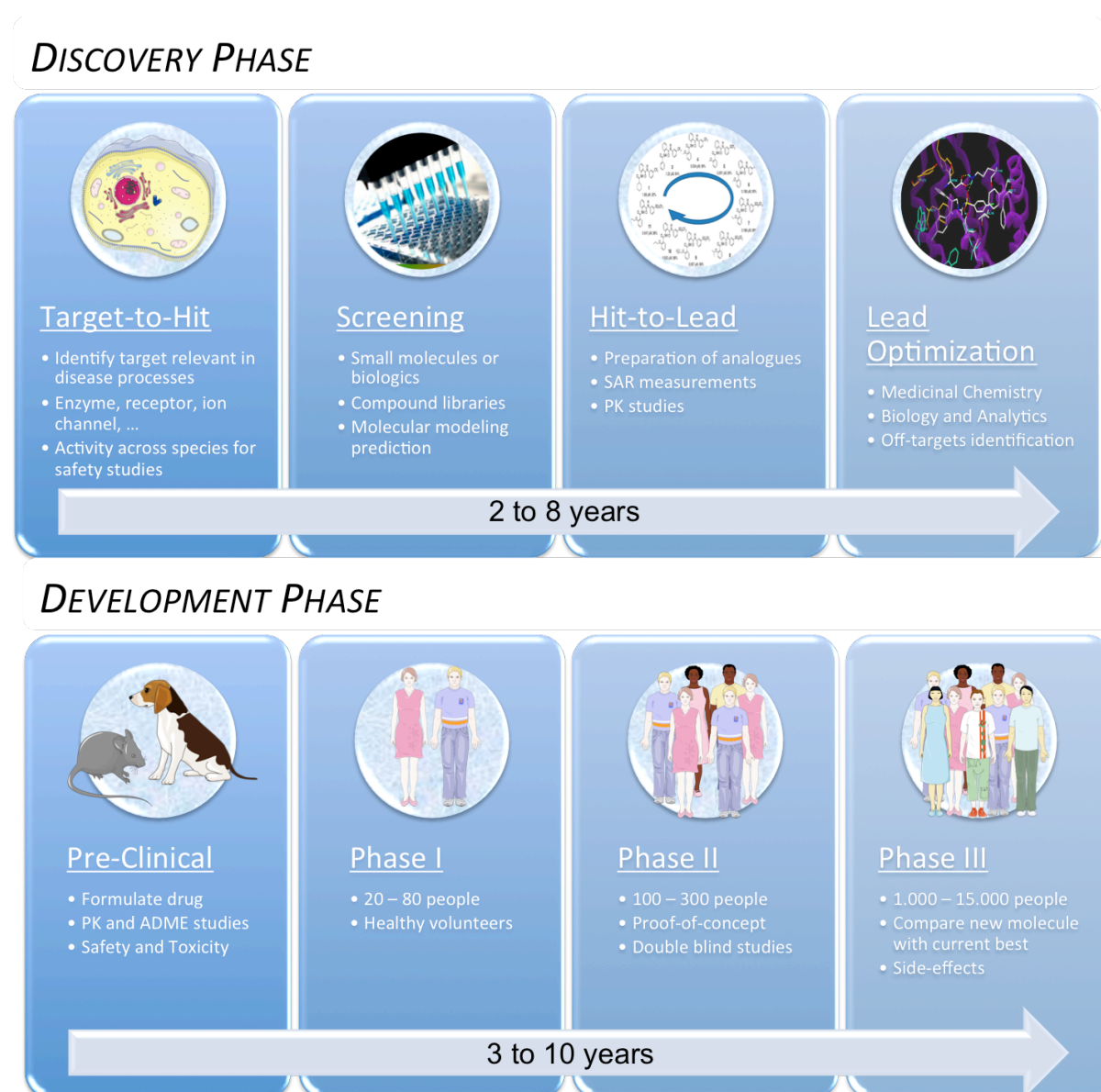


Figure 1-1: Drug Research and Development timeline.

In the initial stage of the discovery phase a target is selected either by actively pursuing an unmet medical need or by screening literature with reports on novel associations with disease states, always guided by the size of the potential market. In the target-to-hit phase it is important to determine the differences and similarities across species for future safety studies translation. Following the target identification, a screening for potential hits is performed using novel high throughput technologies scanning small molecules or biologics, such as antibodies or RNA/DNA-based compounds. Opposite to the large-scale profiling, a more direct approach in drug-design is sometimes utilized via computational molecular modeling prediction systems. Once a potential candidate is identified, a series of analogues are synthesized and structure-activity relationships (SAR) are measured as well as initial pharmacokinetics (PK) studies are performed. In the lead optimization stage, the potential drug is refined and improved for efficacy and potency as well as identification of undesired off-targets. At this stage a drug candidate can enter the development phase and initiate the pre-clinical studies, which include drug formulations compatible with safe administration, further PK studies and ADME (Absorption, Distribution, Metabolism and Excretion) analysis in disease models. Safety and toxicity studies are focused on unwanted effects in cytochrome P450 (CYP) metabolizing enzymes, or specific ion channels that can lead to deleterious consequences. With safety and toxicity parameters in check, the phase I clinical trial consists of a small group of individuals, usually healthy volunteers, where dosages and frequency are tested. In Phase II the cohort is increased and the effectiveness of the compound is proved by double blind studies, which continues on to Phase III with more subjects and also diversified genetic backgrounds to determine observed side effects and establish the general benefits of the new molecular entity in comparison to the current standard of care.

As Figure 1-1 shows, navigating a new medicine to the market is a long and strenuous path. A lot of potential drugs do not move forward in the pipeline because of undesired effects or problems of formulation. A study on the success rates for investigational drugs<sup>2</sup> covering 835 drug developers, including biotech companies as well as specialty and large pharmaceutical firms from 2003 to 2011, reports that from the 7.300 independent drug development paths analyzed, as much as 10.4% of all indication development paths in phase I were approved by the US Food and Drug Administration (FDA). The biggest hurdle along the development chain is the transition from phase II to phase III, with only 32.4% of the drugs advancing in the pipeline, making companies carefully analyze the risk/cost benefits of these undertakings. Hay *et al.*<sup>2</sup> suggest one way to improve the success rates is to improve the predictive animal models, perform earlier toxicology evaluation, biomarker identification and new targeted delivery technologies that may increase future success in the clinic.

## 1.2. DRUG TARGET DECONVOLUTION

One way to improve the success rates in the drug development pipeline, discussed in the previous paragraph, is to implement techniques of drug target deconvolution early on in the process.

Drug target deconvolution is a process where the action of a drug, a small molecule, is characterized by identifying the proteins binding the drug and initiating the biological effect. The biological relevant target has to be extracted, or deconvoluted, from a list of proteins identified in such an approach. Besides the medically desired action of the drug, the identification of other proteins binding the drug can help to identify side effects and toxicity at a very early stage of drug development<sup>3</sup>.

Traditionally, new drugs have been developed following a target-based screening in which a large library of compounds is screened against a single target protein thought to be responsible for the disease, and subsequently the active hits can be optimized through medicinal chemistry efforts. One major limitation of this approach is the fact that many compounds are found to interact with multiple targets. The “one drug, one target” paradigm, thought to be the cornerstone of target-based methods, often does not hold true for compounds identified using this strategy<sup>4</sup>.

One of the major advantages of phenotype-based approaches is that they provide an unbiased way to find active compounds in the context of complex biological systems. Because phenotypic screening takes place in a physiologically relevant environment of cells or whole organism, the results from such screens provide a more direct view of the desired responses as well as highlight potential side effects. More importantly, phenotypic screens can lead to the identification of multiple proteins or pathways that may not have been previously linked to a given biological output. Because target identification from phenotypic screens is expected to generate a spectrum of possible targets, the term “target deconvolution” was coined to more accurately define the process<sup>4</sup>.

Recent developments in chemical proteomics, a multidisciplinary research area integrating biochemistry and cell biology with organic synthesis and mass spectrometry, have enabled a more direct and unbiased analysis of a drug’s mechanism of action in the context of the proteome as expressed in the target cell or the tissue of interest. Advances in quantitative mass spectrometry now enable the detection and quantification of drug-induced changes in protein expression and activation with unprecedented proteome coverage. There are multiple approaches that can be employed in chemical proteomic workflows. These include small molecule affinity-based and activity-based probes that can be used to isolate targets and more recently, *in silico* techniques to predict small molecule binding proteins. Moreover, affinity enrichment strategies using immobilized drugs or tool compounds now allow to characterize the expressed “interactome” of a drug directly from cell extracts<sup>5</sup>.

In drug development, chemical proteomics can shed an unbiased light on the interaction of the drug molecule with the proteome and identify both molecular targets responsible for benign effects and unwanted potentially toxic interactions. Furthermore, a different attachment position of the drug to the rest of the probe results in different interaction profiles with the proteome. This favorable “side effect” of using multi-functional probes may give insight into the structure activity relationship (SAR) of the drug and may serve as starting point for chemical modifications<sup>6</sup>.

### 1.2.1. *In silico* approach

Computer aided drug design is a major pillar of target-based drug discovery. On the basis of docking studies and virtual screening, drug candidates with optimal potency and selectivity can be predicted. With the recent renaissance of phenotype-based drug discovery, these *in silico* technologies have found an important new role in the process of target prediction. Over the last two decades, extensive information regarding activity, structures and targets of small molecule libraries has been deposited into public databases such as ChEMBL, DrugBank and ChemBank. Using these tools, targets of active compounds can be predicted based on similarities in structure between an active hit and well-characterized drugs in these databases. This computer aided target prediction has been widely used to identify new targets of known drugs, to predict the targets of active hits from a library screening, and to investigate the mechanism of action of hits discovered from phenotypic screens<sup>4</sup>.

The previously described strategy relies on molecules that have already been synthesized and studied in a specific system, from which results are extrapolated for a new protein/small-molecule pair. The drug-like chemical space, comprising organic small molecules (MW < 500 Da) of intermediate polarity, is very large and might contain on the order of  $10^{60}$  possible molecules. *De novo* drug design consists in exploring this chemical space in search for bioactive compounds by generating and scoring virtual molecules prior to their synthesis, whereby scoring relies on a variety of virtual screening approaches such as ligand-based and target-based methods. The advantage of *de novo* drug design is that many more molecules can be evaluated than what is possible if considering only already synthesized molecules, a strategy which might help to uncover lead structures and eventually improve clinical success for new drugs<sup>7</sup>.

### 1.2.2. Affinity Chromatography

Affinity purification is the most widely used technique to isolate specific target proteins from a complex proteome. Small molecules identified in phenotypic screens are immobilized onto a solid support that can be used to isolate bound protein targets (Figure 1-2). The small molecules used as selectivity functions in these studies display binding to their target proteins with low nanomolar affinity. This approach relies on extensive washing steps to remove non-binders, followed by specific methods to elute the proteins of interest. The eluted proteins can then either be directly identified using 'shotgun' type sequencing methods with multidimensional liquid chromatography or be further separated by gel electrophoresis and analyzed by mass spectrometry. The identified peptide sequences can then be used in database searches to identify the target protein<sup>4</sup>.

Representative studies utilizing this technique produced so-called kinobeads to study the kinase subproteome from eukaryotic cell lines. These beads carry a number of different small molecule kinase inhibitors and have not only been used to map kinases from complex biological samples, but also to assess the selectivity profiles of kinase inhibitor drugs<sup>8</sup>. Daub and colleagues used a different set of kinase inhibitors to isolate large numbers of kinases from

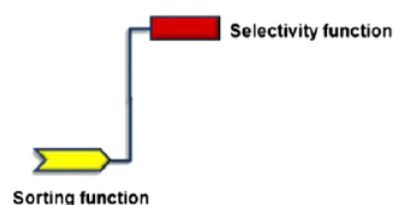


Figure 1-2: Schematic representation of an affinity chromatography pull-down probe. Bi-functional molecule bearing a targeting/selectivity function (red rectangle), corresponding to the small molecule under study, and a sorting function to allow attachment to a solid matrix, usually via biotin/avidin interaction. Reproduced from Lenz et al.<sup>5</sup>

cell lysates, and also focused on the subsequent analysis of the phosphorylation state of the enriched proteins<sup>9</sup>.

The major problem of affinity chromatography and its “pull-down” approach consists in the evaluation of nonspecific binding especially if we take into consideration that some intracellular proteins (e.g. glyceraldehyde-3-phosphate dehydrogenase) are detected as components of various subproteomes. It is also possible that rough elution conditions may remove protein targets exhibiting moderate affinity to ligands used. Affinity-based approaches are also applicable for identification of small-molecule protein targets, but the previously described limitations demand a subsequent analysis of identified proteins with a particular target inhibition assay<sup>10</sup> and are mostly unusable in living cells.

### 1.2.3. Activity-based protein profiling (ABPP)

Activity-based probes are small molecule tools that can be used to monitor the activity of specific classes of enzymes. ABPP probes are characterized by a selectivity function that is capable of covalently reacting with the active sites of target enzymes driven by the catalytic mechanism of the enzyme. By directly modifying the active site amino acid residues, ABPP probes act as suicide inhibitors. Over the past decade and a half, various ABPP probes have been designed to study proteases, hydrolases, phosphatases, histone deacetylases, and glycosidases, and these probes have proven to be valuable in investigating enzyme-related disease mechanisms including cancer and metabolic disorders. Typical activity-based protein profiling follows a similar overall workflow as affinity chromatography, including probe binding, protein separation, sequence analysis, and database searching. However, because most ABPP probes are designed to target a specific enzyme class, they are mostly useful for the development of small-molecules where a specific enzyme or enzyme family is suspected to be involved in a certain disease state or pathway<sup>4,6</sup>.

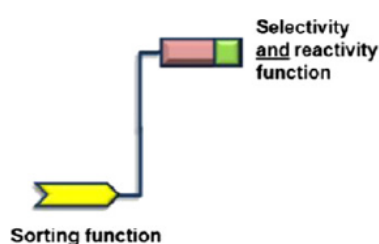


Figure 1-3: Schematic representation of an activity-based protein profiling (ABPP) probe. Typically a bi-functional probe where the small molecule as selectivity function reacts with the active site of the target protein and establishes a covalent bond. The attached sorting function can either be a reporter, such as a fluorophore for visualization, or a tag, such as biotin for isolation and enrichment. Reproduced from Lenz et al.<sup>6</sup>

ABPP probes have three components: a reactive electrophile for covalent modification of enzyme active site, a linker or a specificity group for directing probes to specific enzymes, and a reporter or a tag for separating labeled enzymes (Figure 1-3). Covalent enzyme inhibitors can be readily converted to ABPP probes by attaching a tagging group, and the combined use of covalent inhibitors and ABPP probes in phenotypic screening greatly facilitates target identification and also offers a powerful tool to study function and mechanism of identified proteins. In order to covalently attach ABPP probes to target proteins, an active site nucleophile such as cysteine or serine is required<sup>4,6</sup>.

ABPP probes are not only useful for target identification, but also are powerful tools for the discovery of disease related proteins and the technology has been used to identify serine and cysteine hydrolases from human cancer samples or proteolytic enzymes of the proteasome, for example. Mechanism-based ABPP-probes have also been reported for the profiling of native ATP-binding proteins, in particular kinases. These probes exploit the catalytic reaction of the kinase to form a chemical group that can covalently target lysine residues in the

catalytic sites. Other mechanism-based ABPP-probes were successfully applied for the profiling of tyrosine phosphatases, phospholipases, glycosidases, cytochrome P450 proteins, and the list is growing at a fast pace<sup>6</sup>.

The limitation of ABPP probes in pharmaceutical target research is that most small-molecules are non-covalent binders and modifying the selectivity function where it interacts with the protein would most probably alter its binding affinity. A new design of probe was developed where the small-molecule interacts with the target protein in a natural reversible manner, but an independent photo-reactive moiety forms a covalent ligation to the target allowing for the necessary stringent washing steps to reduce unspecific binders – the Capture Compound<sup>11</sup>.

#### 1.2.4. Capture compound mass spectrometry (CCMS)

Small molecule probes termed Capture Compounds are tri-functional molecules containing a selectivity function, a photoactivatable reactivity function, and a sorting function protruding from a common core atom (Figure 1-4). Binding of the selectivity function occurs non-covalently driven by the thermodynamic equilibrium. Covalent cross-linking to the target protein is accomplished through photo-activation of a separate reactivity function that, in contrast to classic photoaffinity labeling, is not part of the selectivity function, but is located on a different branch of the probe, intentionally at a certain distance from the selectivity function<sup>11</sup>. As a result, all three functional entities exhibit a high degree of freedom independent of each other. In particular, due to the linker between selectivity function and core atom of the probe, the selectivity function binds to the small molecule binding pocket of the target proteins, whereas the reactivity function stays at the protein surface. Therefore, the reactivity function can target surface-exposed structures of the target proteins, and is not structurally confined within the small molecule binding pocket of the protein. This flexibility of the photo-reactive function allows for high cross-link yields<sup>12</sup>.

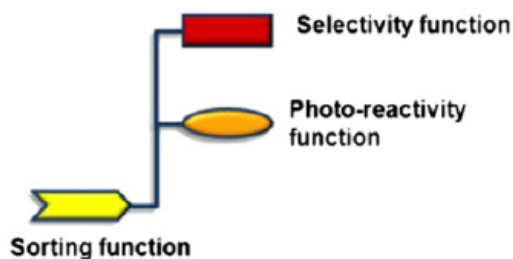


Figure 1-4: Schematic representation of a capture compound. Tri-functional molecule consisting of a selectivity function, formed by the small molecule under study, a reactivity function that establishes a covalent bond with the target protein upon UV irradiation, and a sorting function that can be a fluorophore for visualization or a tag, such as biotin, for enrichment and isolation. Reproduced from Lenz et al.<sup>6</sup>

In a typical CCMS experiment, the selectivity function accomplishes an equilibrium-driven affinity binding to target proteins. In a second step, this equilibrium is “frozen” through photo-activation of the reactivity function. This results in a covalent bond formation between probe and protein target through the reactivity function. Because the equilibrium binding of the target proteins is “frozen” by the covalent cross-link of the reactivity function to the protein, weak, but still specific binders are retained attached to the probe during subsequent isolation and washing steps and can be identified. The third module is a sorting function for isolation of the targeted proteins, usually biotin that can be enriched with streptavidin-coated magnetic beads for subsequent proteomic analysis. The basic experimental workflow of CCMS and the previously described affinity pull-down and ABPP are illustrated in Figure 1-5, on page 19.

Capture compounds with different selectivity functions have been used for the isolation of protein families such as kinases<sup>13,14</sup>, GTPases<sup>15</sup>, cAMP-binding proteins<sup>12</sup>, methyltransferases<sup>16,17</sup>,

and 2-oxoglutarate oxygenases<sup>18</sup> from complex biological mixtures. In each case, specific binders were isolated and identified from cell lysates or subcellular fractions of tissues. In each of the cited capture compound studies, the yield of identified specific binders was shown to be substantially higher than in parallel affinity pull-down experiments without photo-activated cross-linking via the respective reactivity functions<sup>6</sup>. Particularly in the case of methyltransferases that were addressed by a capture compound with the methyltransferase product inhibitor S-adenosyl-L-homocysteine as selectivity function, the results demonstrated that a capture compound based approach, due to the additional photo-activated cross-link to the bound target proteins via the reactivity function, can deal with small molecule-protein interactions in a range of relatively low affinity, i.e., in the micromolar range. These interactions are usually difficult to address by simple affinity pull-down.

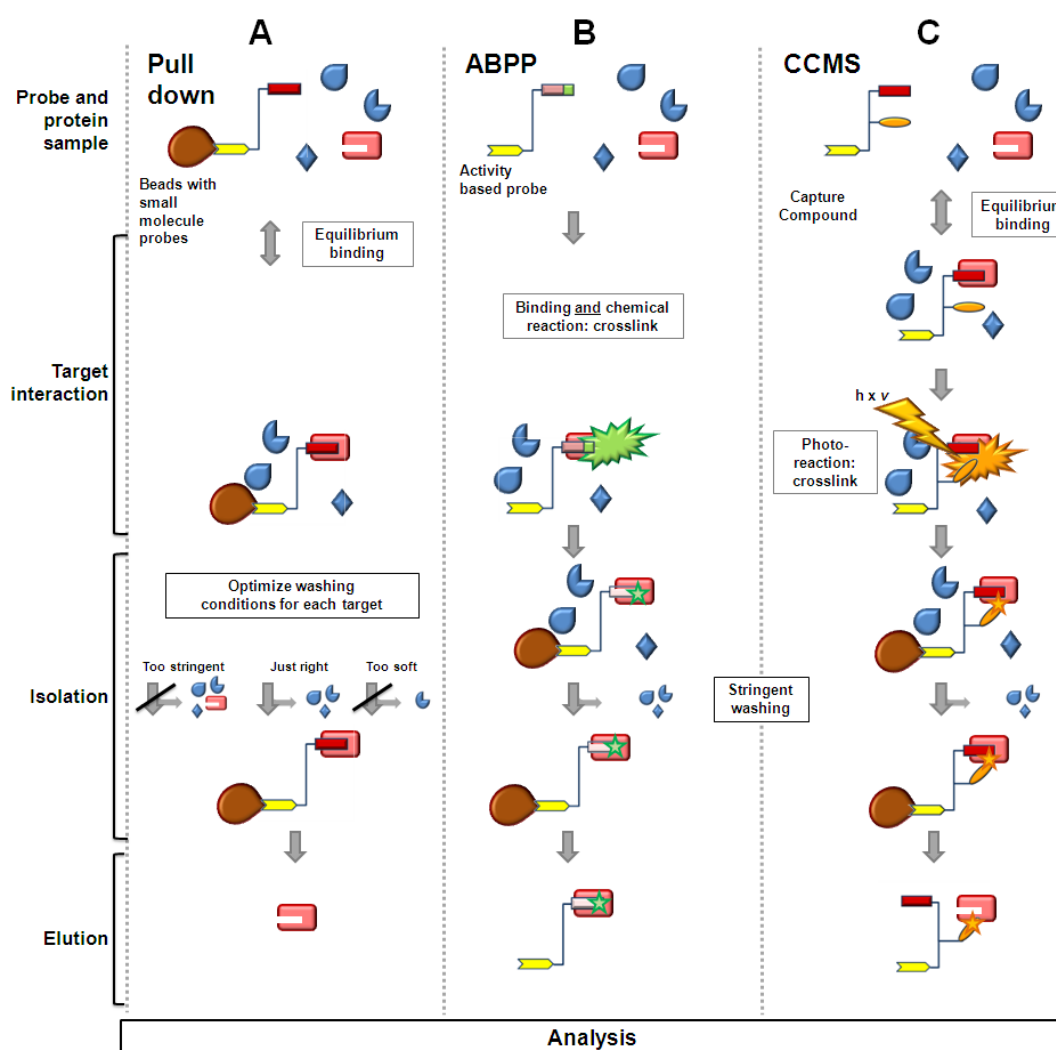


Figure 1-5: Schematic workflows for three different target deconvolution techniques.

In affinity chromatography pull-down experiments (panel A), probes reversibly interact with target proteins defined by a dynamic equilibrium. Non-binding proteins are washed away, and retained proteins are analyzed after elution using denaturing buffer or an excess of free affinity ligand. The choice of buffer conditions requires a tradeoff: low stringency will lead to high unspecific background binding, while high stringency will lead to loss of weakly, but still specifically interacting proteins. In activity-based protein profiling (ABPP) experiments (panel B), the selectivity function of the probe binds to and chemically reacts with the active site of target enzymes. Harsh washing conditions can be applied to remove proteins nonspecifically bound to the solid phase. As a limitation, ABPP can only be used with small molecules that chemically react with their targets. In Capture Compound Mass Spectrometry (CCMS) experiments (panel C) the Capture Compound selectivity function reversibly interacts with target proteins defined by a dynamic equilibrium, and this equilibrium is fixed through a photo-induced cross-linking of the reactivity function. Harsh washing conditions can be applied to remove unspecific background. Some nonspecifically cross-linked proteins are retained as well. Reproduced from Lenz et al.<sup>6</sup>

The prerequisite for the successful functional isolation of proteins from biological samples by small molecule probes is that the proteins are in their native (functional) state. Some proteins tolerate transfer from the cellular context to a cellular lysate, while others may not. It is therefore important to keep the proteins in a state as native as possible in order to reveal physiologically relevant small molecule–protein interactions.

The vast majority of chemical proteomics studies have been conducted on lysate samples<sup>16,19–21</sup>. Ideally, probing of small molecule–protein interactions on intracellular proteins should be conducted in intact cells with membrane-permeable probes. The permeability of the probes can be increased by only adding the tag after the small molecule has found the target and is fixed to it. This is achieved using chemo-selective ligatable probes. The smaller probes comprise only a combined selectivity/reactivity function (in ABPP probes) or separate selectivity and photo-reactivity functions (in capture compounds), but no sorting or detection function. Instead, the probes contain a small functional group, such as an alkyne or azide moiety. This enables chemical ligation of the sorting function later in the workflow. The sorting function is attached to the probe only after the target recognition and (photo-) cross-linking reaction has taken place and cell integrity is no longer necessary. This reaction workflow is called chemo-selective bio-orthogonal chemical ligation. Permeable probes consisting only of selectivity and reactivity function or combined selectivity/reactivity functions have been successfully used to address targets of small molecules within living cells<sup>22–24</sup>.

The in-cell workflow for the application of either a chemically reactive or a photo-reactive probe is depicted in Figure 1-6.

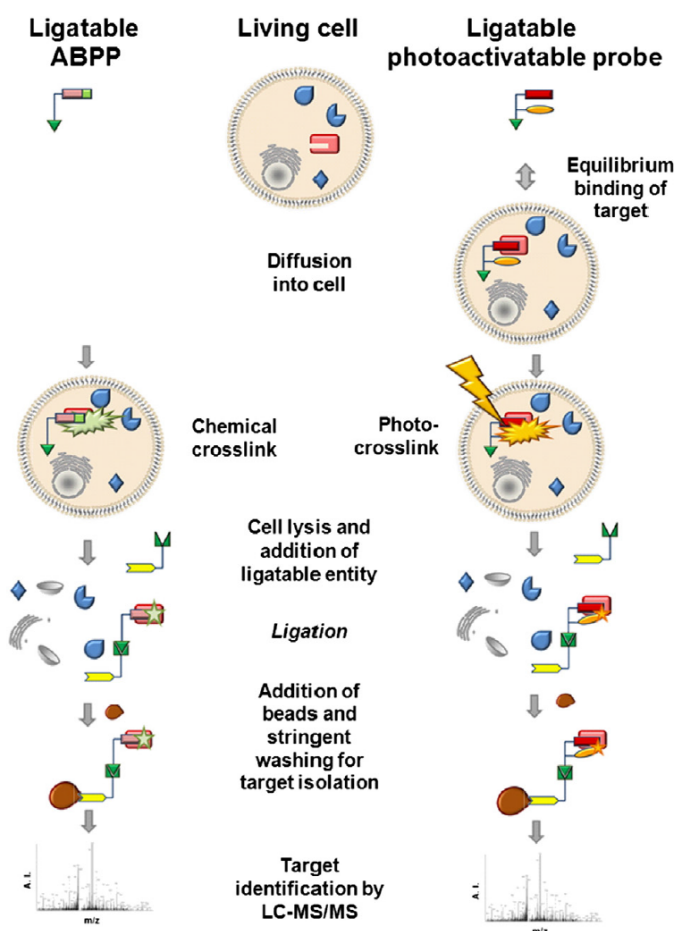


Figure 1-6: Workflow for identification of small-molecule targets in living cells.

Permeable small molecule probes carry a selectivity function and a reactivity function or a combined selectivity/reactivity function, but lack a sorting function. Instead, the probe carries a small functional group that enables addition of a sorting function through a specific ligation reaction later in the workflow. Chemical or photoactivated cross-link can be carried out, and only after that the cell is lysed for ligation to the sorting function. Reproduced from Lenz et al.<sup>6</sup>

An essential condition for this approach is that the functions on the small probe and the sorting function only react with each other and not to any other intracellular component.

In essence, it needs to allow for a bio-orthogonal chemoselective ligation.

### 1.3. CLICK CHEMISTRY AND BIO-ORTHOOGONAL LIGATIONS

In the advent of successfully using green fluorescent protein (GFP) tags to visualize protein dynamics and function in living systems, by cleverly introducing a gene that concomitantly translates with the target protein and produces an active fusion protein, it quickly became clear that this strategy did not allow to study post-translational modifications or other relevant biological molecules such as glycans, lipids, metabolites and nucleic acids<sup>25,26</sup>. To overcome this limitation, a reactivity-based bio-orthogonal chemistry approach was successfully developed.

Bio-orthogonal reactant pairs, which are most suitable for such applications, are molecular groups with the following properties: (i) they are mutually reactive but do not cross-react or interact in noticeable ways with biological functionalities or reactions in a cell, (ii) they and their products are stable and non-toxic in physiological settings, and (iii) ideally, their reaction is highly specific and fast<sup>25,27</sup>. An illustration from Sletten *et al.*<sup>26</sup> depicts the challenge of “fishing” out a specific molecular entity from a “sea” of functional groups that are present in cells (Figure 1-7).

Bio-orthogonal chemical reactions have emerged as highly specific tools that can be used for investigating the dynamics and function of biomolecules in living systems<sup>27–29</sup>. Click chemistry, inspired by nature’s use of simple and powerful connecting reactions, describes the most specific bio-orthogonal reactions that are wide in scope, easy to perform, and usually employ readily available reagents that are insensitive to oxygen and water<sup>30–32</sup>. *In vivo* bio-orthogonal chemistry and click chemistry therefore overlap quite a bit, reflecting the same underlying chemical principles applied in somewhat different ways toward the discovery or development of molecular function and information<sup>25</sup>.

With over 20 bio-orthogonal transformations now reported in the literature and new ones being discovered at a rapid pace, selecting the “best fit” for a given application is non-trivial. The chemistries vary widely in terms of their selectivities and biocompatibilities, and many of their perceived strengths and weaknesses remain anecdotal<sup>29</sup>.

One of the most popular bio-orthogonal functional groups is the azide. The small size, coupled with its inert nature towards endogenous biological functionalities, sets the azide apart. Additionally the azide has unique chemistries with other bio-orthogonal functionalities, most notably phosphines and alkynes<sup>28</sup>. Because of this versatility, old and newly modified reactions based on azides have been the basis for the expansion of click chemistry in the biological context, such as the Staudinger ligation, [3+2] cycloadditions with or without metal catalysts and, more recently, a tetrazine ligation.

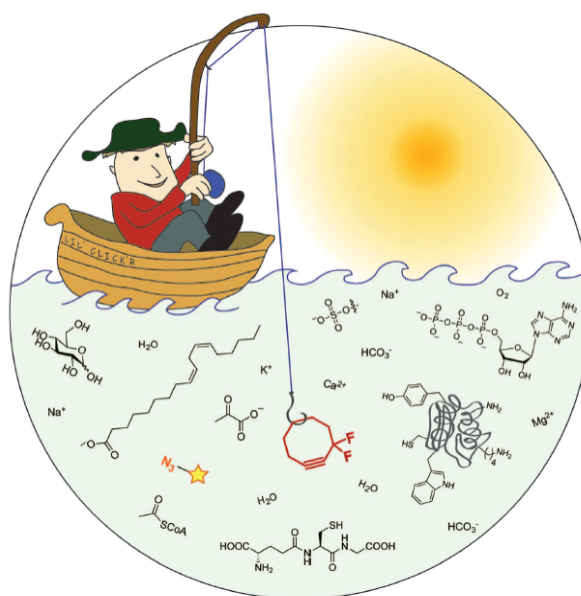


Figure 1-7: Illustration of bio-orthogonal ligation. The bio-orthogonal reactant pairs should react exclusively with each other forming a stable and non-toxic product to the cellular environment. Reproduced from Sletten *et al.*<sup>26</sup>

### 1.3.1. Staudinger ligation

The Staudinger ligation essentially launched the field of bio-orthogonal chemistry, not because it was the first bio-orthogonal reaction per se, but because it was the first among entirely abiotic functional groups and therefore had the potential for translation to live organisms<sup>27</sup>. Its prototype reaction was the Staudinger reduction of azides with triphenylphosphine and water, reported by Hermann Staudinger in 1919. It appeared well suited as a prototype for bio-orthogonal reaction development because the two participants were abiotic, mutually and selectively reactive, mostly unreactive with biological functionalities, and tolerant of water. In 2000, Saxon and Bertozzi<sup>33</sup> were able to adapt this reaction into a ligation method where they successfully labeled modified glycans on the surface of cells via the newly developed Staudinger ligation (Figure 1-8, panel A).

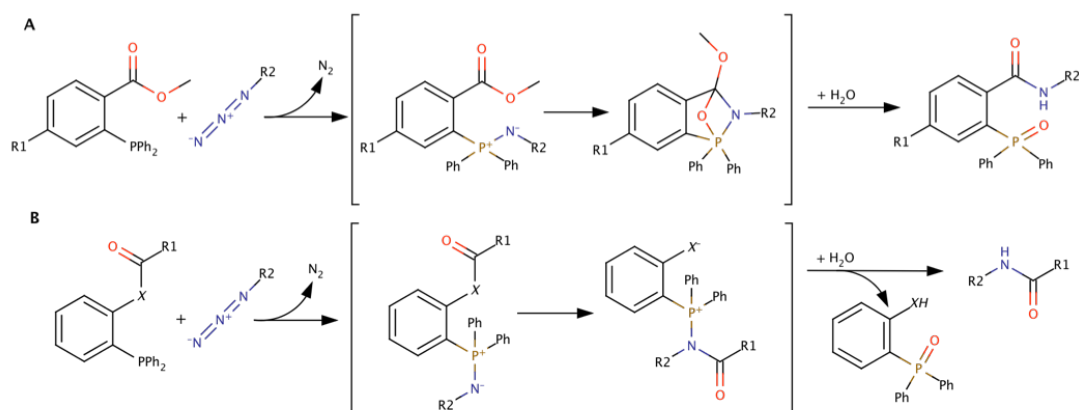


Figure 1-8: Classical (A) and traceless (B) Staudinger ligation

The Staudinger ligation was promising but there were some limitations. The phosphine reagents slowly underwent air oxidation within biological systems and were probably metabolized by cytochrome P450 enzymes in mice. Additionally, the kinetics of the reaction was not fast enough, which necessitated the use of high concentrations of phosphine reagent.

Bertozzi's group overcame this limitation later in the same year by developing a "traceless" Staudinger ligation (Figure 1-8, panel B) where the position of the reporter module in the phosphine reagent was modified. This allowed the phosphine oxide to be expelled during the reaction leaving the two groups linked via an amide bond.

Since this time, the mechanism of the reaction and other details have been probed in depth<sup>34-36</sup>, and a number of iterations have been reported, such as fluorogenic versions, including a FRET-based system, as well as reagents with increased water solubility<sup>37</sup>.

While still the reaction of choice for a wide range of bio-conjugation applications, the slow kinetics of the Staudinger ligation, together with the oxidation liability of its phosphine compounds, remains an unsolved problem and an obstacle for in vivo chemistry. Consequently, most research groups turned their attention to the other mode of bio-orthogonal reactivity exhibited by the azide: its 1,3-dipolar cycloaddition with alkynes.

### 1.3.2. Copper-catalyzed azido-alkyne cycloaddition (CuAAC)

The 1,3-dipolar [3+2] cycloaddition of azides and alkynes was first reported in 1893<sup>38</sup>. But it was only 70 years later that the kinetics and mechanism of the reaction was described by Huisgen<sup>39</sup>, who had his name bestowed upon this azido-alkyne cycloaddition (AAC).

In 2001, Sharpless and his collaborators set out to generate substances by joining small units together with heteroatom links (C-X-C) with the purpose to develop an expanding set of selective and modular “blocks” that would reliably work in both small and large-scale applications. They termed this approach as “click chemistry” and defined a stringent set of criteria for this process<sup>30</sup>. The reaction should be modular, wide-scoped, generate high yields with little or inoffensive byproducts<sup>40</sup>, stable under physiological buffer conditions and insensitive to oxygen. Therefore, click reactions achieve their required characteristics by having a high thermodynamic driving force, as if being “spring-loaded” for a single target in a single trajectory. Among these were the cycloadditions of unsaturated species, especially the 1,3-dipolar cycloaddition reaction<sup>40</sup>.

Being small, incapable of significant hydrogen bonding and relatively non-polar, both azide and alkyne are unlikely to significantly change the properties of structures to which they are attached. Additionally, azides and alkynes are stable in the presence of surrounding nucleophiles, electrophiles and solvents common to standard reaction conditions and complex biological media. However, the rate of this reaction is quite slow, requiring prolonged heating for inactivated alkynes. The AAC process was accelerated by catalysis with copper (I) or ruthenium (II) complexes. Because of its high rate and use of the small and easily synthesized azide and terminal alkyne groups, the copper-catalyzed (CuAAC) version has been the most widely used<sup>40</sup>.

The reaction mechanism was initially proposed by Himo and Sharpless<sup>41</sup> and recently refined by Worrell and Fokin<sup>42</sup>. Copper catalysts change the mechanism and outcome of the thermal reaction of terminal or internal alkynes with organic azides, converting it to a sequence of steps which culminates in the formation of a di-copper intermediate (Figure 1-9).

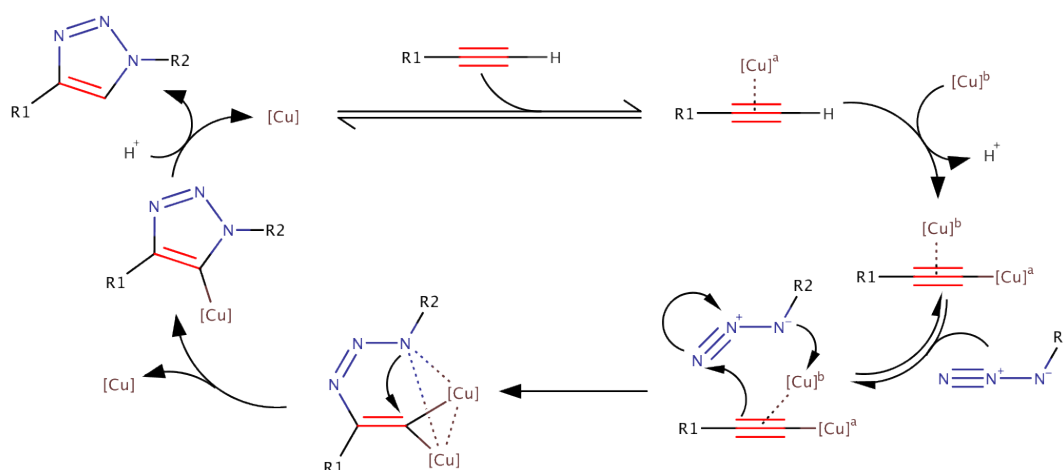


Figure 1-9: Mechanism of the copper-catalyzed azido-alkyne cycloaddition (CuAAC)

The rate of CuAAC is increased by a factor of  $10^7$  relative to the non-catalyzed process, making it conveniently fast and below room temperature<sup>43</sup>.

By 2010, copper stood out as the only metal for the reliable, facile and 1,4-regiospecific catalysis of the azide-alkyne cycloaddition. Fokin's group at the Scripps Institute researched complexes of all first-row transition elements and complexes of Ag(I), Pd(0/II), Pt(II), Au(I/III), and Hg(II), among others, have all failed to produce triazoles in synthetically useful yields; their effect on the rate and selectivity of the cycloaddition was at best marginally noticeable<sup>43</sup>.

In 2005, ruthenium cyclopentadienyl complexes were found to catalyze the formation of the complementary 1,5-disubstituted triazole from azides and terminal alkynes, and also to engage internal alkynes in the cycloaddition<sup>44</sup>. While the scope and functional group compatibility of ruthenium azido-alkyne cycloaddition (RuAAC) are excellent, the reaction is more sensitive to the solvents and the steric demands of the azide substituents than CuAAC<sup>43</sup>. Applications of RuAAC are still scarce<sup>44</sup>.

Meldal and Tornøe<sup>45</sup> published an extensive review on CuAAC showing the effects of the copper source in the reaction and potential side reactions that may prevent this approach to be used in living cells, which ultimately lead to the introduction of copper ligands to perform the cycloaddition safely in intact cells.

### 1.3.2.1. Copper catalysts and ligands

A wide range of experimental conditions for the CuAAC have been employed since its discovery, underscoring the robustness of the process and its compatibility with most functional groups, solvents, and additives regardless of the source of the catalyst. The choice of the catalyst is dictated by the particular requirements of the experiment, and usually many combinations will produce desired results. Copper(I) salts (iodide, bromide, chloride, acetate) and coordination complexes have been commonly employed<sup>43</sup>.

Copper(II) salts and coordination complexes are not competent catalysts. Cupric salts and coordination complexes are well-known oxidizing agents for organic compounds. Alcohols, amines, aldehydes, thiols, phenols, and carboxylic acids may readily be oxidized by the cupric ion, reducing it to the catalytically active copper(I) species in the process<sup>43</sup>. Still, performing the reaction in the presence of mild oxidants allows capture of the triazolyl copper intermediates. Ascorbate, a mild reductant, was introduced by Rostovtsev *et al.*<sup>46</sup> as a convenient and practical alternative to oxygen-free conditions. Its combination with a copper(II) salt, such as the readily available and stable copper(II) sulfate pentahydrate ( $\text{CuSO}_4 \cdot 5\text{H}_2\text{O}$ ) or copper(II) acetate ( $\text{Cu}(\text{CH}_3\text{COO})_2$ ), has been quickly accepted as the method of choice for preparative synthesis of 1,2,3-triazoles. Water appears to be an ideal solvent capable of supporting copper(I) acetylides ( $\text{Cu}_2\text{C}_2$ ) in their reactive state, especially when they are formed in situ. The "aqueous ascorbate" procedure often furnishes triazole products in nearly quantitative yield and greater than 90% purity, without the need for ligands or additives or protection of the reaction mixture from oxygen<sup>43</sup>. Of course, copper(I) salts can also be used in combination with ascorbate, wherein it converts any oxidized copper(II) species back to the catalytically active +1 oxidation state.

Many other copper complexes involving ligands have been reported as catalysts or mediators of the CuAAC reaction. Many reported reactions are performed under widely differing conditions, making quantitative comparisons of ligands performance difficult. The largest and most successful class of ligands for CuAAC catalysis is the one containing heterocyclic donors. The need for these ligands was particularly evident for reactions involving biological molecules that are handled in water in low concentrations and are not stable to heating.

Despite the experimental simplicity and efficiency of the “ascorbate” procedure, the rate of the CuAAC reaction in the absence of an accelerating ligand is simply not high enough when concentrations of reactants are low. The first general solution to the bio-conjugation problem was provided by tris(benzyltriazolyl)methyl amine ligand (TBTA, CC 16 on page 125), prepared using the CuAAC reaction and introduced shortly after its discovery<sup>47</sup>. After its utility in bio-conjugation was demonstrated by the efficient attachment of 60 alkyne-containing fluorescent dye molecules to the azide-labeled cowpea mosaic virus<sup>48</sup> it was widely adopted for use with such biological entities as nucleic acids, proteins, E. coli bacteria, and mammalian cells<sup>43</sup>.

The poor solubility of TBTA in water prompted the development of more polar analogues such as tris(3-hydroxypropyltriazolyl)methyl amine (THPTA, CC 17 on page 125)<sup>49</sup> and a bis(tert-butyltriazolyl) ethanol ligand (BTTE, CC 18 on page 125)<sup>50</sup> that showed tremendous improvement in reaction kinetics compared to the ligand-free cycloaddition in biological conditions.

Despite the accelerated kinetics and reduced copper toxicity by the introduction of ligands in the CuAAC reaction, the Bertozzi group developed more bio-friendly copper-free cycloadditions by using the intrinsic energy of strained cyclic alkynes to drive the reaction<sup>51</sup>.

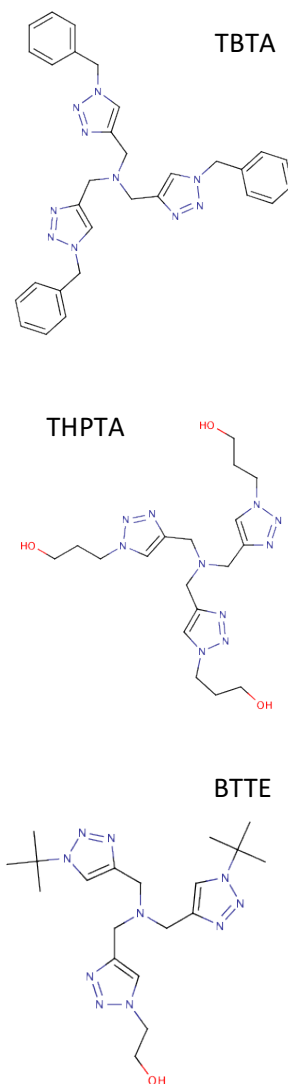


Figure 1-10: CuAAC-accelerating ligands of choice.

### 1.3.3. Metal-free click cycloadditions

Exogenous metals can have mild to severe cytotoxic effects and can thus disturb the delicate metabolic balance of the systems being studied. Copper, for example, exerts its toxicity mainly via free radical-induced oxidative damage<sup>52</sup>.

Based on knowledge that cyclooctyne and phenyl azide “proceeded like an explosion to give a single product” – the triazole, Bertozzi’s lab explored this new click chemistry field to circumvent metal toxicity of the classical cycloadditions.

### 1.3.3.1. Strain-promoted azido-alkyne cycloaddition (SpAAC)

The first cyclooctyne that Bertozzi evaluated underwent cycloaddition with azides to give a triazole, and although its reaction kinetics was vastly accelerated compared to the linear alkynes, there was room for improvement<sup>51</sup>. They sought to reduce the electron density of the alkyne bond by introducing a fluorine atom to the ring system, and this increased the reaction rate constant by 3-fold. With the addition of a second fluorine atom to the ring, to create the compound named DIFO (Figure 1-11), they observed a marked increase in rate constant, making the reaction 60 times faster than the parent compound<sup>28</sup>. While the rate of reaction for DIFO was exceptional, the compound's solubility in water was less than ideal. They then started to fine-tune the molecules with different heteroatoms within the ring structure to achieve a good solubility/reactivity balance, and found a good candidate with DIMAC<sup>53</sup>. At the same time other groups increased the reactivity of the cyclooctynes via introduction of neighboring benzyl rings<sup>54</sup>. Research advanced rapidly and a large myriad of strained alkynes surfaced where in most cases the increased reactivity meant less hydrophilicity and vice-versa<sup>28,55,56</sup>.

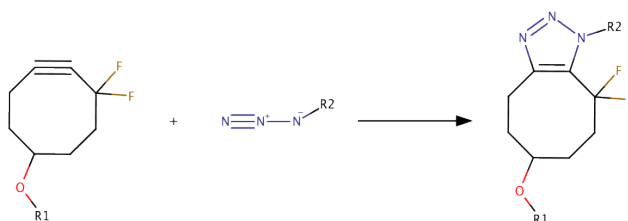


Figure 1-11: Strain-promoted azido-alkyne cycloaddition. Example reaction between DIFO and an azide.

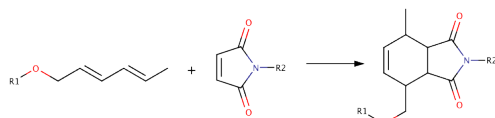
There are numerous applications of cyclooctynes in the context of biological systems. Bertozzi *et al.* proved its applicability on modification of purified proteins<sup>51</sup>, later on the method was extended to *in vivo* experiments<sup>55</sup>. Furthermore, SpAAC was used to image tumors in living mice with the help of nanoparticles<sup>57</sup> and <sup>18</sup>F positron emission tomography (PET)<sup>58</sup>.

Despite some problems in the earlier development of SpAAC such as slow kinetics and spontaneous defluorination of reagents which were overcome by reagent optimization, this method has proven its suitability for *in vivo* labeling several times. The issue of increased unspecific labeling compared to Staudinger ligation remains to be solved.

### 1.3.3.2. Tetrazine ligation

While others were working with alkynes to form triazoles upon cycloaddition with azides, Rutjes and co-workers<sup>59</sup> developed an alkyne surrogate that forms a 1,2,3-triazole product in a two-step reaction that included a retro-Diels-Alder reaction\*.

\* The Diels-Alder reaction is a [4+2] cycloaddition of a conjugated diene and a dienophile (an alkene or alkyne). *E.g.*:



In 2008, the Fox<sup>60</sup> and Hildebrand<sup>61</sup> groups put the inverse electron demand Diels-Alder reaction to use in bio-orthogonal ligation chemistry using a tetrazine to react with a trans-cyclooctene and norbornene, respectively (Figure 1-12).

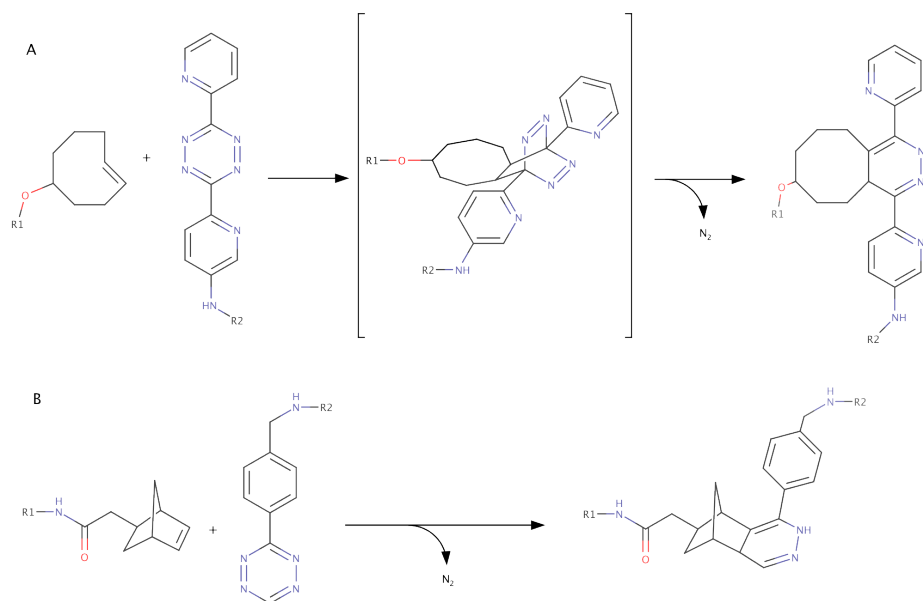


Figure 1-12: Tetrazine ligation.

Example reactions between tetrazines and a trans-cyclooctene (A) as published in Fox et al.<sup>60</sup> and a norbornene (B) as published by Hildebrand and co-workers<sup>61</sup>.

Electron-rich tetrazines are less susceptible to hydrolysis and attack by biological nucleophiles, and are thus more desirable for use *in vivo* and intracellular environments, in particular. Stabilized tetrazines have recently been introduced into recombinant proteins via unnatural amino acid mutagenesis<sup>62</sup>. The heterocyclic amino acid derivatives integrated biological molecules that were then detected with strained alkenes<sup>63</sup>. A head-to-head comparison of the reactions of these various alkenes and tetrazines has not been reported, but combining the best feature of each approach could add valuable tools to the field<sup>28</sup>.

The tetrazine click is showing promising results in the bio-orthogonal chemical ligation field, particularly in the detection of fast biological processes. However, the bulkiness of the molecules involved could hinder some applications of the technique.

Very recently the use of click reactions for chemically triggered release of drugs *in vivo* based on tetrazines and trans-cyclooctenes is being studied<sup>64,65</sup>.

Many other chemical ligations have been explored to be used in biological settings, such as cycloadditions involving nitrile imines or nitrile ylides; azido-alkyne cycloadditions using other metals as catalyst; thiol-ene coupling; palladium-catalyzed coupling reactions; and photo-inducible dipolar cycloadditions. In fact, a cooperation partner of the BioChemLig network in which the research presented in this dissertation was included, published recently novel chemical reactions with potential to originate new bio-orthogonal ligations<sup>66</sup>.

The ligations presented in the previous paragraphs represent the most used and relevant in bio-orthogonal click chemistry research.

## 2. Labeling a protein using click chemistry

---

### 2.1. INTRODUCTION

Cyclic adenosine monophosphate (cAMP) is an important biological second messenger molecule that regulates several cellular events and complex biological processes such as memory consolidation, immune system regulation, insulin secretion and cardiac frequency<sup>67</sup>. cAMP was first described in 1956 by Rall *et al.* when they observed that the increased production of phosphorylase in liver homogenates upon hormonal stimulation was mediated by a heat-stable factor<sup>68</sup>. Soon after that discovery, the same group characterized that factor to be an adenine ribonucleotide<sup>69,70</sup> that was identical to a product isolated at the same time by Cook *et al.* from the alkaline degradation of adenosine triphosphate (ATP)<sup>71</sup>.

cAMP is produced in cells from ATP by adenylyl cyclases that are mainly located in the plasma membrane and these can be regulated in different ways such as via G protein-coupled receptors (GPCRs) that respond to external stimuli in the form of hormones or neurotransmitters<sup>72,73</sup>; intracellular  $\text{Ca}^{2+}$  and bicarbonate regulate cAMP production via a soluble adenylyl cyclase<sup>74,75</sup>; and post-translational modifications such as phosphorylation can also affect the activity of adenylyl cyclases<sup>76,77</sup>. The effector function of cAMP is terminated by specific phosphodiesterases that catalyze the hydrolysis of cAMP into AMP<sup>69</sup>, controlling the pool of available cAMP and regulating the signaling cascade. Additional mechanisms of cAMP production and clearance have been described<sup>72,76</sup>, such as the targeting of specific adenylyl cyclases to membrane microdomains that contribute to the formation of cAMP compartments with clinical relevance<sup>78</sup>, and the efflux of cAMP to the extracellular space through a multidrug resistance transport system<sup>79</sup>.

Protein kinase A (PKA) was the first down-stream target for cAMP to be identified by Walsh *et al.* in 1968<sup>80</sup>. PKA is a heterotetramer composed of two regulatory and two catalytic subunits whose multiple subunits ( $\text{RI}_\alpha$ ,  $\text{RI}_\beta$ ,  $\text{RII}_\alpha$ ,  $\text{RII}_\beta$  and  $\text{C}_\alpha$ ,  $\text{C}_\beta$ ,  $\text{C}_\gamma$ ) possess distinct physical and biological properties, are differentially expressed, and are able to form different isoforms of PKA holoenzymes<sup>81</sup>. Activation of PKA involves the cooperative binding of four cAMP molecules to the two regulatory subunits, inducing a conformational change and releasing both catalytic subunits that are then able to phosphorylate their protein substrates<sup>82</sup>. The regulatory subunits of PKA are also responsible for the binding of scaffolding proteins called A-kinase anchoring proteins (AKAPs) that localize PKA to specific sites in close proximity to its protein substrates<sup>82,83</sup>. A scheme of cAMP synthesis and signaling via PKA is illustrated in Figure 2-1, on page 29.

Additional targets for cAMP have been described that affect the electrical activity of cells, such as hyperpolarization-activated cyclic nucleotide-gated (HCN) channels<sup>84</sup> and directly modulated by cyclic nucleotides (CNG) channels<sup>85</sup>. More recently, exchange proteins activated by cAMP (EPACs) that modulate the activity of the small GTPases Rap1 and Rap2, have been established as a family of proteins that directly bind cAMP<sup>86,87</sup>.

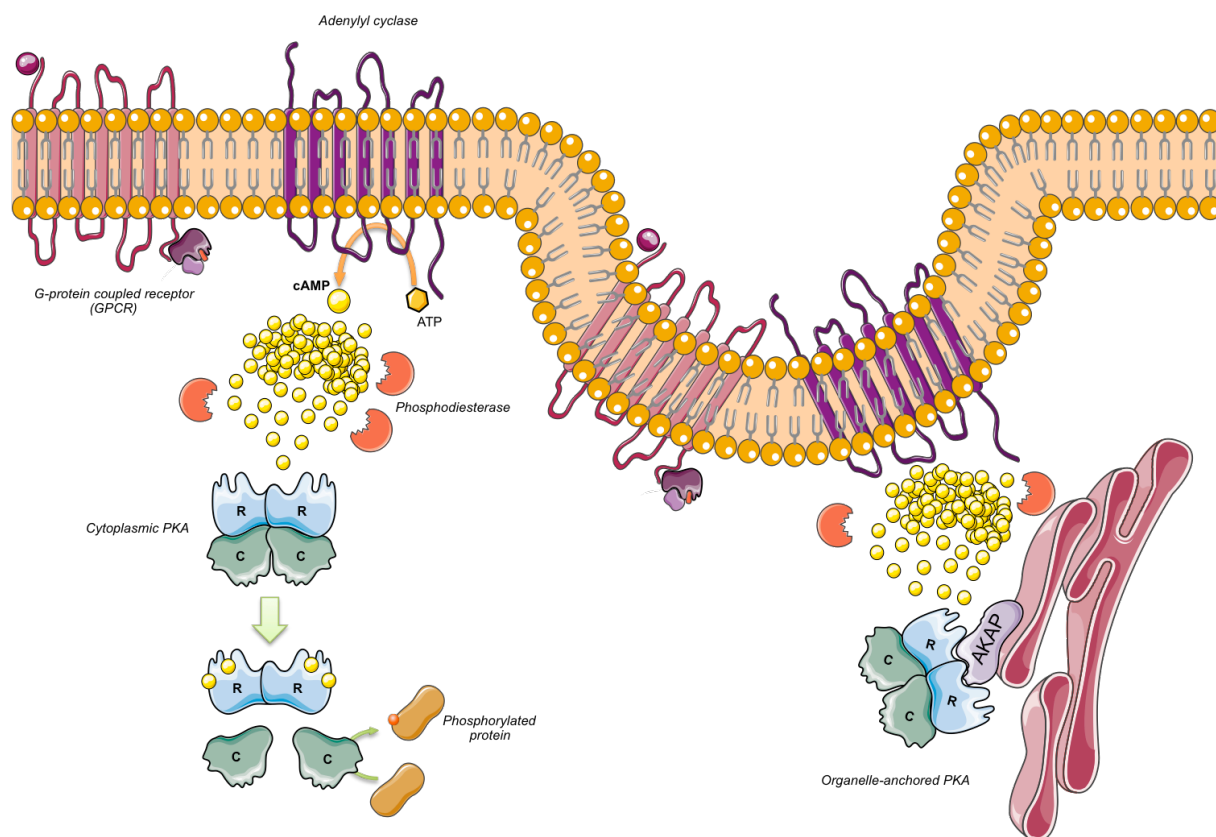


Figure 2-1: cAMP production and activation of PKA.

Ligand binding to G protein-coupled receptors (GPCRs) activates neighboring adenylyl cyclases and generates pools of cAMP from ATP. The distribution and concentration gradient of cAMP is limited by phosphodiesterases. Binding of cAMP to the regulatory (R) subunits of protein kinase A (PKA) releases the catalytic (C) subunits of the heterotetramer allowing them to phosphorylate target substrates. Certain adenylyl cyclases and GPCRs are confined to membrane microdomains in association with intracellular organelles or cytoskeletal constituents. The subcellular structures harbor specific isoforms of PKA that are localized in the vicinity of the receptor and cyclase through anchoring via A kinase anchoring proteins (AKAPs). These mechanisms serve to localize and limit the assembly of the pathway to a defined area of the cell close to the substrate. Adapted from Taskén et al.<sup>81</sup> using Servier Medical Art templates.

Mass spectrometry-based studies on cAMP-binding proteins have identified further targets for the small molecule, in addition to the previously described. Pull-down studies performed on HEK293 cells and different rat tissue lysates<sup>88–90</sup> used cAMP immobilized on agarose beads to enrich, isolate and identify the directly interacting proteins and their interaction partners. The results show that different isoforms of the regulatory subunit of PKA are enriched as well as a set of AKAPs and phosphodiesterases. One particular enriched protein, the oncoprotein sphingosine kinase interacting protein (SKIP) that was not known at the time to be involved in the cAMP pathway, was later established as a new AKAP<sup>91</sup>. The authors also concluded that the cyclic nucleotide proteome is contaminated by abundant proteins<sup>88</sup> and so they sequentially eluted the pulled-down proteins with different nucleotides to further enrich the true cAMP binders. Pull-down strategies with bead-immobilized small-molecules are prone to present high unspecific background because the washing conditions have to be mild and usually consist of only several washes with lysis buffer. These strategies are also little effective in the enrichment of membrane proteins with multiple trans-membrane segments.

In the CCMS approach, as described earlier (1.2.4 Capture compound mass spectrometry (CCMS), on page 18), washing conditions can be more stringent (high salt and detergent) because of the covalent crosslink between the modified small molecule and the target, increasing the signal-to-noise ratio of the true binders of the small molecule. Having a parallel competition assay, in addition to the stringent washing, allows also for a more accurate determination of real targets.

The cAMP-interacting proteome was studied by classical CCMS in HepG2 cells lysate and rat brain synaptosomal fractions<sup>12</sup>. As previous studies have shown, isoforms of the regulatory subunits of PKA were identified using CCMS along with several AKAPs, PKG and EPACs. The novelty was the success in identifying endogenously expressing HCN channels from the synaptosomal fractions, which was a known binding partner of cAMP but not demonstrated before by mass-spectrometry proteomics. Some of the enriched proteins in these experiments were also competed with other nucleotides, confirming the promiscuous binding observed before and they may as well be direct binders of cAMP but lack the cyclic nucleotide binding domain present in the classic targets of the small molecule.

With the knowledge of the strong interaction between cAMP and PKA via its regulatory subunits, a purified recombinant human PKARI was acquired and a cAMP analog was synthesized bearing a photo-reactive moiety and a terminal alkyne reactivity function (CC 2, on page 122) for the establishment of a new CCMS workflow using a two-step bio-orthogonal chemical ligation method.

## 2.2. RESULTS

### 2.2.1. Establishing and optimizing click-capture of PKARI using a cAMP CC

As previously described in the General Introduction (1.3 Click chemistry and bio-orthogonal ligations, on page 21), there are a number of bio-orthogonal ligations described in the literature, but to date the most broadly utilized has been the copper assisted azido-alkyne cycloaddition (CuAAC). This “click” reaction was chosen to establish a labeling method of a protein using a capture compound containing the selectivity and reactivity functions but with an alkyne terminal function in place of the sorting function as in a classical capture compound.

To achieve a successful labeling, different parameters such as capture compound concentration, time of the click reaction, copper concentration and copper ligands were independently varied.

The capture compounds, competitor and ligands utilized in this chapter are illustrated in the Specific Methods section (2.3.1 Structures of used compounds, on page 48)

As a starting point to establish this method in a CCMS workflow, a cAMP-alkyne capture compound (CC 2) was chosen and all reaction optimization steps were performed in a recombinant PKARI solution. The probe was clicked to an azide-biotin (CC 3) for visualization and capture of the target. As a reference, a classical cAMP-capture compound (CC 1) was used in parallel.

#### 2.2.1.1. Effect of cAMP-alkyne capture compound on click yields in a PKARI solution

Initial click reaction conditions were based on a publication by Speers *et al.*<sup>23</sup>. The first step was a concentration-dependent assessment starting from the generic condition to determine the effect of the concentration of cAMP-alkyne capture compound on the labeling of recombinant PKARI using biotin as a label.

16 pmol of PKARI was incubated with cAMP-alkyne capture compound (CC 2) at 5  $\mu$ M, 2.5  $\mu$ M, 1  $\mu$ M, 0.5  $\mu$ M or none for unspecific labeling control. A sample containing 5  $\mu$ M of cAMP full classical compound (CC 1) was used as labeling reference. After 30 min equilibration, samples were irradiated for 10 min at 310 nm in a CaproBox<sup>®</sup>. Next, to the cAMP-alkyne containing samples the following was added: 10  $\mu$ M biotin-azide (CC 3), 50  $\mu$ M CuSO<sub>4</sub>, 250  $\mu$ M TBTA (CC 16) and 2.5 mM sodium ascorbate. The click reaction was performed for 30 min with shaking. To a duplicate sample of cAMP-alkyne capture compound at 5  $\mu$ M, all click reagents except for the biotin-azide were added. The results were visualized by SDS-PAGE followed by Blotting using a streptavidin-horse radish peroxidase (HRP) solution for chemiluminescence readout detected on x-ray film (hereafter referred as biotin blot). Band intensity was measured using ImageJ software.

The biotin blot shown in Figure 2-2, on page 32, reveals that the click reaction takes place and is dependent on the concentration of the cAMP-alkyne capture compound. Figure 2-2 suggests that the click reaction yield with these initial parameters is less than 50% when using the equivalent concentration of cAMP-alkyne capture compound and comparing it to the labeling intensity of the classical full capture compound (Figure 2-2, lane 1 vs. lane 4). Decreasing the clickable capture compound's concentration decreases the intensity of the biotin signal, suggesting the biotin-azide counterpart is in excess and does not cross-link to the protein directly (Figure 2-2, lanes 5 to 7). Additionally, it can be observed that no unspecific reaction occurs in the absence of the alkyne

capture compound (Figure 2-2, lane 2), confirming the bio-orthogonal characteristic of the CuAAC, nor is there an unspecific signal in the absence of the biotin label (Figure 2-2, lane 3).

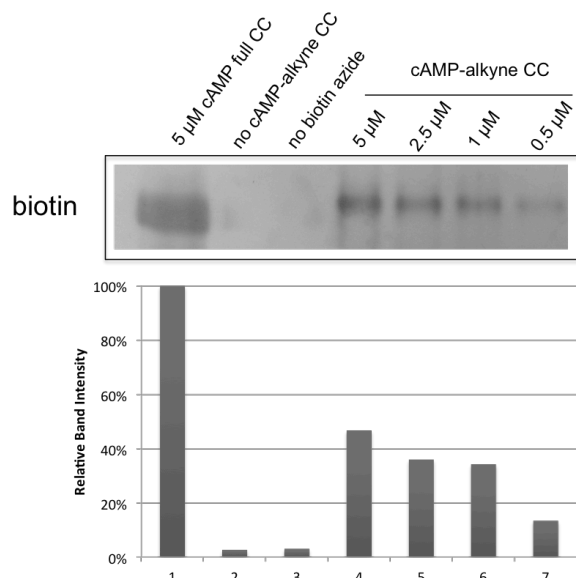


Figure 2-2: Labeling of recombinant PKARI using CuAAC in a serial dilution of cAMP-alkyne capture compound.

16 pmol of PKARI was incubated with: lane 1 – 5  $\mu$ M full cAMP capture compound (CC); lane 2 – no capture compound; lane 3 and lane 4 – 5  $\mu$ M cAMP-alkyne CC; lane 5 – 2.5  $\mu$ M cAMP-alkyne CC; lane 6 – 1  $\mu$ M cAMP-alkyne CC; lane 7 – 0.5  $\mu$ M cAMP-alkyne CC. CuAAC reaction was carried out in lanes 2 to 7 using 50  $\mu$ M CuSO<sub>4</sub>, 250  $\mu$ M TBTA, 2.5 mM sodium ascorbate and 10  $\mu$ M biotin-azide (in lane 3 equivalent volume of water was added instead). Bar plot displays relative intensity of bands measured by densitometry using full capture compound (lane 1) as reference.

This initial experiment seems to suggest that either the new cAMP-alkyne CC binds with less affinity than the original full CC or that the click reaction induces protein degradation or loss. To control the latter, subsequent experiments were probed for PKARI using a specific antibody.

In a new experiment, PKARI samples containing the different concentrations of cAMP-alkyne capture compound were duplicated and pre-incubated with 1 mM free cAMP to act as competitor (Figure 2-3). Subsequent treatment was performed similarly across samples as described previously. In Figure 2-3 intensity bars were plotted as a normalization of the biotin intensity against the total PKARI signal in each lane. The first observation is that protein amount is variable across the clicked samples (Figure 2-3, PKARI panel, lanes 3 – 12). Moreover, consistent competition was not observed in this experiment, except perhaps in samples containing the least amount of cAMP-alkyne compound (Figure 2-3, lanes 11 and 12), but the difference of the amount of PKARI between both samples does not allow a correct evaluation of different biotin signals which allows for the assessment of competition.

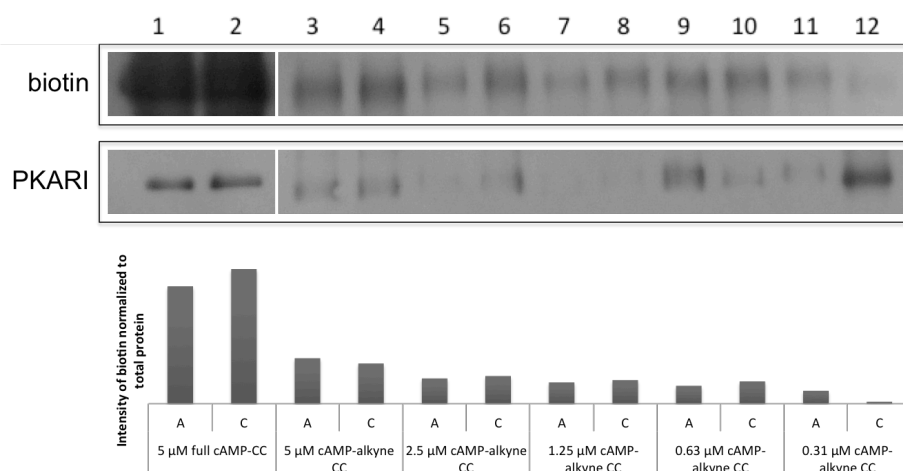


Figure 2-3: Labeling of recombinant PKARI using CuAAC in a serial dilution of cAMP-alkyne capture compound with corresponding competition samples.

16 pmol of PKARI was incubated with (C) or without (A) 1 mM cAMP competitor. Samples in lane 1 and lane 2 were labeled with 5  $\mu$ M full cAMP capture compound (CC); samples in lanes 3 to 12 were incubated with serial dilutions of cAMP-alkyne CC as indicated. CuAAC reaction was carried out in lanes 3 to 12 using 250  $\mu$ M CuSO<sub>4</sub>, 250  $\mu$ M TBTA, 2.5 mM sodium ascorbate and 10  $\mu$ M biotin-azide. Bar plot displays intensity of biotin normalized to intensity of PKARI in corresponding sample.

The experiments illustrated in Figure 2-2 and Figure 2-3, on page 32, demonstrated that the labeling signal obtained with a full classical capture compound is more intense than the one obtained with the new CuAAC method using the cAMP/PKARI system and the original Speers *et al.* CuAAC conditions<sup>23</sup>. Further optimizations on the individual components of the click reaction are necessary and the results from those experiments are described ahead.

### 2.2.1.2. Effect of copper sulfate concentration on click yields in a PKARI solution

To determine the effect of copper sulfate concentration on the biotinylation of PKARI using a cAMP alkyne compound a new experiment was designed with the knowledge obtained from the initial experiments.

16 pmol of PKARI was incubated with 5  $\mu$ M cAMP-alkyne capture compound (CC 2). A sample containing 5  $\mu$ M of cAMP full classical compound (CC 1) was used as labeling reference. After 30 min equilibration, samples were irradiated for 10 min at 310 nm in a CaproBox<sup>®</sup>. Next, to the cAMP-alkyne containing samples the following was added: 10  $\mu$ M biotin-azide (CC 3), 250  $\mu$ M TBTA (CC 16), 2.5 mM sodium ascorbate and different  $\text{CuSO}_4$  concentrations (0, 50  $\mu$ M, 250  $\mu$ M, 500  $\mu$ M and 750  $\mu$ M). The click reaction was performed for 30 min with shaking. To an additional sample containing the cAMP-alkyne capture compound, all click reagents except for the biotin-azide were added. The results were visualized by SDS-PAGE followed by Blotting using a streptavidin-HRP solution for chemiluminescence readout on x-ray film. Band intensity was measured using ImageJ software.

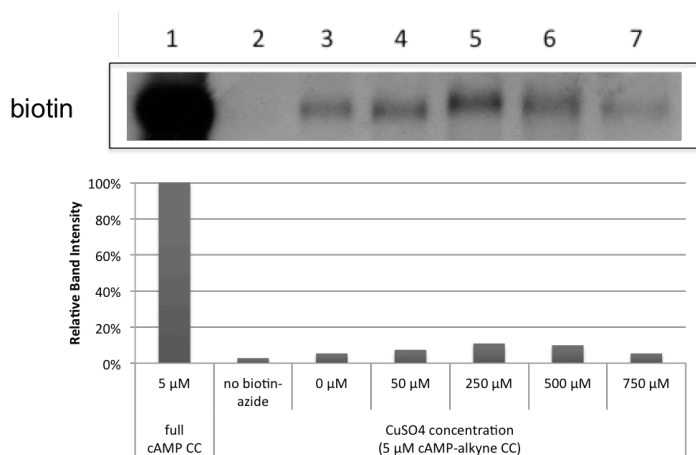


Figure 2-4: Effect of copper sulfate concentration on the click labeling of recombinant PKARI using a cAMP-alkyne capture compound.

16 pmol of PKARI was incubated with 5  $\mu$ M full cAMP capture compound (CC) (lane 1) or 5  $\mu$ M of cAMP-alkyne CC (lanes 2 – 7). CuAAC reaction was carried out in lanes 2 to 7 using 250  $\mu$ M TBTA, 2.5 mM sodium ascorbate, 10  $\mu$ M biotin-azide (in lane 2 equivalent volume of water was added instead) and increasing concentrations of  $\text{CuSO}_4$  (lanes 3 – 7). Bar plot displays relative intensity of bands measured by densitometry using full capture compound (lane 1) as reference.

As depicted in Figure 2-4, in the conditions tested, the increasing concentration of copper sulfate in the click reaction only yields the highest signal at 250  $\mu$ M of  $\text{CuSO}_4$ . Even at this maximum, the signal intensity only accounts for  $\approx$  10% of the labeling obtained with the classical full capture compound (Figure 2-4, lane 5).

To determine if the low yield reaction was due to the presence of the copper ligand TBTA or its ratio to copper sulfate, new samples were prepared and analyzed as previously described.

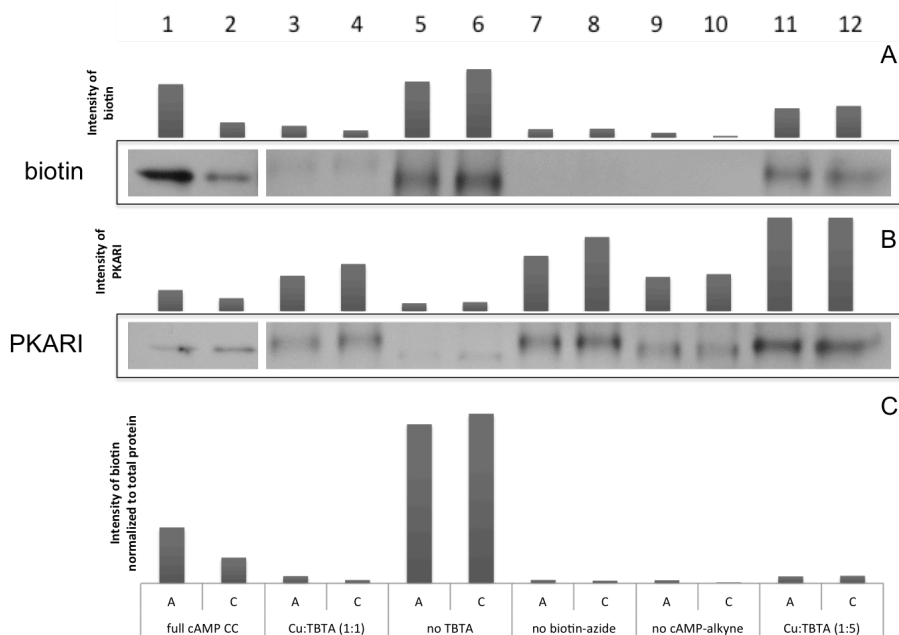


Figure 2-5: Effect of copper ligand TBTA on the click labeling of recombinant PKARI using a cAMP-alkyne capture compound. 16 pmol of PKARI was incubated with (C) or without (A) 1 mM cAMP competitor. Samples were incubated with 5  $\mu$ M full cAMP capture compound (CC) (lanes 1 and 2), 5  $\mu$ M of cAMP-alkyne CC (lanes 3 to 8 and lanes 11 and 12), or none (lanes 9 and 10). CuAAC reaction was carried out in lanes 3 to 12 using 2.5 mM sodium ascorbate, 10  $\mu$ M biotin-azide (except lanes 7-8), 250  $\mu$ M TBTA (except lanes 5 and 6) and either 250  $\mu$ M  $\text{CuSO}_4$  (lanes 3 to 10) or 50  $\mu$ M  $\text{CuSO}_4$  (lanes 11 and 12). Bar plot displays intensity of biotin (panel A), PKARI (panel B) and normalized biotin intensity to PKARI in corresponding sample (panel C).

In the biotin blot illustrated in Figure 2-5, we can observe that labeling is reduced in the competition sample of the classical cAMP capture compound (Figure 2-5, panel A, lane 2) when compared to the corresponding assay (Figure 2-5, panel A, lane 1) as is expected in a CCMS experiment. The samples containing copper sulfate and TBTA at 1:1 ratio present a similar competition pattern, although the overall intensities of the biotin signal are lower (Figure 2-5, panel A, lanes 3 and 4). With higher labeling intensities, although no visible competition, we have the samples reacted with  $\text{CuSO}_4$ :TBTA at 1:5 (Figure 2-5, panel A, lanes 11 and 12) and even higher, comparable to the full classical capture compound, the samples without TBTA (Figure 2-5, panel A, lanes 5 and 6).

The signal for total PKARI is variable across the samples (Figure 2-5, panel B), as seen previously in Figure 2-3, on page 32. Due to this variability, the signal obtained in the biotin blot was normalized to the intensity of PKARI detected in the corresponding sample. The results of this normalization are plotted in Figure 2-5, panel C. The outcome of the normalization shows that the clicked samples without TBTA present the highest biotinylation yields but no competition is observed (Figure 2-5, panel C, lanes 5 and 6). This could be a skewed result from the much lower abundance of the signal from the total protein in these samples (Figure 2-5, panel B, lanes 5 and 6). These observations suggest that free copper sulfate, in the absence of a ligand, promotes the cycloaddition reaction but at a cost of degrading protein. The presence of TBTA minimizes the protein degradation but also diminishes the yield of the CuAAC reaction.

Overall, these results seem to indicate that TBTA is not an adequate copper ligand for our click approach workflow. New ligands should be investigated if they produce a more efficient reaction yield in the CuAAC.

### 2.2.1.3. Testing time of CuAAC reaction on click yields and protein stability in a PKARI solution

The yields of the click reaction in a semi-complex system such as the cAMP-alkyne capture compound and biotin-azide in a recombinant PKARI solution could be time-dependent, but a protein in solution will tend to degrade throughout this process. It is therefore important to determine a time-point for the click reaction where the labeling yields are satisfactory and the target protein is mostly intact in the reaction vial.

Previous results described in the previous paragraph 2.2.1.2 and illustrated in Figure 2-5, have suggested that the copper ligand so far utilized was not adequate for the new click workflow to be implemented. Hong *et al.* produced a water-soluble copper ligand, THPTA (CC 17), and showed that it has higher kinetics in the CuAAC reaction when compared to the traditionally utilized TBTA (CC 16)<sup>49</sup>. We set out to determine the optimal time for the click reaction of a cAMP-alkyne capture compound to a biotin-azide in a recombinant PKARI solution using the new ligand THPTA.

Recombinant PKARI was incubated with cAMP-alkyne capture compound (CC 2) at 5  $\mu$ M, cAMP full classical compound (CC 1) at 5  $\mu$ M or none for unspecific labeling control. After 30 min equilibration, samples were irradiated for 10 min at 310 nm in a CaproBox<sup>®</sup>. Next, to the cAMP-alkyne containing samples the following was added: 10  $\mu$ M biotin-azide (CC 3), 250  $\mu$ M CuSO<sub>4</sub>, 250  $\mu$ M THPTA (CC 17) and 2.5 mM sodium ascorbate. To an additional sample containing cAMP-alkyne capture compound at 5  $\mu$ M, all click reagents except for the biotin-azide were added. The click reaction was performed up until 180 min shaking and aliquots were collected at determined time points. The results were visualized by SDS-PAGE followed by Blotting using a streptavidin-HRP solution for chemiluminescence readout on x-ray film. Band intensity was measured using ImageJ software.

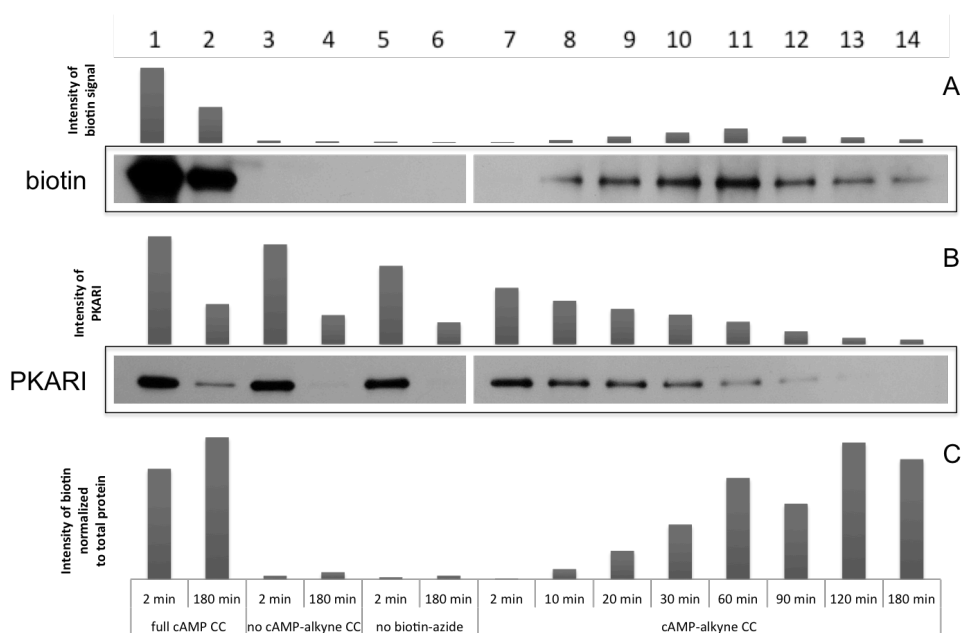


Figure 2-6: Labeling of recombinant PKARI using a cAMP-alkyne capture compound at different CuAAC reaction times. PKARI was incubated with 5  $\mu$ M full cAMP capture compound (CC) (lanes 1 and 2), 5  $\mu$ M of cAMP-alkyne CC (lanes 5 – 14) or none (lanes 3 and 4). Aliquots were recovered at described time points of the CuAAC reaction containing 250  $\mu$ M CuSO<sub>4</sub>, 250  $\mu$ M THPTA, 10  $\mu$ M biotin-azide (in lanes 5 and 6 equivalent volume of water was added instead) and 2.5 mM sodium ascorbate. Samples with the classical full cAMP CC were treated similarly and also collected at different time points. Bar plot displays intensity of biotin (panel A), PKARI (panel B) and normalized biotin intensity to PKARI in corresponding sample (panel C).

Figure 2-6, on page 35, shows that detection of PKARI decreases as the time of CuAAC reaction increases (Figure 2-6, panel B), most likely due to protein degradation. We can also observe in these results that the degradation is independent of the presence of either the cAMP-alkyne CC or the biotin-azide counterpart (Figure 2-6, panel B, lanes 3 – 6). In panel A of Figure 2-6, we can see that the biotin labeling obtained via the CuAAC reaction reaches a maximum at 60 min (Figure 2-6, panel A, lane 11), although this signal is still a fraction of the one obtained by using the classical full capture compound (Figure 2-6, panel A, lanes 1 and 2). When the biotin signal is normalized to the amount of PKARI detected in the sample (Figure 2-6, panel C) we can observe an approximation of the signal intensity between the classical full capture compound and the clickable compound at, *e.g.*, 60 min of reaction which was previously mentioned as the maximum biotin signal in the CuAAC reaction samples measured (Figure 2-6, panel C, lane 11). Higher normalized intensities can be observed at 120 min of reaction (Figure 2-6, panel C, lane 13), but these results are overestimated due to the decreasing intensity of the total PKARI detection when compared to the initial time point (Figure 2-6, panel B, lanes 7 and 13), probably due to protein degradation, precipitation or denaturation.

The chosen CuAAC reaction time for future experiments was between 30 and 60 min.

#### **2.2.1.4. Optimization of biotin-azide concentration in CuAAC reaction for detection of PKARI**

In order to achieve maximum reaction yield, we researched the influence of the concentration of biotin-azide in the CuAAC reaction using a recombinant PKARI solution and the cAMP-alkyne capture compound as the primary probe.

PKARI samples for competition assays were pre-incubated with 1 mM free cAMP (CC 13) and to normal assay samples the equivalent volume of water was added. Competition and normal assay samples were then incubated with with 5  $\mu$ M cAMP-alkyne capture compound (CC 2). Assay and competition samples containing 5  $\mu$ M of cAMP full classical compound (CC 1) were used as labeling reference. After 30 min equilibration, samples were irradiated for 10 min at 310 nm in a CaproBox<sup>®</sup>. Next, to the cAMP-alkyne containing samples the following was added: 250  $\mu$ M copper sulfate, 250  $\mu$ M THPTA (CC 17), 2.5 mM sodium ascorbate and different biotin-azide concentrations (0, 5  $\mu$ M, 10  $\mu$ M, 20  $\mu$ M and 30  $\mu$ M). The click reaction was performed for 30 min shaking. To an additional control sample containing the cAMP-alkyne capture compound, all click reagents except for the biotin-azide were added. The results were visualized by SDS-PAGE followed by Blotting using a streptavidin-HRP solution for chemiluminescence readout on x-ray film. Band intensity was quantified using the ImageJ software.

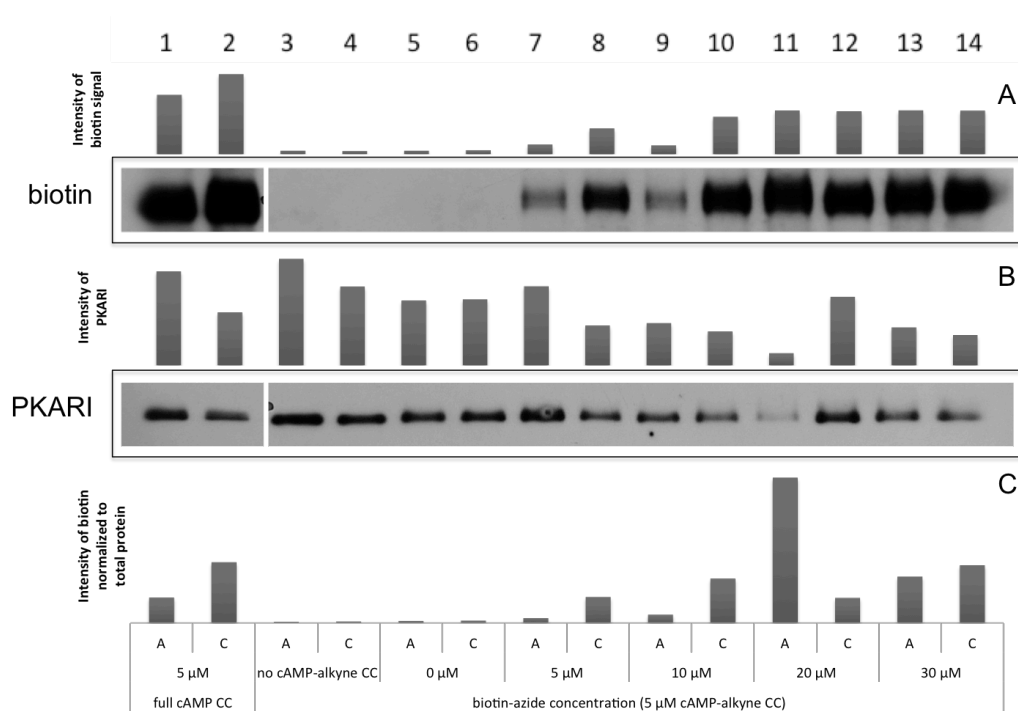


Figure 2-7: Labeling of recombinant PKARI using CuAAC with different biotin-azide concentrations.

16 pmol of PKARI was incubated with (C) or without (A) 1 mM cAMP competitor. Samples in lane 1 and lane 2 were labeled with 5 μM full cAMP capture compound (CC); samples in lanes 5 to 14 were incubated with 5 μM cAMP-alkyne CC and samples in lanes 3 and 4 were used as control. CuAAC reaction was carried out in lanes 3 to 14 using 250 μM CuSO<sub>4</sub>, 250 μM THPTA, 2.5 mM sodium ascorbate and varying concentrations of biotin-azide as indicated. Bar plot displays intensity of biotin (panel A), PKARI (panel B) and normalized biotin intensity to PKARI in corresponding sample (panel C).

Figure 2-7 shows the bio-orthogonal characteristic of the CuAAC reaction demonstrated by the absence of a biotinylation signal in samples lacking either the cAMP-alkyne capture compound or the biotin azide (Figure 2-7, panel A, lanes 3 to 6). The same blot also shows the biotin signal increasing with more biotin-azide in solution and saturating at 20 μM of azide, which is still a fraction of the signal obtained with the classical full capture compound but higher than in any previously presented result. Figure 2-7 also shows that increased amounts of biotin-azide in solution has an effect on the detection of PKARI but the intensity of these samples is always higher than 50% of the signal detected in the sample without biotin-azide (Figure 2-7, panel B, lanes 5 and 6), except in lane 11 where detection is considerably lower and was considered an outlier. Analyzing the plot obtained when the biotin labeling is normalized to the total PKARI (Figure 2-7, panel C) we can observe that the pre-incubation with excess free cAMP competitor did not produce the expected reduction in the biotin signal for those samples when compared to the assay pair (e.g., Figure 2-7, panels A and C, lanes 1 and 2). Also, reacting more than 10 μM of biotin-azide apparently does not improve further the biotin signal readout.

### 2.2.1.5. Capture of PKARI with a clickable cAMP capture compound using CuAAC

After the conditions for the biotin labeling of PKARI using a CuAAC reaction were optimized, as described in the previous paragraphs of this chapter, we set out to capture it using magnetic streptavidin beads.

Recombinant PKARI was initially incubated with (C) or without (A) excess free cAMP (CC 13) for 10 min and then added to the samples cAMP-alkyne capture compound (CC 2) at 5  $\mu$ M or cAMP full classical compound (CC 1) at 5  $\mu$ M. After 90 min equilibration, samples were irradiated for 10 min at 310 nm in a CaproBox<sup>®</sup>. Next, to the cAMP-alkyne containing samples the following was added: 10  $\mu$ M biotin-azide (CC 3), 50  $\mu$ M CuSO<sub>4</sub>, 250  $\mu$ M THPTA (CC 17) and 2.5 mM sodium ascorbate. To the full classical compound samples, the same volume of water was added. The click reaction was run for 30 min. An aliquot was removed and labeled as *input* for visualization on gel. To the remainder of the reaction, streptavidin magnetic beads were added and mixed for 1 hour. In the end, the beads were collected with a CaproMag<sup>®</sup>, washed and boiled in Laemmli buffer to extract the bound proteins. Several fractions of the samples were recovered for analysis: (1) the sample after cross-linking the capture compound before beads were added, (2) the beads with the captured compound and (3) the remainder supernatant after beads were recovered. All fractions were visualized by SDS-PAGE followed by Blotting using a streptavidin-HRP solution for chemiluminescence readout on x-ray film. Band intensity was measured using ImageJ software.

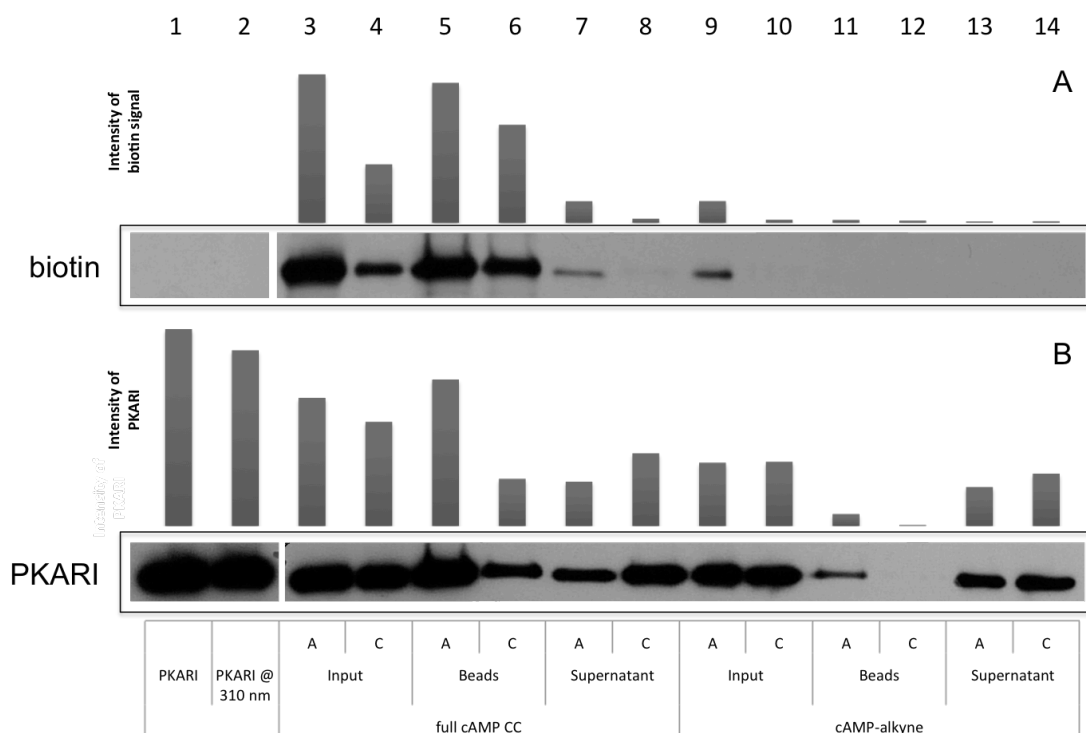


Figure 2-8: Click-capture of PKARI using a cAMP alkyne capture compound.

PKARI was pre-incubated with (C) or without (A) excess free cAMP. The samples were then incubated with 5  $\mu$ M full cAMP capture compound (CC) (lanes 3 – 8), 5  $\mu$ M of cAMP-alkyne CC (lanes 9 – 14) or none (lanes 1 and 2). Fractions analyzed: before addition of beads (input), bead capture (beads) and remaining sample after bead incubation (supernatant). The effect of UV irradiation to PKARI detection was analyzed (PKARI @ 310 nm). Bar plot displays intensity of biotin (panel A) and PKARI (panel B).

In this initial click-capture experiment we also analyzed the effect of the UV radiation used to cross-link the capture compounds to the target protein on the detection of PKARI. In fact, the UV radiation decreases the detection of PKARI by 10% (Figure 2-8, panel B, lanes 1 and 2), not by inducing degradation of the protein but by promoting dimerization of PKARI, which was observable as a band next to 130 kDa marker only in the irradiated sample.

When looking at the results obtained using the classical full capture compound (Figure 2-8, lanes 3 to 8) it is clear that pre-incubation with excess cAMP competitor prevents the biotinylated capture compound to bind to PKARI and hence reduce the detection of biotin in that sample (Figure 2-8, panel A, lane 4) when compared to the normal assay (Figure 2-8, panel A, lane 3). This competition effect is once again observed in the captured beads fraction and success is confirmed by the differential detection of total PKARI between assay and competition (Figure 2-8, panel B, lanes 5 and 6). Some PKARI remains in solution after the bead capture with a reversed intensity profile (Figure 2-8, panel B, lanes 7 and 8), mainly due to the fact that it was not carrying the biotinylated capture compound (Figure 2-8, panel A, lanes 7 and 8) and therefore did not bind to the streptavidin magnetic beads.

Results from the new click capture workflow are also shown (Figure 2-8, lanes 9 to 14). The biotin signal in the assay sample and almost undetectable in the competition sample before adding the beads (Figure 2-8, panel A, lanes 9 and 10) suggests that having a two step approach provides for a more evident competition effect. The corresponding PKARI blot for these samples (Figure 2-8, panel B, lanes 9 and 10) shows that the amount of protein present is similar between them and therefore a true competition effect on the labeling using the new click workflow was obtained. Analyzing the captured beads fraction of the click samples no biotinylation is detected (Figure 2-8, panel A, lanes 11 and 12), which would suggest that the target protein was not successfully captured, but looking at the PKARI blot for the same samples (Figure 2-8, panel B, lanes 11 and 12) we can observe that the protein was indeed successfully captured in the assay sample and is not detected in the competition. This discrepant observation would suggest that detection of biotin is not sensitive enough to determine with certainty the success of a capture experiment and should be taken into account in future experiments. It is also important to consider that non-cross-linked compounds are still able to pull-down the target and after the sample treatment no biotin signal is detected. The overall capture yield in the new click chemistry workflow is less than when using the exhaustively optimized classical capture but it appears to be “cleaner”.

Overall, the new CuAAC capture method of PKARI using a clickable cAMP capture compound presented in this experiment was successful and this workflow can be used as a starting point for capturing in more complex systems such as a cellular lysate or living cells. Before increasing the complexity of the system, a new copper ligand was introduced in the workflow to increase the yields of the CuAAC reaction.

### 2.2.1.6. Using BTTE as copper ligand and adjusting reaction pH increases PKARI click labeling yield

Soriano del Amo *et al.* demonstrated BTTE (CC 18), a new copper ligand, to have increased reaction kinetics in comparison to the previously used TBTA (CC 16) and THPTA (CC 17)<sup>50</sup>. We investigated the effect of this new ligand on the efficiency of click labeling PKARI with the cAMP-alkyne with the previously established parameters.

Up until this experiment, labeling efficiency of the click method was directly compared to the normal classical compound and the maximum labeling achieved with the cAMP-alkyne compound was around 50% of the one obtained with the original full compound. In order to discard potential affinity differences towards PKARI between the classical and the clickable cAMP compounds, the cAMP-alkyne compound was pre-clicked to the biotin-azide (CC 4) before incubation with the recombinant protein and used as an additional control.

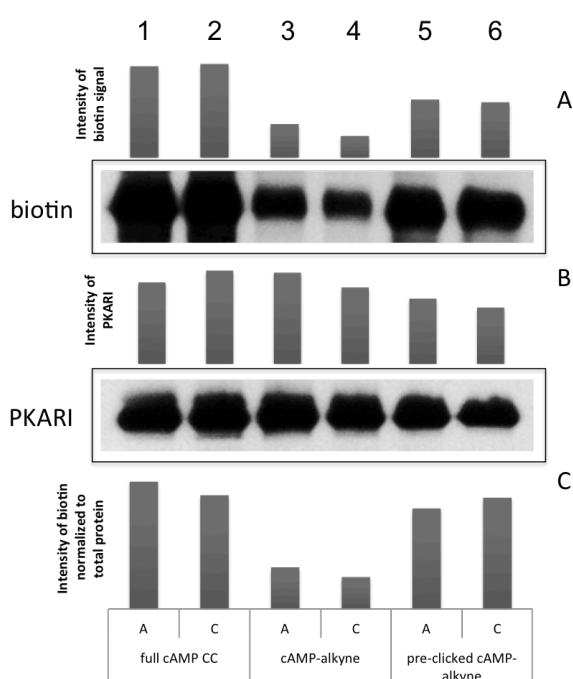


Figure 2-9: Labeling of PKARI with a cAMP-alkyne capture compound clicked to a biotin-azide using CuAAC with BTTE as copper ligand.

PKARI was pre-incubated with (C) or without (A) excess free cAMP. The samples were then incubated with 5  $\mu$ M full cAMP capture compound (CC) (lanes 1 and 2), 5  $\mu$ M of cAMP-alkyne CC (lanes 3 and 4) or 5  $\mu$ M of pre-clicked cAMP-alkyne-azide-biotin (lanes 5 and 6). Bar plot displays intensity of biotin (panel A), PKARI (panel B) and normalized biotin intensity to PKARI in corresponding sample (panel C).

As seen in Figure 2-9, the pre-clicked cAMP compound labels PKARI similarly to the full classical capture compound (Figure 2-9, panel C, lanes 1-2 and 5-6) confirming that the affinity of these molecules to the recombinant protein is guided by the selectivity function and that the rest of the compound has no impact on the labeling. However, when the CuAAC reaction is performed after the cAMP-alkyne is cross-

linked to the PKARI protein there is a substantial decrease in biotin labeling (Figure 2-9, panel C, lanes 3 and 4). These observations suggest that the compounds remain intact after the click reaction but within a protein solution the yields are drastically reduced.

### 2.2.1.7. Introducing TAMRA as a detection function using a clickable cAMP capture compound for PKARI labeling

Biotin has been used as a label within the probes used so far mainly due to the fact that the original cAMP capture compound (CC 1) carries it and it was used as reference for the optimization of PKARI labeling using the CuAAC reaction. This molecule is widely used for pull-down/capture experiments due to its high-affinity towards streptavidin. Working with a purified protein such as PKARI presents little challenges when using biotinylation as a readout system, but when moving towards labeling proteins within complex media, such as cellular lysates and whole living cells, it can be a hindrance because these proteomes contain endogenously biotinylated proteins which will interfere with the readout.

Introducing a non-natural stable molecule with fluorescence properties such as TAMRA for labeling/capturing in complex media reduces the background originated by biotin.

Recombinant PKARI was labeled as previously established using the optimal determined conditions: 5  $\mu\text{M}$  cAMP-alkyne capture compound (CC 2), 100  $\mu\text{M}$   $\text{CuSO}_4$ , 200  $\mu\text{M}$  BTTE (CC 18), 5 mM sodium ascorbate and 10  $\mu\text{M}$  TAMRA-azide (CC 5). Aliquots of samples were taken out at different time points during the course of the CuAAC reaction and analyzed by SDS-PAGE/W. Blot.

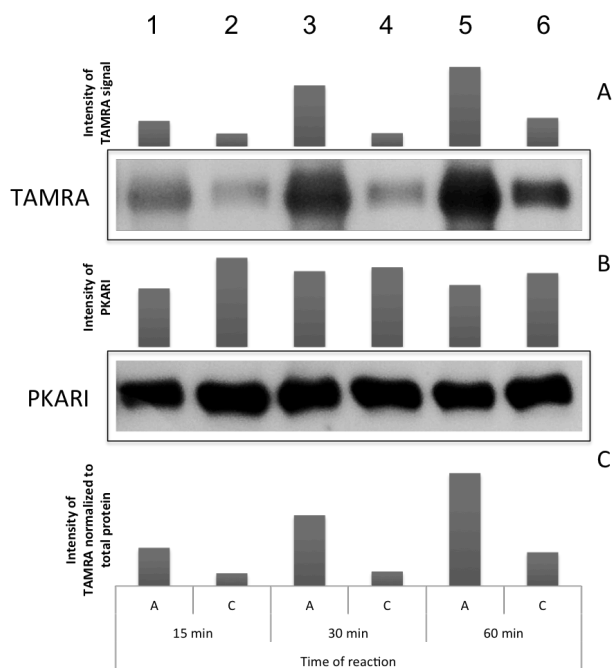


Figure 2-10: Effect of time of CuAAC reaction on the labeling of PKARI with a cAMP-alkyne capture compound and a TAMRA-azide.

PKARI was pre-incubated with (C) or without (A) excess free cAMP. The samples were then incubated with 5  $\mu\text{M}$  of cAMP-alkyne CC, 10  $\mu\text{M}$  TAMRA-azide, 200  $\mu\text{M}$   $\text{CuSO}_4$ , 400  $\mu\text{M}$  BTTE and 5 mM sodium ascorbate. Aliquots were taken at 15, 30 and 60 min of CuAAC reaction. Bar plot displays intensity of TAMRA (panel A), PKARI (panel B) and normalized TAMRA intensity to PKARI in corresponding sample (panel C).

Figure 2-10, shows that using the new TAMRA-azide is compatible to the CuAAC reaction for PKARI labeling. The TAMRA label is observable only after 15 min of reaction and the intensity continues to increase until 60 min of CuAAC reaction always with the expected competition effect, where the intensity is lower in the samples pre-incubated with excess cAMP. In fact, the results also show that the protein integrity is not affected during the CuAAC reaction using the TAMRA-azide and the described conditions, as it was previously observed when running the equivalent time course experiment with the biotin-azide counterpart (see Figure 2-6, on page 35).

This approach using the TAMRA label should be used for future experiments in complex media such as cellular lysates where the click reaction efficiency can be more easily determined without the confounding background of biotinylated proteins when using the biotin-azide for the CuAAC. After the parameters for the reaction are determined for the specific target being evaluated in a particular lysate, the biotin click will have to be used for the capture and enrichment of the targets because of the available streptavidin-magnetic beads system.

## 2.2.2. Mass Spectrometry analysis of captured proteins from HEK293 and HepG2 lysates using a classical and clickable cAMP capture compound

With all optimization steps put in place, we set out to find whether PKAR was enriched and captured from a cellular lysate using CuAAC reaction.

In an initial experiment different lysis buffers were used to solubilize cellular pellets. HEK293 cells were lysed in a buffer containing or not n-Dodecyl  $\beta$ -D-maltoside (DDM). Alternatively, ready-made HepG2 lysates were obtained from InVivo. The different lysates were incubated with the cAMP capture compounds in optimized conditions as previously described in the labeling experiments. After the CuAAC reaction proteins were either precipitated or not to remove excess non-reacted biotin-azide and re-solubilized before incubation with the streptavidin-coated magnetic beads. A detailed description of the method can be found in 2.3.4 Click capture of cAMP-binding proteins from cell lysates, on page 53.

Table 2–1 gathers the data obtained from the proteomics analysis of the experiment.

	Classical cAMP-CC		Clickable cAMP-CC (no precipitation)		Clickable cAMP-CC (with precipitation)	
	Assay	Competition	Assay	Competition	Assay	Competition
<b>Total proteins identified (LFQ&gt;0)</b>						
• HEK293 (+DDM)	901	1354	640	1448	1435	1467
• HEK293 (-DDM)	1004	1045	991	1333	1394	1389
• HepG2	892	1256	1417	345	1459	1545
<b>Assay/Competition fold-change &gt; 2 (% of total proteins in Assay)</b>						
	24		15		2	
• HEK293 (+DDM)	170 (18.9%)		98 (15.3%)		124 (8.6%)	
• HEK293 (-DDM)	209 (20.8%)		189 (19.1%)		163 (11.7%)	
• HepG2	118 (13.2%)		1226 (86.5%)		178 (12.2%)	
<b>Assay/Competition fold-change &gt; 2 across the different workflows</b>						
• HEK293 (+DDM)			5			
• HEK293 (-DDM)			1			
• HepG2			3			

Table 2–1: Summary of identifications from cAMP capture experiments in HEK293 and HepG2 lysates.

List of proteins was obtained using MaxQuant v1.2.2.4. Numbers for positive protein identifications in each sample are given and intensity-based calculated fold-changes between assays and corresponding competitions as well as across all samples within each lysate are also presented.

Table 2–1, on page 42, shows that using different lysis buffers to solubilize the proteome of the same cell line will produce different results not only in specifically competed proteins, ranging from 98 up to 209 depending on the capture method, but also in the total of identified proteins which was of only 640 in the click-capture without precipitation method and as high as 1467 different proteins in the competition sample of the click-capture followed by precipitation method. In the commercial HepG2 lysate there was a low value of 345 identified proteins in one of the samples which by default greatly increases the calculated number of specifically competed proteins, but that could have been an experimental error. When the calculated competed proteins in each lysate subset are compared between them according to the capture method, 24 proteins are identified as commonly competed for the classical capture compound across the different lysates, 15 for the clickable cAMP capture compound and only 2 when an additional step of protein precipitation is added to the clickable capture compound. These proteins are not common across all samples and methods but there are two proteins that are competed in all lysates identified both with the classical capture compound and the clickable cAMP capture compound without protein precipitation – RPS8, a ribosomal protein and SRRM2, a protein involved in pre-mRNA splicing.

The different methods utilized in the experiment did not successfully produce a common specific binder across all proteomes and capture methods although some commonly competed proteins were identified across the different methods within one type of lysate. These commonly competed proteins were mostly ribosome-associated proteins, which are usually considered unspecific background (Table 2–2).

Table 2–2: Proteins identified as specifically competed with cAMP across the different capture methods in each type of cellular lysate.

Protein Gene Name	HEK293 (+DDM)	HEK293 (-DDM)	HepG2
H1F3	✓		
RPS19	✓		
RPL27A	✓		✓
RPS18	✓		
HABP1	✓		
SERPINB6		✓	
HRNPG			✓
RPL21			✓

Comparing the competed proteins between each lysate within the same capture method ranges between 37 and 54 for the classical cAMP capture compound, 20 and 82 for the clickable cAMP capture compound without the protein precipitation step and when this protein precipitation step is introduced it ranges between 18 and 25. These values are represented in Table 2–3 highlighted in bold. It is interesting to notice that the number of commonly identified as competed proteins using the clickable cAMP capture compound with a precipitation step is greatly reduced in comparison to the other two methods but the overall number of identified proteins is similar. Also highlighted in Table 2–3 in italic are the number of commonly identified proteins as competed by cAMP from the same lysate but using different capture methods.

		Classical cAMP-CC			Clickable cAMP-CC (no precipitation)			Clickable cAMP-CC (with precipitation)		
		HEK293 (+DDM)	HEK293 (-DDM)	HepG2	HEK293 (+DDM)	HEK293 (-DDM)	HepG2	HEK293 (+DDM)	HEK293 (-DDM)	HepG2
Classical cAMP-CC	HEK293 (+DDM)									
	HEK293 (-DDM)	<b>54</b>								
	HepG2	<b>49</b>	<b>37</b>							
Clickable cAMP-CC (no precipitation)	HEK293 (+DDM)	<b>42</b>	<b>25</b>	<b>31</b>						
	HEK293 (-DDM)	<b>37</b>	<b>20</b>	<b>19</b>	<b>20</b>					
	HepG2	<b>118</b>	<b>140</b>	<b>68</b>	<b>55</b>	<b>82</b>				
Clickable cAMP-CC (precipitation)	HEK293 (+DDM)	<b>18</b>	<b>18</b>	<b>7</b>	<b>8</b>	<b>14</b>	<b>70</b>			
	HEK293 (-DDM)	<b>14</b>	<b>15</b>	<b>7</b>	<b>6</b>	<b>10</b>	<b>103</b>	<b>25</b>		
	HepG2	<b>25</b>	<b>22</b>	<b>5</b>	<b>8</b>	<b>15</b>	<b>102</b>	<b>18</b>	<b>24</b>	

Table 2–3: Number of proteins identified as competed by cAMP in common between the different samples.

Highlighted values in bold represent the competed proteins between different lysates using the same capture method; highlighted values in italic represent the number of proteins from one particular lysate competed across the different capture methods.

Focusing on the results obtained for PKA, Table 2–4 compiles the calculated fold-change of assay and competition intensities and the number of MS spectra obtained for each identified subunit of PKA (three regulatory subunits – PRKAR1A, PRKAR2A and PRKAR2B – and one catalytic subunit – PKACA).

Protein <i>Gene name</i>	Classical full cAMP-CC			Clickable cAMP-CC (no precipitation)			Clickable cAMP-CC (with precipitation)		
	Intensity fold- change (log <sub>2</sub> )	MS Counts		Intensity fold- change (log <sub>2</sub> )	MS Counts		Intensity fold- change (log <sub>2</sub> )	MS Counts	
(Assay)		(Comp.)	(Assay)		(Comp.)	(Assay)		(Comp.)	
<b>PRKAR1A</b>									
• HEK293 (+DDM)	14.4	10	0	0.0	0	0	0.0	1	0
• HEK293 (-DDM)	7.8	9	0	0.1	0	0	-0.1	0	1
• HepG2	13.9	10	0	-8.9	0	0	2.8	2	1
<b>PRKAR2A</b>									
• HEK293 (+DDM)	6.9	12	0	4.1	0	0	0.9	2	1
• HEK293 (-DDM)	6.7	10	0	-0.9	0	0	0.9	2	0
• HepG2	8.7	16	0	7.7	0	0	-0.3	4	2
<b>PRKAR2B</b>									
• HEK293 (+DDM)	8.2	1	0	0.0	0	0	0.0	0	0
• HEK293 (-DDM)	8.4	2	0	0.0	0	0	0.0	0	0
• HepG2	8.2	3	0	0.0	0	0	0.0	0	0
<b>PKACA</b>									
• HEK293 (+DDM)	0.0	0	0	0.0	0	0	7.8	0	0
• HEK293 (-DDM)	0.0	0	0	-7.9	0	0	0.0	0	0
• HepG2	0.0	0	0	9.1	2	0	0.0	0	0

Table 2–4: Calculated intensity fold-changes (assay vs. competition) and MS counts for identified PKA subunits in each sample.

As seen on Table 2–4, the classical full cAMP capture compound specifically captures the regulatory subunits of PKA across all types of cell lysate, ranging from 6.7 to 14.4 log<sub>2</sub> fold-change between the assay and the corresponding competition. Additionally, no MS spectra were obtained in the competition samples using the classical full capture compound, confirming the successful blockage of the capture compound by free cAMP competitor.

Results on the click approach are more variable. Table 2–4, on page 45, shows that there is a big reduction on the number of identified MS spectra in assays using the clickable capture compound when compared to the classical full capture compound, meaning that there is little enrichment of these subunits of PKA. Although with only few MS spectra, and sometimes none, PKA regulatory subunit 2A (PRKAR2A) is successfully identified as competed using the new developed CuAAC approach in both HEK293 and HepG2 cells with or without protein precipitation. Additionally, PRKAR1A is also specifically identified with positive MS spectra in HepG2 lysate when using a protein precipitation step after the CuAAC reaction with the clickable cAMP capture compound.

From an overall observation of the results presented in Table 2–4, either HEK293 cells lysed with a DDM-containing buffer or HepG2 lysate obtained externally can be used for further experiments to improve the method of capturing cAMP-binding proteins in cellular lysates using the CuAAC reaction. No exact data on efficiency or reproducibility of this new method could be extracted from this experiment due to its design lacking technical replicates; therefore, a new capture experiment of cAMP-binding proteins using CuAAC reaction was performed.

HEK293 cells lysed in a buffer containing DDM were incubated with either classical full cAMP capture compound or with clickable cAMP-alkyne capture compound. To corresponding competition samples free cAMP was added prior to the capture compounds. Additionally, control samples containing no capture compound were processed in parallel. After photo-crosslinking and CuAAC reaction all samples were submitted to methanol precipitation and reconstituted before incubation with streptavidin-coated magnetic beads. All samples were processed in technical triplicates to estimate reproducibility and calculate significance of identifications.

Table 2–5 below presents the summary of identifications and calculated specific and significant proteins in a capture experiment using cAMP capture compounds in HEK293 lysate.

	Classical cAMP-CC		Clickable cAMP-CC	
	Assay	Competition	Assay	Competition
<b>Total proteins identified</b>	1462	1429	1591	1637
<b>Student's t-test &lt; 0.05 (% of total proteins in Assay)</b>		27 (1.8%)		50 (3.1%)
<b>Assay/Competition fold-change &gt; 2 (% of total proteins in Assay)</b>		382 (26.1%)		177 (11.1%)
<b>Competed and significant proteins (% of total)</b>		21 (1.4%)		17 (1.1%)

Table 2–5: Summary of identifications from cAMP capture experiments in HEK293 lysates. List of proteins was obtained using MaxQuant v1.2.2.4. Numbers for positive protein identifications in each sample are given and intensity-based calculated fold-changes between assays and corresponding competitions.

Having replicate samples allows for the calculation of the significance of the calculated intensity fold-change between assays and competitions. This statistical analysis method narrows down 382 potential competed hits to only 21 with 95% confidence in the capture experiments using the classical full cAMP capture compound. In the CuAAC reaction method using the cAMP-alkyne compound the potential hits with significant values are 17 in total (Table 2–5).

In a non-biased approach the list of significantly competed proteins for both sets of capture compounds would be presented, but the purpose of this experiment design is to focus on the cAMP-binding protein PKA. The results focused on PKA subunits are presented in Table 2–6.

Protein <i>Gene name</i>	Intensity fold-change ( $\log_2$ )	Student's t-test ( <i>p</i> value)	Sum of Spectral Counts	
			(Assay)	(Comp.)
<b>PRKAR1A</b>				
• full cAMP-CC	13.1	0.048	5	0
• clickable cAMP-CC	-0.1	0.932	2	1
<b>PRKAR2A</b>				
• full cAMP-CC	2.4	0.027	5	0
• clickable cAMP-CC	-0.1	0.927	2	4
<b>PRKAR2B</b>				
• full cAMP-CC	-	-	2	0
• clickable cAMP-CC	-	-	0	0
<b>PRKACA</b>				
• full cAMP-CC	-	-	0	0
• clickable cAMP-CC	-11.1	0.192	2	4

Table 2–6: Calculated intensity fold-changes (assay vs. competition) and corresponding significance value for identified PKA subunits from capture experiments using full and clickable cAMP capture compounds. Sum of spectral counts of triplicate assays and competitions is also shown.

The classical full cAMP capture compound was able to specifically capture two different regulatory subunits of PKA – PRKAR1A and PRKAR2A – from the HEK293 lysate. Intensity fold-changes of 13.1 and 2.4 with 5 identified MS spectra for both regulatory subunits were, respectively, obtained (Table 2–6).

The method used with the clickable cAMP capture compound was able to produce more MS spectra for PRKAR1A in the assays compared to the controls, but the corresponding intensities when fold-changes were calculated give result to a negative value (-0.1) although non-significant (*p* value = 0.932). For PRKAR2A, more MS spectra were identified in the competition samples of the clickable capture compound and intensity fold-change was also negative (Table 2–6). The lack of significance of these results does not allow any conclusive analysis on the performance of the method to be made.

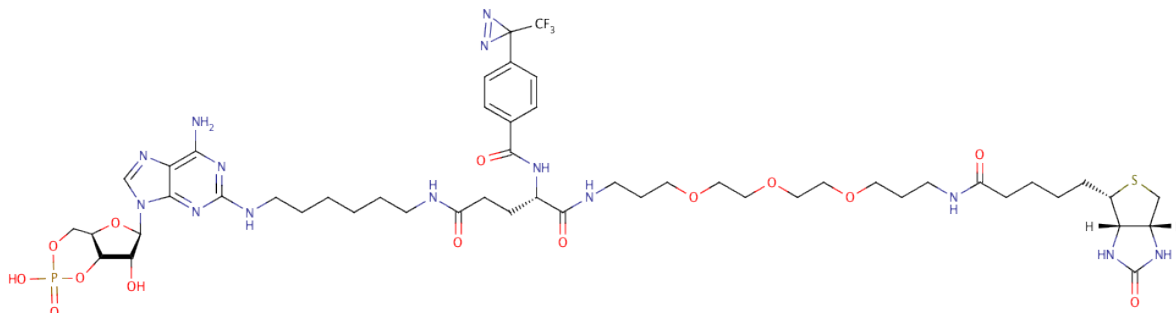
Previous experiments presented in this chapter have shown a lack of reproducibility regarding the competition effect expected when excess free cAMP competitor is added to the samples (as example, see Figure 2-7 and Figure 2-9, on pages 37 and 40, respectively). Even if this lack of competition would be further investigated and resolved, the natural high concentration of cAMP in a cellular environment is not the optimal system to further proceed with capturing targets in an intact cell environment.

A non-natural selectivity function such as the drug dasatinib was chosen for subsequent experiments.

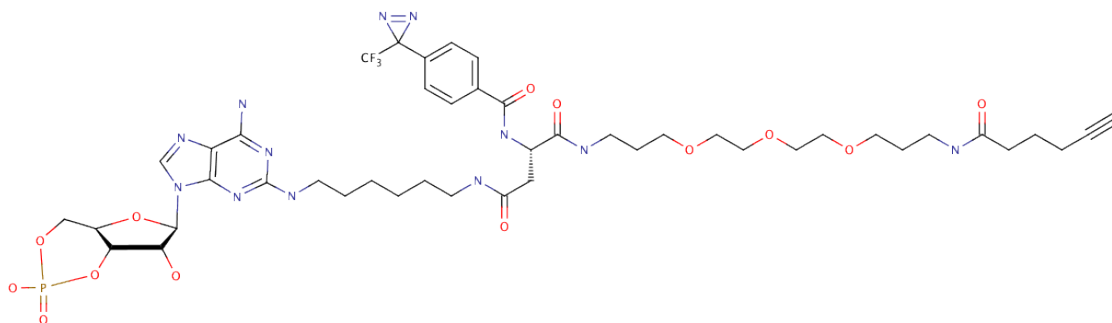
## 2.3. SPECIFIC METHODS FOR THE cAMP/PKARI SYSTEM

### 2.3.1. Structures of used compounds

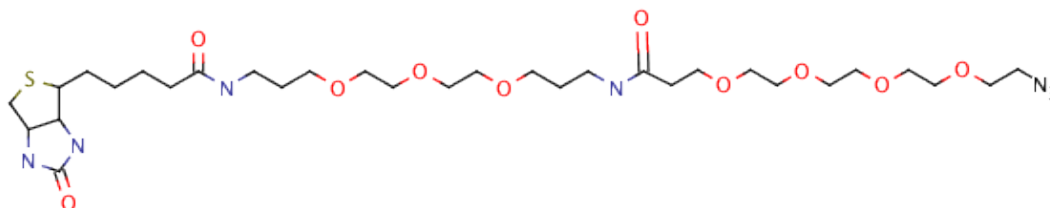
CC 1: Classical full cAMP capture compound



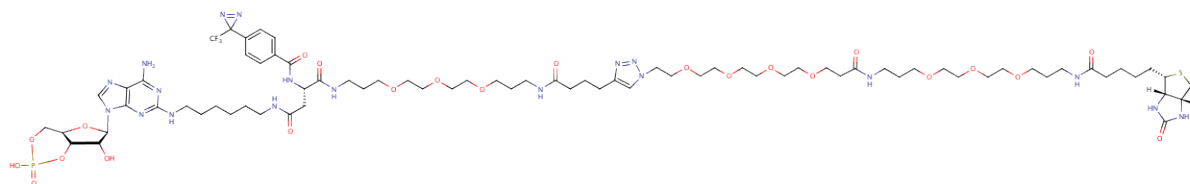
CC 2: Clickable cAMP alkyne capture compound (contains selectivity and photoreactive functions)



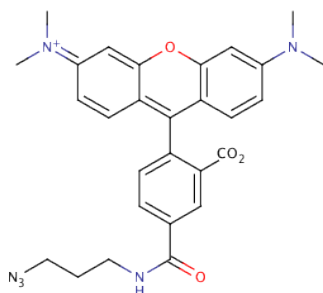
CC 3: Clickable biotin-PEG-azide (contains labeling function)



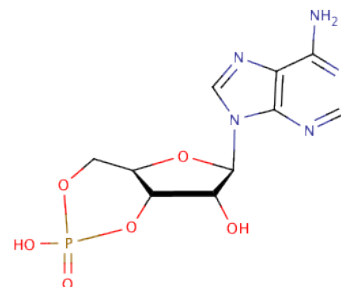
CC 4: Clicked cAMP-biotin capture compound. Reaction product of CC 2 and CC 3



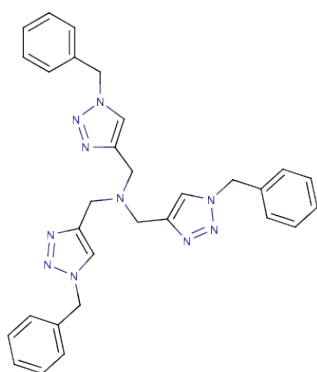
CC 5: Clickable TAMRA [tetramethylrhodamine] azide  
(contains labeling function)



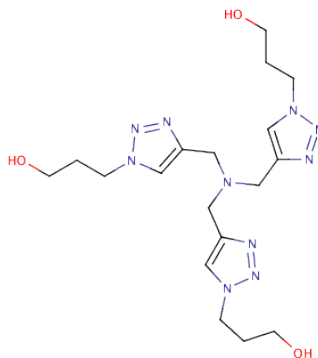
CC 13: cAMP competitor



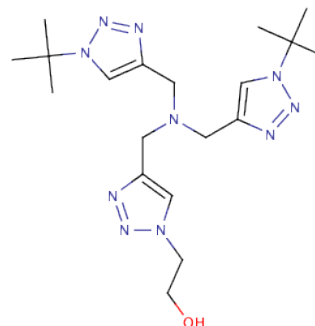
CC 16:  
Copper-chelating ligand TBTA  
Tris(benzyltriazolylmethyl)  
amine



CC 17:  
Copper-chelating ligand THPTA  
Tris(3-hydroxypropyltriazolylmethyl)  
amine



CC 18:  
Copper-chelating ligand BTTE  
bis(tert-butyltriazolyl)ethanol



### 2.3.2. Establishing and optimizing click-capture of PKARI using a cAMP CC

16 pmol of recombinant human PKARI was pipetted into 200  $\mu$ L PCR-tubes and diluted with Capture Buffer and water to a final concentration of 0.1  $\mu$ M. To the competition samples, 1, 2 or 4 mM of cAMP (CC 13) was added and incubated at least 10 min on ice. Next, cAMP-alkyne capture compound (CC 2) was added to the samples at different concentrations ranging from 0.31  $\mu$ M to 10  $\mu$ M. The samples were incubated at least 30 min rotating at 4  $^{\circ}$ C and then UV-irradiated for 10 min at 310 nm in a CaproBox™ to promote photo crosslinking. To the samples containing cAMP-alkyne, reagents for the CuAAC reaction were added and tested at different concentrations: biotin-azide (CC 3) was present between 5  $\mu$ M and 30  $\mu$ M; CuSO<sub>4</sub> between 50  $\mu$ M and 750  $\mu$ M; and three different copper ligands used individually – TBTA (CC 16) at 250  $\mu$ M, THPTA (CC 17) at 150  $\mu$ M or 250  $\mu$ M, or BTTE (CC 18) used at 150  $\mu$ M or 200  $\mu$ M. To initiate the click reaction, sodium ascorbate was always added lastly at a final concentration of 2.5 mM. The CuAAC time of reaction was performed at different times. A new TAMRA-labeled azide (CC 5) was also clicked to the cAMP-alkyne capture compound in one set of samples at a final concentration of 5  $\mu$ M. All parameters tested for each experiment and corresponding obtained results are specified in Table 2–7 on the following 2 pages.

In some experiments, parallel to the click samples, the full classical cAMP capture compound (CC 1) was added at a final concentration of 5  $\mu$ M to be used as a reference control. To these controls, all click reagents except for the azide were added.

The results were visualized by SDS-PAGE followed by Blotting with chemiluminescence readout on x-ray film using either a streptavidin-HRP solution (for biotin-labeled samples) or IgG anti-TAMRA followed by anti-IgG-HRP secondary antibody (for TAMRA-labeled samples).

Band intensity was measured using ImageJ software for fold-change calculations.

### 2.3.3. Preparation of HEK293 lysates

HEK293 cell pellets were lysed in 2X their volume with a hypotonic buffer (10 mM HEPES pH7.9, 1.5 mM MgCl<sub>2</sub>, 10 mM KCl) containing (+) or not (-) 0.5%(w/v) DDM. Both buffers were supplemented with proteinase inhibitors and benzonase at the time of lysis. After 30 min incubation on ice, the lysate was dounced 20X using a tight pestle and then run through a 21G needle with a syringe. Remaining debris was pelleted by refrigerated centrifugation at 15.000 rpm for 30 min. The supernatant was recovered and the leftover pellet was discarded. The lysates were aliquoted and snap-frozen in liquid nitrogen. Samples were stored at -80  $^{\circ}$ C until use.

Protein concentration of lysates was determined by the BCA assay as described in the General Methods section (6.2.1 Protein concentration determination, on page 118).

## PARAMETER OPTIMIZATION FOR LABELING AND CAPTURING OF PKARI USING CLICK CHEMISTRY

	cAMP-alkyne CC	cAMP competitor	CuAAC reaction	biotin-azide	TAMRA-azide	CuSO <sub>4</sub>	Copper ligand			sodium ascorbate
							TBTA	THPTA	BTTE	
<b>Experiment 1</b>	5 $\mu$ M	-								
	2.5 $\mu$ M	-								
Results 2.2.1.1 (Figure 2-2)	1 $\mu$ M	-	30 min	10 $\mu$ M	-	50 $\mu$ M	250 $\mu$ M	-	-	2.5 mM
	0.5 $\mu$ M	-								
	0 $\mu$ M	-								
<b>Experiment 2</b>	5 $\mu$ M									
	2.5 $\mu$ M									
Results 2.2.1.1 (Figure 2-3)	1.25 $\mu$ M	1 mM	30 min	10 $\mu$ M	-	250 $\mu$ M	250 $\mu$ M	-	-	2.5 mM
	0.63 $\mu$ M									
	0.31 $\mu$ M									
<b>Experiment 3</b>						0 $\mu$ M				
						50 $\mu$ M				
Results 2.2.1.2 (Figure 2-4)	5 $\mu$ M	-	30 min	10 $\mu$ M	-	250 $\mu$ M	250 $\mu$ M	-	-	2.5 mM
						500 $\mu$ M				
						750 $\mu$ M				
<b>Experiment 4</b>										
						250 $\mu$ M	0 $\mu$ M			
Results 2.2.1.2 (Figure 2-5)	5 $\mu$ M	2 mM	30 min	10 $\mu$ M	-	50 $\mu$ M	250 $\mu$ M	-	-	2.5 mM
							250 $\mu$ M			
<b>Experiment 5</b>			2 min							
			10 min							
			20 min							
Results 2.2.1.3 (Figure 2-6)	5 $\mu$ M	-	30 min	10 $\mu$ M	-	250 $\mu$ M	-	250 $\mu$ M	-	2.5 mM
			60 min							
			90 min							
			120 min							
			180 min							

## PARAMETER OPTIMIZATION FOR LABELING AND CAPTURING OF PKARI USING CLICK CHEMISTRY

	cAMP-alkyne CC	cAMP competitor	CuAAC reaction	biotin-azide	TAMRA-azide	CuSO <sub>4</sub>	Copper ligand			sodium ascorbate
							TBTA	THPTA	BTTE	
<b>Experiment 6</b>				0 μM 5 μM						
Results 2.2.1.4 (Figure 2-7)	5 μM	2 mM	30 min	10 μM 20 μM 30 μM	-	250 μM	-	250 μM	-	2.5 mM
<b>Experiment 7</b>										
Results 2.2.1.5 (Figure 2-8)	5 μM	2 mM	20 min	10 μM	-	50 μM	-	150 μM	-	2.5 mM
<b>Experiment 8</b>										
Results 2.2.1.6 (Figure 2-9)	5 μM	2 mM	10 min	10 μM	-	50 μM	-	-	150 μM	2.5 mM
<b>Experiment 9</b>										
Results 2.2.1.7 (Figure 2-10)	5 μM	2 mM	15 min 30 min 60 min	-	5 μM	100 μM	-	-	200 μM	2.5 mM
<b>Experiment 10</b>										
Results 2.2.2	10 μM	4 mM	30 min	20 μM	-	100 μM	-	-	200 μM	2.5 mM

Table 2-7: Summary of parameters utilized in PKARI labeling and capturing with a cAMP capture compound via a CuAAC reaction

### 2.3.4. Click capture of cAMP-binding proteins from cell lysates

HEK293 and HepG2 cellular lysates were pre-cleared of endogenously biotinylated proteins by incubating with streptavidin-coated magnetic beads prior to the capture experiment. The lysates were incubated with the beads for 45 min rotating at 4 °C and then these were removed using the caproMag™.

The cleared lysate was distributed in 200 µL PCR-tube strips and diluted with water and 5X Capture Buffer. To the competition samples, 4 mM of cAMP (CC 13) was added and the corresponding volume of water was added to the assay samples. The vials were incubated for 10 min on ice and then 10 µM of either cAMP-alkyne (CC 2) or classical full cAMP (CC 1) capture compounds were added to the designated tubes. The samples were incubated for 1h rotating at 4 °C and then irradiated for 10 min at 310 nm in a caproBox™ to promote photo-crosslinking of the compounds to the binding targets. To the vials containing the cAMP-alkyne capture compound the CuAAC reaction was performed by adding 20 µM biotin-azide (CC 3), 100 µM CuSO<sub>4</sub>, 200 µM BTTE (CC 18) and 2.5 mM sodium ascorbate. To the vials containing the classical full cAMP capture compound, the same volume of water was added. The click reaction ran for 30 min shaking at room temperature.

The clicked samples were divided in two and one set was mixed with methanol pre-cooled at -20 °C to precipitate proteins and leave non-clicked biotin-azide in solution. These samples were stored over-night at -80 °C to allow for precipitation. The other fraction of clicked samples and the samples containing the classical full capture compound were snap-frozen in liquid nitrogen and kept at -80 °C for the duration of the precipitation procedure. The precipitated samples were pelleted for 20 min spinning at 15.000 rpm. The supernatant was discarded and the tubes let to dry at room temperature. The precipitate was washed three times by resuspending it in fresh cold methanol and vigorously vortexing to homogenize the pellet. After the last wash, the pellets were resuspended in 4% SDS and sonicated until a clear solution was obtained. The samples were diluted with PBS to a final concentration of 0.4% SDS and incubated with streptavidin-coated magnetic beads for capturing of biotinylated proteins. The non-precipitated samples were thawed and also incubated with the beads for capturing.

The magnetic beads were incubated with the lysates for at least 1h rotating at 4 °C and then recovered using a caproMag™. The beads were then washed six times with wash buffer followed by three times wash with 80% acetonitrile and a final wash with MS-grade water.

0.5 µg of trypsin in ammonium bicarbonate was added to the beads and incubated over-night shaking at 37 °C. The supernatant containing the tryptic digest was recovered to clean tubes; next, the beads were washed with MS-grade water and the wash solution pooled with the original supernatant. All samples were lyophilized and analyzed by LC-MS/MS following the protocol described in the General Methods section (6.3 Mass Spectrometry, on page 121).

## 3. Identifying Dasatinib targets in cells

---

### 3.1. INTRODUCTION

Having implemented the basic steps for a novel click-capture system in a cell lysate with the cAMP capture compound, the next step would be to proceed to a living cell capture. cAMP is a non-permeable highly abundant molecule in cells, in the micromolar range, which makes it non-ideal to establish a new workflow for a living cell capturing system. Ideally, the capture compound to be used for target identification in cell culture should be a non-naturally occurring molecule. With this in mind, a collaboration was established with Prof. Yao from the University of Singapore who published a paper on the cellular targets of dasatinib using a clickable capture compound<sup>92</sup>.

Dasatinib (CC 14) is a protein tyrosine kinase inhibitor initially developed by Bristol-Meyers Squibb (commercialized as Sprycel) to treat imatinib-resistant chronic myeloid leukemia<sup>93</sup>.

Chronic myeloid leukemia (CML) accounts for 15% of all new cases of leukemia in the Western hemisphere with a prevalence of 1/100.000 per year, which untreated has a median survival of 5 to 7 years<sup>94</sup>. In CML the hematopoietic stem cells possess an abnormal chromosome, the Philadelphia chromosome, which originates from the reciprocal translocation of a region of chromosome 9 that contains the Ablason oncogene (*ABL*) and the break cluster region (*BCR*) gene from chromosome 22. This translocation produces a new fusion gene that ends up being translated into the BCR-ABL protein. The ABL family of protein tyrosine kinases, which is comprised of ABL1 and ABL2 (also known as ARG), link diverse extracellular stimuli to signaling pathways that control cell growth, survival, invasion, adhesion and migration. There is a strong relationship between deregulation of this family of protein kinases and cancer, from leukemia to solid tumors<sup>95</sup>. Whilst in most leukemia the deregulation originates from chromosome translocations that produce fusion proteins, in solid tumors the activation of the ABL kinases is driven by their over-expression, chemokine receptors, oxidative stress and/or inactivation of negative regulatory proteins<sup>95</sup>.

ABL1 and ABL2 function redundantly in some cellular contexts, but also have unique roles, owing to distinct and conserved sequences and structural domains (Figure 3-1, on page 55). *ABL1* encodes a non-receptor tyrosine kinase that phosphorylates substrate proteins with crucial cellular activities such as increased proliferation, loss of stromal adhesion, and resistance to apoptosis<sup>94</sup>. *Ab11*-knockout mice exhibit diverse abnormalities leading to premature senescence and neonatal morbidity. By contrast, *Ab12*-knockout mice are viable though they exhibit neuronal defects<sup>96</sup>.

Unlike PKA with its single activating molecule cAMP (as discussed in the previous chapter), the ABL kinase is activated by many different extrinsic ligands, such as epidermal growth factor receptor (EGFR), platelet-derived growth factor receptor (PDGFR), vascular endothelial growth factor receptor (VEGFR), and others<sup>95</sup>. The ABL kinase is also activated by intrinsic signals such as DNA damage and oxidative stress<sup>97</sup>.

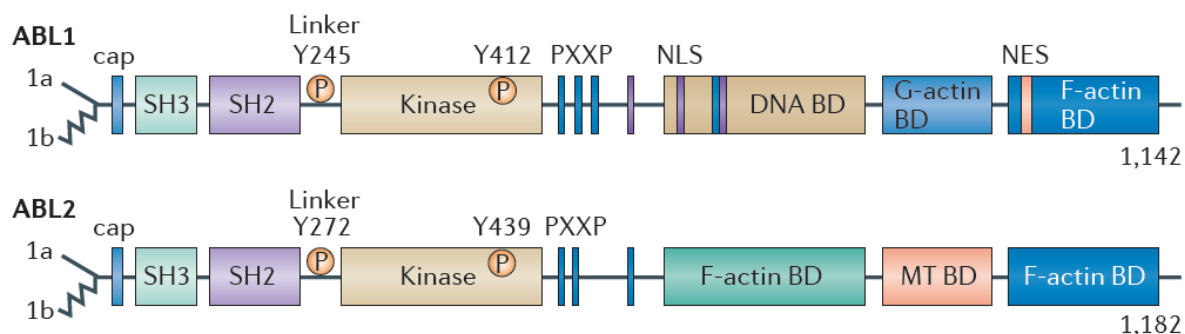


Figure 3-1: Schematic representation of the modular domains of the ABL kinases.

Alternative splicing of ABL1 and ABL2 produces several isoforms, including the 1a isoforms (as shown by the straight line) and the 1b isoforms (jagged line); the 1b isoforms are targeted for amino-terminal myristoylation. The ABL N termini are comprised of the SRC homology 3 (SH3), SH2 and SH1 (tyrosine kinase) domains. The ABL carboxyl termini contain a conserved filamentous (F)-actin-binding domain (BD). ABL1 has a globular (G)-actin-binding domain and a DNA-binding domain, whereas ABL2 has a second internal F-actin-binding domain and a microtubule (MT)-binding domain. ABL1 has three nuclear localization signal (NLS) motifs and one nuclear export signal (NES) in its C terminus. Both ABL1 and ABL2 have conserved PXXP motifs to mediate protein–protein interactions. Phosphorylation (P) of ABL1 at Y412 within the activation loop (Y439 in ABL2) and Y245 in the SH2–kinase domain linker (Y272 in ABL2) stabilizes the active conformation. Reproduced from Greuber et al.<sup>95</sup>

The catalytic activities of the ABL kinases are tightly regulated by inter and intramolecular interactions, and post-translational modifications (Figure 3-2). The intramolecular inhibition is obtained by the formation of a clamp structure involving a SRC homology (SH) 3 domain\*, a SH2 domain and a SH1 domain. ABL activity can be negatively or positively regulated by intermolecular interactions with distinct binding partners. In general, the intermolecular interactions that disrupt the autoinhibitory interactions and stabilize the active (open) conformation of the ABL kinases promote increased enzymatic activity. For example, the catalytic efficiency of ABL can be enhanced by interactions with adaptor proteins such as Ras and Rab interactor 1 (RIN1), which interacts both with the SH3 and SH2 domains<sup>95</sup>.

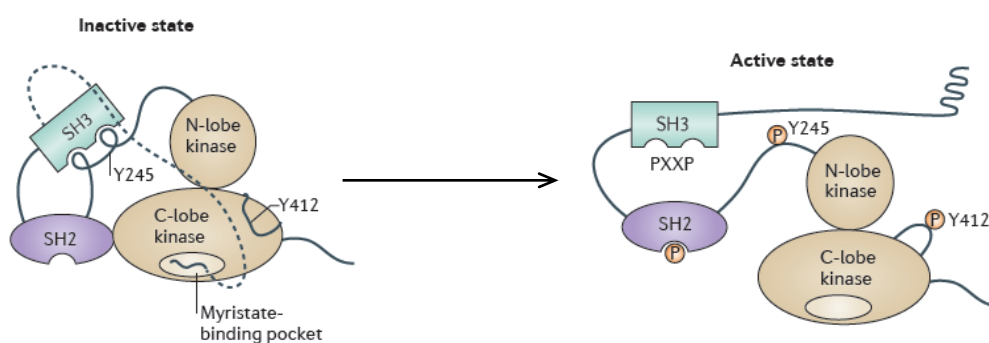


Figure 3-2: Representation of auto-inhibited (closed) and active (open) ABL kinases.

Intramolecular interactions play a role in the regulation of ABL kinase activity. The SH3 domain binds to the linker sequence connecting the SH2 and the kinase domains, and the SH2 domain interacts with C-terminal lobe of the kinase (SH1) domain forming an SH3–SH2 clamp structure. The myristoylated residue in the N terminus of the 1b ABL isoforms binds to a hydrophobic pocket within the C-lobe of the kinase domain, stabilizing the auto-inhibited conformation. The configuration and interactions of the ABL C-terminal sequences are not included in the model. Dashed line represents ABL N-terminal sequences upstream of the SH3 domain that fold over to promote binding of the myristoyl group to a pocket in the C-lobe of the kinase domain. Adapted from Greuber et al.<sup>95</sup>

\* SRC homology (SH) domains are divided in three categories: SH1 domain refers to the tyrosine kinase domain which was first identified in the SRC kinase; SH2 domain is a protein module that binds to tyrosine phosphorylated sites in a sequence-specific context; SH3 domain is a protein module that binds to proline-rich sequences.



Dasatinib is an ATP-competitive protein tyrosine kinase inhibitor, which was originally identified as a potent inhibitor of SRC family kinases (including SRC, LCK, HCK, YES, FGR, LYN and FYN) and was subsequently found to have activity against ABL, KIT, the macrophage colony stimulating factor receptor (FMS), the platelet-derived growth factor receptor (PDGFR) and the ephrin receptor family members EPHB1, EPHB2 and EPHB4<sup>113</sup>. The receptor tyrosine kinase DDR1 and the oxidoreductase NQO2 have also been recently identified as specific binders of dasatinib<sup>19</sup>. The exact mechanism of dasatinib action in CML is still unknown and there are many theories<sup>114</sup>. Some studies have shown that dasatinib induces defects in spindle formation, cell cycle arrest, and centrosome alterations in leukemic cells, tumor cell lines, as well as in normal cells<sup>115</sup>. The mechanisms of dasatinib and its role in CML as well as how to decrease the toxicity of dasatinib require further investigation<sup>114</sup>, so an unbiased full proteome analysis of dasatinib binders might elucidate some of those mechanisms.

In 2012, Shi *et al.*<sup>92</sup> characterized the proteome of dasatinib targets by use of clickable capture compounds. The uniqueness of this approach was to address those targets directly in living cells, where the protein-ligand, as well as native protein-protein interactions would be more natural, as opposed to potential artifacts and alternative protein conformations created during cell lysate preparations that are commonly used in binding/inhibition assays. Although they identified some protein and non-protein kinases in living K562 cells\*, none of them were the ABL or SRC family of proteins; these were only identified when the capture was performed in lysate (supplementary data tables from Shi *et al.*<sup>92</sup>). Also lacking in this study is a parallel competition assay to correctly determine specific binders of dasatinib.

Based on the work from Shi *et al.*<sup>92</sup> and having a direct collaboration with that group, we set out to capture dasatinib targets in living cells using our established and optimized click capture workflow described in the previous chapter.

---

\* K562 cells: cell line containing the Philadelphia chromosome and therefore carrying the BCR-ABL fusion protein. Used as cell model of chronic myeloid leukemia (CML)

## 3.2. RESULTS

### 3.2.1. Introducing a new copper-chelating azide in the CuAAC reaction

The experiments done so far to optimize the CuAAC reaction were all performed using a commercially available biotin-azide (CC 3, on page 122) as described in the previous chapter (2.2.1 Establishing and optimizing click-capture of PKARI using a cAMP CC, on page 31).

Valentina Bevilacqua, a fellow member of the BioChemLig consortium, synthesized new copper-chelating azides to be used in bioconjugation experiments<sup>116</sup>. The most efficient azide regarding reaction kinetics at the time was chosen and a biotin (CC 7) or TAMRA (CC 8) anchors were attached to it to perform labeling and capture experiments. The structures of the compounds are illustrated on the Specific Methods section (3.3.1 Structures of used compounds), on page 77.

An initial experiment was designed to test the efficiency of this new azide in the labeling of recombinant SRC protein solution or in K562 cells lysate using a clickable dasatinib capture compound (CC 6). The previously optimized click reaction parameters with the cAMP capture compound were used as reference and the conditions used to measure the reaction kinetics in Bevilacqua's system were also used. The parameters used in the reaction kinetics experiments seemed from the start to be too harsh for a biological system; hence, a new set of parameters was designed and included in the labeling experiment.

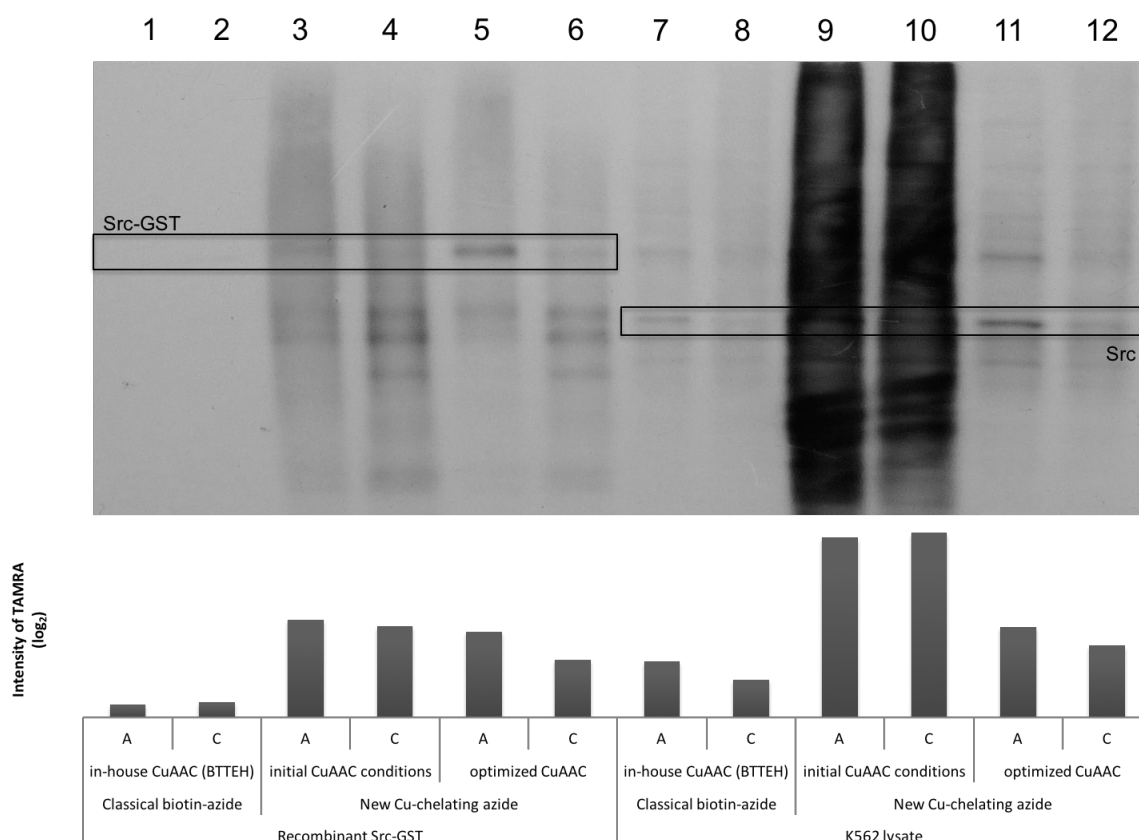


Figure 3-4: Labeling of recombinant SRC and K562 cell lysate with a clickable dasatinib-alkyne capture compound using a new copper-chelating azide with a TAMRA label.

Recombinant SRC (lanes 1 – 6) or K562 cell lysate (lanes 7 – 12) were pre-incubated with (C) or without (A) excess free dasatinib. The samples were then incubated with dasatinib-alkyne CC and clicked with classical biotin-azide and BTTEH (lanes 1, 2, 7 and 8), Bevilacqua's initial conditions with the copper-chelating azide (lanes 3, 4, 9 and 10) and a new optimized CuAAC reaction with the new copper-chelating azide (lanes 5, 6, 11 and 12). Bar plot displays intensity of TAMRA from the bands within the drawn box.

As seen on Figure 3-4, on page 58, the previously established CuAAC reaction conditions show the faintest signal when compared to the other samples (Figure 3-4, in-house CuAAC lanes in both recombinant Src-GST and K562 lysate groups). On the other hand, the in vitro conditions developed by the authors of the new molecule show an intense labeling but also unspecific, as revealed by the smeared lanes (Figure 3-4, initial CuAAC conditions on both recombinant Src-GST and K562 lysate groups). The newly established parameters for the CuAAC reaction with the new copper-chelating azide presented optimal results, with a clear Src-GST band in the assay lane and clear competition in the adjacent lane (Figure 3-4, optimized CuAAC in the Src-GST group) as well as in the full lysate labeling (Figure 3-4, optimized CuAAC in the K562 lysate group).

The newly established parameters for the CuAAC reaction with 20  $\mu\text{M}$  TAMRA copper-chelating-azide (CC 8), 100  $\mu\text{M}$   $\text{CuSO}_4$  and 2.5 mM sodium ascorbate at pH 8.5 were used for future labeling experiments. Further adjustments in concentrations of the corresponding biotin copper-chelating azide (CC 7) were fine-tuned for capture experiments.

### 3.2.2. Capturing dasatinib targets in K562 cell lysate using CuAAC

Proteins from 100 µg of K562 cell lysate were enriched using a clickable and photoreactive dasatinib capture compound (CC 6) produced in the Yao laboratory and their initial results published in Shi *et al.*<sup>92</sup>. The probes were clicked to the new biotin copper-chelating azide (CC 8) using the conditions described in the Specific Methods (3.3.3 Capturing dasatinib targets in K562 cell lysate using CuAAC, on page 79).

Capture experiments were performed following two different workflows: click and pre-clicked.

#### 3.2.2.1. Pre-clicked compound workflow

In the pre-clicked workflow, competition samples were pre-incubated with free dasatinib competitor and assay samples with equivalent volume of DMSO. The complete dasatinib capture compound containing the sorting function (CC 9) was produced *a priori* and added to all samples. The samples were then photo-crosslinked and enriched with streptavidin-coated magnetic beads.

Following the enrichment, trypsin was added to the samples and the resulting peptides were recovered and analyzed by LC-MS/MS.

Table 3–1 shows the summary of identifications on both sets obtained from triplicates of each type of sample.

	Pre-clicked		Click	
	Alignment-based	MS-based	Alignment-based	MS-based
<b>Total proteins identified</b>	1764	1355	1764	1582
<b>Student's t-test &lt; 0.05 (% of total)</b>	158 (9.0%)	136 (10.0%)	246 (13.9%)	198 (12.5%)
<b>Assay/Competition fold-change &gt; 2 (% of total)</b>	69 (3.9%)	50 (3.7%)	186 (10.5%)	155 (9.8%)
<b>Competed and significant proteins (% of total)</b>	7 (0.4%)	7 (0.5%)	48 (2.7%)	47 (3.0%)
<b>Total kinases identified (% of total proteins)</b>	93 (5.3%)	77 (5.7%)	93 (5.3%)	78 (4.9%)
<b>Student's t-test &lt;0.05 (% of total kinases)</b>	14 (15.1%)	14 (18.2%)	17 (18.3%)	12 (15.4%)
<b>Assay/Competition fold-change &gt; 2 (% of total kinases)</b>	15 (16.1%)	14 (18.2%)	15 (16.1%)	11 (14.1%)
<b>Competed and significant kinases (% of total kinases)</b>	6 (6.5%)	6 (7.8%)	5 (5.4%)	5 (6.4%)
<b>(% of total competed and significant proteins)</b>	<b>(85.7%)</b>	<b>(85.7%)</b>	<b>(10.4%)</b>	<b>(10.6%)</b>

Table 3–1: Summary of identifications from dasatinib capture experiments in K562 lysate.

List of proteins was obtained using MaxQuant v1.3.0.3. Numbers for identifications based on spectral counts (MS-based) and alignment-based are given.

As mentioned previously, dasatinib inhibits the BCR-ABL fusion protein but other proteins, mainly kinases, have been described to be targeted by this small molecule<sup>19,117,118</sup>. In fact, in the pre-clicked workflow both BCR and ABL1 are clearly identified as significantly competed proteins in the K562 lysate, alongside five other kinases (ABL2, SRC, YES1, RIPK2 and EPHB4). Table 3–2 and Figure 3-5 compile the data for this set of proteins.

Protein <i>Gene name</i>	Total MS counts			Enrichment (Assay / DMSO)		Specificity (Assay / Competition)	
	DMSO	Assay	Comp.	Intensity fold-change ( $\log_2$ )	Student's t-test ( <i>p</i> value)	Intensity fold-change ( $\log_2$ )	Student's t-test ( <i>p</i> value)
<b>ABL1<sup>k</sup></b>	2	55	4	5.4	0.021	3.8	0.022
<b>ABL2<sup>k</sup></b>	0	16	0	6.7	0.009	4.0	0.011
<b>BCR</b>	0	48	6	5.8	0.007	3.0	0.008
<b>EPHB4<sup>k</sup></b>	0	12	0	4.0	0.036	7.6	0.035
<b>RIPK2<sup>k</sup></b>	0	5	0	10.5	0.017	9.4	0.017
<b>SRC<sup>k</sup></b>	0	9	0	12.1	0.036	11.1	0.047
<b>YES1<sup>k</sup></b>	0	19	5	8.0	0.038	3.5	0.044

Table 3–2: List of competed and significant hits in dasatinib capture experiments in K562 lysate using a pre-clicked workflow. Total MS counts from technical replicates (*n* = 3) of DMSO control, assay and competition (comp.) samples. Intensity fold-change and significance levels are given for enrichment (assay versus DMSO control) and specificity (assay versus competition) of hits. <sup>k</sup> = kinase

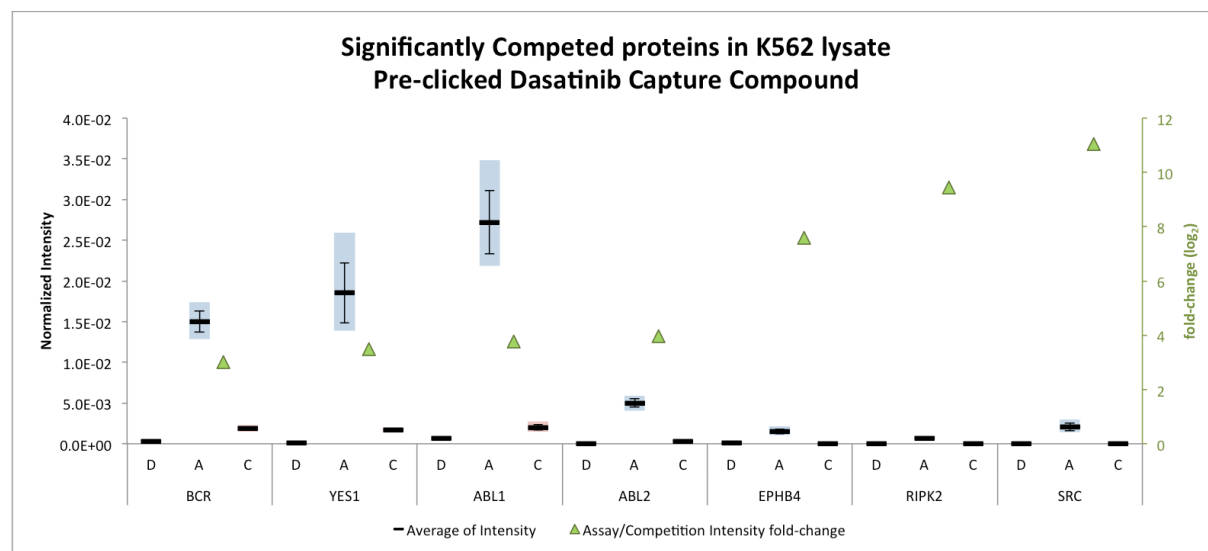


Figure 3-5: CCMS chart of significantly competed hits in Dasatinib capture experiment in K562 lysate using a pre-clicked workflow. Boxes: minimum and maximum intensity values for DMSO control (D), assay (A) and competition (C) samples. Black bar: Average of intensity (*n*=3)  $\pm$  SEM. Green triangle:  $\log_2$  fold-change between average intensities from assay and competition samples. Proteins are displayed by increasing specificity *p* value from left to right.

As seen in the CCMS chart (Figure 3-5, above), all hits were identified in low abundance in the DMSO control samples and significantly enriched in the assay samples. BCR and ABL1, have been extensively described as strong dasatinib binders<sup>19,108,109,113,114</sup> and were here identified with high intensities in the assays relatively to most of the other also significantly competed proteins. YES1 was identified with high intensity in the assay samples as well; it belongs to the tyrosine protein kinase as ABL1 and to the SRC protein kinases subfamily.

SRC is also identified as a significantly competed protein in this set. ABL2 is the other tyrosine protein kinase from the ABL family with an over-lapping role in some biological processes carried out by ABL1<sup>94,95</sup> and was also identified as a significant hit for dasatinib using this method. EPHB4 is a receptor tyrosine kinase previously reported to be inhibited by dasatinib as well<sup>113</sup>. Lastly, the serine/threonine protein kinase RIPK2 is also specifically captured in this workflow, which was also previously described as being inhibited by dasatinib<sup>117</sup>.

When the targets are surveyed for their interactions using the STRING database<sup>119</sup>, an intricate network of binding and activities can be observed between them (Figure 3-6, below).

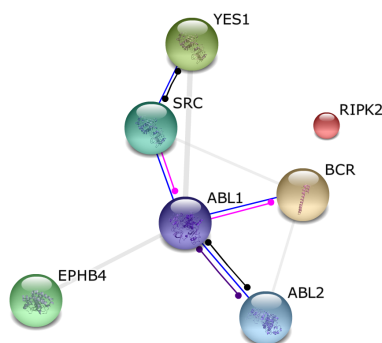


Figure 3-6: STRING protein interaction analysis of significantly competed proteins in dasatinib capture experiment in K562 lysate using the pre-clicked workflow.

Blue: binding; black: reaction; pink: post-translational modification; purple: catalysis; gray: association in curated databases.

With this experiment we have shown that *bona fide* dasatinib targets can be identified in whole cell lysates from K562 cells using a clickable photo-reactive dasatinib probe that was reacted *a priori* with a new biotin copper-chelating azide, by a bio-orthogonal chemical ligation method, to enrich and identify the interaction partners via a LC-MS/MS shotgun analysis. Interestingly, Shi *et al.*<sup>92</sup> were unable to identify these targets in their experiments with K562 lysates, allowing for a possible interpretation that the probe did not have the same affinity as free dasatinib but we can now assure that known dasatinib targets can be addressed with the dasatinib-alkyne capture compound (CC 6).

With these results, we set out to evaluate the proteins identified with the clickable dasatinib-alkyne capture compound in a K562 lysate but performing the CuAAC reaction after the capture compound is photo cross-linked to the binding partner.

### 3.2.2.2. Click workflow

In the click workflow, the dasatinib capture compound (CC 6) was added to the lysate in the assay sample as well as the competition sample that was previously incubated with excess free dasatinib (CC 14). After equilibration, the samples were irradiated with UV light to promote cross-linking of the probe to the interacting proteins. Next, the counter-probe containing the sorting function (CC 7) and the reagents for the CuAAC reaction were added and, lastly, the labeled proteins were enriched with streptavidin-coated magnetic beads.

Following the enrichment, trypsin was added to the samples and the resulting peptides were recovered and analyzed by LC-MS/MS. A detailed method description can be found in the Specific Methods section (3.3.3 Capturing dasatinib targets in K562 cell lysate using CuAAC, on page 79).

A total of 48 of potential hits were identified. Fold-changes and corresponding *p* values for intensity differences are summarized in Table 3–3, below.

Protein <i>Gene name</i>	Enrichment (Assay / DMSO)		Specificity (Assay / Competition)	
	Intensity fold-change (log <sub>2</sub> )	Student's t-test ( <i>p</i> value)	Intensity fold-change (log <sub>2</sub> )	Student's t-test ( <i>p</i> value)
<b>ADH5</b>	10.7	0.007	1.8	0.006
<b>AMMECR1;AMMECR1L</b>	8.1	0.011	2.2	0.044
<b>ANXA6</b>	7.4	0.008	6.5	0.008
<b>ATIC</b>	12.2	0.002	1.4	0.001
<b>BRIX1</b>	0.8	0.096	1.2	< 0.001
<b>CALML5</b>	1.8	0.071	1.1	0.032
<b>CBR1;CBR3</b>	7.8	0.019	2.3	0.033
<b>CLIC1</b>	6.6	0.004	1.1	0.010
<b>DBT</b>	-1.6	0.004	3.9	0.044
<b>DDX42</b>	9.5	0.013	1.1	0.040
<b>DLST</b>	-4.0	0.002	2.5	0.007
<b>ENO1</b>	4.3	0.022	1.4	0.038
<b>EPB41L2</b>	9.6	0.011	1.0	0.031
<b>ETFA</b>	8.1	0.026	1.4	0.047
<b>FTSJ3</b>	0.9	0.013	1.2	0.006
<b>GSTP1</b>	8.0	0.014	1.5	0.022
<b>HARS</b>	4.8	< 0.001	1.1	0.001
<b>HIST1H1B</b>	2.9	0.007	1.1	0.023
<b>HIST1H1C</b>	3.1	0.028	1.4	0.045
<b>LCP1</b>	6.0	< 0.001	1.9	< 0.001
<b>MAPK14<sup>k</sup></b>	10.0	0.010	1.7	0.010
<b>MDH2</b>	4.9	< 0.001	1.2	< 0.001
<b>MMTAG2</b>	-1.4	0.027	6.7	0.012
<b>MYH9</b>	6.2	0.014	1.4	0.020
<b>MYL12B;MYL12A;MYL9</b>	6.1	0.007	1.1	0.019
<b>NANS</b>	10.7	0.005	1.2	0.004
<b>OGDH</b>	-5.4	< 0.001	1.3	0.001
<b>PFAS</b>	9.5	0.040	2.6	0.036
<b>PFN1</b>	6.3	0.002	1.1	0.002
<b>PGK1<sup>k</sup></b>	4.1	0.001	1.1	0.001
<b>PMPCA</b>	10.6	0.007	1.5	0.006

Protein <i>Gene name</i>	Enrichment (Assay / DMSO)		Specificity (Assay / Competition)	
	Intensity fold-change ( $\log_2$ )	Student's t-test ( $p$ value)	Intensity fold-change ( $\log_2$ )	Student's t-test ( $p$ value)
PREP	4.1	0.001	1.2	0.011
PRPF4B <sup>k</sup>	2.1	0.006	1.3	0.022
PSAT1	6.9	0.003	3.2	0.003
TAOK3 <sup>k</sup>	7.8	0.007	1.5	0.046
TOMM5	10.6	0.010	1.4	0.021
TPI1	3.4	0.001	1.5	0.002
TPM3	2.2	0.012	1.2	0.026
TSFM	10.0	0.007	1.2	0.047
TXLNG	9.0	0.001	1.8	0.046
TXNRD1	8.4	0.009	1.1	0.014
U2SURP	9.2	0.027	1.8	0.040
UBA1	11.4	0.015	1.0	0.037
UBA6	8.8	0.006	1.1	0.006
UBE2L3	5.2	0.002	1.4	0.002
UQCRFS1	1.8	0.079	1.5	0.046
UQCRQ	4.5	0.006	1.1	0.013
VRK1 <sup>k</sup>	9.7	0.009	4.5	0.007

Table 3-3: List of competed and significant hits in Dasatinib capture experiments in K562 lysate using a click workflow. Intensity fold-change and significance levels are given for enrichment (assay versus DMSO control) and specificity (assay versus competition) of hits. <sup>k</sup> = kinase

Some kinases are identified using the click workflow in lysate: PGK1, VRK1, MAPK14, PRPF4B and TAOK3. No interactions between them are known according to the STRING database (Figure 3-7).

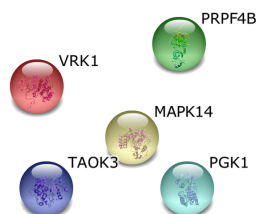


Figure 3-7: STRING protein interaction analysis of significantly competed kinases in Dasatinib capture experiment in K562 lysate using the click workflow.

According to a recent publication by Kitagawa *et al.*<sup>118</sup>, where tyrosine kinase inhibitors, including dasatinib, were profiled against a panel of 310 kinases, MAPK14 shows an IC<sub>50</sub> of 330 nM for dasatinib whereas the small molecule does not inhibit PGK1. TAOK3 was not included in this study but the authors profiled TAOK2, which was also not inhibited by dasatinib. In the study from Davis *et al.*<sup>108</sup>, some additional kinases were profiled against dasatinib and results showed that TAOK3 presented a K<sub>d</sub> of 2300 μM for dasatinib, VRK2 (not VRK1) a K<sub>d</sub> of 3200 μM and PRPF4B showed no data. The CCMS data for these significantly identified kinases in the click workflow are presented in Figure 3-8.

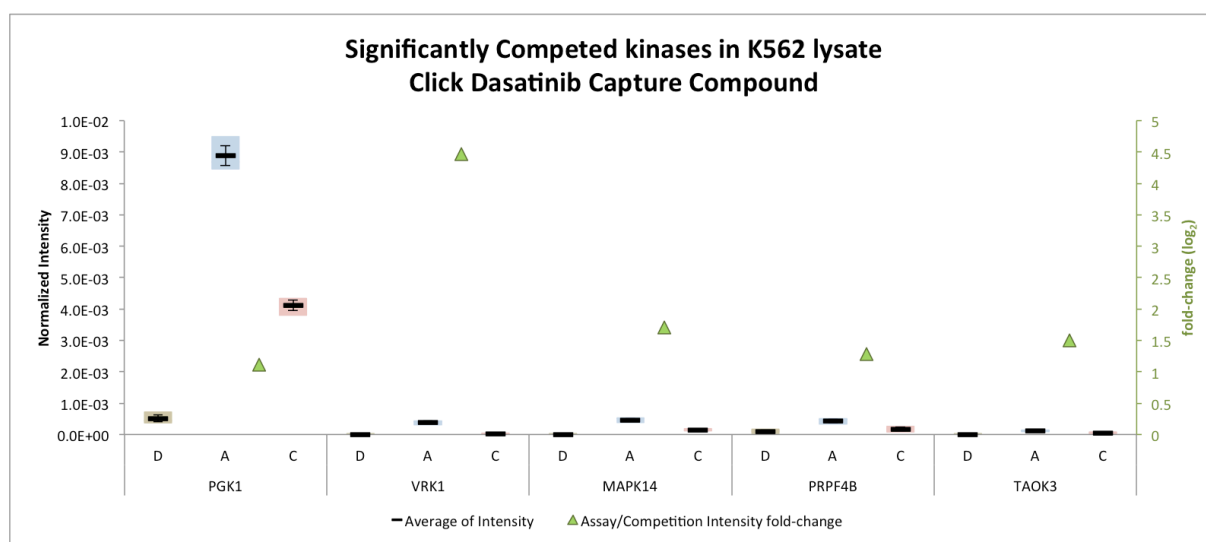


Figure 3-8: CCMS chart of significantly competed kinases in Dasatinib capture in K562 lysate using CuAAC.

Boxes: minimum and maximum intensity values for DMSO control (D), assay (A) and competition (C) samples. Black bar: Average of intensity ( $n=3$ )  $\pm$  SEM. Green triangle: log<sub>2</sub> fold-change between average intensities from assay and competition samples. Proteins are displayed by increasing specificity  $p$  value from left to right.

BCR, ABL and SRC were not identified as significantly competed in the click workflow. Table 3–4 presents the values for the expected targets of dasatinib as previously observed in the pre-clicked workflow.

Protein Gene name	Total MS counts			Enrichment (Assay / DMSO)		Specificity (Assay / Competition)	
	DMSO	Assay	Comp.	Intensity fold-change (log <sub>2</sub> )	Student's t-test (p value)	Intensity fold-change (log <sub>2</sub> )	Student's t-test (p value)
ABL1 <sup>k</sup>	2	10	3	2.1	0.003	0.4	0.018
ABL2 <sup>k</sup>	0	0	0	2.2	0.009	0.2	0.531
BCR	0	6	7	3.3	0.016	0.3	0.262
SRC <sup>k</sup>	0	0	0	7.3	0.068	6.4	0.069

Table 3-4: Values for expected targets of Dasatinib in K562 lysate using a click workflow.

Total MS counts from technical replicates ( $n = 3$ ) of DMSO control, assay and competition (comp.) samples. Intensity fold-change and significance levels are given for enrichment (assay versus DMSO control) and specificity (assay versus competition) of hits. <sup>k</sup> = kinase

All proteins presented in Table 3–4, on page 65, are enriched when compared to the DMSO controls. Even in the absence of spectral counts, MaxQuant software is able to retrieve data from other runs and search for the intensity of that event in the sample being analyzed<sup>120</sup>. This explains the positive intensity value when no MS count for a specific protein is observed in that sample.

The specificity fold-change obtained for BCR and ABL2 are purely random, as suggested by the high  $p$  values of 0.262 and 0.531, respectively. However, the low intensity fold-change between assay and competition for ABL1 is valid ( $p = 0.018$ ), suggesting that the clickable dasatinib probe addresses this target but the overall capture yields are smaller compared to the pre-clicked compound workflow. In fact, when looking at the spectral counts for this protein, the assay clearly shows more identified peptides (10) than the DMSO (0) and competition (3) controls. In an opposite situation is SRC, where no MS counts were identified but alignment data reveals high enrichment and specificity ( $\log_2$  fold-change of 7.3 and 6.4, respectively), and even though it does not meet the inclusion criteria of  $p < 0.05$ , the difference to the threshold is less than 0.02.

When the 48 specific targets obtained in the click workflow are submitted to the STRING protein interaction database, the loose network depicted in Figure 3-9 (on page 67) is obtained. In fact, by analyzing further this network searching for enrichment of Gene Ontology terms, “small molecule metabolic process” and “cellular nitrogen compound metabolic process” are obtained (Table 3–5), suggesting the hits shown on Table 3–3, on page 64, are not specific targets of dasatinib but general drug metabolizing enzymes.

Gene Ontology Term – Biological Process	Number Of Genes	$p$ -value	$p$ -value_FDR	$p$ -value_bonferroni
<b>cofactor metabolic process</b>	6	3.86E-06	2.61E-02	4.87E-02
<b>cellular amino acid metabolic process</b>	7	4.14E-06	2.61E-02	5.22E-02
<b>small molecule metabolic process</b>	13	3.45E-04	1.00E+00	1.00E+00
<b>cellular nitrogen compound metabolic process</b>	18	1.84E-03	1.00E+00	1.00E+00

Table 3–5: Gene Ontology term enrichment from significantly competed proteins in Dasatinib capture experiment in K562 lysate using a click workflow.

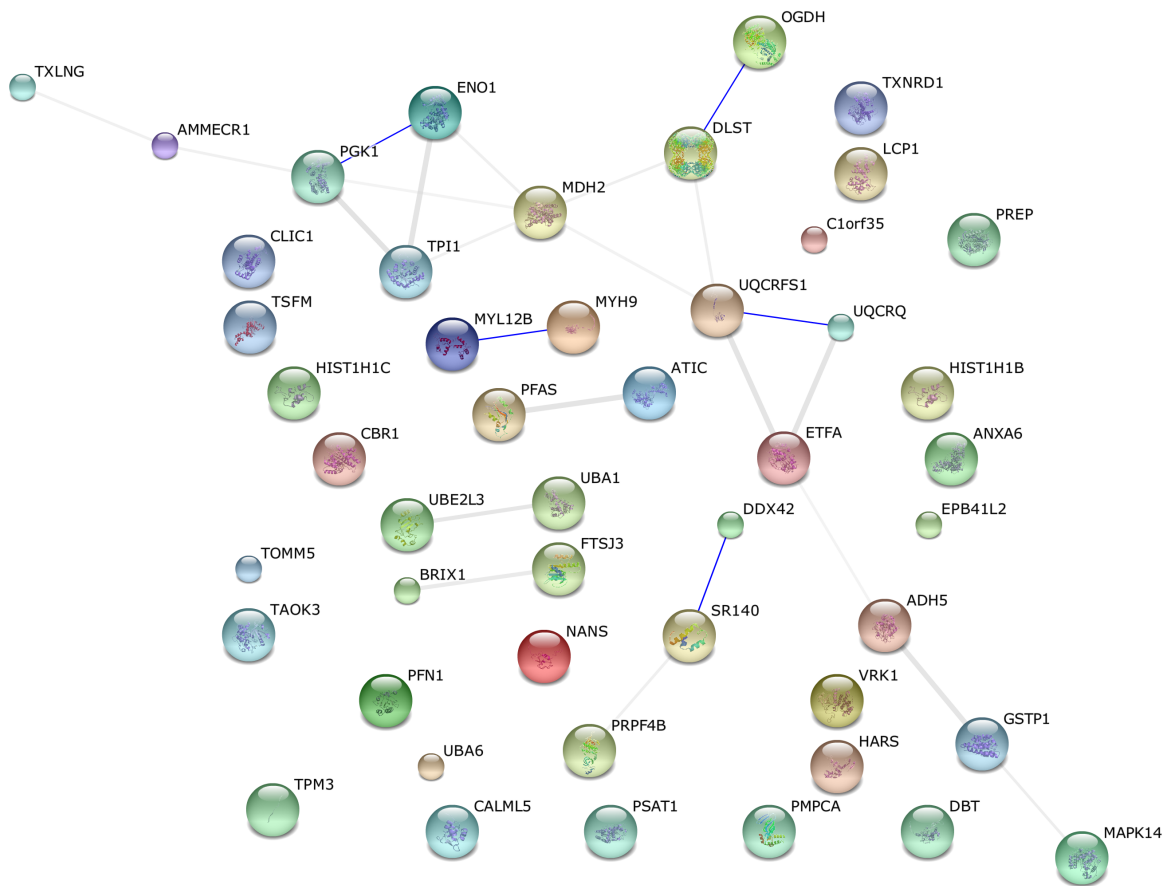


Figure 3-9: STRING protein interaction analysis of significantly competed proteins in dasatinib capture experiment in K562 lysate using the click workflow.  
 Blue: binding; gray: association in curated databases.

The results obtained using the dasatinib-alkyne capture compound in a post-irradiation click using K562 lysate do not reflect the previously obtained known targets of dasatinib. However, this probe was developed to be cell permeable and used in a living cell system. Therefore, we moved on establishing the click capture conditions in living K562 cells knowing the probe is able to identify *bona fide* dasatinib targets, as seen on the pre-click workflow.

### 3.2.3. Cell viability assay for dasatinib compounds in K562 cells

Before performing capture experiments in living cells, it is important to determine if dasatinib and the clickable dasatinib probe affect cell viability at the used concentrations in capture experiments since it could introduce a bias in the subsequent data analysis due to differences in cell numbers and consequent protein amounts.

To determine the cell viability of K562 cells after incubation with dasatinib and dasatinib clickable probe, the CellTiter-Glo<sup>®</sup> Luminescent Cell Viability Assay from Promega<sup>™</sup> was used. Generally, this method determines the number of viable cells in culture based on quantitation of the ATP present, which signals the presence of metabolically active cells. The kit includes a thermo-stable luciferase that provides the luminescent signal that can be measured.

The experiment was performed on a 96-well plate, where a dilution series of K562 cells (in triplicate) was used to establish a calibration curve for the corresponding ATP present in each cell dilution. A regression curve was determined based on the average of the measured signal. Assay wells were prepared containing 100.000 cells and either dasatinib (CC 14 – Dasa in Figure 3-10) or clickable dasatinib-alkyne capture compound (CC 6 – CPT392 in Figure 3-10) at different concentrations and incubation times. The luminescent signals measured in the assay wells were converted to ATP concentration values and corresponding viable cell numbers by interpolation from the calibration curve. The percentage of viable cells was then calculated based on the initial input of cells. Additional wells containing only compounds without cells were also prepared to rule out any effect of the compound on the luminescent signal. Figure 3-10 illustrates the multi-well plate scheme.

	1	2	3	4	5	6	7	8	9	10	11	12
A	100.000	50.000	25.000	12.500	6.250	3.125	1.563	781	391	195	98	0
B	100.000	50.000	25.000	12.500	6.250	3.125	1.563	781	391	195	98	0
C	100.000	50.000	25.000	12.500	6.250	3.125	1.563	781	391	195	98	0
D	100 nM Dasa	500 nM Dasa	2.5 µM Dasa	12.5 µM Dasa	100 nM Dasa	500 nM Dasa	2.5 µM Dasa	12.5 µM Dasa		100 nM Dasa	100 nM CPT392	
E	100 nM Dasa	500 nM Dasa	2.5 µM Dasa	12.5 µM Dasa	100 nM Dasa	500 nM Dasa	2.5 µM Dasa	12.5 µM Dasa		500 nM Dasa	500 nM CPT392	
F	100 nM CPT392	500 nM CPT392	2.5 µM CPT392	12.5 µM CPT392	100 nM CPT392	500 nM CPT392	2.5 µM CPT392	12.5 µM CPT392		2.5 µM Dasa	2.5 µM CPT392	
G	100 nM CPT392	500 nM CPT392	2.5 µM CPT392	12.5 µM CPT392	100 nM CPT392	500 nM CPT392	2.5 µM CPT392	12.5 µM CPT392		12.5 µM Dasa	12.5 µM CPT392	
H												

1h30
30 min
no cells

# cells  
(calibration curve)

Concentration @  
1.000.000 cells/mL

Figure 3-10: Scheme of multi-well plate for cell viability assay of dasatinib (Dasa) and dasatinib clickable compound (CPT392) in K562 cells. **Wells A1 to C12:** Dilution series of K562 cells. **Wells D1 to G8:** 100.000 cells were incubated for 30 or 90 min with either dasatinib (Dasa) or dasatinib clickable compound (CPT392) at 100 nM, 500 nM, 2.5 µM and 12.5 µM. **Wells D10 to G11:** only compound was added.

Luminescence signal was obtained using an Imaging System (Syngene G:BOX XT4) and the image obtained was analyzed with ImageJ software to extract the intensities of each well. Data was further processed in Microsoft Excel to calculate the effect of the compounds on the viability of K562 cells (Figure 3-11, on page 69).

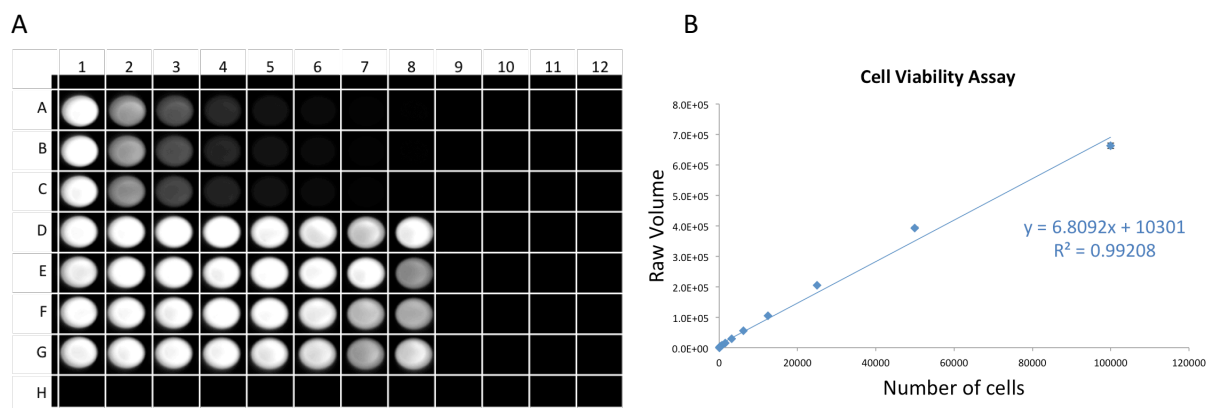


Figure 3-11: Luminescence detection of cell viability assay of dasatinib and clickable dasatinib-alkyne capture compound in K562 cells. (Panel A) Wells A1 to C12: Dilution series of K562 cells. Wells D1 to G8: 100,000 cells were incubated for 30 or 90 min with either dasatinib or clickable dasatinib capture compound at 100 nM, 500 nM, 2.5  $\mu$ M and 12.5  $\mu$ M. Wells D10 to G11: only compound was added. (Panel B) Plot of number of cells versus luminescence intensity (raw volume) from non-incubated cells. Linear regression of points is presented.

Calculated values for the viability of K562 cells after incubation with dasatinib or dasatinib-clickable compound are presented in Table 3–6.

Compound concentration	% of viable K562 cells			
	dasatinib		dasatinib-alkyne capture compound	
	30 min	90 min	30 min	90 min
12.5 $\mu$ M	75%	100%	74%	97%
2.5 $\mu$ M	90%	99%	68%	95%
500 nM	95%	98%	90%	95%
100 nM	99%	93%	95%	93%

Table 3–6: Effect of dasatinib or clickable dasatinib-alkyne capture compound on K562 cell viability.

As observed in Table 3–6, increasing concentrations of both compounds reduce cell viability to 74-75% when incubated for a short period of 30 min. At 90 min incubations, this effect is no longer visible and cell viability remains over 90%. This could indicate a cellular response mechanism to both small molecules that leads to the increase of ATP production after the initial toxic effect. Also interesting to notice is that both compounds have the same effect pattern indicating a similar mechanism of action. At lower concentrations (100 nM or 500 nM), both dasatinib and the dasatinib-alkyne capture compound do not appear to be toxic to the cells despite the incubation time.

The lack of cytotoxicity is rather surprising but this absent effect could be due to an acquired resistance to dasatinib from the particular strain of K562 cells used for the experiments or, more likely, due to the short incubation times that are insufficient to trigger cell death.

Nevertheless, the identification of dasatinib binders in living cells by click CCMS was carried out since the targets were confirmed in the lysate of the same strain of cells.

Living cell capture of dasatinib targets was then performed on K562 cells using low concentrations of compounds and short incubation times.

### 3.2.4. Capturing in living K562 cells

Current small-molecule target interaction profiling is mainly done in solution. Certain protein conformations are modified during the preparation of lysates and, consequently, putatively important protein-protein interactions are lost. Devising a new strategy to address small-molecule targets in their natural cellular environments allows for a more accurate profiling of targets and partner interactions as well as directly demonstrating target engagement. Using a small clickable compound allows to overcome the limitations of a complete probe in terms of cellular permeability and to reduce non-specific scaffold interactions. A CCMS workflow strategy for capture of dasatinib targets in living K562 cells was developed using the click conditions previously established and optimized in lysates.

Briefly, the cells are grown in multi-well plates to a fixed concentration and supplemented with medium containing dasatinib for the competition samples or DMSO for the assays. After that, the clickable dasatinib probe is added to all wells and further incubated in a controlled atmosphere. The medium is removed and the cells are washed with PBS. The plates are then irradiated with UV light to promote the crosslinking of the reactivity function in the capture compound to the bound protein. The cells are recovered, lysed and then clicked to the counter-probe containing the sorting function using the reagents for the CuAAC reaction and, lastly, the labeled proteins are enriched with Streptavidin-coated magnetic beads. Following the enrichment, trypsin is added to the samples and the resulting peptides are recovered and analyzed by LC-MS/MS.

A total of nine individual experiments each with triplicate samples were analyzed. Table 3–7 summarizes the results obtained.

	Experiment								
	A	B	C	D	E	F	G	H	I
<b>Total proteins identified</b>	1322	1322	884	1096	1430	1653	921	921	1428
<b>Student's t-test &lt;0.05</b>	99	33	3	33	73	30	21	70	197
(% of total)	(7.5%)	(2.5%)	(0.3%)	(3%)	(5.1%)	(1.8%)	(2.3%)	(7.6%)	(13.8%)
<b>Assay/Competition fold-change &gt; 2</b>	577	118	16	89	73	65	83	40	160
(% of total)	(43.6%)	(8.9%)	(1.8%)	(8.1%)	(5.1%)	(3.9%)	(9%)	(4.3%)	(11.2%)
<b>Competed and significant proteins</b>	93	5	0	14	5	4	9	2	14
(% of total)	(7%)	(0.4%)	(0%)	(1.3%)	(0.3%)	(0.2%)	(1%)	(0.2%)	(1%)
<b>Total kinases identified</b>	55	55	31	50	69	89	30	30	64
(% of total proteins)	(4.2%)	(4.2%)	(3.5%)	(4.6%)	(4.8%)	(5.4%)	(3.3%)	(3.3%)	(4.5%)
<b>Student's t-test &lt;0.05</b>	4	1	0	2	2	3	0	4	16
(% of total kinases)	(7.3%)	(1.8%)	(0%)	(4%)	(2.9%)	(3.4%)	(0%)	(13.3%)	(25%)
<b>Assay/Competition fold-change &gt; 2</b>	31	8	1	3	9	7	4	2	6
(% of total kinases)	(56.4%)	(14.5%)	(3.2%)	(6%)	(13%)	(7.9%)	(13.3%)	(6.7%)	(9.4%)
<b>Competed and significant kinases</b>	3	1	0	1	1	1	0	0	1
(% of total kinases)	(5.5%)	(1.8%)	(0%)	(2%)	(1.4%)	(1.1%)	(0%)	(0%)	(1.6%)
<b>(% of total competed and significant proteins)</b>	<b>(3.2%)</b>	<b>(20%)</b>	<b>(0%)</b>	<b>(7.1%)</b>	<b>(20%)</b>	<b>(25%)</b>	<b>(0%)</b>	<b>(0%)</b>	<b>(7.1%)</b>

Table 3–7: Summary of identifications from dasatinib capture experiments in K562 living cells in nine separate experiments. (A – I) each consisting of at least three technical replicates. List of proteins was obtained using MaxQuant v1.3.0.3.

As seen in Table 3–7, on page 70, the number of significantly competed proteins varies between 0 and 93, with a calculated median of 5. The identified proteins within these numbers are also variable between each experiment, which hinders the correct identification of potential targets for dasatinib using this workflow.

One possible way to extract significant information from this combined set of data is to develop a scoring method to rank the proteins according to the frequency they were significantly competed in each experiment. A value of 1 is attributed to each protein that was significantly competed in the experiment and the final score is the sum across all experiments. Using this analysis method, four proteins have a score higher than 1, meaning they were significantly competed in more than one experiment. Table 3–8, on page 72, summarizes the values for specificity fold-change and corresponding *p* value for these targets in each experiment. Additionally, results for ABL and BCR are also presented in Table 3–8. SRC was not identified in any experiment using this workflow.

The protein with the highest score was CSK, a non-receptor tyrosine-protein kinase. CSK was identified as specifically competed in 3 out of 9 experiments and is then the highest potential candidate to be inhibited by dasatinib in a natural cell environment. CSK phosphorylates tyrosine residues located in the C-terminal tails of Src-family kinases regulating their activity and therefore plays an important role in the regulation of cell growth, differentiation, migration and immune response<sup>121</sup>. It. According to Kitagawa *et al.*<sup>118</sup>, dasatinib has an IC<sub>50</sub> of 3.2 nM against CSK. Additionally, dasatinib binding to CSK in living cells was previously observed in Kim *et al.* using magnetic biotin particles<sup>122</sup>.

Another potential target for dasatinib was WARS, Tryptophan--tRNA ligase that regulates ERK, Akt, and eNOS activation pathways that are associated with angiogenesis, cytoskeletal reorganization and shear stress-responsive gene expression<sup>123,124</sup>. Interestingly, an association between WARS and dasatinib was previously reported in a PhD thesis by Brendan Martin Corkery, entitled “Tyrosine Kinase Inhibitors in Triple Negative Breast Cancer”<sup>125</sup>. In this work, it was observed a highly confident increase of WARS (annotated as IPF53 in the manuscript) in dasatinib-treated versus non-treated cells using a DIGE-MALDI-TOF/TOF analysis approach.

The other two potential candidates for dasatinib targets were PSMC4 (26S protease regulatory subunit 6B) and RPS17 (40S ribosomal protein S17). No literature about any interactions between these proteins and dasatinib was found.

In summary, the profile differs from what is observed in the lysate. This could be attributed to a lower efficiency of the method or that living cells are a more complex system, though more realistic, making the analysis more difficult.

Experiment <i>Gene name</i>	Specificity (Assay / Competition)																			Score
	Intensity fold-change ( $\log_2$ )									Student's t-test ( $p$ value)										
	A	B	C	D	E	F	G	H	I	A	B	C	D	E	F	G	H	I		
CSK	<b>3.87</b>	<b>9.19</b>	#N/I	0.09	<b>1.02</b>	0.63	#N/I	#N/I	<b>3.86</b>	0.210	<b>0.005</b>	#N/I	0.950	<b>0.040</b>	0.685	#N/I	#N/I	<b>0.001</b>	3	
WARS	<b>1.86</b>	<b>6.21</b>	-1.08	<b>1.18</b>	0.23	0.16	0.65	-0.18	0.64	<b>0.031</b>	0.425	0.480	<b>0.048</b>	0.633	0.645	0.196	0.599	<b>0.012</b>	2	
PSMC4	<b>2.59</b>	0.69	0.13	0.68	-0.23	-1.02	-0.01	0.31	<b>1.24</b>	<b>0.014</b>	0.287	0.786	0.241	0.261	0.572	0.973	0.073	<b>0.042</b>	2	
RPS17;RPS17L	<b>4.60</b>	0.54	#N/I	0.75	-0.61	-1.26	0.32	0.20	<b>1.06</b>	<b>&lt;0.001</b>	0.461	#N/I	0.471	0.209	0.608	0.545	0.279	<b>0.020</b>	2	
ABL1;ABL2	<b>6.42</b>	0.24	#N/I	-0.76	0.05	#N/I	-0.21	-0.09	<b>1.34</b>	<b>0.022</b>	0.797	#N/I	0.405	0.685	#N/I	0.099	0.926	0.156	1	
BCR	<b>3.18</b>	-0.13	-0.89	0.50	0.43	#N/I	#N/I	#N/I	0.68	<b>0.003</b>	0.883	0.482	0.591	0.356	#N/I	#N/I	#N/I	0.351	1	

Table 3–8: Excerpt of potential hits for dasatinib in K562 living cell capture using a click workflow from 9 individual experiments (A – I) each consisting of triplicates for assays and competitions. Values in bold mark specific ( $\log_2$  fold-change > 1) and significant ( $p$  value < 0.05) results for a given experiment. Score is calculated by the sum of number of results that fulfilled both the criteria of specificity and significance. #N/I : not identified

An alternative analysis method to bypass the variability observed between each experiment is to analyze all samples together as technical replicates, calculating a unique fold-change and associated  $p$  value between the average normalized intensity obtained from all assays and competitions.

With this method of analysis only two proteins are identified as significantly competed by dasatinib: ALDOC (Fructose-bisphosphate aldolase C) and, once again, CSK.

Table 3–9 lists the fold-change and  $p$  values for the top 20 competed proteins (approximately top 1% of all identifications) when these are sorted by increasing statistical significance.

Protein <i>Gene name</i>	Specificity (Assay / Competition)		Protein <i>Gene name</i>	Specificity (Assay / Competition)	
	Intensity fold-change ( $\log_2$ )	Student's t-test ( $p$ value)		Intensity fold-change ( $\log_2$ )	Student's t-test ( $p$ value)
<b>ALDOC*</b>	0.97	0.008	<b>NHP2</b>	4.48	0.112
<b>CSK*<sup>k</sup></b>	1.33	0.044	<b>AZGP1</b>	1.72	0.121
<b>HBA1</b>	2.19	0.050	<b>SARS</b>	0.55	0.122
<b>GSTO1</b>	0.85	0.073	<b>NAP1L1</b>	1.19	0.123
<b>ESF1</b>	1.92	0.084	<b>RAB21</b>	1.20	0.125
<b>FAU</b>	7.55	0.087	<b>GAR1</b>	1.78	0.134
<b>ABL2;ABL1<sup>k</sup></b>	3.33	0.088	<b>BCR</b>	0.75	0.136
<b>KRI1</b>	5.27	0.099	<b>AHCY</b>	0.45	0.139
<b>TSR1</b>	2.86	0.104	<b>GARS</b>	0.54	0.140
<b>EEF2</b>	0.63	0.112	<b>SLC1A5</b>	0.36	0.145

Table 3–9: Top20 list (sorted by increasing  $p$  value) of dasatinib-competed proteins when calculating values for all runs from all experiments 26 assays and 26 competitions. \* = significant and competed; <sup>k</sup> = kinase

The results obtained for ALDOC, CSK, ABL and BCR in each individual experiment can be observed in Figure 3-12, on page 74. ALDOC was the protein from this list which was more often identified across experiments but reduced intensity values in the competition were only observed significantly in two experiments (A and F) as opposed to CSK which, as said previously, was significantly competed in three separate experiments (A, E and I). BCR and ABL are only competed with a significant  $p$  value in one experiment (A).

Analyzing the overall results, it becomes more apparent that dasatinib primarily engages CSK in K562 cells. In fact, CSK was one of the top tyrosine kinases identified by Shi *et al.* when performing the *in vitro* click capture in K562 lysate<sup>92</sup>. Also, CSK has been previously captured with a dasatinib capture compound in HepG2 lysate using the classical CCMS workflow<sup>13</sup> and in the analysis performed by Davis *et al.*<sup>108</sup> dasatinib inhibits CSK with a  $K_d$  of 1 nM (this protein is represented in Figure 3-3, on page 56, as being inhibited by dasatinib but not by the other represented tyrosine kinase inhibitors).

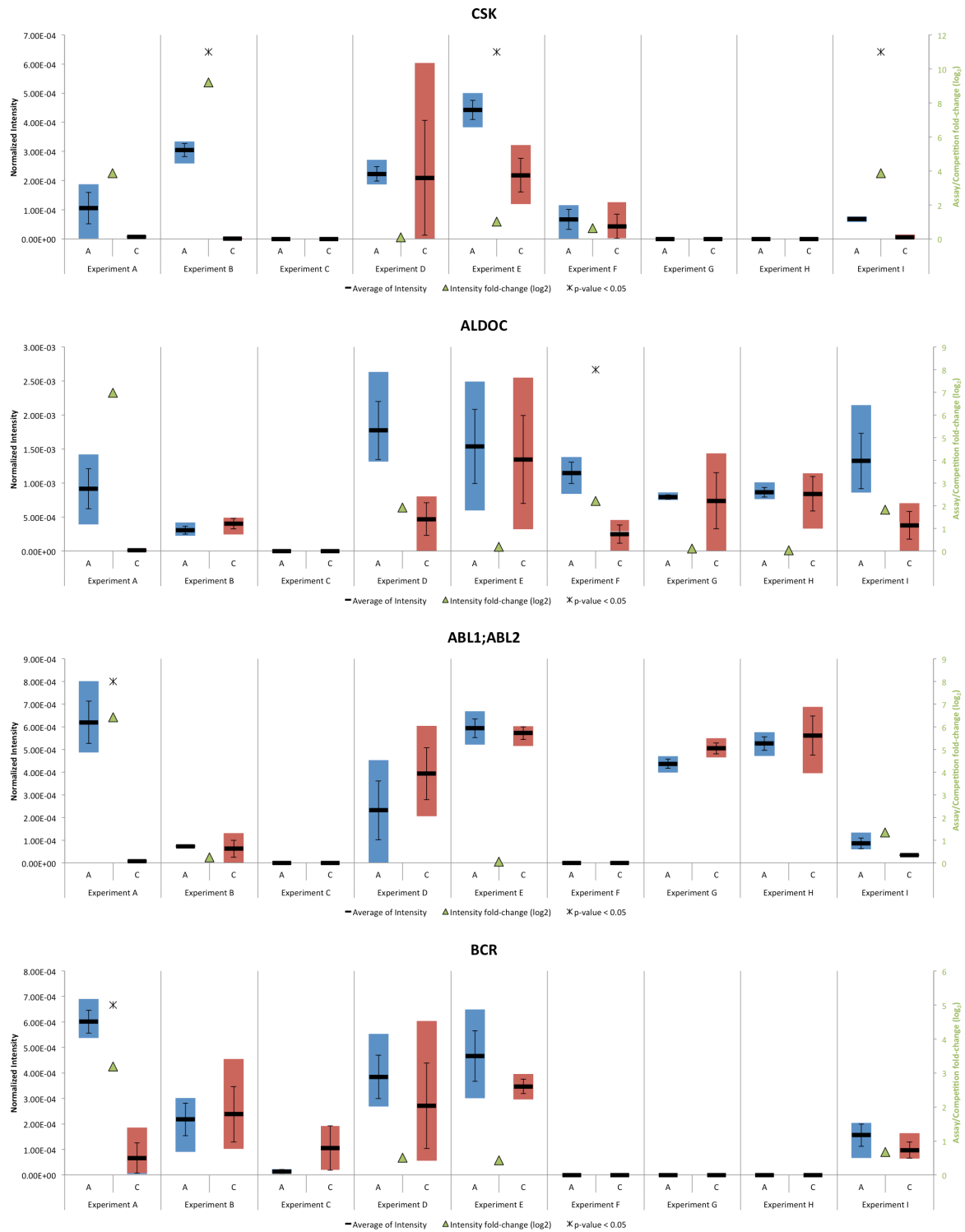


Figure 3-12: CCMS charts of CSK, ALDOC, ABL and BCR proteins in Dasatinib capture experiment in K562 living cells using a click workflow. Boxes: minimum and maximum intensity values for assay (A / blue) and competition (C / red) samples. Black bar: Average of intensity (n=3) ± SEM. Green triangle: log<sub>2</sub> fold-change between average intensities from assay and competition samples. \* significant fold-change (p value < 0.05)

When the protein list from Table 3–9, on page 73, is analyzed with STRING, a network of enriched interactions is obtained (Figure 3-13). Most of the interacting proteins are associated to ribosomes or to the cellular translational machinery. The other smaller network observed in Figure 3-13 is between ABL1, ABL2 and BCR while all other identified proteins have little interaction with each other according to this database.

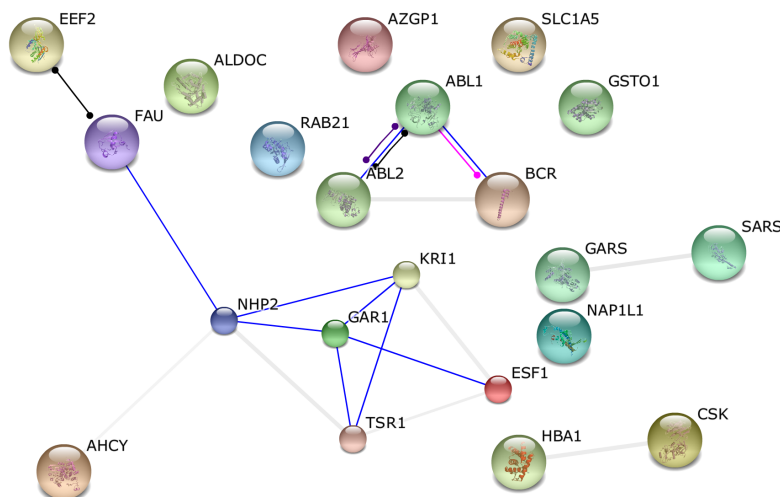


Figure 3-13: STRING protein interaction analysis of significantly competed proteins in dasatinib capture experiment in K562 lysate using the click workflow.

Blue: binding; black: reaction; pink: post-translational modification; purple: catalysis; gray: association in curated databases.

Further analysis of the network for Gene Ontology terms reveals a significant enrichment of protein tyrosine kinases as well as other functions related to general small molecule binding properties (Table 3–10). Lastly, correlation analysis of this network for related diseases identifies chronic myeloid leukemia as a top candidate, which is in accordance of dasatinib therapeutic use and K562 cell biology.

Gene Ontology Term – Molecular Function	Number Of Genes	<i>p</i> value	<i>p</i> value_FDR	<i>p</i> value_bonferroni
poly(A) RNA binding	8	3.94E-06	7.62E-03	1.51E-02
heterocyclic compound binding	14	6.71E-06	7.62E-03	2.57E-02
non-membrane spanning protein tyrosine kinase activity	3	6.75E-06	7.62E-03	2.59E-02
organic cyclic compound binding	14	7.94E-06	7.62E-03	3.05E-02

Table 3–10: Gene Ontology term enrichment from significantly competed proteins in dasatinib capture experiment in K562 living cells using a click workflow.

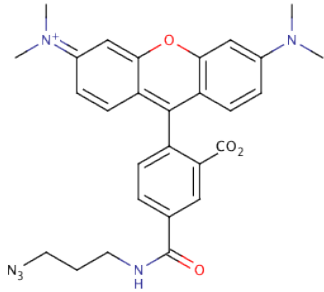
Although the first system established to identify small molecule targets in living cells via a bio-orthogonal chemical ligation method did not deliver the expected results, important information can be retrieved. Living cell systems have inherent high variability in several structural, biological and biochemical characteristics due to different cell cycle stages, which can influence the uptake of small molecules and introduce unforeseen bias. One way to tackle this issue could be to synchronize cells prior to experimentation but this would be less representative of how dynamic a biological system is and the main objective of introducing this new approach to identify small molecule targets is to be as close to the natural system as possible. An alternative, which was confirmed in the final analysis, is to increase the number of biological and technical replicates to have strong statistics and confidence in the obtained results.

With this in mind, the next step was to identify targets from a small molecule with poorly understood mode of action.

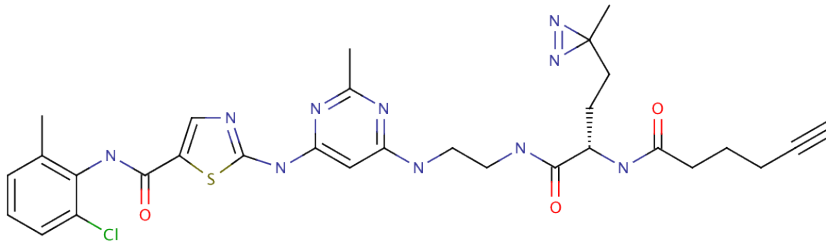
### 3.3. SPECIFIC METHODS FOR THE DASATINIB SYSTEM

#### 3.3.1. Structures of used compounds

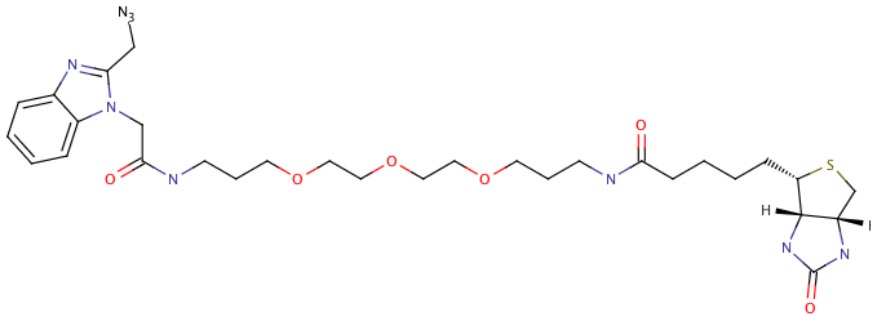
CC 5: Clickable TAMRA [tetramethylrhodamine] azide (contains labeling function)



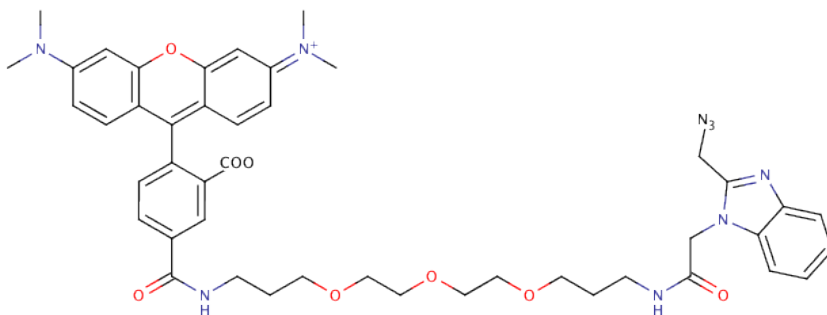
CC 6: Clickable Dasatinib alkyne capture compound (contains selectivity and photoreactive functions)



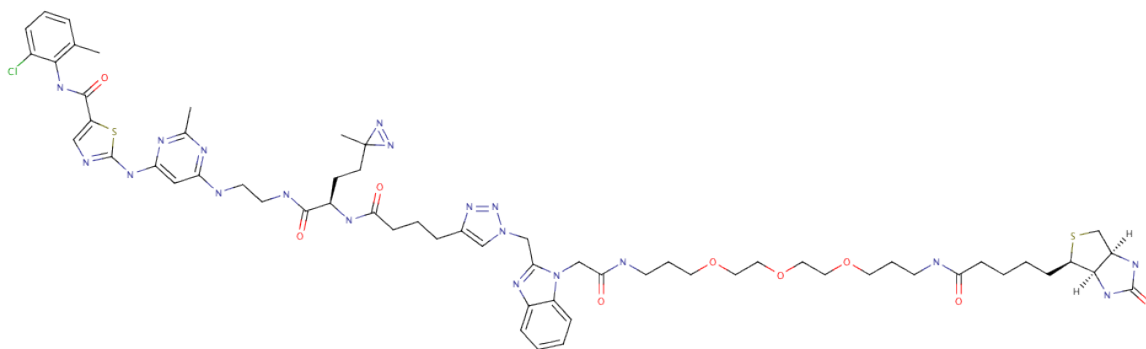
CC 7: Clickable biotin-PEG copper-chelating azide (contains labeling and copper ligand functions)



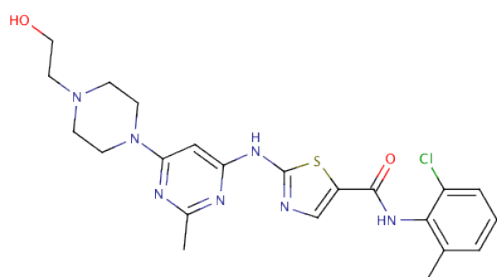
CC 8: Clickable TAMRA-PEG copper-chelating azide (contains labeling and copper ligand functions)



CC 9: Clicked dasatinib-biotin capture compound. Reaction product of CC 6 and CC 7

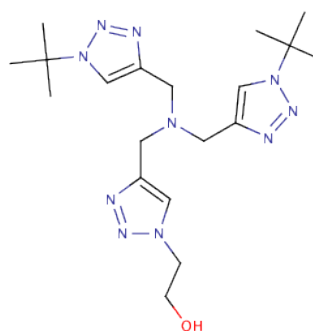


CC 14: Dasatinib competitor



CC 18:

Copper-chelating ligand BTTE  
bis(tert-butyltriazoly)ethanol



### 3.3.2. Optimizing CuAAC reaction parameters with new copper-chelating azide

160 pmol of recombinant human SRC or 50  $\mu\text{g}$  of K562 cell lysate was distributed in 200  $\mu\text{L}$  PCR-tube strips and diluted with water and 5X Capture Buffer. To the competition samples, 500  $\mu\text{M}$  of dasatinib competitor (CC 14) was added and the corresponding volume of water was added to the assay samples. The vials were incubated for 10 min on ice and then 20  $\mu\text{M}$  of dasatinib-alkyne capture compound (CC 6) was added. The samples were incubated for 90 min rotating at 4  $^{\circ}\text{C}$  and then irradiated for 10 min at 350 nm in a caproBox™ to promote photo-crosslinking of the compounds to the binding targets. The CuAAC reaction was performed in three different sets to compare efficiencies: (i) previously established conditions with 20  $\mu\text{M}$  TAMRA-azide (CC 5), 100  $\mu\text{M}$   $\text{CuSO}_4$ , 200  $\mu\text{M}$  BTTE (CC 18) and 2.5 mM sodium ascorbate at pH 8.5; (ii) Bevilacqua's chemistry parameters with 10  $\mu\text{M}$  TAMRA copper-chelating-azide (CC 8), 200  $\mu\text{M}$   $\text{CuSO}_4$  and 5 mM sodium ascorbate; (iii) newly designed mixture with 20  $\mu\text{M}$  TAMRA copper-chelating-azide (CC 8), 100  $\mu\text{M}$   $\text{CuSO}_4$  and 2.5 mM sodium ascorbate at pH 8.5. The click reaction ran for 30 min shaking at room temperature. Concentrated Laemmli buffer was added to the samples and then boiled for 10 min at 100  $^{\circ}\text{C}$ .

The results were visualized by SDS-PAGE followed by Blotting with chemiluminescence readout on x-ray film using IgG anti-TAMRA followed by anti-IgG-HRP secondary antibody.

Band intensity was measured using ImageJ software for fold-change calculations.

### 3.3.3. Capturing dasatinib targets in K562 cell lysate using CuAAC

K562 cell lysate was prepared as described in the General Methods (6.1.2.1 K562 lysate preparation, on page 116).

A full dasatinib-biotin capture compound (CC 9) was prepared *a priori* to be used as a reference: 500  $\mu\text{M}$  of biotin copper-chelating-azide (CC 7) was equilibrated with 5 mM of  $\text{CuSO}_4$  for 10 min at R.T. and then reacted with 500  $\mu\text{M}$  of dasatinib-alkyne capture compound (CC 6) in PBS at pH 8.5 by adding 2.5 mM of sodium ascorbate. The vial was shaken vigorously for 10 min at R.T.

100  $\mu\text{g}$  of K562 cell lysate was distributed in 200  $\mu\text{L}$  PCR-tube strips and either 125  $\mu\text{M}$  of dasatinib competitor (CC 14) was added to the competition samples or the corresponding volume of DMSO was added to the assay samples. The vials were incubated for 30 min on ice and then added 5  $\mu\text{M}$  of dasatinib-alkyne capture compound (CC 6) for post-click samples or 5  $\mu\text{M}$  of pre-clicked dasatinib-biotin capture compound (CC 9) to the pre-click samples. To additional control samples with or without dasatinib competitor, the equivalent volume of water was added. All samples were incubated for 90 min rotating at 4  $^\circ\text{C}$  and then irradiated for 10 min at 350 nm in a caproBox™ to promote photo-crosslinking of the compounds to the binding targets. The CuAAC reaction was performed in the samples containing the dasatinib-alkyne capture compound (CC 6) by adding 5  $\mu\text{M}$  of biotin copper-chelating-azide (CC 7) (pre-equilibrated with two-times excess  $\text{CuSO}_4$ ) and 2.5 mM of sodium ascorbate. To control and pre-clicked samples, the equivalent volume of PBS was added. The click reaction ran for 30 min shaking at room temperature.

Streptavidin-coated magnetic beads were washed with PBS and incubated with the samples for 1 h rotating at 4  $^\circ\text{C}$ . The beads were recovered using a caproMag™ and then washed six times with wash buffer followed by three times wash with 80% acetonitrile and a final wash with MS-grade water.

0.5  $\mu\text{g}$  of trypsin in ammonium bicarbonate was added to the beads and incubated over-night shaking at 37  $^\circ\text{C}$ . The supernatant containing the tryptic digest was recovered to clean tubes; next, the beads were washed with MS-grade water and the wash solution pooled with the original supernatant. All samples were lyophilized and analyzed by LC-MS/MS following the protocol described in the General Methods section (6.3 Mass Spectrometry, on page 121).

### 3.3.4. Cell viability assay for dasatinib compounds in K562 cells

To determine the cell viability of K562 cells after incubation with dasatinib (CC 14) and clickable dasatinib-alkyne capture compound (CC 6), the CellTiter-Glo® Luminescent Cell Viability Assay from Promega™ was used.

CellTiter-Glo® Reagent was prepared as described by the manufacturer and the assay was performed in triplicate in an opaque 96-well multiplate. To establish a calibration curve, 100  $\mu\text{L}$  of K562 cells at a concentration of  $1 \times 10^6$  cells/mL in RPMI medium was dispensed in the starting well and diluted sequentially in the same medium with a dilution factor of two. Control wells containing medium without cells were also prepared to determine the value for background luminescence. Assay wells were prepared with 100,000 cells and either dasatinib (CC 14) or dasatinib-alkyne capture compound (CC 6) were added and incubated for 30 or 90 min at 37  $^\circ\text{C}$  (5%  $\text{CO}_2$ ). The plate

and its contents was equilibrated at room temperature for 30 min. 100  $\mu\text{L}$  of CellTiterGlo<sup>®</sup> Reagent was added to the wells and the plate was mixed for 2 min on an orbital shaker. The plate was then allowed to incubate for 10 min at room temperature.

The luminescence signal was recorded in an Imaging System (Syngene G:BOX XT4) and the image obtained was analyzed with the ImageJ software to extract the intensities of each well. Data was further processed in Microsoft Excel to calculate the effect of the compounds on the viability of K562 by interpolation from the calibration curve.

### 3.3.5. Capture of dasatinib targets in living K562 cells using CuAAC

K562 cells were resuspended in RPMI 1640 medium without phenol red, supplemented with 10% FBS and 1% penicillin/streptomycin, when used for experiments.  $1 \times 10^6$  K562 cells were plated onto 6-wells multiplates and left over-night in a cell incubator at 37 °C (5%  $\text{CO}_2$ ). The cells were pelleted for 5 min at 1.000  $xg$ , resuspended in serum-free RPMI medium and returned to their original wells.

10  $\mu\text{M}$  of dasatinib competitor (CC 14) or equivalent volume of DMSO was added to the competition wells or to the assay, respectively. The plates were returned for 15 min to the cell incubator. Then, 1  $\mu\text{M}$  of dasatinib alkyne capture compound (CC 6) was added to all wells and the cells were further incubated for 90 min at 37 °C (5%  $\text{CO}_2$ ). The plates were placed in a CaproBox<sup>™</sup> and irradiated for 10 min at 350 nm. The cells were recovered to tubes and pelleted for 5 min at 1.000  $xg$ , and washed with D-PBS.

The treated cells were lysed for 30 min on ice with 100  $\mu\text{L}$  of RIPA buffer (50 mM Tris-HCl pH8.0, 150 mM NaCl, 1% IGEPAL CA-630, 0.5% Sodium deoxycholate, 0.1% SDS) supplemented with 0.2 mM DTT, 0.5  $\mu\text{L}/\text{mL}$  benzonase and proteinase inhibitors. The crude lysate was transferred to 500  $\mu\text{L}$  eppies and centrifuged for 10 min at 15.000 r.p.m. to remove cell debris.

The supernatant containing the solubilized proteins was transferred to 200  $\mu\text{L}$  PCR strips to which was added 1  $\mu\text{M}$  biotin copper-chelating azide (CC 7) (previously incubated with 10-fold excess  $\text{CuSO}_4$ ) and 2.5 mM sodium ascorbate. The click reaction ran for 30 min shaking at room temperature.

Streptavidin-coated magnetic beads were washed with PBS and incubated with the samples for 1 h rotating at 4 °C. The beads were recovered using a caproMag<sup>™</sup> and then washed six times with wash buffer followed by three times wash with 80% acetonitrile and a final wash with MS-grade water.

0.5  $\mu\text{g}$  of trypsin in ammonium bicarbonate was added to the beads and incubated over-night shaking at 37 °C. The supernatant containing the tryptic digest was recovered to clean tubes; next, the beads were washed with MS-grade water and the wash solution pooled with the original supernatant. All samples were lyophilized and analyzed by LC-MS/MS following the protocol described in the General Methods section (6.3 Mass Spectrometry, on page 121).

## 4. Phenobarbital: new binders for an old drug

### 4.1. INTRODUCTION

Phenobarbital (PB) was first produced in 1912 by Bayer and commercialized as Luminal®. It was widely used as a hypnotic/sedative for the treatment of epilepsy until the later introduction of benzodiazepines, almost 50 years later. To this day, PB continues to be administered to patients with established *status epilepticus*, the most severe form of epilepsy usually resistant to benzodiazepine treatment, despite phenobarbital's suboptimal safety profile<sup>126</sup>. PB is known to promote hepatocellular carcinomas in both rat and mice livers but, interestingly, the same effect has not been observed in humans<sup>127</sup>, and the pathway associated to this mechanism of action remains to be elucidated.

It is largely known that PB induces the expression of specific cytochrome P450 (CYP) genes, amongst other metabolizing enzymes present in liver microsomes<sup>127-130</sup>. The CYP superfamily of proteins, comprised of at least 27 distinct gene families, is a collection of structurally related haemoprotein mono-oxygenase enzymes that hydroxylate a large number of steroid hormones, fatty acids, drugs, carcinogens, and environmental chemicals<sup>129</sup>. In rat liver, PB induces mainly the expression of CYP2B1 and CYP2B2 but only with high concentrations of the drug. The PB receptor, if it truly exists, has low affinity for PB<sup>127</sup>. Even though CYP2B1 and CYP2B2 are the primary members of the P450 superfamily induced by PB, they do not appear to metabolize the drug<sup>127</sup>. This known induction of CYPs by PB is actually used as reference to determine the hepatotoxicity of other drugs and categorize them as "PB-like" inducer if the response is positive<sup>130</sup>.

There are several reasons to think that "PB-type" induction of CYPs is involved in hepatic tumor promotion by PB. A detailed analysis on PB mechanistic data and risk assessment has been covered by Whysner *et al.*<sup>127</sup> Induction by PB of P450 enzymes is part of a complex, pleiotropic response. PB has many effects on liver that may or may not be mediated by P450 induction, such as effects on gap junctions, effects on apoptosis, effects on EGF receptors, and effects on proliferation. In fact, there are paradoxical effects of PB on mouse hepatocarcinogenesis<sup>131</sup>, making it difficult to extrapolate experimental data from laboratory animals to human risk assessment. In rats and mice pre-initiated with genotoxic carcinogens, PB administration increases the number of hepatocellular tumors by approximately 5-fold despite its non-genotoxicity. However, in mice PB occasionally exhibits strong inhibitory effects on hepatocarcinogenesis initiated with the potent carcinogen diethylnitrosamine. Both positive and negative effects of phenobarbital on hepatocytic proliferation and apoptosis, which are mechanistically involved in the promotion stage of hepatocarcinogenesis, have been described.

Understanding the activation mechanism through which PB induces CYP expression might prove crucial to a better clarification of the observed inter-species effect variance.



Figure 4-1: Luminal (phenobarbital) as it was packaged in 1940/1945. Picture from product on display at the Stadtgeschichtliches Museum Leipzig.

Several studies have demonstrated that intracellular phosphorylation events control the PB induction of CYP2B genes<sup>132–134</sup>, with some suggesting that both energy status and nutritional environment of the cell can influence PB regulation of CYP2B gene expression, although the exact mechanism was not understood at the time. In 2005, Rencurel *et al.* provided evidence that AMP-activated kinase (AMPK) mediates the PB induction of CYP2B genes expression<sup>135</sup>, which they later confirmed with AMPK knockout experiments<sup>136</sup>. AMPK is a ubiquitously expressed metabolic-stress-sensing protein kinase that regulates metabolism in response to energy demand and supply by directly phosphorylating rate-limiting enzymes in metabolic pathways as well as controlling gene and protein expression. If the energy stock decreases, AMP/ATP ratio increases followed by activation of AMPK which subsequently turns off ATP-consuming pathways such as fatty acid, triglycerides and cholesterol synthesis as well as protein synthesis and transcription, and switches on catabolic pathways such as glycolysis and fatty acid oxidation. AMPK activity is activated by a wide array of metabolic stresses, including hypoxia, ischemia, and oxidative and hyperosmotic stresses<sup>137</sup>.

In the proposed mechanism by Rencurel *et al.*<sup>135,136</sup>, PB increases the AMP/ATP ratio that activates AMPK through phosphorylation of its Thr172, a reaction later proposed to be carried out by the LKB1 enzyme<sup>138</sup>. A connection between AMP and its main binder PKA (already described in a previous Chapter) and the PB effect on CYP expression had been established by Joannard *et al.*<sup>139</sup> who observed a competition between the two systems, suggesting that the activation of the AMP/PKA pathway down-regulated the induction of CYP2B1/2 by PB.

In 1999, Kawamoto *et al.*<sup>132</sup> discovered that the constitutive androstane receptor (CAR), sometimes also referred to as constitutively active receptor, translocated from the cytoplasm to the nucleus upon PB stimulus. CAR was originally described as a regulator of gene expression from retinoic acid-responsive elements and is now associated to a series of regulation mechanisms involved in the metabolism and transport of various xenobiotics and endogenous chemicals<sup>140</sup>. Upon PB treatment, the signaling cascade leads to a recruitment of CAR in the nucleus where it binds to the phenobarbital responsive enhancer module (PBREM) present in the CYP2B gene family and induces the expression of P450 enzymes. In 2007, Shindo *et al.*<sup>141</sup>, established the missing link between AMPK activation/phosphorylation and CAR nuclear translocation to enhance CYP2B expression, confirming that PB utilizes the AMPK pathway as signaling molecules leading to CYP2B gene expression, although not exclusively with data suggesting the presence of other activation pathways.

A more cohesive theory for the phenobarbital activation and signaling pathway has arisen during the development of the work here presented. Mutoh and co-workers<sup>142</sup> discovered that PB indirectly activates CAR by inhibiting the epidermal growth factor receptor (EGFR). The activation of CAR through dephosphorylation is catalyzed by phosphatase PP2A when associated to dephosphorylated RACK1. Dephosphorylated CAR translocates to the nucleus, interacts with retinoid X receptor (RXR), and activates the transcription of CYP2B through the PBREM enhancer. Inhibition of EGFR with PB prevents the receptor to be activated and impedes RACK1 phosphorylation, possibly through the Src kinase, allowing its association with PP2A and subsequent CAR activation.

The interaction of CAR with the EGFR signaling pathway was previously described by Meyer *et al.* in 1989<sup>143</sup>, where the results showed the affinity of EGF to its receptor was diminished in PB-treated rat primary hepatocytes although the abundance of EGFR was unchanged. The experiments performed at the time indicated the inhibition was not a direct competition for the receptor but

acted through some other underlying mechanism. Even though earlier results contradicted the current findings, the author of the initial research has published a letter in support of Mutoh's achievements<sup>144</sup>.

A recent publication provides evidence for the missing link between Mutoh's proposal and the observed AMPK phosphorylation in association with CAR translocation. Joseph *et al.*<sup>145</sup> have shown that AMPK is dephosphorylated by PP2A, the same phosphatase shown to coordinate with RACK1 to dephosphorylate CAR and lead to the translocation of the latter towards the nucleus. PB binds to EGFR preventing its activation and RACK1 phosphorylation, which binds to PP2A, preventing the phosphatase to continue acting on AMPK and thus leads to an increase on AMPK phosphorylation levels.

A scheme depicting the proposed mechanism is illustrated in Figure 4-2.

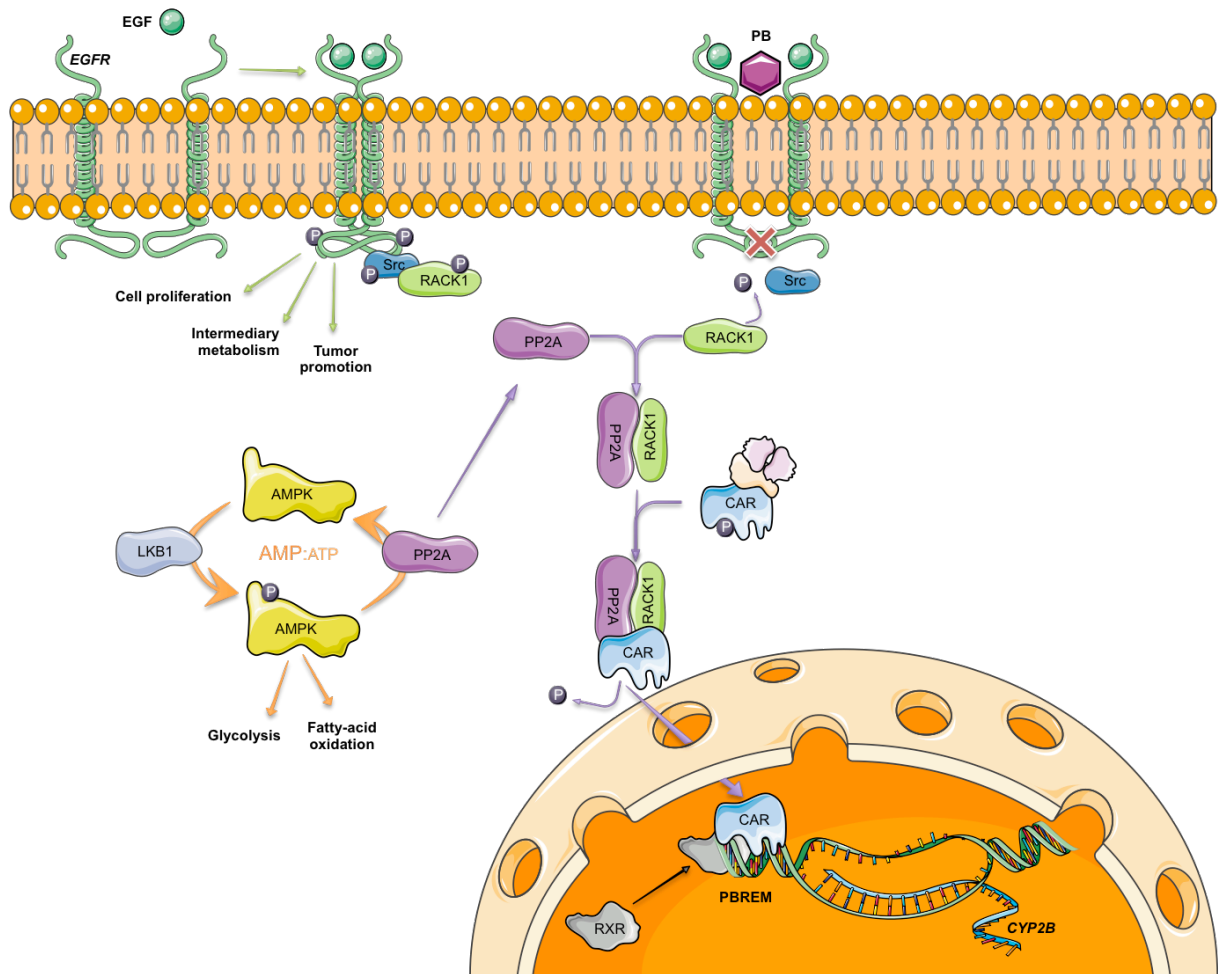


Figure 4-2: Phenobarbital induces CYP2B expression via EGFR inhibition

Epidermal growth factor (EGF) binding to its high-affinity receptor (EGFR) induces dimerization and autophosphorylation of its intracellular tyrosines. The activated receptor generates adapting protein docking sites to trigger several downstream effector pathways, including those stemming from the tyrosine-specific phosphorylation of Src. Activated Src in turn phosphorylates RACK1, thus inactivating RACK1-assisted dephosphorylation of CAR. Increasing AMP:ATP ratios activates cytosolic AMPK, via phosphorylation by LKB1, increasing ATP-generating intracellular processes such as glycolysis and fatty-acid oxidation. The AMPK activity is regulated by PP2A, which dephosphorylates the kinase. Phenobarbital (PB) binding to EGFR prevents the receptor's activation, suppressing RACK1 phosphorylation and promoting the binding to PP2A. The RACK1:PP2A complex recruits CAR and catalyzes its dephosphorylation. Dephosphorylated CAR translocates to the nucleus, interacts with the retinoid X receptor (RXR), and activates the transcription of CYP2B through the phenobarbital responsive enhancer module (PBREM). Adapted from Meyer and Jirtle<sup>144</sup>, based on Mutoh *et al.*<sup>142</sup> and Joseph *et al.*<sup>145</sup> using Servier Medical Art templates.



### 4.2.2. Developing a phenotypic assay to evaluate phenobarbital effect

Selection of adequate experimental systems is key in understanding the underlying mechanisms of action of a specific drug. In 1984, Ferro *et al.*<sup>146</sup> showed the induction of cytochrome P450 (CYP) by phenobarbital in a rat hepatoma cell line (MH<sub>1</sub>C<sub>1</sub>), making it a good candidate as a biological system to identify phenobarbital targets and characterize its phenotypic effect. A later study on the effect of phenobarbital on some CYPs and other liver metabolizing enzymes in six different rat hepatoma cell lines confirmed that MH<sub>1</sub>C<sub>1</sub> cells compared better to primary hepatocytes in their expression of biotransformation activities<sup>147</sup>. The goal of implementing a read-out system for the effect of phenobarbital is to use it later once potential target candidates are identified by CCMS and measure if ablating or reducing their expression produces the same type of response observed with the use of the small-molecule.

To develop a phenotypic assay, three different approaches with known phenobarbital responses, as described in the literature, to phenobarbital stimulation were pursued simultaneously: constitutive androstane receptor translocation; AMP activated protein kinase phosphorylation; and cytochrome P450 induction.

#### 4.2.2.1. Constitutive Androstane Receptor (CAR) translocation

The constitutive androstane receptor (CAR) is a known responder to phenobarbital stimulus<sup>148–150</sup> via an indirect activation mechanism. Phenobarbital activates a pathway that translocates CAR from the cytoplasm to the cellular nucleus where it will induce gene expression<sup>132</sup>.

MH<sub>1</sub>C<sub>1</sub> cells were submitted to cellular fractionation using a commercially available kit that isolates nuclei from cytoplasm as described in the specific methods section (4.3.3 Subcellular fractionation of MH<sub>1</sub>C<sub>1</sub> cells, on page 106). The isolated fractions were resolved by SDS-PAGE and transferred onto nitrocellulose membrane for probing using a specific anti-CAR antibody (Figure 4-4).

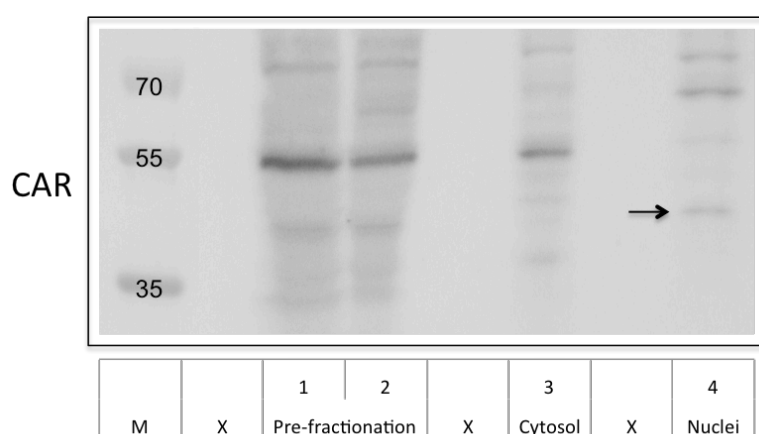


Figure 4-4: Western Blot analysis of CAR in isolated nuclei and cytosol from MH<sub>1</sub>C<sub>1</sub> cells. Expected molecular weight for CAR: 46 kDa (arrow indicates possible CAR)

The anti-CAR blot shown in Figure 4-4 reveals that the antibody produces considerable background, having the strongest reaction at unexpected 55 kDa. The expected reaction for CAR at 46 kDa is very faint in the pre-fractionated samples (Figure 4-4, lanes 1 and 2), mostly absent in the cytosol fraction (Figure 4-4, lane 3) but becoming clearer in the nuclear fraction (Figure 4-4, lane 4). The cells used in this experiment were not treated with phenobarbital therefore the presence of CAR in the nucleus and its absence in the cytoplasm was unexpected, suggesting a pre-activation of the pathway.

A new experiment was designed to evaluate if the result presented in Figure 4-4 confirms the presence of CAR in the nucleus in untreated cells or if upon treatment with phenobarbital more CAR is recruited to this subcellular fraction.

MH<sub>1</sub>C<sub>1</sub> cells were treated with phenobarbital at different concentrations (0, 1 μM, 10 μM, 100 μM, 250 μM or 500 μM) during 1 h, 2 h, 4 h or 6 h. The detection of CAR in each subcellular fraction by western blot is shown in Figure 4-5.

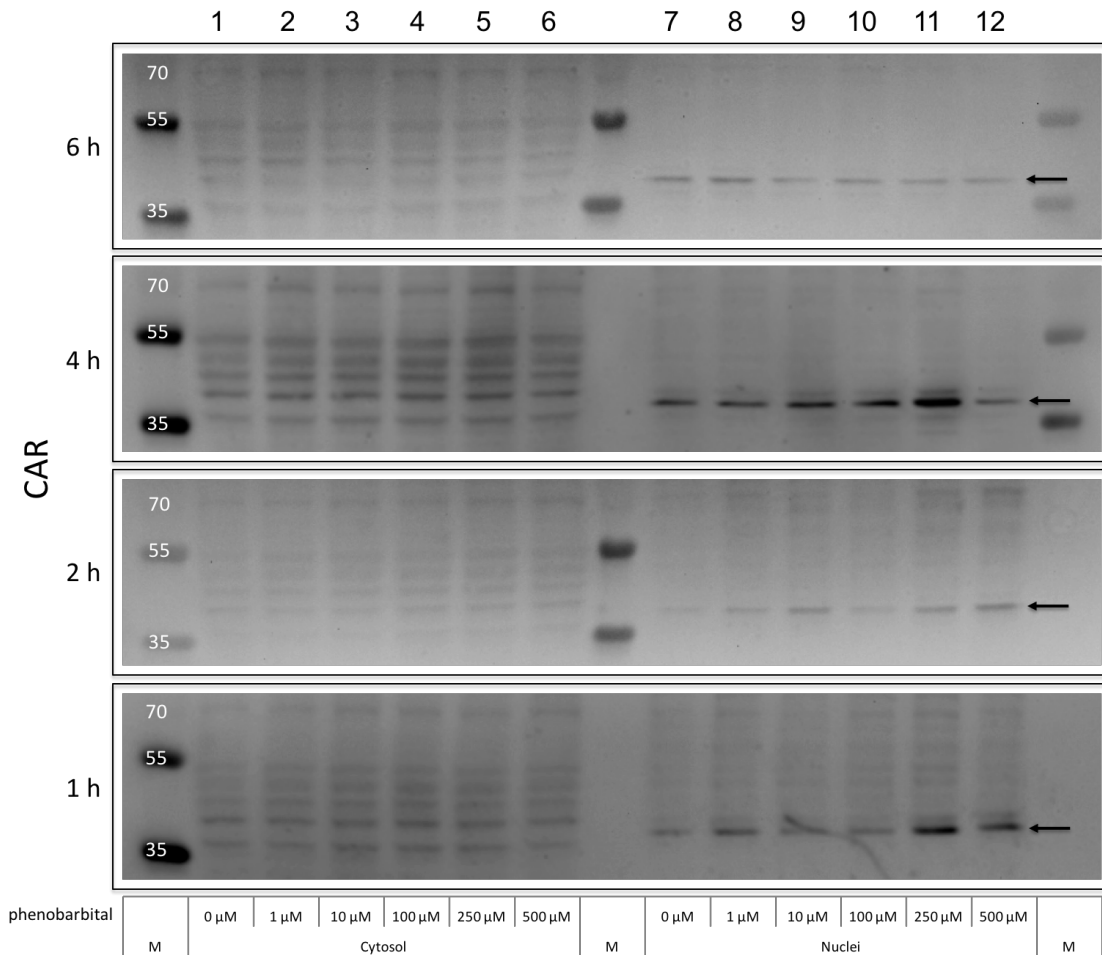


Figure 4-5: Effect of phenobarbital on CAR translocation from cytosol to nucleus in MH<sub>1</sub>C<sub>1</sub> cells. Cells were incubated with 0 – 500 μM phenobarbital for 1 h, 2 h, 4 h or 6 h followed by subcellular fractionation. The individual fractions were analyzed by western blot for CAR detection. Arrow indicates possible CAR. Expected molecular weight for CAR: 46 kDa

The results presented in Figure 4-5 show once again the high background created by the antibody used for the detection of CAR. The expected molecular weight for CAR (46 kDa) can be attributed to several bands detected between the 55 kDa and 35 kDa markers in the cytosolic fractions independently of the different phenobarbital stimulus (Figure 4-5, lanes 1 – 6). The strongest reaction observed in the picture is a band slightly over the 35 kDa marker in the nucleus fraction (Figure 4-5, lanes 7 – 12) which, if in fact corresponds to CAR, confirms that the protein is already present without phenobarbital stimulus (Figure 4-5, lane 7) and the intensity of that band does not show linearity with increasing phenobarbital concentrations or time of stimulation.

The overall results are not clear and suggest that CAR translocation is not a good readout system for phenobarbital effect on MH<sub>1</sub>C<sub>1</sub> cells.

#### 4.2.2.2. Phosphorylation of AMP activated protein kinase (AMPK)

AMP-activated kinase (AMPK) is described as a cellular energy sensor, sensitive to AMP:ATP ratios, which is activated upon phosphorylation of its threonine 172 (T172) residue<sup>151</sup>. Rencurel *et al.*<sup>135,136</sup> have demonstrated a relationship between phenobarbital stimulus and AMPK activation via T172 phosphorylation in hepatic cells from different species.

MH<sub>1</sub>C<sub>1</sub> cells cultured in complete DMEM medium (10% FBS, 1% pen/strep) were starved in fresh serum-free medium prior to the incubation with phenobarbital. The cells were incubated for 1 h, 2 h, 4 h or 6 h with phenobarbital at 0, 1 μM, 10 μM, 100 μM, 250 μM or 500 μM. After treatment the medium was removed, the cells were washed with D-PBS and recovered for fractionation. The cytosolic fractions of each sample were analyzed by western blot using antibodies against total AMPK and specific phosphorylation on T172 (pAMPK). The results are presented in Figure 4-6, on page 88.

The results of phenobarbital effect on AMPK phosphorylation in MH<sub>1</sub>C<sub>1</sub> cells after serum starvation show that concentrations of phenobarbital higher than 10 μM reduce the overall amount of AMPK in the cytosol (Figure 4-6, lanes 13 – 24, middle panel), only after 1 h incubation, which is also obtained with 10 μM phenobarbital but with 6 h incubation time (Figure 4-6, lane 12, middle panel). The phosphorylation of AMPK (pAMPK) fluctuates over time with a tendency to be maintained at higher concentrations of phenobarbital but still in fewer amounts compared to the smaller time incubation (Figure 4-6, top panel).

Looking at the control samples, which were not stimulated with phenobarbital (Figure 4-6, lanes 1 – 4) it is clear that AMPK activation/phosphorylation is cyclic. After 1 h of the start of the experiment, AMPK is phosphorylated; it gets inactivated after 2 h incubation; at 4 h is again phosphorylated and in the end of the experiment it is again de-phosphorylated.

A clearer picture of the effect of phenobarbital on AMPK activation is obtained when the intensity of the phosphorylation is normalized to the intensity of the total AMPK present in the sample (Figure 4-6, bottom panel). Different patterns of the time incubation effect emerge when using different concentrations of phenobarbital, suggesting that an analysis of the effect of concentration at specific time points could prove more useful to withdraw conclusions.

Figure 4-7, on page 88, shows the phosphorylation of AMPK normalized to the total amount of AMPK in the sample and in relation to the phenobarbital-free control at each time of incubation. Incubating the cells for 1 h shows a variation on AMPK activation between a 3% decrease with 10 μM and a 3% increase with 500 μM phenobarbital in comparison with the control. At 2 h incubation the variation is the highest with an increase of 33% of AMPK phosphorylation using 250 μM of phenobarbital, which is also observed at 6 h with an increase of 26% in comparison to the corresponding control. With longer incubation with phenobarbital at 6 h, the overall effect on the phosphorylation of AMPK is observed even at lower concentrations of the drug.

This method of analysis suggests that phenobarbital has in fact an effect on AMPK activation, although very variable and dependent on time of incubation.

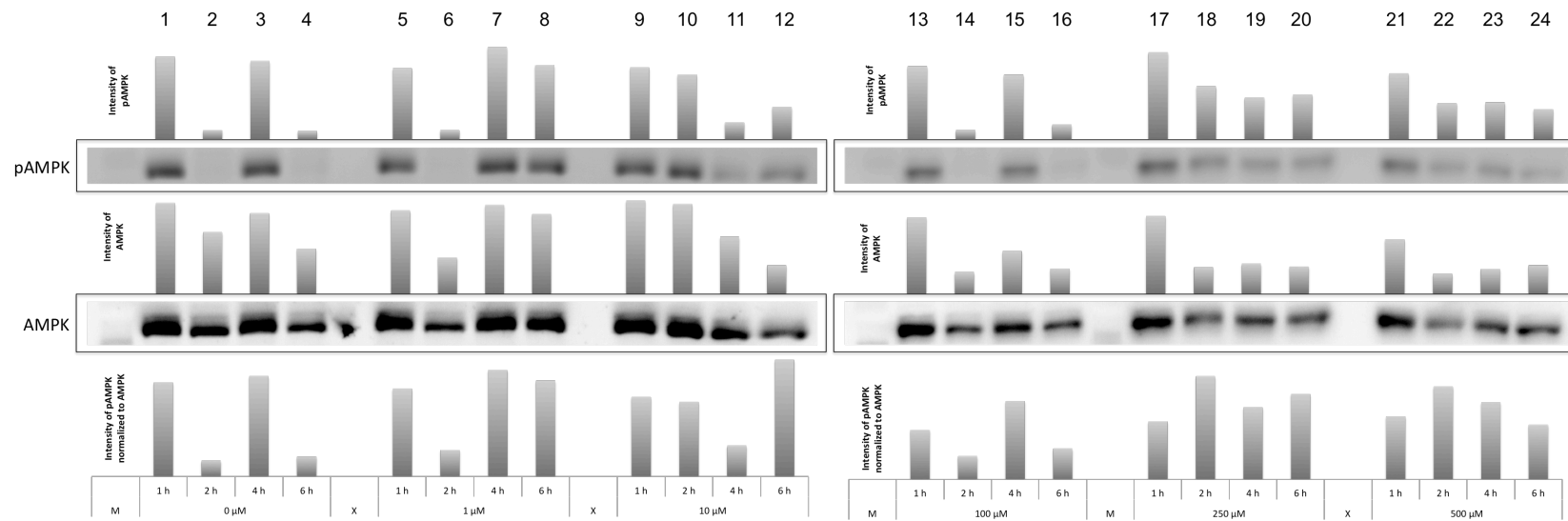


Figure 4-6: Effect of phenobarbital on AMPK phosphorylation (pAMPK) in  $MH_1C_1$  cells treated in serum-free medium.  $MH_1C_1$  cells were incubated for 1 h, 2 h, 4 h or 6 h in serum-free DMEM containing phenobarbital at 0  $\mu M$  (lanes 1 – 4), 1  $\mu M$  (lanes 5 – 8), 10  $\mu M$  (lanes 9 – 12), 100  $\mu M$  (lanes 13 – 16), 250  $\mu M$  (lanes 17 – 20) or 500  $\mu M$  (lanes 21 – 24). Samples were analyzed by western blot for AMPK and pAMPK detection. Bar plot displays intensity of phosphorylated (p) AMPK (top), total AMPK (middle) and normalized pAMPK intensity to total AMPK intensity for each sample (bottom).

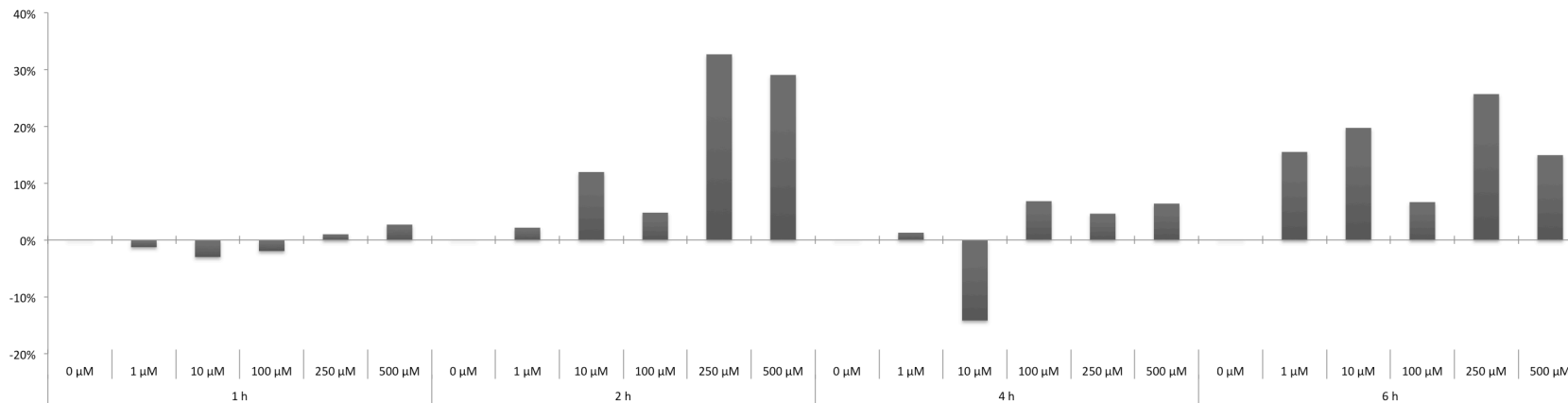


Figure 4-7: Comparative analysis of the effect of phenobarbital on AMPK phosphorylation for each time incubation point in  $MH_1C_1$  cells treated in serum-free DMEM. Bar plots display the normalized pAMPK intensity to total AMPK intensity (as presented in Figure 4-6, bottom panel) in relation to the intensity calculated for the medium control (0  $\mu M$ ) at each time point.

Considering the cyclic nature of AMPK's activation over the time course of the experiment, observed in the control samples (Figure 4-6, lanes 1 – 4, on page 88) and the variable results obtained in the samples stimulated with phenobarbital, a new experimental design is necessary to eliminate that variability. In fact, Ching *et al.*<sup>152</sup> showed that AMPK phosphorylation is elevated in serum-starved cells in comparison to control cells, which could be the cause for the unstable state of activation of AMPK observed in the control samples and, possibly, affecting the effect of phenobarbital stimulation.

A new experiment was performed in MH<sub>1</sub>C<sub>1</sub> cells grown and incubated in serum-supplemented medium. An additional serum-free control was added in this experiment.

As observed previously, serum-free samples present phosphorylation of AMPK in non-treated cells (Figure 4-9, lanes 1, 7, 13 and 19, top panel, on page 90). Likewise, the new control samples treated in complete medium but absent of phenobarbital stimulation also show an active AMPK (Figure 4-9, lanes 2, 8, 14 and 20, top panel, on page 90). In fact, as shown below in Figure 4-8, comparing the phosphorylation of AMPK normalized to the total amount of AMPK in the sample between cells grown in complete or serum-free media show no distinct differences throughout the incubation times (with the exception of a reduction in 2 h incubation in complete medium).

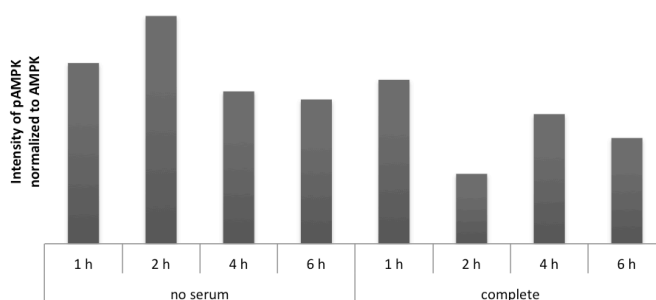


Figure 4-8: Effect of serum supplementation in AMPK phosphorylation (pAMPK) from non-treated (0  $\mu$ M phenobarbital) MH<sub>1</sub>C<sub>1</sub> cells. Bar plot displays the normalized pAMPK intensity to total AMPK intensity (as presented in Figure 4-9, bottom panel) in the different incubation time-points (1 h, 2 h, 4 h or 6 h) for serum-deprived or complete DMEM growth media.

The results for the treatment with phenobarbital are shown in Figure 4-9, on page 90.

Treatment with phenobarbital for 1 or 6 h show no marked differences on the relative phosphorylation of AMPK with increasing concentrations of the drug (Figure 4-9, lanes 3 – 6 and lanes 21 – 24, bottom panel, on page 90). Incubating MH<sub>1</sub>C<sub>1</sub> cells for 4 h results in the same relative phosphorylation using the lowest and the highest concentration of phenobarbital, with a reduction on AMPK activation observed in the mid concentrations utilized (Figure 4-9, lanes 15 – 18, bottom panel, on page 90). The 2 h incubation time with phenobarbital (Figure 4-9, lanes 9 – 12, bottom panel, on page 90) presents some dose response but lacks linearity; AMPK activation is lowest in the control, increasing with 1  $\mu$ M phenobarbital and having a maximum value with 10  $\mu$ M, but dropping to the same phosphorylation value as the control when using 100  $\mu$ M phenobarbital and rising again with 500  $\mu$ M.

Looking at the relative activation of AMPK in comparison to the control at the same time point (Figure 4-10, on page 90) it is possible to say that at two hours incubation with phenobarbital at 10  $\mu$ M produces the highest activation of AMPK when compared to the control, but the overall picture suggests that there is no dose-response effect of phenobarbital on AMPK phosphorylation.

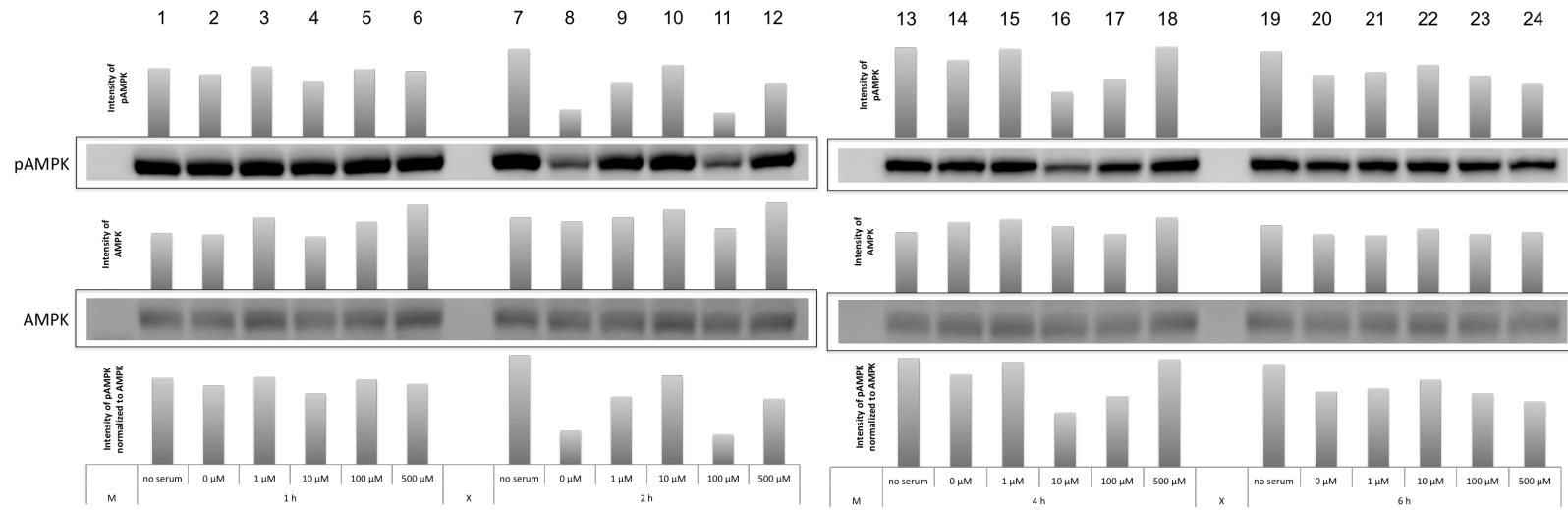


Figure 4-9: Effect of phenobarbital on AMP activated protein kinase (AMPK) phosphorylation (pAMPK) in a rat hepatoma cell line treated in complete medium. *MH<sub>1</sub>C<sub>1</sub>* cells were incubated for 1 h, 2 h, 4 h or 6 h in FBS-supplemented DMEM containing phenobarbital at 0  $\mu\text{M}$  (lanes 1 – 4), 1  $\mu\text{M}$  (lanes 5 – 8), 10  $\mu\text{M}$  (lanes 9 – 12), 100  $\mu\text{M}$  (lanes 13 – 16), 250  $\mu\text{M}$  (lanes 17 – 20) or 500  $\mu\text{M}$  (lanes 21 – 24). Samples were analyzed by western blot for AMPK and pAMPK detection. Bar plot displays intensity of phosphorylated (p) AMPK (top), total AMPK (middle) and normalized pAMPK intensity to total AMPK intensity for each sample (bottom).

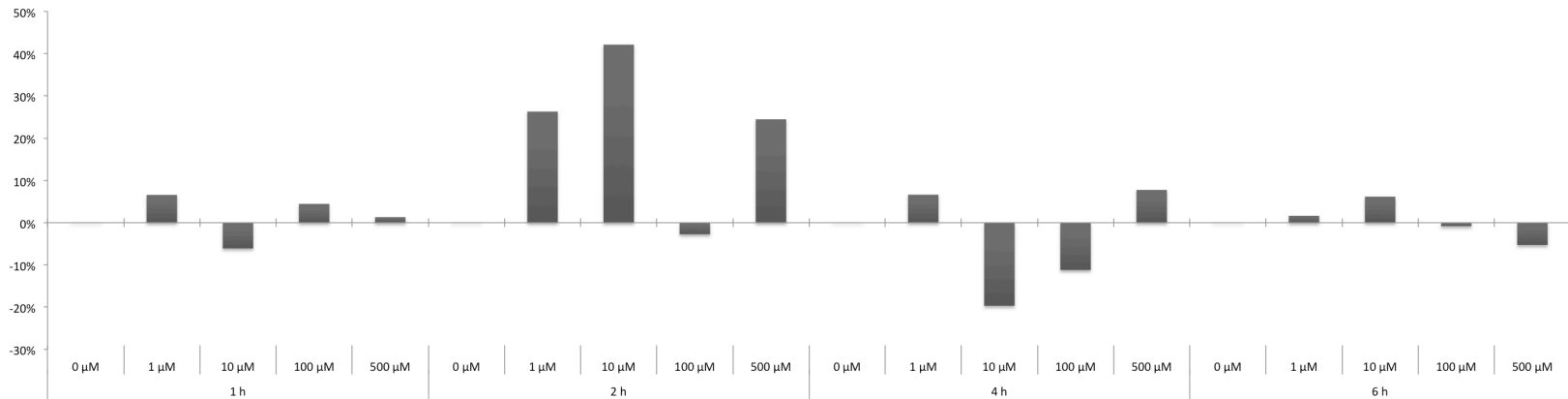


Figure 4-10: Comparative analysis of the effect of phenobarbital on AMPK phosphorylation for each time incubation point in *MH<sub>1</sub>C<sub>1</sub>* cells treated in FBS-supplemented DMEM. Bar plots display the normalized pAMPK intensity to total AMPK intensity (as presented in Figure 4-9, bottom panel) in relation to the intensity calculated for the medium control (0  $\mu\text{M}$ ) at each time point.

Once again, the variability of the effects of phenobarbital on the phosphorylation/activation of AMPK and its endogenous cyclic activated state in MH<sub>1</sub>C<sub>1</sub> cells proves difficult to interpret the results and establish this method as a reliable phenotypic assay to measure the effect of phenobarbital stimulation.

#### 4.2.2.3. Induction of cytochrome P450 (CYP) 2B1 and 2B2

The ability of PB to induce expression of P450 genes has been investigated and reviewed extensively<sup>129,153,154</sup>. The major P450 types induced by PB in rat liver are P450b (CYP2B1) and P450e (CYP2B2)<sup>127</sup>.

The same treatment of phenobarbital in a rat hepatoma cell line, as the previous experiments, was used to determine the effect of the drug in CYP2B1 and CYP2B2 detection by western blot. MH<sub>1</sub>C<sub>1</sub> cells were treated with 0 – 500  $\mu$ M phenobarbital in complete medium for 1 h or 6 h and unfractionated cell lysates were probed with an antibody that detects both CYP2B1 and CYP2B2. The results are shown in Figure 4-11.

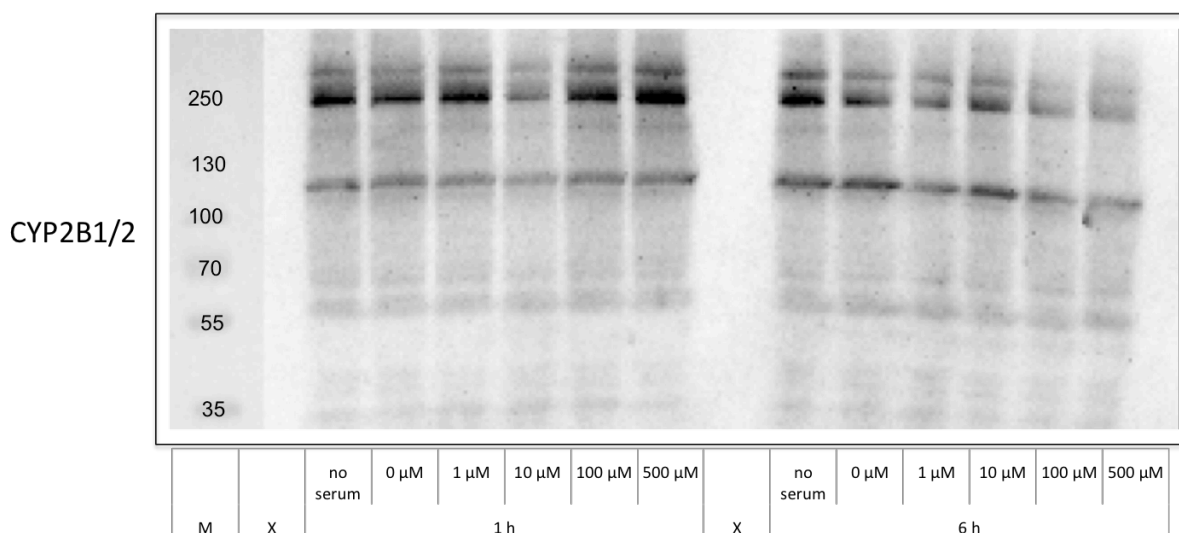


Figure 4-11: Effect of phenobarbital in CYP2B1/2 detection in a rat hepatoma cell line. MH<sub>1</sub>C<sub>1</sub> cells were treated for 1 h or 6 h in FBS-supplemented DMEM containing phenobarbital at 0  $\mu$ M, 1  $\mu$ M, 10  $\mu$ M, 100  $\mu$ M or 500  $\mu$ M. Expected molecular weight: 50 kDa

CYP2B1 and CYP2B2 were not detected in MH<sub>1</sub>C<sub>1</sub> cells after treatment with phenobarbital (Figure 4-11). The blot shows the absence of a band at the expected 50 kDa molecular weight. Other bands are detected with this antibody at higher molecular weights but none changes with phenobarbital, suggesting a case of unspecific antibody binding.

To evaluate the quality of the antibody against CYP2B1 and CYP2B2, different fractions of rat liver isolated for another project were loaded on the gel, and a new experiment with MH<sub>1</sub>C<sub>1</sub> cells treated with higher phenobarbital concentrations (1 mM and 2 mM) was probed simultaneously (see details in specific methods 4.3.4 Treatment of MH<sub>1</sub>C<sub>1</sub> cells with high concentration of phenobarbital, on page 106). Results are presented in Figure 4-12, on page 92.

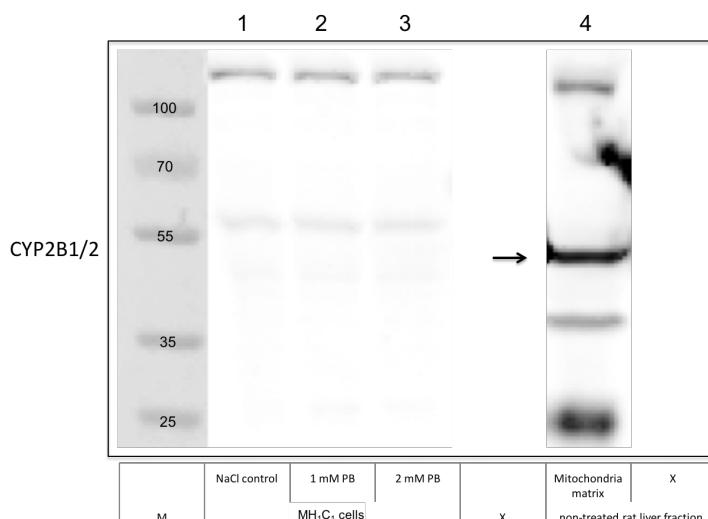


Figure 4-12: Effect of high concentration phenobarbital on the detection of CYP2B1/2 in MH<sub>1</sub>C<sub>1</sub> cells using rat liver mitochondria matrix fraction as positive control for antibody reaction quality.

Rat liver mitochondria were probed with an anti-CYP2B antibody and the presence of a reaction below the 55 kDa marker band confirms the presence of this protein and the capacity of the antibody to detect it (Figure 4-12, arrow, lane 4). This new protocol allowed for the detection of a faint band in MH<sub>1</sub>C<sub>1</sub> cells (Figure 4-12, lanes 1 – 3), although still a bit lower in molecular weight as compared to the rat liver samples. The results also show that treatment with phenobarbital as high as 2 mM does not increase the detection of CYP2B1 or CYP2B2 compared to the negative control.

Since the new method for treatment of MH<sub>1</sub>C<sub>1</sub> cells with higher concentration of phenobarbital revealed improvements in the detection of P450 proteins, the same protocol was applied for the detection of AMPK and its phosphorylation state.

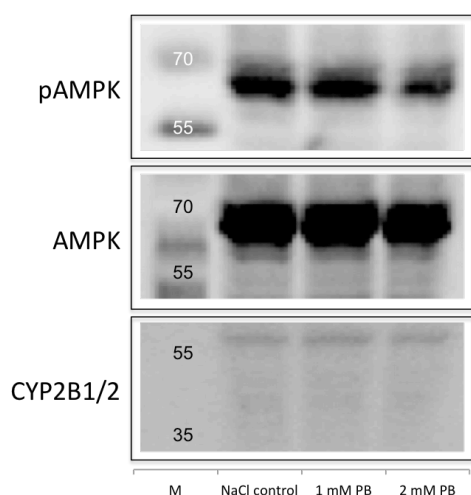


Figure 4-13: Effect of high concentration phenobarbital on the detection of CYP2B1/2 and AMPK phosphorylation in a rat hepatoma cell line. MH<sub>1</sub>C<sub>1</sub> cells were treated with 0 mM (NaCl control), 1 mM or 2 mM phenobarbital and analyzed by SDS-PAGE followed by Western Blot.

The new protocol confirmed that even with high concentration of phenobarbital (1 mM or 2 mM), MH<sub>1</sub>C<sub>1</sub> cells do not show differences in AMPK phosphorylation in comparison to the negative control (Figure 4-13)

#### 4.2.2.4. Detection of D-amino acid oxidase (DAO) in MH<sub>1</sub>C<sub>1</sub> cells

Unpublished CCMS data suggested D-amino acid oxidase as a possible target of phenobarbital in rat liver mitochondria. D-Amino acid oxidase is a FAD-dependent enzyme that catalyzes oxidative deamination of D-amino acids. In 1965, Giuditta and Casola<sup>155</sup> determined that phenobarbital had an inhibitory constant ( $K_i$ ) of  $4 \times 10^{-3}$  M against D-amino oxidase.

To determine if DAO could be used as a phenotypic assay to monitor response to phenobarbital treatment, MH<sub>1</sub>C<sub>1</sub> cell lysate in a serial dilution was probed for the protein by western blot. Results show that DAO is undetectable in MH<sub>1</sub>C<sub>1</sub> lysate (Figure 4-14, lanes 6 – 10), even at the highest input of 50  $\mu$ g total protein. To confirm antibody specificity, purified DAO was loaded also in serial dilution (Figure 4-14, lanes 1 – 5).

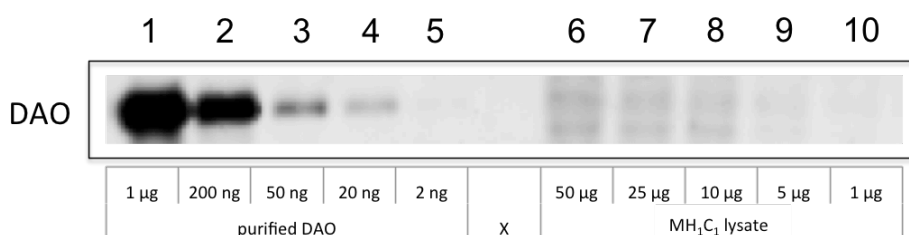


Figure 4-14: Detection of D-amino acid oxidase (DAO) in purified fractions and MH<sub>1</sub>C<sub>1</sub> lysate.

Parallel experiments to determine the inhibitory action of phenobarbital on DAO were performed at caprotec by Dr. Yan Luo. She produced recombinant DAO and tested for phenobarbital inhibition via an Amplex Red based assay. Results confirmed that phenobarbital affinity is low for rat DAO (both recombinant and from liver mitochondria) with an  $IC_{50} > 400$   $\mu$ M and inactive against DAO from a human hepatocyte cell line (HepG2) with an  $IC_{50} > 10$  mM.

#### 4.2.2.5. Effect of phenobarbital treatment in rat primary hepatocytes

Despite all efforts to develop a phenotypic assay for the effect of phenobarbital in a rat hepatoma cell line, the results were so far negative or inconclusive. The genetic and physiological differences induced during the establishment of the cell line could be responsible for the ineffectiveness of the established assays. For this reason, a new biological system, less manipulated, was selected to develop further phenotypic assays: rat primary hepatocytes.

The rat primary hepatocytes were obtained frozen and used always in the first passage. The previously established phenotypic assays to determine AMPK phosphorylation, CAR translocation, CYP2B1/2 and DAO detection in response to phenobarbital treatment were performed in rat primary hepatocytes.

The results of the effect of 1 mM phenobarbital on rat primary hepatocytes are presented in Figure 4-15, on page 94.

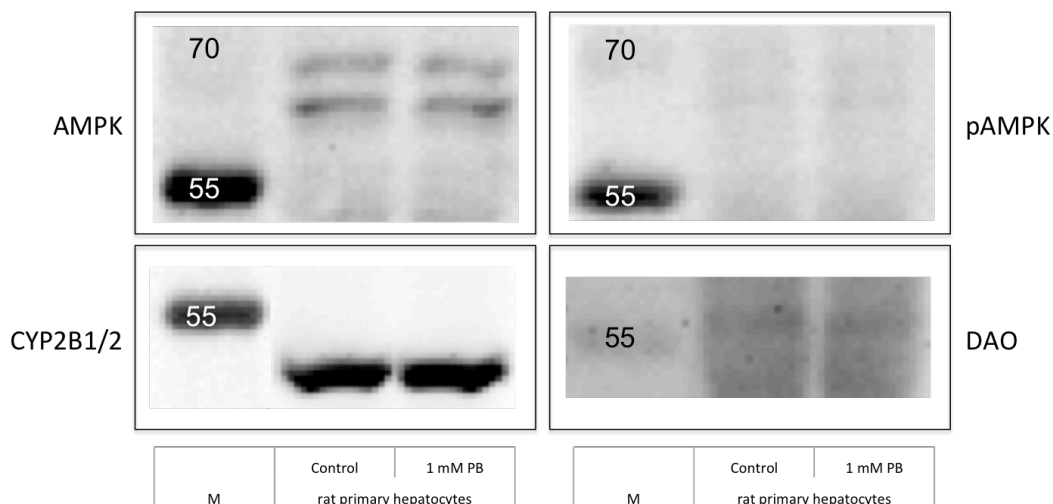


Figure 4-15: Effect of phenobarbital in the detection of D-amino acid oxidase (DAO), CYP2B1/2 and AMPK phosphorylation (pAMPK) from rat primary hepatocytes.

As seen in Figure 4-15, rat primary hepatocytes treated with 1 mM phenobarbital show no differences to control regarding AMPK detection and the drug also does not promote the phosphorylation of AMPK at its threonine 172. Similarly, CYP2B1 or CYP2B2 detection is also not affected by the phenobarbital stimulus. Finally, DAO is not detected in either control or treated rat primary hepatocytes.

The results here presented are sufficient to question the published data regarding western blot methods as a readout system for the effect of phenobarbital in rat hepatocytes from both primary and hepatoma origins.

An alternative method of detection for all the previously described markers was developed, using mRNA expression as a readout system.

#### 4.2.2.6. Effect of phenobarbital on CYP2B1 and CYP2B2 mRNA expression in rat hepatocytes

Reverse-transcription polymerase chain reaction (RT-PCR) is a well-established method to evaluate the effect of compounds in living cells. A semi-quantitative RT-PCR method was used to compare treated samples to controls. Extracted RNA and synthesized cDNA was quantified and loaded in the same amounts at each step for all samples, and the housekeeping gene *G3PDH* was used as internal control to confirm equal loading between samples. Detailed methods are described in 4.3.6 RT-PCR, on page 107.

Non-treated MH<sub>1</sub>C<sub>1</sub> cells were used initially to establish the RNA extraction and cDNA synthesis protocols, followed by specific amplification of the housekeeping gene *G3PDH*. The quality of each step was analyzed by agarose gel electrophoresis and is presented in Figure 4-16, on page 95.

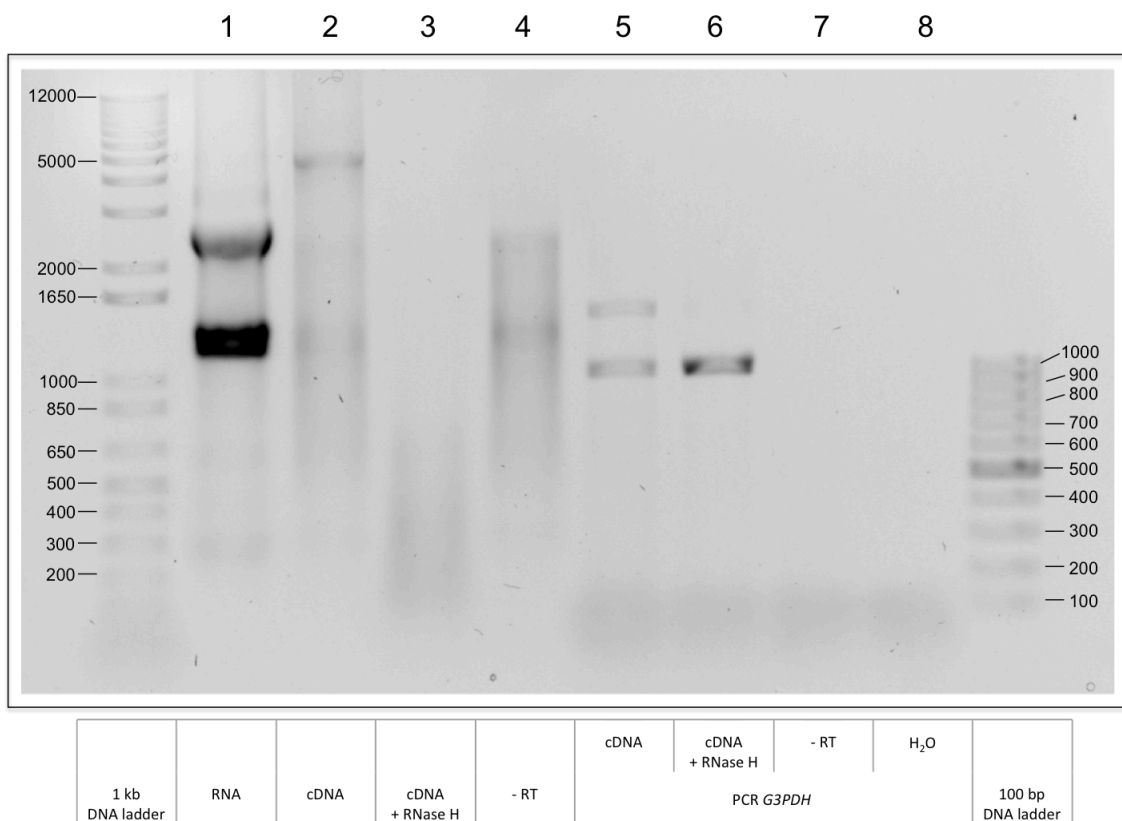


Figure 4-16: Agarose gel electrophoresis of RNA, cDNA and PCR products. Quality control for RNA extraction from *MH<sub>1</sub>C<sub>1</sub>* cells, cDNA synthesis and PCR for the housekeeping gene *G3PDH*

As seen on Figure 4-16, lane 1, total RNA was successfully extracted from the rat hepatoma cell line and the 28S and 18S rRNA bands are clearly visible. The reverse transcription of poly-A mRNA was also successful although some remaining RNA is still detected after purification of the cDNA (Figure 4-16, lane 2), which can be specifically degraded by adding RNase H after the cDNA synthesis (Figure 4-16, lane 3). The purification process done in a sample without reverse transcriptase (Figure 4-16, lane 4) shows the same leftover RNA but no additional impurities. To confirm cDNA quality, the specific amplification of the housekeeping gene *G3PDH* was done in both cDNA samples (Figure 4-16, lanes 5 and 6) containing or not RNase H and a single intense band at the expected 983 bp confirms that samples should be treated with the RNase H enzyme after cDNA synthesis. Additional negative controls (Figure 4-16, lanes 7 and 8) in pure water or lacking the reverse transcriptase enzyme were amplified with the specific primers for *G3PDH* but presented no visible band, confirming the quality of the samples and the specificity of the PCR.

Having confirmed each step of the RNA extraction, cDNA synthesis and gene-specific PCR, *MH<sub>1</sub>C<sub>1</sub>* cells treated with either 1 mM or 2 mM phenobarbital were subjected to the same protocol. Untreated *MH<sub>1</sub>C<sub>1</sub>* cells and rat liver tissue were used as controls to monitor the expression of *CYP2B1*, as was previously tested by western blot but yielded no discernible results (see Results 4.2.2.3 Induction of cytochrome P450 (CYP) 2B1 and 2B2, on page 91).

Figure 4-17, on page 96, clearly shows an increase of *CYP2B1* mRNA expression upon treatment with phenobarbital.

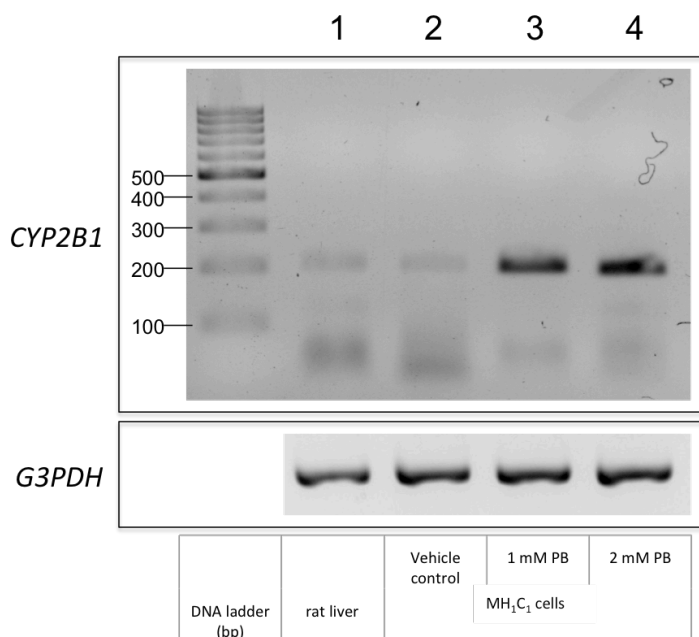


Figure 4-17: Effect of phenobarbital on CYP2B1 mRNA expression in a rat hepatoma cell line. MH<sub>1</sub>C<sub>1</sub> cells were treated with 1 or 2 mM phenobarbital (PB) and one vehicle control (0.9% NaCl) over-night at 37 °C (5% CO<sub>2</sub>). Total RNA was extracted from the cells and the mRNA was specifically transcribed into cDNA using a reverse transcriptase and oligo (dT)<sub>20</sub> primers. RNA extraction and cDNA synthesis was also done from a rat liver sample. CYP2B1 was amplified by PCR using specific primers and the product was run on a 2% agarose gel in TBE. The expected amplification product is 204 bp (top panel). The housekeeping gene G3PDH was used as loading control (bottom panel).

Rat liver tissue and MH<sub>1</sub>C<sub>1</sub> cells have the same level of CYP2B1 mRNA expression (Figure 4-17, lanes 1 and 2, top panel). The rat hepatoma cell line when treated with phenobarbital increases the production of CYP2B1 mRNA (Figure 4-17, lanes 3 and 4). The results of the effect of phenobarbital on the expression of the cytochrome P450 are confirmed by the unchanged intensity of the housekeeping gene G3PDH used as loading control (Figure 4-17, lane 1 – 4, bottom panel).

This phenotypic assay was replicated and more genes were probed for changes with phenobarbital treatment in primary rat hepatocytes. Figure 4-18, shows the effects of 1 mM phenobarbital treatment on the expression of D-amino acid oxidase (DAO), cytochrome P450 2B1 (CYP2B1) and cytochrome P450 2B2 using two different pairs of primers that amplify different regions of the gene (CYP2B2 and CYP2B2.1). Again, the housekeeping gene G3PDH was used as loading control.

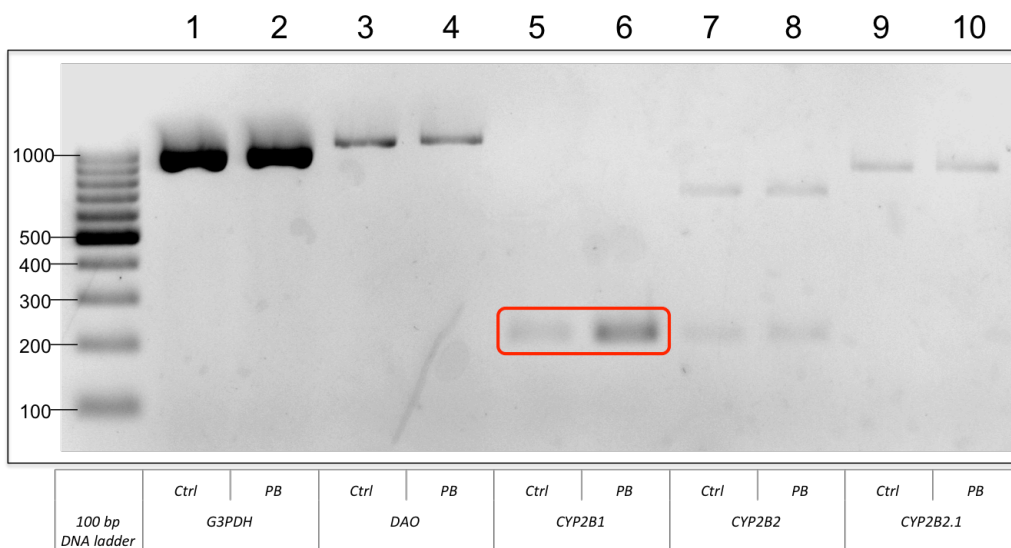


Figure 4-18: Effect of phenobarbital on CYP2B1 mRNA expression in rat primary hepatocytes. Rat primary hepatocytes ( $1 \times 10^6$  cells) were seeded in a 6-well plate with supplemented William's E medium and allowed to adhere and differentiate for 6 hours. The cells were then treated with 1 mM phenobarbital (PB) and 0.9% NaCl vehicle control (Ctrl) over-night at 37 °C (5% CO<sub>2</sub>). Total RNA was extracted from the cells and the mRNA was specifically transcribed into cDNA using a reverse transcriptase and oligo (dT)<sub>20</sub> primers. Target genes were amplified by PCR using specific primers and the products run on a 2% agarose gel in TBE.

Rat primary hepatocytes were treated with 1 mM phenobarbital and monitored for the effect on the expression of mRNA from different genes. The similar level of expression of *G3PDH* in control (Ctrl) and treated (PB) samples allows to establish that any difference observed in other amplification products is due to amount of sample (Figure 4-18, lanes 1 and 2).

Previous western blot results (Figure 4-15, on page 94) had failed to elucidate whether rat primary hepatocytes contained DAO. In Figure 4-18, it is clear that these cells express *DAO* mRNA but its expression is not affected by treatment with phenobarbital (Figure 4-18, lanes 3 and 4). One of the analyzed cytochrome P450 mRNA (*CYP2B2*) did not show a visible increase in expression after phenobarbital stimulus even when analyzing the gene expression with two different sets of specific primers (Figure 4-18, lanes 7 – 10).

The expression of *CYP2B1* mRNA from rat primary hepatocytes, however, is clearly increased after phenobarbital treatment (Figure 4-18, lanes 5 and 6), as highlighted in the red box, confirming the same effect observed previously in  $MH_1C_1$  cells (Figure 4-17, on page 96).

These results confirm the establishment of a working phenotypic assay for the effect of phenobarbital in rat liver cells. This effect can be monitored by semi-quantitative RT-PCR of *CYP2B1* mRNA expression. This also confirms that both rat primary hepatocytes and  $MH_1C_1$  cells can be used to identify specific binding partners of phenobarbital in living cells through the previously established CCMS using click chemistry.

### 4.2.3. Capturing phenobarbital targets in $MH_1C_1$ cell lysate

The initial experiment to identify phenobarbital targets was performed in lysate from the rat hepatoma  $MH_1C_1$  cell line. Only phenobarbital capture compounds A (CC 10) and C (CC 12) were used because, as described previously, compound B (CC 11) did not yield sufficient amounts for a comprehensive study. Also, even though the permeability of compound C (CC 12) was determined as being low (see 4.2.1 Determining permeability of phenobarbital-alkyne capture compounds, on page 84), the initial approach was designed in lysate, where compound permeability does not play a role, in order to cast a wider net for the identification of putative phenobarbital targets.

Three separate experiments were performed (I, II and III) with varying compound and competitor (CC 15) concentrations, as well as individual and combined data analyses. Detailed information on the experiment protocol is described in the Specific Methods section 4.3.7 Capture of phenobarbital targets in  $MH_1C_1$  cell lysate, on page 109.

Table 4–2 on the following page shows the summary of the identifications on the individual experiments or in combined analysis. More specifically, results were combined for both capture compounds in each experiment or for all experiments to allow for an investigative analysis on the reproducibility of the CCMS outcome.

Compound	Experiment									
	I			II			III		I+II+III	
	CC10	CC12	CC10 + CC12	CC10	CC12	CC10 + CC12	CC10 1 $\mu$ M 5 $\mu$ M		CC10	CC12
<b>Total proteins identified</b>	1190	1181	1265	920	958	1013	976	2020	2020	1460
<b>Student's t-test &lt; 0.05 (% of total)</b>	123 (10%)	26 (2.2%)	18 (1.4%)	25 (2.7%)	175 (18%)	126 (12%)	55 (5.6%)	17 (0.8%)	2 (0.1%)	2 (0.1%)
<b>Assay/Competition fold-change &gt; 2 (% of total)</b>	139 (12%)	74 (6.3%)	133 (11%)	48 (5.2%)	41 (4.3%)	51 (5.0%)	33 (3.4%)	70 (3.5%)	146 (7.2%)	98 (4.9%)
<b>Competed and significant proteins (% of total)</b>	37 (3.1%)	5 (0.4%)	2 (0.2%)	0 (0%)	8 (0.8%)	2 (0.2%)	2 (0.2%)	7 (0.3%)	2 (0.1%)	0 (0%)

Table 4–2: Summary of identifications from phenobarbital capture experiments in  $MH_1C_1$  cell lysate.

Three different experiments (I, II and III), each consisting of multiple technical replicates, were analyzed for putative targets of two different phenobarbital capture compounds (CC10 and CC12). These results were analyzed with MaxQuant v.1.3.0.3 in an independent manner or in combination (symbolized by +)

Table 4–2 shows that the total number of identifications between experiments varied between 920 and 2020 but more strikingly that putative targets for phenobarbital, here referred to as competed and significant hits, spans from none to 37 using the same compound.

An extensive analysis on each individual and combined result could be presented but the variability of results would confound the analysis. To find the minimal common denominator all experiments performed with the permeable compound CC10 were analyzed together, treating samples as technical replicates, and 2 proteins are identified as significantly competed by phenobarbital (Table 4–2, I+II+III, CC10).

The first, Wdr1, also known as WD repeat\* -containing protein 1, has a fold-change of 11.8 between assays and competitions with a calculated  $p$ -value of 0.024. According to Uniprot, this protein induces disassembly of actin filaments and is involved in platelet degranulation. Its association to any commonly reported phenobarbital effect is at first glance distant, but it has been published that phenobarbital increases the expression of Wdr1 mRNA in mouse liver phenobarbital-induced tumors and is dependent on CAR since the same effect was not observed in tumors from CAR knock-out mice (supplementary tables S3E and S3I in Phillips and Goodman<sup>149</sup>). The direct implication of this putative direct binder of phenobarbital should be further investigated since WD-repeat containing proteins are known to be involved in several important biological functions such as signal transduction, transcription regulation and are associated with different human diseases<sup>156</sup>. It is interesting to note that RACK1, a protein thought to have a role in phenobarbital effect<sup>142</sup>, as described in the Introduction section, is a WD-repeat protein.

Ybx1 was also found to be significantly competed by phenobarbital with a fold-change of 2.6 and  $p$ -value of 0.046. Ybx1, known as nuclease-sensitive element-binding protein 1, would as well appear not to be related to known phenobarbital effects in a superficial analysis. However, an alternative name for this protein, CCAAT-binding transcription factor I subunit A suggests otherwise. As described in the introduction, CYP2B genes possess a phenobarbital responsive enhancer module

\* WD repeat proteins are defined by the presence of four or more repeating units containing a conserved core of approximately 40 amino acids that usually end with tryptophan-aspartic acid (WD)

(PBREM) composed by a binding site for nuclear factor-1 (NF-1) flanked by two DR-4 nuclear receptor (NR) binding sites for a heterodimer of constitutive androstane receptor (CAR) and retinoid X receptor (RXR)<sup>132,157</sup>. Interestingly, NF-1 binds to a so-called Y-box or CCAAT-box, much like Ybx1<sup>158–160</sup>. Among several functions attributed to Ybx1, there is another association of this protein to a known phenobarbital effect, namely regarding the small molecule's interaction with EGFR<sup>161</sup>. Ybx1, also referred to as YB-1, was shown to bind to the EGFR promoter and reducing YB-1 levels resulted in the down-regulation of EGFR<sup>162</sup>. The capture of Ybx1 with the phenobarbital capture compound suggests a direct binding and, given the function of this protein in the regulation of several genes, this could be a contributing factor to the cellular pleiotropic effect of phenobarbital.

In order not to lose information on each individual experiment, a comparison between the different results using a scoring method (as previously done in 3.2.4 Capturing in living K562 cells, Table 3–8, on page 72) was used to retrieve the most relevant putative hits for phenobarbital capture in MH<sub>1</sub>C<sub>1</sub> lysate. Analyzing the data with values based on MS-positive identifications (LFQ values in MaxQuant software), a total of 19 hits were identified in more than one experiment and the fold-change and corresponding *p*-values are presented in Table 4–3, on page 100. This list includes the previously described Wdr1 and Ybx1 but also reveals other interesting hits regarding previously described associations with phenobarbital interacting mechanisms. Running a STRING interaction analysis, two clusters of interacting proteins are revealed (Figure 4-19) and a pathway analysis indicates that AMPK pathway proteins are enriched in this list, namely the different subunits of PP2A phosphatase that has been described in the EGFR signaling pathway in the introduction (see Figure 4-2: Phenobarbital induces CYP2B expression via EGFR inhibition, on page 83).

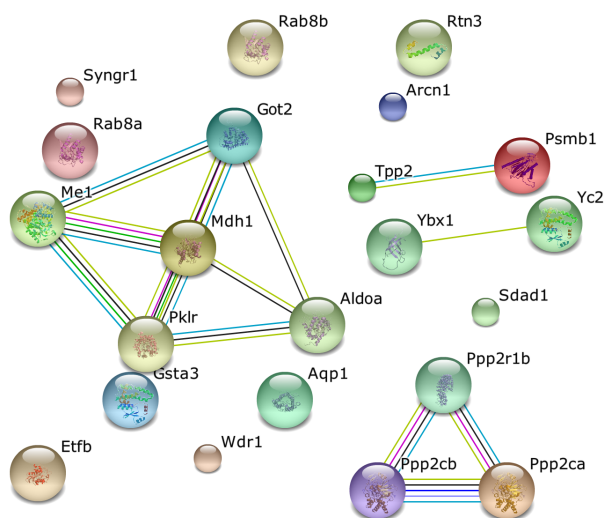


Figure 4-19: STRING protein interaction analysis of significantly competed proteins in phenobarbital capture experiments in MH<sub>1</sub>C<sub>1</sub> lysate  
Blue: binding; black: reaction; pink: post-translational modification; purple: catalysis; green: association in curated databases.

Three proteins were identified in 3 different experiments as phenobarbital binder candidates: Psmb1, Aqp1 and Gsta3/Gsta5. Psmb1 is a proteasome subunit that has been mentioned to increase its mRNA expression upon phenobarbital stimulus, but this effect was only observed in a subset of the experiment and its relevance remains dubious<sup>163</sup>. A surprising hit was

Aqp1, aquaporin-1, which regulates the influx of water in cells. It has been described that phenobarbital increases and decreases Aqp1 mRNA expression and that CAR is involved in the process<sup>164,165</sup>. Interestingly, Aqp1 and the larger aquaporin family of proteins play a relevant role in epilepsy<sup>166–168</sup>, the initial therapeutic use of phenobarbital. Lastly, glutathione S-transferase alpha subunits (Gsta3/Gsta5) were targeted by phenobarbital in the capture experiments. This family of proteins is involved in the protection against stress sensors in the cellular environment and its stimulation by phenobarbital is well established in the literature<sup>169</sup>.

Experiment	Specificity (Assay / Competition)																	Score				
	Intensity fold-change (log <sub>2</sub> )									Student's t-test (p value)												
	I		II*		III		I+II+III			I		II*		III		I+II+III						
compound	CC10	CC12	CC10	CC12	CC10	CC10	CC12	CC10 + CC12	CC10	CC12	CC10	CC12	CC10	CC10	CC12	CC10	CC12	CC10 + CC12				
Gene name	10 μM	10 μM	10 μM	10 μM	1 μM	5 μM	1 μM	5 μM	10 μM	10 μM	10 μM	10 μM	10 μM	1 μM	5 μM	1 μM	5 μM	1 μM	5 μM	10 μM	10 μM	10 μM
Aqp1	0.3	<b>12.6</b>	1.0	<b>1.1</b>	0.1	0.3	0.3	<b>3.4</b>	0.6	0.233	<b>0.028</b>	0.189	<b>0.028</b>	0.880	0.669	0.480	0.085	0.142	3			
Gsta3;Gsta5	<b>2.8</b>	0.1	#N/I	#N/I	0.7	<b>1.7</b>	<b>2.3</b>	0.1	<b>1.8</b>	<b>0.033</b>	0.552	#N/I	#N/I	0.219	<b>0.030</b>	0.175	0.917	0.170	3			
Psemb1	<b>12.9</b>	0.2	#N/I	-7.2	<b>1.2</b>	<b>9.5</b>	<b>5.7</b>	0.1	<b>1.6</b>	<b>0.014</b>	0.900	#N/I	0.423	0.627	<b>0.036</b>	0.100	0.933	0.189	3			
Aldoa	<b>2.0</b>	-0.8	-1.0	-0.9	0.7	<b>1.6</b>	<b>1.6</b>	-0.8	0.8	<b>0.001</b>	0.489	0.238	<b>0.022</b>	0.400	0.061	0.225	0.533	0.398	2			
Arcn1	0.2	-0.1	-0.3	-0.6	0.4	<b>8.7</b>	0.2	-0.1	0.1	0.312	0.772	0.088	<b>0.029</b>	<b>0.016</b>	<b>0.005</b>	0.858	0.922	0.936	2			
Etfb	<b>11.8</b>	#N/I	#N/I	#N/I	<b>9.8</b>	<b>9.6</b>	<b>10.5</b>	#N/I	<b>10.2</b>	0.500	#N/I	#N/I	#N/I	<b>0.003</b>	0.188	0.082	#N/I	0.082	2			
Got2	<b>3.0</b>	0.1	-0.5	-0.6	0.9	<b>1.3</b>	<b>1.9</b>	-0.2	<b>1.5</b>	<b>0.036</b>	0.879	<b>0.012</b>	<b>0.047</b>	0.142	0.244	0.118	0.763	0.125	2			
Mdh1	<b>1.0</b>	0.1	-0.5	-0.6	<b>1.2</b>	<b>1.5</b>	1.0	#N/I	0.6	0.247	0.961	<b>0.041</b>	<b>0.035</b>	<b>0.048</b>	0.092	0.415	0.997	0.464	2			
Me1	<b>3.5</b>	-1.0	-0.6	-0.9	<b>1.4</b>	<b>2.5</b>	<b>2.4</b>	-1.0	<b>1.5</b>	0.063	0.716	0.199	<b>0.032</b>	0.091	<b>0.010</b>	0.117	0.575	0.175	2			
Pklr	#N/I	#N/I	-1.0	-0.7	0.8	<b>1.3</b>	0.6	-0.7	0.4	#N/I	#N/I	0.272	0.165	0.152	<b>0.016</b>	0.211	0.473	0.398	2			
Ppp2cb;Ppp2ca	<b>1.7</b>	<b>12.4</b>	#N/I	#N/I	-5.6	<b>6.5</b>	<b>1.6</b>	<b>11.0</b>	<b>2.5</b>	0.255	<b>0.046</b>	#N/I	#N/I	0.391	0.389	0.389	0.179	0.107	2			
Ppp2r1b	-11.5	-11.1	0.6	<b>8.7</b>	-4.5	0.4	-2.9	-1.9	-2.4	0.500	0.500	0.702	<b>0.001</b>	0.391	0.391	0.340	0.509	0.224	2			
Rab8a;Rab8b	<b>11.2</b>	<b>1.0</b>	#N/I	#N/I	#N/I	-12.0	<b>11.2</b>	<b>1.0</b>	<b>2.1</b>	<b>0.024</b>	0.482	#N/I	#N/I	#N/I	0.391	0.164	0.532	0.145	2			
Rtn3	#N/I	#N/I	0.6	<b>2.4</b>	0.8	<b>10.2</b>	<b>1.0</b>	<b>2.4</b>	<b>1.2</b>	#N/I	#N/I	0.162	<b>0.035</b>	0.437	0.391	0.258	0.146	0.139	2			
Sdad1	-0.3	-0.1	<b>1.2</b>	<b>7.7</b>	#N/I	0.9	-0.3	-0.1	-0.2	0.071	0.891	0.132	<b>0.013</b>	0.912	0.211	0.839	0.960	0.854	2			
Syng1	-0.3	<b>12.3</b>	<b>1.6</b>	<b>2.7</b>	-0.9	0.4	-0.2	<b>6.0</b>	0.6	0.395	0.109	0.162	<b>0.013</b>	0.434	0.391	0.854	0.133	0.490	2			
Tpp2	<b>1.5</b>	<b>1.4</b>	-0.3	-0.2	<b>1.3</b>	1.0	<b>1.2</b>	<b>1.0</b>	<b>1.1</b>	0.317	0.342	<b>0.050</b>	0.353	<b>0.015</b>	0.179	0.268	0.375	0.150	2			
Wdr1	#N/I	#N/I	#N/I	#N/I	<b>12.1</b>	<b>11.2</b>	<b>11.8</b>	#N/I	<b>11.8</b>	#N/I	#N/I	#N/I	#N/I	<b>0.001</b>	0.391	<b>0.024</b>	#N/I	<b>0.026</b>	2			
Ybx1	#N/I	#N/I	-6.7	<b>5.3</b>	<b>7.9</b>	<b>3.3</b>	<b>2.6</b>	<b>4.6</b>	<b>2.7</b>	#N/I	#N/I	0.423	0.423	0.067	<b>0.023</b>	<b>0.041</b>	0.374	<b>0.038</b>	2			

Table 4–3: Potential hits for phenobarbital in a rat hepatoma cell line (MH<sub>1</sub>C<sub>1</sub>) from 3 individual experiments using a MS-based analysis

(I - III) each consisting of 2 – 4 replicates for assays and competitions using two pre-clicked phenobarbital capture compounds (CC10 and CC12). Values in bold mark specific (log<sub>2</sub> fold-change > 1) and significant (p value < 0.05) results for a given experiment. Score is calculated by the sum of number of results that fulfilled both the criteria of specificity and significance. #N/I : not identified. \*CC10 subset of experiment II was analyzed individually with MaxQuant software and was added to the score calculations.

#### 4.2.4. Capture of phenobarbital targets in living MH<sub>1</sub>C<sub>1</sub> cells

The capture of phenobarbital targets in living cells was done to improve upon the already successful results obtained in the capture experiments from lysate samples and establish a new method for the identification of small-molecule binding partners that better resembles the delivery system of drugs in living organisms.

The experiment was done with living MH<sub>1</sub>C<sub>1</sub> cells using triplicates of assays and competitions and the detailed protocol is described in the Specific Methods section 4.3.8 Capture of phenobarbital targets in living MH<sub>1</sub>C<sub>1</sub> cells, on page 110.

Table 4–4 gathers the summary of the identifications in each subset of the experiment.

	Pre-clicked		Click	
	Alignment-based	MS-based	Alignment-based	MS-based
<b>Total proteins identified</b>	740	735	1363	1362
<b>Student's t-test &lt; 0.05 (% of total)</b>	41 (5.5%)	43 (5.9%)	52 (3.8%)	44 (3.2%)
<b>Assay/Competition fold-change &gt; 2 (% of total)</b>	16 (2.2%)	33 (4.5%)	21 (1.5%)	49 (3.6%)
<b>Competed and significant proteins (% of total)</b>	2 (0.3%)	1 (0.1%)	1 (0.1%)	1 (0.1%)

Table 4–4: Summary of identifications from phenobarbital capture experiments in MH<sub>1</sub>C<sub>1</sub> living cells. List of proteins was obtained using MaxQuant v1.3.0.3. Numbers for identifications based on spectral counts (MS-based) and alignment-based are given.

One immediate observation of Table 4–4 is that a larger number of proteins is identified in samples where the click reaction was done after the photo-crosslink to the target, 740 vs. 1363 where the capture compound was pre-clicked to the biotin anchor during the cell incubation. The difference in numbers could be explained by the probable impermeability of the larger pre-clicked compound, preventing it to diffuse into the cell and therefore mainly targeting surface proteins or only after endocytosis. A different perspective suggests that the larger number of identifications in click samples could be due to unspecific capture inherent to the CuAAC reaction, although initial experiments (described in Chapter 2. Labeling a protein using click chemistry) show that the CuAAC is rather clean but with low yields.

Even though a large number of proteins were identified, only four pass the competition and reproducibility criteria. The values for these putative phenobarbital binders are presented in Table 4–5, on the following page.

Protein  <i>Gene name</i>	Specificity (Assay / Competition)					
	Total MS counts		Alignment-based		MS-based	
	Assay	Comp.	Intensity fold-change (log <sub>2</sub> )	Student's t-test ( <i>p</i> value)	Intensity fold-change (log <sub>2</sub> )	Student's t-test ( <i>p</i> value)
	<i>Pre-click</i>					
<b>Them6</b>	11	5	<b>1.6</b>	<b>0.002</b>	<b>1.4</b>	<b>0.014</b>
<b>Anxa4</b>	1	1	<b>1.2</b>	<b>0.022</b>	<b>9.6</b>	0.423
	<i>Click</i>					
<b>Arf5</b>	3	0	<b>4.5</b>	<b>0.032</b>	-7.9	0.423
<b>Dnm2</b>	3	0	0.1	0.761	<b>12.7</b>	<b>0.008</b>

Table 4–5: List of competed and significant hits in phenobarbital capture experiments in MH<sub>1</sub>C<sub>1</sub> living cells. Total MS counts from technical replicates (*n* = 3) of assay and competition (comp.) samples. Intensity fold-change and significance levels are given for specificity (assay versus competition) of hits. Values in bold indicate either FC>2 or *p*val<0.05.

The list of proteins identified in the capture experiment using phenobarbital in living MH<sub>1</sub>C<sub>1</sub> cells, presented in Table 4–5, do not coincide with the previously described putative binders obtained with the capture in lysate of the same cell line. There is, however, a common denominator to all these identified proteins: EGFR.

Them6 is a rather uncharacterized thioesterase with only seven references on Pubmed and 9 known protein interactions. The thioesterases, or thioester hydrolases, comprise a large enzyme group whose members hydrolyze the thioester bond between a carbonyl group and a sulfur atom. Interestingly, Them6 has been co-immunoprecipitated with EGFR<sup>170</sup> and was also previously identified as a potential phenobarbital target in Experiment B of the capture in MH<sub>1</sub>C<sub>1</sub> lysate described in the previous paragraph (the alignment-based values for Them6 revealed a log<sub>2</sub> fold-change between assays and competitions of 1.3 with an associated *p*-value of 0.002).

Annexin A4, Anxa4, is a calcium/phospholipid-binding protein that promotes membrane fusion and is involved in exocytosis. Anxa4 has clinical significance in cancer<sup>171</sup>, and even if this specific member of the annexin family has not been described in EGFR transduction context, several other annexins have been associated with endocytosis and EGFR signaling<sup>172,173</sup>.

Arf5, also known as ADP-ribosylation factor 5 is a GTP-binding protein that is involved in protein trafficking<sup>174</sup> and recently found to co-localize with EGFR in A431 cells<sup>175</sup>.

Dnm2, Dynamin-2, is a microtubule-associated force-producing protein involved in producing microtubule bundles and able to bind and hydrolyze GTP. Dnm2 plays an important role in vesicular trafficking processes, in particular endocytosis<sup>176</sup>. Association of Dnm2 to EGFR has also been described in multiple publications as an EGF-induced EGFR-associated protein<sup>177,178</sup>.

Once again, results seem to point towards a connection with EGFR, in line with Mutho's recent findings<sup>142</sup>, but the question that remains is why isn't EGFR captured in these experiments. Are these the true phenobarbital binders that establish the connection between EGFR signaling and phenobarbital phenotypic effect or are these interacting proteins captured due to unspecific cross-linking to neighboring proteins inherent to the design of capture compounds? It can also be postulated that EGFR peptides are not identified in the CCMS experiments because the attached capture compound alters the mass of the peptides and affects the analysis in the database search.

#### 4.2.5. Capturing phenobarbital targets in tissue with high EGFR expression

With piling evidence that phenobarbital targets proteins related to EGFR, and given the recent publication of Mutoh and co-workers<sup>142</sup> that confirms EGFR as a target for phenobarbital, it would be interesting to verify if capture experiments determine the receptor as a primary binder, or if the associated proteins identified in the previous paragraphs are still preferential to the drug in a tissue expressing high levels of EGFR.

According to the Human Protein Atlas, a tissue-based map of the human proteome<sup>179</sup>, trophoblastic cells from placenta present a high expression of EGFR protein.

Human placenta lysate was used as sample to identify phenobarbital targets using a complete pre-clicked phenobarbital capture compound. Detailed protocol is described in Specific Methods section 4.3.9 Capture of phenobarbital targets in human placenta lysate, on page 111.

	Pre-click		
	Alignment-based	MS-based	
<b>Total proteins identified</b>	2054	2047	<i>Table 4–6: Summary of identifications from phenobarbital capture experiment in human placenta lysate. List of proteins was obtained using MaxQuant v1.3.0.3. Numbers for identifications based on spectral counts (MS-based) and alignment-based are given.</i>
<b>Student's t-test &lt; 0.05 (% of total)</b>	80 (3.9%)	64 (3.1%)	
<b>Assay/Competition fold-change &gt; 2 (% of total)</b>	51 (2.5%)	78 (3.8%)	
<b>Competed and significant proteins (% of total)</b>	4 (0.2%)	3 (0.1%)	

From over 2000 protein identifications, only 6 were competed by phenobarbital in a reproducible manner. These identifications, summarized in Table 4–6, yield different results when analyzing the values based on alignment features or exclusively on sequenced peptides, with only one significantly competed target identified in both methods.

The list of significantly competed proteins with phenobarbital in human placenta lysate is presented in Table 4–7.

Protein	Specificity (Assay / Competition)					
	Total MS counts		Alignment-based		MS-based	
	Assay	Comp.	Intensity fold-change (log <sub>2</sub> )	Student's t-test (p value)	Intensity fold-change (log <sub>2</sub> )	Student's t-test (p value)
<i>Gene name</i>						
<b>SRP72</b>	52	37	<b>2.4</b>	<b>&lt;0.001</b>	0.2	0.087
<b>YBX1/3/5</b>	4	3	<b>1.5</b>	<b>0.001</b>	<b>13.3</b>	<b>&lt;0.001</b>
<b>MICALL1</b>	4	1	<b>1.7</b>	<b>0.011</b>	<b>1.4</b>	0.378
<b>TMEM97</b>	3	4	<b>1.1</b>	<b>0.045</b>	<b>1.3</b>	0.073
<b>MESDC2</b>	3	1	0.1	0.673	<b>12.4</b>	<b>&lt;0.001</b>
<b>GAK</b>	3	2	0.8	<b>0.047</b>	<b>12.2</b>	<b>&lt;0.001</b>
<b>EGFR</b>	33	30	0.1	0.761	0.14	0.129

*Table 4–7: List of competed and significant hits in phenobarbital capture experiments in human placenta lysate. Total MS counts from technical replicates (n = 3) of assay and competition (comp.) samples. Intensity fold-change and significance levels are given for specificity (assay versus competition) of hits. EGFR is added separately for failing criteria. Values in bold indicate either FC>2 or pval<0.05.*

The first observation of the phenobarbital capture experiment in a tissue expressing high levels of EGFR is that the receptor is indeed captured but the competition with free phenobarbital competitor does not exceed the two-fold ratio between assays and competitions, nor is the confidence level of the identifications acceptable.

Interestingly, the only positive identification using either an alignment or MS-based analysis is YBX, the previously described Y-box-binding protein identified as a target in rat hepatoma cell lysate. The results in placenta do not allow for a definite identification of the YBX isoform since the quantified peptide is common to YBX1, YBX3 and YBX5. Data suggests it to be YBX1, just as in the MH<sub>1</sub>C<sub>1</sub> cell lysate experiment, because an additional YBX1 peptide was identified although without a significant competition effect.

The other identified putative targets for phenobarbital are also described to have an association to EGFR, with the exception of the signal recognition particle subunit SRP72. MICALL1, Molecule Interacting with CasL (MICAL)-like1 protein, has been described to be involved in receptor-mediated endocytosis and, in complex with Rab protein, regulates EGFR trafficking<sup>180</sup>. Cyclin G-associated kinase (GAK) is a serine/threonine kinase with a relevant role in cellular traffic of clathrin-coated vesicles and it was shown that its down-regulation resulted in an enhancement of EGFR signaling<sup>181</sup>. Although not directly associated with EGFR, MESDC2 is a chaperone protein specifically assisting the beta-propeller/EGF modules within the family of low-density lipoprotein receptors<sup>182</sup> and transmembrane protein TMEM97 was correlated with EGFR in a study from Tong *et al.*<sup>178</sup>.

To overcome the incongruous results obtained when using a different value output from the MaxQuant analysis software and the way each contributing peptide generates the intensity for a whole protein, the experimental data obtained from the phenobarbital capture in human placenta lysate was analyzed at the peptide level. Out of 12188 identified peptides only 710 (6%) were competed and of these only 26 (0.2%) were identified with a *p* value of less than 0.05.

These 26 unique peptides, peptides corresponding exclusively to a specific protein, were submitted to the protein interaction database STRING and revealed an intricate network that shows EGFR and YBX1 as central nodes (Figure 4-20).

Gathered evidence suggests that phenobarbital binds primarily to YBX1 and there is a high affinity towards proteins associated to EGFR signaling.

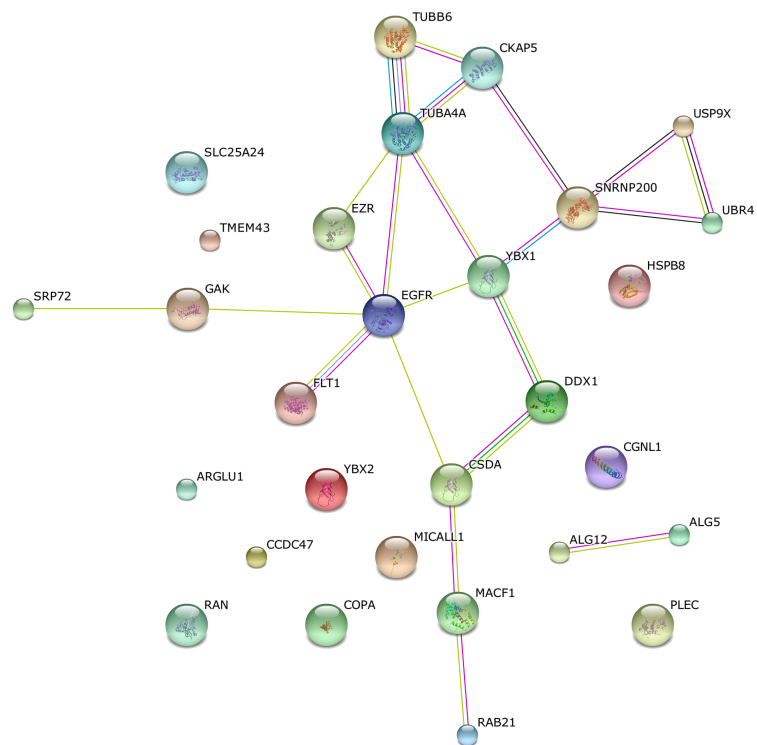


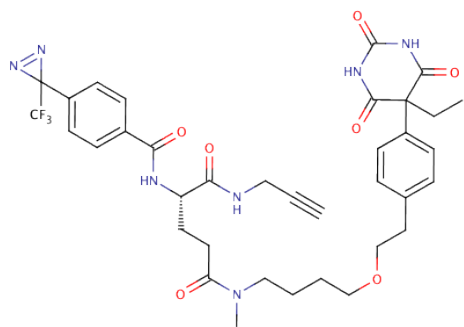
Figure 4-20: STRING protein interaction analysis of significantly competed proteins in phenobarbital capture experiments in human placenta lysate.

Blue: binding; pink: post-translational modification; purple: catalysis; green: association in curated databases.

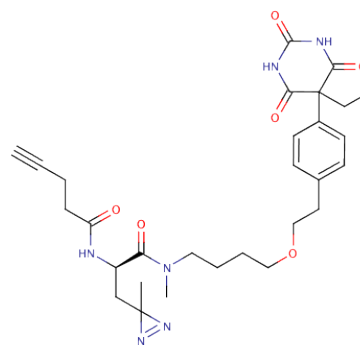
## 4.3. SPECIFIC METHODS FOR THE PHENOBARBITAL SYSTEM

### 4.3.1. Structures of used compounds

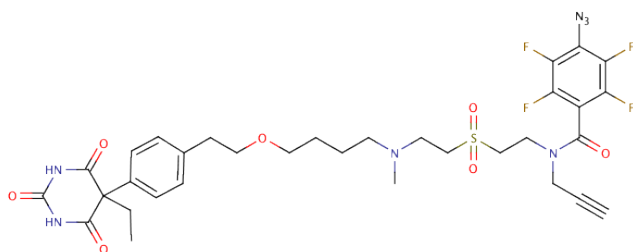
CC 10: Clickable phenobarbital alkyne capture compound A (contains selectivity and a trifluoromethyl-phenyl-diazirine photoreactive functions)



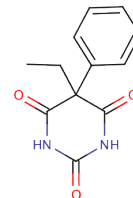
CC 11: Clickable phenobarbital alkyne capture compound B (contains selectivity and a methyl-diazirine photoreactive functions)



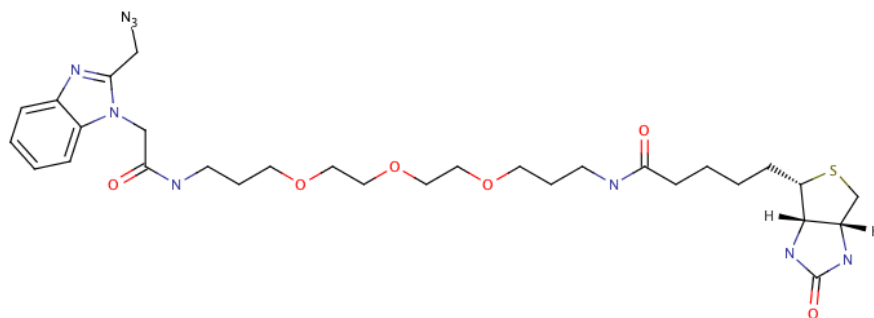
CC 12: Clickable phenobarbital alkyne capture compound C (contains selectivity and a azido-tetrafluorobenzene photoreactive functions)



CC 15: Phenobarbital competitor



CC 7: Clickable biotin-PEG copper-chelating azide (contains labeling and copper ligand functions)



### 4.3.2. Treatment of MH<sub>1</sub>C<sub>1</sub> cells with phenobarbital

The rat hepatoma cell line MH<sub>1</sub>C<sub>1</sub> was treated with increasing concentration of phenobarbital for the analysis of CAR translocation, AMPK phosphorylation and CYP2B1/2B2 analysis by Western Blotting.

MH<sub>1</sub>C<sub>1</sub> cells in DMEM (10% FBS, 1% pen/strep) were seeded in 6-well plates at  $2 \times 10^6$  cells/well and incubated over-night at 37 °C (5% CO<sub>2</sub>). Confluent cells were starved over-night by removing the medium and adding serum-free DMEM.

Phenobarbital diluted in DMEM was added to the wells at different concentrations: 0, 1 μM, 10 μM, 100 μM, 250 μM and 500 μM. Plates were incubated at 37 °C (5% CO<sub>2</sub>) for 1 h, 2 h, 4 h or 6 h.

After treatment, the medium was removed and the cells were washed with 1 mL D-PBS. Cells were scraped in 1 mL of fresh D-PBS and transferred to 1.5 mL microtubes for cellular fractionation (as described in 4.3.3 Subcellular fractionation of MH<sub>1</sub>C<sub>1</sub> cells, below).

The cellular fractions and the unfractionated samples were resolved on a SDS-PAGE and transferred to a nitrocellulose membrane for specific antibody probing as described in the general methods section (6.2 Biochemistry General Methods, on page 118).

### 4.3.3. Subcellular fractionation of MH<sub>1</sub>C<sub>1</sub> cells

MH<sub>1</sub>C<sub>1</sub> cell pellets from culture in 6-well plates for phenobarbital treatment were fractionated using the NE-PER® Nuclear and Cytoplasmic Extraction kit (Pierce Biotechnology™).

Cells were scraped in 1 mL D-PBS and transferred to 1.5 mL microtubes to pellet by centrifugation at 500 *xg* for 3 min. The supernatant was carefully removed with a micropipette and discarded, leaving a dry pellet with  $\approx 15 \mu\text{L}$  of packed volume. 150 μL of ice-cold CER I reagent was added to the cell pellet and the tube was stirred in a vortex at maximum speed for 15 seconds to resuspend the cells. The tube was incubated on ice for 10 min. 8.25 μL of ice-cold CER II reagent was added to the tube, following 5 seconds vortex and 1 min incubation on ice. The tube was again vortexed for 5 seconds and centrifuged for 5 min at 17.000 *xg*. The supernatant containing the cytoplasmic fraction was transferred to a clean pre-chilled tube and stored at -80 °C. The remaining pellet, containing the nuclei, was resuspended in 75 μL of NER reagent. The tube was vortexed at maximum speed for 15 seconds every 10 min for a total of 40 min, keeping it on ice in between. The tube was centrifuged for 10 min at 17.000 *xg* and the supernatant containing the nuclear extract was transferred to a pre-chilled clean tube and stored at -80 °C.

### 4.3.4. Treatment of MH<sub>1</sub>C<sub>1</sub> cells with high concentration of phenobarbital

MH<sub>1</sub>C<sub>1</sub> cells in DMEM (10% FBS, 1% pen/strep) were seeded in 6-well plates at  $2 \times 10^6$  cells/well and incubated over-night at 37 °C (5% CO<sub>2</sub>). Confluent cells were starved for 2.5 h by removing the medium and adding serum-free DMEM. Phenobarbital diluted in 0.9% NaCl at a final concentration of 0, 1 mM or 2 mM was added to the wells and incubated over-night at 37 °C (5% CO<sub>2</sub>). The medium was removed and the cells were washed with 1 mL D-PBS.

To the wells for protein analysis, 100 μL of 2X Laemmli Buffer (containing benzonase) was added to disrupt the cells. The samples were transferred to microtubes, sonicated and boiled, and stored at -20 °C until analysis by SDS-PAGE and Western Blotting (as described in the general methods section (6.2 Biochemistry General Methods, on page 118).

For RT-PCR analysis, the cells were processed as described in 4.3.6 RT-PCR, on page 107.

### 4.3.5. Treatment of rat primary hepatocytes with phenobarbital

Rat primary hepatocytes were plated as described in the General Methods section (6.1.4 Rat primary hepatocytes culture, on page 117).

The cells were incubated over-night with 1 mM phenobarbital diluted in 0.9% NaCl. The medium was removed and the hepatocytes were washed with 1 mL D-PBS.

To the wells for protein analysis, 100  $\mu$ L of 2X Laemmli Buffer (containing benzoylcholine) was added to disrupt the cells. The samples were transferred to microtubes, sonicated and boiled, and stored at -20 °C until analysis by SDS-PAGE and Western Blotting (as described in the general methods section (6.2 Biochemistry General Methods, on page 118).

For RT-PCR analysis, the cells were processed as described below.

### 4.3.6. RT-PCR

Reverse-transcription polymerase chain reaction (RT-PCR) is a commonly used technique to semi-quantitatively measure the expression of specific genes. RNA is converted into a complementary DNA (cDNA) library that can then be probed for target genes using appropriate primers. One of the advantages of this technique is the need for very little sample quantity to detect the targets of interest.

#### 4.3.6.1. RNA extraction using RNeasy Protect Mini Kit

RNA was extracted from either MH<sub>1</sub>C<sub>1</sub> cells or rat primary hepatocytes in culture, treated or not with phenobarbital, using a commercially available kit from Qiagen™ (RNeasy Protect Mini Kit).

1 x 10<sup>7</sup> cells were collected to a 15 mL Falcon tube and lysed in 600  $\mu$ L RLT buffer (supplemented with DTT). The tube was vortexed and the lysate was homogenized by passing it five times through a 20-gauge needle attached to a RNA-free sterile syringe. 600  $\mu$ L of 70% ethanol was added to the tube and mixed by pipetting. The solution was divided and transferred to two RNeasy spin columns placed in 2 mL microtubes. The samples were spun down for 30 s at 10.000 *xg*. The flow-through was discarded and 700  $\mu$ L of buffer RW1 was added to the spin column. The tubes were centrifuged 30 s at 10.000 *xg*. 500  $\mu$ L of RPE buffer was added to the spin column and again centrifuged 30 s at 10.000 *xg*. Fresh 500  $\mu$ L of RPE buffer was added to the column and the tubes spun down for 2 min at 10.000 *xg*. The spin column was transferred to a clean 2 mL microtube and spun down for 1 min at maximum speed (16.000 *xg*). The spin column was placed in a clean 1.5 mL microtube and RNA was eluted with 40  $\mu$ L of RNase-free water. The column was centrifuged 1 min at 10.000 *xg* to elute the RNA. Samples were snap frozen in liquid nitrogen and stored at -80 °C until further use.

#### 4.3.6.2. RNA quantification and purity calculation

Nucleic acids have absorbance maxima at 260 nm. Historically, the ratio of this absorbance maximum to the absorbance at 280 nm has been used as a measure of purity in both DNA and RNA extractions. A 260/280 ratio of approximately 1.8 is generally accepted as “pure” for DNA; a ratio of approximately 2.0 is generally accepted as “pure” for RNA.

Extracted RNA from MH<sub>1</sub>C<sub>1</sub> cells and rat primary hepatocytes was diluted in PBS (pH 7.4) and the absorption at 260 nm and 280 nm was measured in a Varian Cary 50 Bio UV-Vis Spectrophotometer.

The purity of RNA was calculated according to the formula:  $\frac{A_{260}(\text{sample}) - A_{260}(\text{blank})}{A_{280}(\text{sample})}$ .

The concentration of RNA was determined by:

$$C = \frac{A_{260}(\text{sample}) - A_{260}(\text{blank})}{25} \times \text{dilution factor}.$$

The obtained RNA concentrations from different extractions varied between 0.5 µg/µL and 1 µg/µL with a purity always higher than 2.

#### 4.3.6.3. cDNA synthesis from extracted mRNA

1 µg of total RNA extracted from MH<sub>1</sub>C<sub>1</sub> cells, rat primary hepatocytes or rat liver tissue was reverse-transcribed into cDNA using the Superscript III reverse transcriptase kit from Invitrogen™.

1 µL of oligo(dT)<sub>20</sub> primers at 50 µM was mixed with 1 µg of total RNA, 1 µL of dNTP mix at 10 mM and water to normalize volume to 13 µL. The mixture was heated for 5 min at 65 °C in a thermomixer and placed on ice for over 1 min. The tubes were spun down and added 4 µL of 5x First Strand Buffer, 1 µL of DTT at 0.1 M and 1 µL SuperScript III reverse-transcriptase (at 200 U/µL). The samples were mixed by gently pipetting and incubated for 60 min at 50 °C in a thermomixer. The reaction was inactivated by heating 15 min at 70 °C. 1 µL of RNase H was added for 20 min at 37 °C in some cases to remove RNA complementary to the first strand cDNA.

#### 4.3.6.4. Polymerase Chain Reaction (PCR) of specific genes

The cDNA library from MH<sub>1</sub>C<sub>1</sub> cells, rat primary hepatocytes or rat liver tissue, treated or not with phenobarbital, was used as template to search for specific genes: *CYP2B1* (using two different pairs of primers), *CYP2B2*, *DAO* and *G3PDH* as a housekeeping gene control. The sequences for the primers are described below:

	Forward primer	Reverse primer	Expected product
<i>G3PDH</i>	5'-TGAAGGTCGGTGTCAACGGATTTGGC-3'	5'-CATGTAGGCCATGAGGTCCACCAC-3'	983 bp
<i>CYP2B1</i>	5'-CTGTGGGTCATGGAGAGCTG-3'	5'-TCACACCGGCTACCAACCCT-3'	201 bp
<i>CYP2B2</i>	5'-CTGTGGGTCATGGAGAGCTG-3'	5'-TCTCACAGGCACCATCCCT-3'	201 bp
<i>CYP2B2.1</i>	5'-GCTCTCCTGTGGGCTTCTT-3'	5'-AGGACTCACTTCTCCATGCG-3'	804 bp
<i>DAO</i>	5'-ATCCTGCTGGAGACAGGTC-3'	5'-TCTCCTCCATCACTCCATC-3'	1510 bp

The optimization of the different parameters of PCR, such as cDNA input amount, MgCl<sub>2</sub> concentration, primer concentration, and number of cycles, was done according to the Taguchi method<sup>183</sup>.

The final parameters used for the experiments presented in the results section (4.2.2.6 Effect of phenobarbital on CYP2B1 and CYP2B2 mRNA expression in rat hepatocytes, on page 94) were:

	cDNA	F. primer	R. primer	10x PCR buffer	dNTP mix	<i>T.aq</i> polymerase	MgCl <sub>2</sub>	H <sub>2</sub> O
Volume (μL)	1.5	2	2	5	1	0.2	1.5	38.3

#### 4.3.6.5. Agarose gel electrophoresis

RNA quality and PCR products were analyzed by horizontal agarose gel electrophoresis.

0.8% – 1.2% (w/v) agarose gels were prepared by mixing the weighed amount of agarose in 50 mL of Tris/Borate/EDTA (TBE) buffer. The solution was boiled in a microwave and cooled down before adding 3 μL of SYBR® Safe dye and casting onto the electrophoresis tray.

The tray containing the gel was immersed in the electrophoresis unit filled with TBE buffer and samples mixed with 6x loading dye were loaded in the wells. Appropriate DNA ladders were added as reference. The gel electrophoresis was carried out for 45 min at 100 V and bands visualized using a UV trans-illuminator in an Imaging System (Syngene G:BOX XT4).

#### 4.3.7. Capture of phenobarbital targets in MH<sub>1</sub>C<sub>1</sub> cell lysate

MH<sub>1</sub>C<sub>1</sub> cell lysate was prepared as described in the General Methods (6.1.3.1 MH<sub>1</sub>C<sub>1</sub> lysate preparation, on page 117).

Full pre-clicked capture compounds were prepared *a priori*: 500 μM of biotin copper-chelating-azide (CC 7) was equilibrated with 5 mM of CuSO<sub>4</sub> for 10 min at R.T. and then reacted with 500 μM of phenobarbital-alkyne capture compound (CC 10 or CC 12) in PBS at pH 8.5 by adding 2.5 mM of sodium ascorbate. The reaction was shaken vigorously for 10 min at R.T.

400 μg of MH<sub>1</sub>C<sub>1</sub> cell lysate was distributed in 200 μL PCR-tube strips and either 330 μM or 1 mM of phenobarbital competitor (CC 15) was added to the competition samples or the corresponding volume of DMSO was added to the assay samples. The vials were incubated for 30 min on ice and then added 5 μM or 10 μM of pre-clicked phenobarbital-biotin capture compound. All samples were incubated for 60 min rotating at 4 °C and then irradiated for 15 min at 310 nm in a caproBox™ to promote photo-crosslinking of the compounds to the binding targets. Streptavidin-coated magnetic beads were washed with PBS and incubated with the samples for 1 h rotating at 4 °C. The beads were recovered using a caproMag™ and then washed six times with wash buffer followed by three times wash with 80% acetonitrile and a final wash with MS-grade water.

0.5 μg of trypsin in ammonium bicarbonate was added to the beads and incubated over-night shaking at 37 °C. The supernatant containing the tryptic digest was recovered to clean tubes; next, the beads were washed with MS-grade water and the wash solution pooled with the original supernatant. All samples were lyophilized and analyzed by LC-MS/MS following the protocol described in the General Methods section (6.3 Mass Spectrometry, on page 121).

#### 4.3.8. Capture of phenobarbital targets in living MH<sub>1</sub>C<sub>1</sub> cells

MH<sub>1</sub>C<sub>1</sub> cells were seeded on 6-well plates in DMEM, supplemented with 10% FBS and 1% penicillin/streptomycin, and grown to 85% confluence in a cell incubator at 37 °C (5% CO<sub>2</sub>). The medium was removed and the cells were washed with D-PBS to starve with serum-free DMEM for 2 h at 37 °C (5% CO<sub>2</sub>).

A pre-clicked phenobarbital capture compound (CC 10) with a biotin-copper chelating azide (CC 7) was produced *a priori*: 500 µM of biotin copper-chelating-azide (CC 7) was equilibrated with 5 mM of CuSO<sub>4</sub> for 10 min at R.T. and then reacted with 500 µM of phenobarbital-alkyne capture compound (CC 10) in PBS at pH 8.5 by adding 2.5 mM of sodium ascorbate. The vial was shaken vigorously for 10 min at R.T.

2 mM of phenobarbital competitor (CC 15) or equivalent volume of DMSO diluted in fresh medium was added to the competition wells or to the assay, respectively. 20 µM of phenobarbital capture compound (CC 10) as is or pre-clicked to biotin (CC 10-CC 7) was then added to the wells. The plates were returned for 35 min to the cell incubator. The medium was removed and the cells washed with fresh D-PBS. The plates were placed in a CaproBox™ and irradiated for 4 min at 310 nm. The cells were recovered to tubes with scraping and pelleted for 10 min at 400 xg.

The cells treated with the pre-clicked compound were lysed for 30 min shaking vigorously with 1 mL of RIPA buffer (50 mM Tris-HCl pH 8.0, 150 mM NaCl, 1% IGEPAL CA-630, 0.5% Sodium deoxycholate, 0.1% SDS) supplemented with 0.2 mM DTT, 0.5 µL/mL benzonase and proteinase inhibitors. The samples incubated with the unclicked phenobarbital capture compound were lysed in 500 µL of Lysis Buffer E as described in 6.1.3.1 MH<sub>1</sub>C<sub>1</sub> lysate preparation, on page 117. The crude lysates from both preparations were transferred to 500 µL eppies and centrifuged for 30 min at 17.000 r.p.m. to remove cell debris.

The CuAAC reaction was performed in the samples containing the unclicked capture compound by adding 5 µM of biotin copper-chelating-azide (CC 7) (pre-equilibrated with two-times excess CuSO<sub>4</sub>), 10 µM BTTE (CC 18) pre-equilibrated with two-times excess CuSO<sub>4</sub>, and 2.5 mM of sodium ascorbate. The click reaction ran for 30 min shaking at room temperature.

Streptavidin-coated magnetic beads were washed with PBS and incubated with the samples for 30 min rotating at 4 °C. The beads were recovered using a caproMag™ and then washed six times with wash buffer followed by three times wash with 80% acetonitrile and a final wash with MS-grade water.

0.5 µg of trypsin in ammonium bicarbonate was added to the beads and incubated over-night shaking at 37 °C. The supernatant containing the tryptic digest was recovered to clean tubes; next, the beads were washed with MS-grade water and the wash solution pooled with the original supernatant. All samples were lyophilized and analyzed by LC-MS/MS following the protocol described in the General Methods section (6.3 Mass Spectrometry, on page 121).

#### 4.3.9. Capture of phenobarbital targets in human placenta lysate

Human placenta tissue was purchased from in.Vent, Berlin-Hennigsdorf, and was obtained according to relevant ethical guidelines with informed consent of donor.

400  $\mu$ L of human placenta lysate, containing around 2000  $\mu$ g protein, from the BioBank at caprotec bioanalytics, were incubated with phenobarbital competitor (CC 15) at 2 mM final concentration or with equivalent volume of DMSO in case of control samples and 5X Capture Buffer. The samples were equilibrated for 20 min rotating at 4 °C.

Full pre-clicked capture compounds were prepared *a priori*: 500  $\mu$ M of biotin copper-chelating-azide (CC 7) was equilibrated with 5 mM of  $\text{CuSO}_4$  for 10 min at R.T. and then reacted with 500  $\mu$ M of phenobarbital-alkyne capture compound (CC 10) in PBS at pH 8.5 by adding 2.5 mM of sodium ascorbate. The reaction was shaken vigorously for 10 min at R.T.

Streptavidin-coated magnetic beads were pre-loaded with the pre-clicked phenobarbital capture compound using excess capture compound to saturate the beads, shaking for 5 min at room temperature. The excess unbound capture compound was removed and the beads were washed two times with Capture Buffer.

The pre-loaded magnetic beads with phenobarbital capture compound were added to the samples and incubated for 2 h rotating at 4 °C. The beads were then collected using a caproMag™ and resuspended in 100  $\mu$ L of Capture Buffer. The suspended beads were irradiated for 4 min (two times 2 min, shaking the tubes in between) at 310 nm in a caproBox™ to promote photo-crosslinking. The magnetic beads were recovered using a caproMag™ and then washed six times with wash buffer followed by three times wash with 80% acetonitrile and a final wash with MS-grade water.

0.5  $\mu$ g of trypsin in ammonium bicarbonate was added to the beads and incubated over-night shaking at 37 °C. The supernatant containing the tryptic digest was recovered to clean tubes; next, the beads were washed with MS-grade water and the wash solution pooled with the original supernatant. All samples were lyophilized and analyzed by LC-MS/MS following the protocol described in the General Methods section (6.3 Mass Spectrometry, on page 121).

## 5. Conclusions and Outlook

---

The current challenges in drug discovery have strengthened the development of new technologies for target deconvolution in an unbiased approach to identify unwanted off-targets or reveal a new path for development early in the pipeline. Recent developments in chemical proteomics associated to advances in quantitative mass spectrometry have enabled the detection and quantification of low abundant binders or drug-induced changes in protein expression with large proteome coverage.

Capture compound mass spectrometry (CCMS) introduced a novel design for small molecule probes that allow the identification of low abundant and lower affinity targets in a complex biological sample. The capture compounds traditionally consist of a selectivity function carrying the small molecule under study that is attached to a scaffold bearing a tag for visualization or enrichment, such as a fluorophore or biotin, and also a protruding photo-reactive moiety with enough distance and flexibility from the central core to covalently bind the probe to the surface of the target protein.

One of the major limitations of capture compounds in their originally published design and other affinity-based probes is that most cannot permeate through cells due to their size, reducing the application to cell-surface targets or the need to prepare lysates if the aimed protein is intracellular. The drawback of working with protein lysates is that not all cellular proteins are easily solubilized, thus excluding part of the proteome, and the lysis process might in fact alter the native conformation of proteins, which can affect the interaction with the drug molecule. Subcellular fractionation instead of full lysate has been developed as a strategy to overcome some of these obstacles.

Bio-orthogonal chemistry was initially developed to study post-translational modifications but quickly expanded to a broader use to study dynamics and function of biomolecules. Several reactant pairs have been developed but the azide and alkyne reaction still remain the better suited for living cell applications due to their reduced size. The biggest disadvantage of this bio-orthogonal ligation is the need to accelerate it with metals, copper being the most widely used, which can induce stress in cells. Advances in the technology were made with the introduction of chelating agents that improve the reaction kinetics and reduce the metal-induced stress.

Establishing a new drug deconvolution method that allows the identification of targets in their natural cell environment was set as a primary goal in this research project. The strategy was to combine the strength of capture compounds in the enrichment of low abundant and lower affinity targets with the versatility of bio-orthogonal ligation chemistry. The new probe design would allow it to be small enough and increase cell permeability to target intracellular proteins and specifically capture them with a controlled chemical click reaction. One main advantage of such a workflow would be to identify drug-binding proteins directly under conditions that are used in phenotypic screening-based drug discovery.

A modified capture compound bearing cAMP as selectivity function and a photo-reactivity function, but having a reactive alkyne instead of the traditional labeling function, was synthesized to establish copper-assisted azido-alkyne cycloaddition (CuAAC) click chemistry in the context of CCMS. The optimization steps to establish the click reaction conditions were initially established in a solution of recombinant PKARI, the subunit of protein kinase A that binds cAMP. A biotin-azide was

used as label to monitor this reaction and results were analyzed by western blot. The initial experiments confirmed the specific nature of the azido-alkyne cycloaddition where no signal was observed in samples lacking the capture compound (Figure 2-2, on page 32) but also showed that the signal was a fraction of the one obtained with a classical cAMP capture compound. Different parameters from the CuAAC reaction were modified to improve the labeling of PKARI such as copper and ligands concentrations; time and pH of reaction; biotin-azide and alkyne capture compound concentrations; and a new fluorescent label that promised to be better suited for the labeling of complex samples, such as cellular lysates. The optimization efforts yielded some improvement from the initial experiments but still did not achieve the same results as with the classical cAMP capture compound.

Capturing PKA subunits from cell lysates with the optimized parameters proved to be sub-optimal when using the new click workflow and comparing it to results obtained with the classical cAMP capture compound. Although the results suggested an enrichment of PKA-related peptides, the intensity ratio between assays and competitions and their statistical significance did not allow for a conclusive analysis on the performance of the method. The lack of competition in several experiments proved to be a challenge if further efforts would be made to resolve this issue, especially when the subsequent step would be to establish the click capture in living cells, where the natural concentration of cAMP is very high. Nevertheless, the system was useful to establish technical aspects of the click reaction in the context of the use of capture compounds. However, because of the impermeability of cAMP as such, a different selectivity function was required for the next steps. With this in mind, a new non-natural selectivity function was used for target identification in cell lysates and living cells using the new click reaction.

The kinase inhibitor drug Dasatinib was used for its clinical relevance and well-known targets. Concomitantly to this new alkyne dasatinib capture compound, a new azide was also produced in collaboration with the group of Taran, from the CEA Saclay, member of the BioChemLig consortium. The new azide, bearing the biotin or fluorescent TAMRA as tags, also had a copper-chelating moiety that better accelerated the cycloaddition reaction. The well characterized target profile of dasatinib was well suited as reference to judge the effectiveness of the new approach. A previously published study on living cell capture with a dasatinib probe failed to produce a meaningful target profile<sup>92</sup>, so there was obvious room and need for a better workflow. Using the dasatinib capture compound pre-clicked to the copper-chelating biotin allowed for the successful identification of *bona fide* dasatinib targets in a BCR-ABL-positive cell lysate, such as ABL1, ABL2, BCR and SRC, as well as other kinases (Table 3-2 and Figure 3-5, on page 61). Even though the new click workflow did not produce the same results as the full compound in lysate, these proteins were enriched when comparing to the negative control but were not competed enough by free dasatinib to pass the inclusion criteria of two-times fold-change and *p* value less than 0.05. Other known dasatinib inhibited kinases were successfully identified using this protocol.

Searching for dasatinib targets in living cells showed that a large number of biological and technical replicates is necessary to achieve statistical significance when probing living cells. Individually, each experiment consisting of technical replicates yielded very different results regarding potential targets (Table 3-7, on page 70). Calculating the intensity differences between assays and competitions of all experiments as one or attributing a re-incidence score allowed a better understanding of the results. In fact, using this strategy, known dasatinib targets were

competitively identified for the first time in living cells, with special relevance to the C-Src kinase (CSK), as well as the *bona fide* dasatinib-binder ABL1/ABL2.

Having successfully implemented the capture of small molecule targets in living cells, the new methodology was used to identify new binders for phenobarbital, a drug that has been in use for 100 years and still has unknown mechanisms of action regarding its toxicity. The hepatocarcinogenic effect of phenobarbital in some species was the focus of this endeavor, and at the time experiments were being performed it was not known that EGFR could bind phenobarbital and elicit a cellular response, as published by Mutoh *et al.* in 2013<sup>142</sup>.

In order to later be able to associate capture results to phenotypic effects, the first objective was to implement a phenotypic assay that would serve as a validation method once the phenobarbital target candidate was identified by mass spectrometry. Several systems were tested, such as AMPK phosphorylation or CAR translocation that according to literature happens upon phenobarbital stimulation, but the results obtained did not confirm that and could therefore not be used as reliable readouts. The constitutive androstane receptor (CAR) was already found in the nucleus of unstimulated cells and AMPK phosphorylation was cyclic making them poor candidates as a validation method. The successful phenotypic assay turned out to be the expression of cytochrome P450 2B1 mRNA that clearly increases upon high dosage of phenobarbital (Figure 4-18, on page 96) in both rat hepatoma cell line and primary hepatocytes. Unfortunately, by the time mass spectrometry results indicated potential targets to be validated, there was no further possibility to continue the research due to time constraints.

The mass spectrometry analysis of the initial capture experiments using a pre-clicked phenobarbital capture compound in lysate from a rat hepatoma cell line provided interesting results. Most of the putative hits had been previously associated to some phenobarbital effect and some had also known interactions with EGFR. In those experiments, subunits from the phosphatase PP2A responsible for the de-phosphorylation of AMPK and RACK1, the EGFR-associated kinase that aids the translocation of CAR to the nucleus, were identified as candidate binders of phenobarbital. Even more interestingly, Wdr1 and Ybx1 were also presented as putative targets of phenobarbital. The first being a WD repeat-containing protein, characteristic shared with RACK1, and the second a protein that binds Y-boxes, specific sequences in gene promoters, that are part of the phenobarbital response enhancer module (PBREM) present in CYP2B genes.

Results from capture experiments with phenobarbital probes in living MH<sub>1</sub>C<sub>1</sub> cells continued pointing towards a connection to the EGFR signaling pathway. Different proteins were identified depending on whether the capture compound was pre-clicked or not, but all have documented association with EGFR: a thioesterase (Them6) and annexin A4 (Anxa4) were identified as potential targets in samples probed with a complete phenobarbital capture compound; and ADP-ribosylation factor 5 (Arf5) and dynamin-2 (Dnm-2) were found as binders in samples with the clickable phenobarbital capture compound.

All the identifications in the phenobarbital experiments directed the attention for EGFR but this protein was never specifically captured. To answer the posing question of whether the receptor was not targeted because it is not a direct binder of phenobarbital or if it was only due to low abundance in the sample, a last experiment was performed in a tissue that expresses high levels of EGFR. The results from the capture in human placenta lysate confirmed some previously identified proteins as putative targets of phenobarbital and its connection to the EGFR signaling pathway, but

the receptor itself was not competed by phenobarbital. A recurrent candidate as the primary binder of phenobarbital was YBX1, and given its role as transcription factor and direct binder of EGFR, the pleiotropic effects and the modulation of the EGFR signaling cascade in response to phenobarbital treatment could be explained. Further validation is necessary to confirm that YBX1 is inhibited by phenobarbital.

A point of concern, in hindsight, is that the phenotypic effect elicited by phenobarbital only occurs at high compound concentrations, close to the millimolar range, suggesting low affinity towards the pathway under study. To further pursue CCMS in living cells with permeable capture compounds, the focus should be on more potent small molecules, eliciting effects in the nanomolar range.

Amongst the drug target deconvolution techniques, CCMS remains the most robust and with higher potential to innovate. At the time, probing living cells with bio-orthogonal capture compounds is a reality but the results are still far from ideal. Efforts must be put in reducing background of capture and mass spectrometry methods as well as experimenting with new clickable pairs that allow for a better reaction yield and, consequently, better identifications.

In my opinion, the best strategy presently for drug target deconvolution is to firstly identify which subcellular structures contain the target, using bio-orthogonal reactions and microscopy analysis, fractionate and enrich those organelles and then use CCMS in those subproteomes.

## 6. General Methods and Materials

---

### 6.1. CELL CULTURE

#### 6.1.1. HEK293 cell culture

Human embryonic kidney (HEK) cells, clone 293, were used in cAMP/PKA capture experiments (as described in 2. Labeling a protein using click chemistry, on page 28).

HEK293 cells were cultured in Dulbecco's Modified Eagle Medium (DMEM) supplemented with 10% heat-inactivated fetal bovine serum (FBS) and 1% of penicillin/streptomycin in a 5% CO<sub>2</sub> incubator at 37 °C. The cells were subcultured at a 1:5 – 1:6 dilution every 2-3 days by mechanical detachment.

##### 6.1.1.1. HEK293 lysate preparation

HEK293 cell pellets were lysed in 2X their volume with a hypotonic buffer (10 mM HEPES pH7.9, 1.5 mM MgCl<sub>2</sub>, 10 mM KCl) containing or not 0.5% (w/v) DDM. Both buffers were supplemented with proteinase inhibitors and benzonase at the time of lysis. After 30 min incubation on ice, the lysate was dounced 20X using a tight pestle and then run through a 21G needle with a syringe. Remaining debris was pelleted by refrigerated centrifugation at 15.000 rpm for 30 min. The supernatant was recovered and the leftover pellet was discarded. Aliquots were made and snap-frozen in liquid nitrogen. Samples were stored at -80 °C until use.

#### 6.1.2. K562 cell culture

Human K562 cells originate from a chronic myeloid leukemia in blast crisis, and were used in the identification of dasatinib targets experiments (as described in 3. Identifying Dasatinib targets in cells, on page 54).

K562 cells were cultured in RPMI-1640 medium supplemented with 10% heat-inactivated fetal bovine serum (FBS) and 1% penicillin/streptomycin in a 5% CO<sub>2</sub> incubator at 37 °C. The cells were split every 3 days at a 1:3 – 1:5 dilution by pelleting the suspension cells for 10 min at 1000 xg.

##### 6.1.2.1. K562 lysate preparation

K562 cell pellets were lysed in either (1) RIPA buffer (50 mM Tris-HCl pH 8.0, 150 mM NaCl, 1% IGEPAL® CA-630, 0.5% (w/v) sodium deoxycholate, 0.1% (w/v) SDS) supplemented with 0.2 mM DTT; or (2) Lysis Buffer E (50 mM Tris-HCl, 100 mM NaCl, 1.5 mM MgCl<sub>2</sub>, 0.2% (v/v) IGEPAL® CA-630, 0.5% (w/v) DDM, 5% (v/v) glycerol) supplemented with 1 mM DTT. Both buffers were additionally supplemented with proteinase inhibitors and 0.5 µL/ml benzonase.

After 30 min incubation on ice, the lysate was dounced 20X using a tight pestle and then run through a 21G needle with a syringe. Remaining debris was pelleted by refrigerated centrifugation at 15.000 rpm for 30 min. The supernatant was recovered and the leftover pellet was discarded. Aliquots were made and snap-frozen in liquid nitrogen. Samples were stored at -80 °C until use.

### 6.1.3. MH<sub>1</sub>C<sub>1</sub> cell culture

A rat clonal strain of epithelial cells derived from Morris hepatoma #7795, MH<sub>1</sub>C<sub>1</sub> cell line, was used in phenobarbital experiments (as described in 4. Phenobarbital: new binders for an old drug, on page 81).

MH<sub>1</sub>C<sub>1</sub> cells were cultured in Dulbecco's Modified Eagle Medium (DMEM) supplemented with 10% heat-inactivated fetal bovine serum (FBS) and 1% penicillin/streptomycin in a 5% CO<sub>2</sub> incubator at 37 °C. The cells were split using trypsin/EDTA once or twice per week at a 1:2 – 1:4 dilution.

#### 6.1.3.1. MH<sub>1</sub>C<sub>1</sub> lysate preparation

MH<sub>1</sub>C<sub>1</sub> cell pellets were lysed in Lysis Buffer E (50 mM Tris-HCl, 100 mM NaCl, 1.5 mM MgCl<sub>2</sub>, 0.2% (v/v) IGEPAL® CA-630, 0.5% (w/v) DDM, 5% (v/v) glycerol) supplemented with 1 mM DTT, proteinase inhibitors and 0.5 µL/ml benzonase.

After 30 min incubation on ice, the lysate was dounced 20X using a tight pestle and then run through a 21G needle with a syringe. Remaining debris was pelleted by refrigerated centrifugation at 15,000 rpm for 30 min. The supernatant was recovered and the leftover pellet was discarded. Aliquots were made and snap-frozen in liquid nitrogen. Samples were stored at -80 °C until use.

### 6.1.4. Rat primary hepatocytes culture

Rat (male Sprague-Dawley) cryopreserved hepatocytes were used in phenobarbital experiments (as described in 4. Phenobarbital: new binders for an old drug, on page 81).

The cryopreserved hepatocytes were thawed in a 37 °C water bath for less than 2 min and transferred to a pre-warmed tube containing Williams Medium E and Hepatocyte Plating Supplement Pack (Thermo Fisher Scientific). The cells were centrifuged at 55 xg for 3 min at room temperature.

The supernatant was discarded and 1 mL per 1 x 10<sup>6</sup> cells of plating medium was added. The hepatocytes were diluted and seeded in collagen I-coated 24-well plates at a concentration of 8 x 10<sup>5</sup> cell per well (500 µL). The plate was incubated for 4 h at 37 °C to allow adherence and formation of monolayer. After incubation the plate was agitated to release unattached debris and the medium was aspirated and replaced with fresh complete medium.

The rat primary hepatocytes were used for RT-PCR experiments (as described in 4.3 Specific methods for the phenobarbital system, 4.3.6 RT-PCR, on page 107).

## 6.2. BIOCHEMISTRY GENERAL METHODS

### 6.2.1. Protein concentration determination

Total protein concentration from cell lysates was determined using the commercially available BCA Protein Assay Reagent (Pierce™, Prod. #23225). The BCA Protein Assay was introduced by Smith, et al. in 1985<sup>184</sup>. The main benefit of this assay is the compatibility with a wide range of detergents normally used in cellular lysates. The assay relies on a colorimetric detection of copper reduction by bicinchoninic acid (BCA).

A standard curve of bovine serum albumin (BSA) (Pierce™, Prod #23209) was prepared in a dilution series using the same lysis buffer of the cellular lysate to be quantified. The samples to be quantified were also diluted (1:4 – 1:20) in buffer to assure the measurement is within the range of the standards.

10 µL of BSA standard or sample were pipetted in triplicates into a 96-well flat-bottom plate and 200 µL of working reagent (50:1, reagent A : reagent B) were added to the wells. The plates were incubated for 30 min at 37°C and the light absorbance read in a multiplate reader (Anthos 2010, Anthos Mikrosysteme GmbH) with a 562 nm filter.

The values were inserted in a spreadsheet and the average of the standards was used to plot and calculate a linear regression curve. The total protein concentration in the samples was calculated by inference and corrected for the dilution factor.

### 6.2.2. SDS-PAGE

Sodium Dodecyl Sulfate Polyacrylamide Gel Electrophoresis (SDS-PAGE) is a protein analytical method established by Maizel<sup>185</sup> in 1963 as an advancement of the original PAGE developed by Weintraub in 1959<sup>186</sup>. The current method mostly used around the world was optimized by Laemmli in 1970<sup>187</sup>. For an insight on the development and establishment of SDS-PAGE as a reference protein analytical method see Maizel's review published in 2000<sup>188</sup>.

Protein solutions, cellular lysates or whole cells were mixed with Laemmli Buffer to a final 1X concentration (50 mM Tris-base, 2.5% (w/v) SDS, 10% Glycerol, 0.32 mM β-mercaptoethanol, bromophenol blue). Samples were loaded on pre-casted 4-20% Tris-Glycine gels (anamed Elektrophorese GmbH, Germany) and proteins were separated for 35 min at 300V on a XCell SureLock® Mini-Cell electrophoresis chamber (Life Technologies™ GmbH, Germany) filled with SDS Running Buffer (25 mM Tris base, 192 mM Glycine, 0.1% (w/v) SDS). A pre-stained protein molecular weight marker was always loaded in one well as a reference.

After separation, gels were directly stained using Coomassie Blue or Silver staining, or transferred onto nitrocellulose membranes for Western Blotting.

### 6.2.3. Polyacrylamide Gel Staining

Resolved proteins on polyacrylamide gels can be visualized with specific dyes. The type of dye to use will depend on the abundance of the proteins of interest. The first dye of choice is usually Coomassie Brilliant Blue because of its simple protocol and the signal-to-background is, in most cases, sufficient to make an assessment of the experiment. More sensitive dyes, such as the ones using Silver, usually take longer procedures but are necessary when dealing with low abundant proteins.

#### 6.2.3.1. Coomassie Blue

The Coomassie-based gel stain used to visualize proteins on gels was the SimplyBlue™ SafeStain from Invitrogen®. It contains a proprietary Coomassie G-250 stain for a fast sensitive detection without requiring the use of methanol or acetic acid.

The protocol was followed as described by the manufacturer. After electrophoresis, the gel was rinsed 3 times for 5 min with ultrapure water to remove SDS and buffer salts. The gel was then incubated for at least 1 h with the coomassie solution, gently shaking at room temperature. The gel was then washed with ultrapure water for the necessary time to reduce background and increase contrast with stained bands. The gel was kept in water if further mass spectrometry analysis of individual bands was performed.

#### 6.2.3.2. Silver Stain

The ProteoSilver™ Silver Stain Kit (Sigma®) was used to detect low abundant proteins. ProteoSilver uses silver nitrate, which binds to selective amino acids on the proteins under weakly acidic or neutral pH conditions. The protein bound silver ions are reduced by formaldehyde at alkaline pH to form metallic silver in the gel.

The protocol was followed according to manufacturer's guidelines. The polyacrylamide gel was fixed for at least 20 min in fixing solution (50% ethanol, 10% acetic acid), followed by a wash with 30% ethanol and a wash with ultrapure water, 10 min each. The gel was then incubated for 10 min in sensitizer solution (contents not described) and then washed two times for 10 min with ultrapure water. After that, the gel was equilibrated in silver solution for 10 min followed by a quick wash with ultrapure water and immediately soaked in developer solution (contents not described). Incubation times in this solution varied until desired bands were visualized. To stop further development and increase of background the reaction was terminated by adding stop solution (contents not described) directly to the immersed gel. The solution was discarded and the gel was washed for 15 min in ultrapure water. The stained gel could be kept in fresh ultrapure water until further analysis was necessary, such as mass spectrometry analysis of individual protein bands.

### 6.2.4. Western Blotting

In 1979, Harry Towbin developed a method to allow for the probing of any electrophoretically separated protein with antibodies or serum<sup>189</sup>. The principle behind it was to create a copy of the electrophoretic pattern obtained on the gel by transferring it to a nitrocellulose membrane<sup>189</sup>. Two years later, Burnette<sup>190</sup> made a few modifications to the transfer buffer conditions to allow a complete and quantitative elution of proteins from the SDS gel onto the nitrocellulose membrane and coined it “Western Blotting”. This method is still today the most commonly used for protein transfer.

After gel electrophoresis, the resolved proteins were transferred onto a nitrocellulose membrane (0.2  $\mu\text{m}$ , Whatmann™) using a wet-transfer blotting tank (Biozym™) in either a Tris-glycine homemade transfer buffer or a proprietary Western Blot Transfer Buffer from Pierce™. A stack of (bottom-to-top) three layers of Whatmann paper, the nitrocellulose membrane, the polyacrylamide gel, and another three layers of Whatman paper was assembled in a blotting chamber. All layers were soaked with blotting buffer and electrotransfer was performed at 1 mA/cm<sup>2</sup> (45 mA per gel). To visualize proteins, the nitrocellulose membrane was stained with Ponceau S solution. The stain was removed with TBS-T washing and blocked in 2% (w/v) non-fat milk in TBS-T for at least 1 h at room temperature or over-night at 4°C.

For detection of biotinylated proteins, the membrane was incubated with infrared (IR) or horseradish peroxidase (HRP)-conjugated streptavidin diluted 1:1000 in blocking solution for 2 h at room temperature or over-night at 4°C. Blots were then washed three times with TBS-T for 10 min and kept in TBS until readout.

For specific proteins detection, the membrane was washed three times with TBS-T for 10 min and then incubated with primary antibody solution (diluted in blocking solution) for 2 h at room temperature or over-night at 4°C. After three 10 min washes in TBS-T, the membrane was exposed to IR or HRP-conjugated secondary antibody solution (diluted in blocking solution) for 1 h at room temperature. Finally, the blot was washed three times in TBS-T for 10 min and kept in TBS until image acquisition.

IR-labeled blots were directly acquired in the imaging system (Syngene G:BOX XT4) using the appropriate combination of excitation light and cutoff filters.

For HRP-labeled blots, the membranes were incubated with enhanced chemiluminescence (ECL) detection reagent (Pierce®) and the emitting light was recorded in the imaging system in the dark without any filter.

## 6.3. MASS SPECTROMETRY

### 6.3.1. Sample acquisition and database match identification

Tryptic digests were analyzed by online nanoflow liquid chromatography tandem MS (LC-MSn) on an UltiMate 3000 RSLCnano System (Dionex, part of Thermo Fisher Scientific, Germany) coupled to a LTQ-Orbitrap Velos instrument (Thermo Fisher Scientific, Germany) through a Proxeon nanoelectrospray ion source (Proxeon, part of Thermo Fisher Scientific, Germany). For chromatographic separation, samples were first loaded on a reversed phase (RP) pre-column (Acclaim PepMap100, 5 mm, 100 Å, 100 µm i.d. x 20 mm) and separated on a RP analytical column (Acclaim PepMap RSLC C18, 2 µm, 100 Å, 75 µm i.d. x 150 mm, Dionex, part of Thermo Fisher Scientific, Germany) performing a 96 min gradient (5 – 45% acetonitrile, 0.1% formic acid).

MS detection was performed in the data-dependent mode allowing to automatically switch between Orbitrap-MS and LTQ-MS/MS acquisition in a top 20 configuration at 60 K resolution for a full scan with subsequent collision induced dissociation (CID) fragmentation. Full scan MS spectra (from  $m/z$  300–2000) were acquired in the Orbitrap analyzer after accumulation to a target value of  $1 \times 10^6$  in the linear ion trap. The most intense ions (up to twenty, depending on signal intensity) with charge state  $\geq 2$  were sequentially isolated at a target value of 5000 and fragmented in the linear ion trap using low energy CID with normalized collision energy of 35%. Target ions already mass selected for CID were dynamically excluded for the duration of 60 s. The minimal signal required for MS<sup>2</sup> was 1000 counts. An activation  $q$  of 0.25 and an activation time of 10 ms were applied for MS<sup>2</sup> acquisitions.

All MS/MS data were analyzed using Andromeda implemented in MaxQuant<sup>120</sup>. Automated database searching against the human UniProtKB/Swiss-Prot database was performed with 6 ppm precursor tolerance, 0.5 Da fragment ion tolerance, full trypsin specificity allowing for up to 2 missed cleavages and methionine oxidation as variable modification. The maximum false discovery rates were set to 0.01 both on protein and peptide level, the maximum PEP to 1, and 7 amino acids were required as minimum peptide length. The label free quantification option was selected with a maximal retention time window of 2 min for the alignment between LC-MS/MS runs.

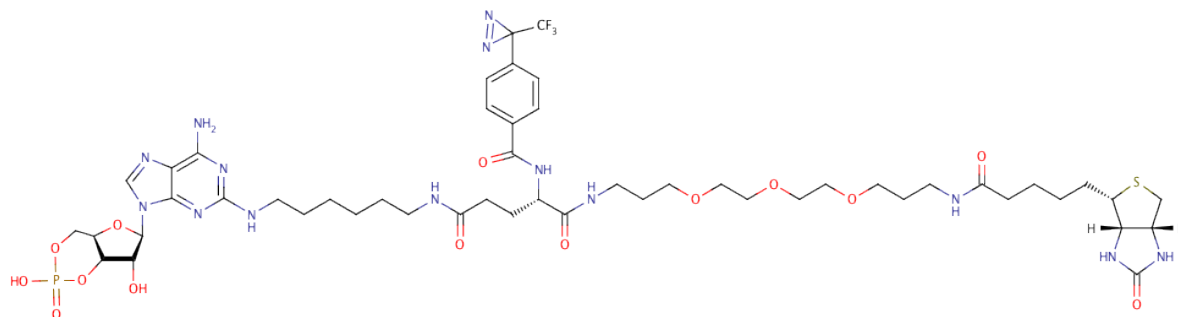
Calculations for fold-change between different subsets of samples and Student's t-Test were performed manually in Excel spreadsheets using both MS-based values (LFQ values from MaxQuant) and alignment-based intensity values.

CCMS charts were developed to comprehensively display the multi-parameter results obtained in CCMS experiments for individual proteins, plotting minimum and maximum intensity values as a box with a black horizontal bar for the median value  $\pm$  the standard error of the mean (SEM). In a separate axis, the fold-change between the subsets of samples is plotted as a green triangle and significant ( $p < 0.05$ ) differences are highlighted with an asterisk (\*).

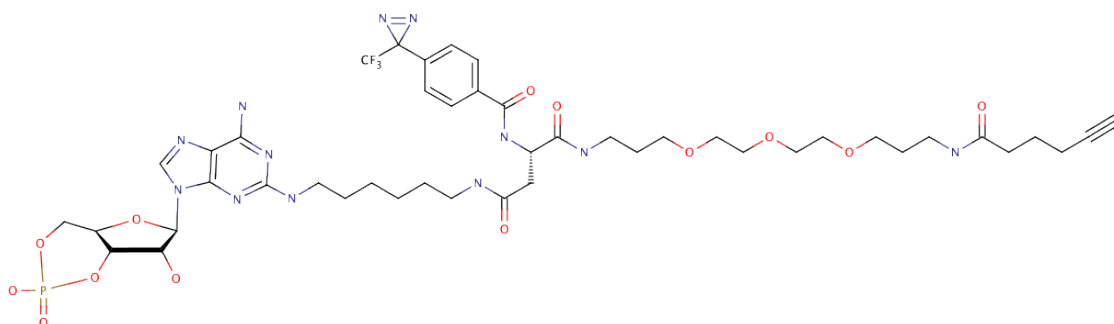
## 6.4. MOLECULAR STRUCTURES OF COMPOUNDS

### 6.4.1. Capture compounds

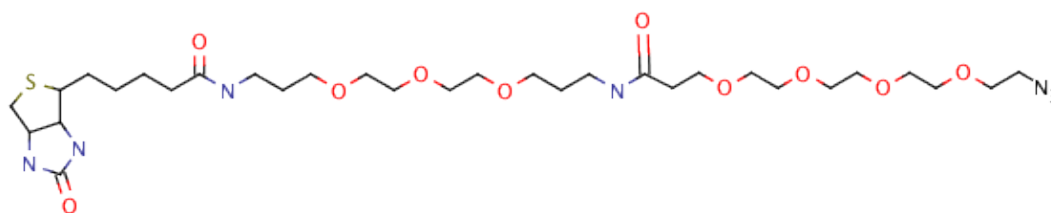
CC 1: Classical full cAMP capture compound



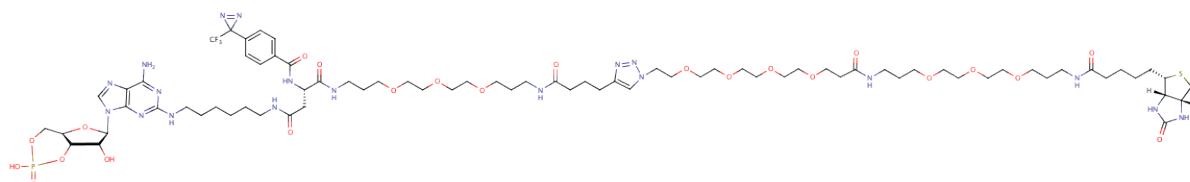
CC 2: Clickable cAMP alkyne capture compound (contains selectivity and photoreactive functions)



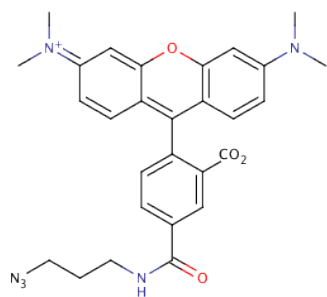
CC 3: Clickable biotin-PEG-azide (contains labeling function)



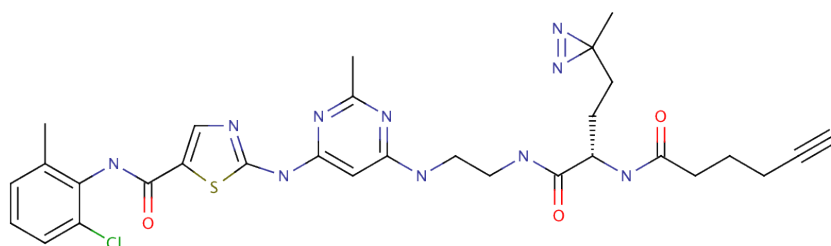
CC 4: Clicked cAMP-biotin capture compound. Reaction product of CC 2 and CC 3



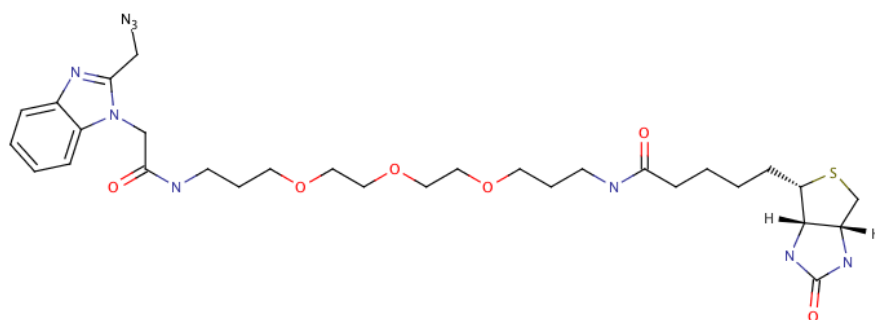
CC 5: Clickable TAMRA [tetramethylrhodamine] azide (contains labeling function)



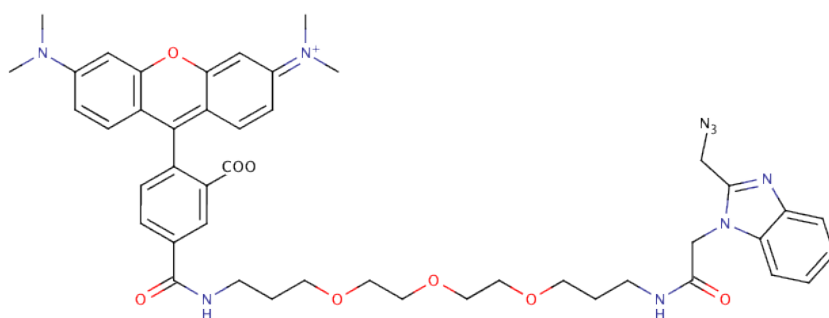
CC 6: Clickable Dasatinib alkyne capture compound (contains selectivity and photoreactive functions)



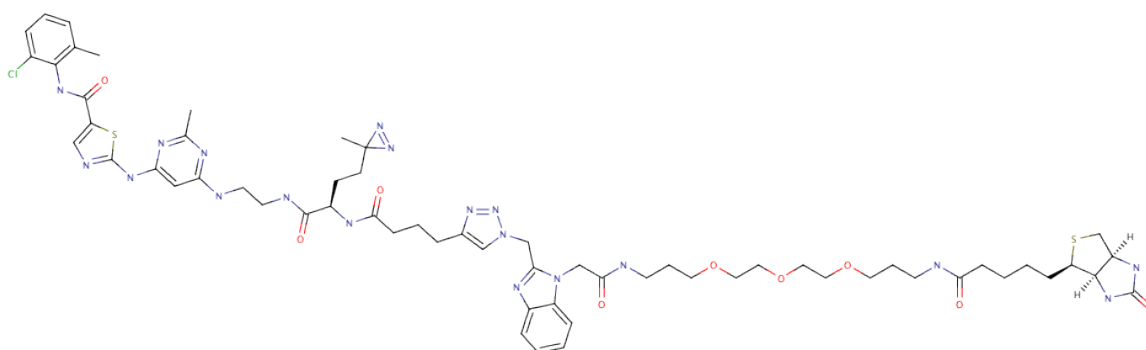
CC 7: Clickable biotin-PEG copper-chelating azide (contains labeling and copper ligand functions)



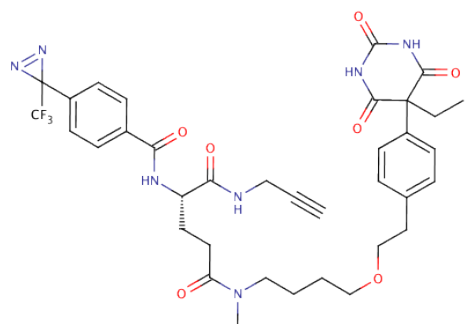
CC 8: Clickable TAMRA-PEG copper-chelating azide (contains labeling and copper ligand functions)



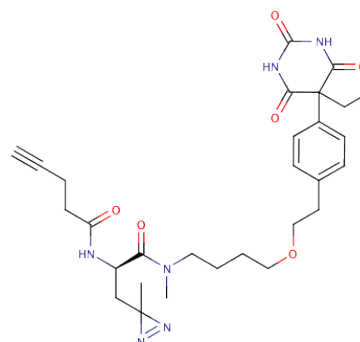
CC 9: Clicked dasatinib-biotin capture compound. Reaction product of CC 6 and CC 7



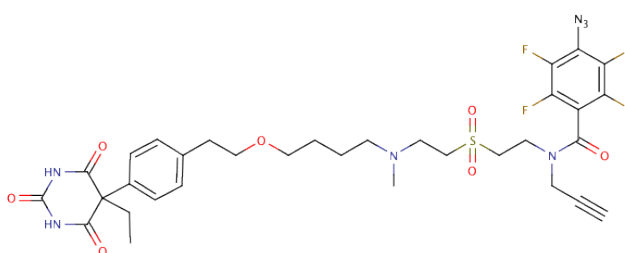
CC 10: Clickable phenobarbital alkyne capture compound A (contains selectivity and a trifluoromethyl-phenyl-diazirine photoreactive functions)



CC 11: Clickable phenobarbital alkyne capture compound B (contains selectivity and a methyl-diazirine photoreactive functions)

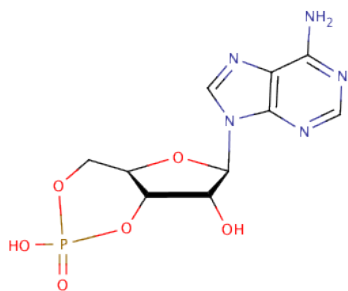


CC 12: Clickable phenobarbital alkyne capture compound C (contains selectivity and a azido-tetrafluorobenzene photoreactive functions)

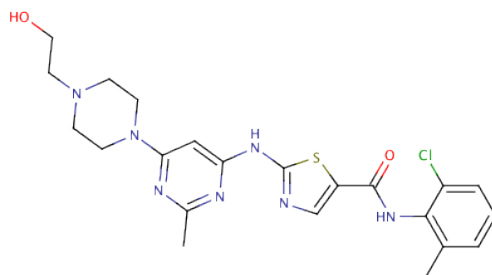


### 6.4.2. Competitors

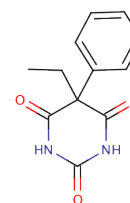
CC 13: cAMP competitor



CC 14: Dasatinib competitor

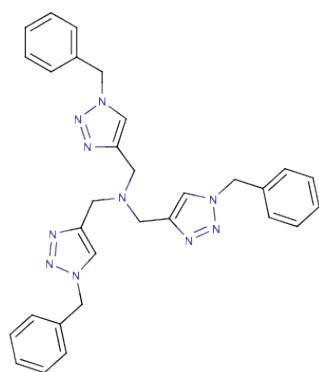


CC 15: Phenobarbital competitor

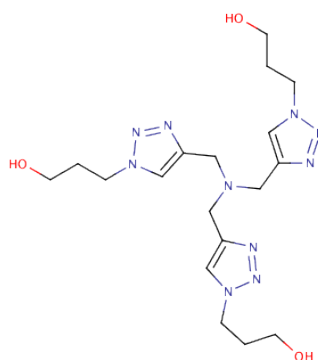


### 6.4.3. Ligands

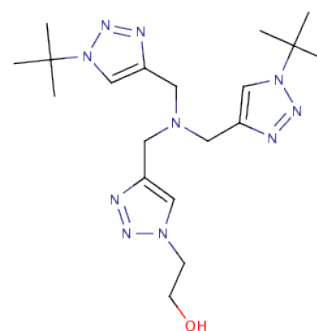
CC 16:  
Copper-chelating ligand TBTA  
Tris(benzyltriazolylmethyl)  
amine



CC 17:  
Copper-chelating ligand THPTA  
Tris(3-hydroxypropyltriazolylmethyl)  
amine



CC 18:  
Copper-chelating ligand BTTE  
bis(tert-butyltriazolyl)ethanol



## 6.5. MATERIALS

### 6.5.1. Chemical reagents

Chemical name	Molecular Formula	Molar mass (g/mol)	CAS	Supplier	Risk and Safety Statements
<b>(+)-Sodium L-ascorbate</b>	C <sub>6</sub> H <sub>7</sub> NaO <sub>6</sub>	198.11	134-03-2	Sigma	-
<b>Acetonitrile (HPLC grade)</b>	C <sub>2</sub> H <sub>3</sub> N	42.05	75-05-8	Sigma	R: 11-20/21/22-36 S: 16-36/37
<b>Ammonium bicarbonate</b>	NH <sub>4</sub> HCO <sub>3</sub>	79.06	1066-33-7	Sigma	R: 22
<b>Biotin</b>	C <sub>10</sub> H <sub>16</sub> N <sub>2</sub> O <sub>3</sub> S	244.31	58-85-5	BioMag	-
<b>Bromophenol Blue sodium salt</b>	C <sub>19</sub> H <sub>9</sub> Br <sub>4</sub> NaO <sub>5</sub> S	692.00	34725-61-6	Serva	S: 22-24/25
<b>Copper(II) sulfate pentahydrate</b>	CuSO <sub>4</sub> • 5H <sub>2</sub> O	249.69	7758-99-8	Alpha Caesar	R: 22-36/38-50/53 S: 22-60-61
<b>Dimethyl sulfoxide</b>	C <sub>2</sub> H <sub>6</sub> SO	78.13	67-68-5	Acros	-
<b>DL-Dithiothreitol</b>	C <sub>4</sub> H <sub>10</sub> O <sub>2</sub> S <sub>2</sub>	154.25	3483-12-3	Fluka	R:22-36/37/38 S:26-36
<b>EDTA-Na<sub>2</sub></b>	C <sub>10</sub> H <sub>14</sub> N <sub>2</sub> Na <sub>2</sub> O <sub>8</sub> • 2H <sub>2</sub> O	372.24	6381-92-6	Gerbu	-
<b>Formic acid</b>	CH <sub>2</sub> O <sub>2</sub>	46.03	64-18-6	Fluka	R: 35 S: 23-26-45
<b>Glycerol</b>	C <sub>3</sub> H <sub>8</sub> O <sub>3</sub>	92.09	56-81-5	Gerbu	-
<b>Glycine</b>	C <sub>2</sub> H <sub>5</sub> NO <sub>2</sub>	75.07	56-40-6	Gerbu	S: 22-24/25
<b>Hepes</b>	C <sub>8</sub> H <sub>18</sub> N <sub>2</sub> O <sub>4</sub> S	238.30	7365-45-9	Gerbu	-
<b>Hydrochloric acid</b>	HCl	36.46	7647-01-0	Sigma	R: 34-37 S: 26-45
<b>IGEPAL® CA-630</b>	(C <sub>2</sub> H <sub>4</sub> O) <sub>n</sub> C <sub>14</sub> H <sub>22</sub> O	-	9036-19-5	Fluka	R: 41-50 S: 26-39-61
<b>Iodoacetamide</b>	C <sub>2</sub> H <sub>14</sub> I NO	184.96	144-48-9	Applichem	R: 25-42/43-53 S: 22-36/37-45
<b>Lutensol® GD70</b>	-	-	31799-71-0	BASF	R: 41 S: 39-26
<b>Magnesium acetate tetrahydrate</b>	C <sub>4</sub> H <sub>14</sub> MgO <sub>8</sub> • 4H <sub>2</sub> O	214.45	16674-78-5	Sigma	-
<b>Potassium acetate</b>	C <sub>2</sub> H <sub>3</sub> KO <sub>2</sub>	98.14	127-08-2	Sigma	-
<b>Potassium hydroxide</b>	KOH	56.11	1310-58-3	Sigma	R: 22-35 S: 26-36/37/39-45
<b>Sodium chloride</b>	NaCl	58.44	7647-14-5	Roth	-
<b>Sodium deoxycholate</b>	C <sub>24</sub> H <sub>39</sub> NaO <sub>4</sub>	414.55	302-95-4	Sigma	R: 22-37
<b>Sodium dodecyl sulfate</b>	C <sub>12</sub> H <sub>25</sub> NaO <sub>4</sub> S	288.38	151-21-3	Gerbu	R: 11-21/22-36/37/38 S: 26-36/37
<b>Sodium hydroxide</b>	NaOH	40.00	1310-73-2	Carl Roth	R: 35 S: 26-37/39-45
<b>Trifluoroacetic acid (99%)</b>	C <sub>2</sub> HF <sub>3</sub> O <sub>2</sub>	114.02	76-05-1	Acros	R: 20-35-52/53 S: 9-26-27-28-45-61
<b>Tris(hydroxymethyl) aminomethane</b>	C <sub>4</sub> H <sub>11</sub> NO <sub>3</sub>	121.14	77-86-1	VWR	R: 36/38
<b>Triton™ X-100</b>	C <sub>14</sub> H <sub>22</sub> O(C <sub>2</sub> H <sub>4</sub> O) <sub>n</sub> , n= 9-10	$\bar{x}$ =625	9002-93-1	Fluka	R: 22-36-51/53 S: 26-39-61
<b>Trypan blue</b>	C <sub>34</sub> H <sub>24</sub> N <sub>6</sub> Na <sub>4</sub> O <sub>14</sub> S <sub>4</sub>	960.82	72-57-1	Fluka	R: 45 S: 53, 45

Chemical name	Molecular Formula	Molar mass (g/mol)	CAS	Supplier	Risk and Safety Statements
Trypsin (sequencing grade, modified, porcine)	-	-	9002-07-7	Promega	R: 36/37/38-42-42/43 S: 22-24-26-36/37-45-23
Tween® 20	-	1228	9005-64-5	Sigma	-
B-Mercaptoethanol	C <sub>2</sub> H <sub>6</sub> OS	78.13	60-24-2	Appllichem	R: 23/24/25-38-41-43-48/22-50/53 S: 26-36/37/39-45-60-61
N-Dodecyl β-D-maltoside	C <sub>24</sub> H <sub>46</sub> O <sub>11</sub>	510.62	69227-93-6	Sigma	-

### 6.5.2. Kits and Consumables

Category	Product	Manufacturer
Antibody	PKAR1α	BD Biosciences
Antibody	AMPKα1/2 (H-300)	Santa Cruz Biotechnology
Antibody	CAR1/2 (M-127)	Santa Cruz Biotechnology
Antibody	p-AMPKα1/2 (Thr 172)	Santa Cruz Biotechnology
Antibody	CYP2B1/2B2 (9.14)	Santa Cruz Biotechnology
Biotin detection	HRP-conjugated Streptavidin	Sigma
Blotting Buffer	10X Western Blot Transfer Buffer, Methanol-free	Pierce, Thermo
Cell Fractionation	NE-PER® Nuclear and Cytoplasmic Extraction Reagents	Pierce Biotechnology
Gel Staining	SimplyBlue™ SafeStain	Invitrogen
Gel Staining	ProteoSilver™ Silver Stain Kit	Sigma
Horseradish peroxidase detection	SuperSignal West Dura Chemiluminescent Substrate	Pierce, Thermo
Magnetic Beads	DynaBeads	
Membrane Stain	Ponceau	
Molecular weight marker	PageRuler Plus Prestained Protein Ladder	Pierce, Thermo
Polyacrylamide Gels	4-20% Tris-Glycin Gel	Anamed Elektrophorese GmbH
Protease inhibitor	cOmplete, Mini, EDTA-free Protease Inhibitor Cocktail Tablets	Roche
Protein Quantification Assay	BCA Protein Assay Reagent	Pierce, Thermo

## 6.5.3. Buffers, media and solutions

	Stock Solution		Work Solution	
<b>SDS Electrophoresis Running Buffer</b>	10x	250 mM Tris 1.92 M Glycine 1% (w/v) SDS	1x	For 1 L: 100 mL stock + 900 mL H <sub>2</sub> O
<b>Blotting Buffer</b>	10x	478 mM Tris 386 mM Glycine 0.37% (w/v) SDS	1x	For 1 L: 100mL stock + 700 mL H <sub>2</sub> O + 200 mL Methanol
<b>Tris Buffered Saline (TBS)</b>	10x	0,5 M Tris 1,5 M NaCl pH 7.5 (with HCl)	1x	For 1 L: 100 mL stock + 900 mL H <sub>2</sub> O
<b>Laemmli Buffer</b>	4x	200 mM Tris-Base pH 6.8 10% (w/v) SDS 40% (v/v) Glycerol 1.28 M β-Me Bromophenol blue	2x	For 1 mL: 500 μL stock + 500 μL H <sub>2</sub> O
<b>Radioimmunoprecipitation assay (RIPA) buffer</b>	1x	150 mM NaCl 1% (v/v) IGEPAL® CA-630 0.5% (w/v) sodium deoxycholate 0.1% (w/v) SDS 50 mM Tris pH 8.0		Use stock
<b>Washing Buffer</b>	5x	250 mM Tris 5 mM EDTA-Na <sub>2</sub> 5 M NaCl 0.25% (v/v) Lutensol GD70 pH 7.5 (with HCl)	1x	For 1 mL: 200 μL stock + 800 μL H <sub>2</sub> O
<b>Capture Buffer</b>	5x	100 mM HEPES 250 mM Potassium acetate 50 mM Magnesium acetate tetrahydrate pH 7.9 (with 1 M KOH) 50% (v/v) Glycerol	1x	For 1 mL: 200 μL stock + 800 μL H <sub>2</sub> O
<b>Lysis Buffer E</b>	1x	50 mM Tris-HCl 100 mM NaCl 1.5 mM MgCl <sub>2</sub> 0.2% (v/v) IGEPAL® CA-630 0.5% (w/v) DDM 5% (v/v) Glycerol 1 mM DTT		Use stock
<b>Cell Culture Media and Supplements</b>		<b>Cell line</b>		
<b>RPMI 1640</b>		K562; HEK293		
<b>Williams Medium E</b>		Primary hepatocytes		
<b>DMEM</b>		MH <sub>1</sub> C <sub>1</sub>		
<b>Heat inactivated fetal bovine serum (FBS)</b>		-		
<b>Penicillin/Streptomycin solution</b>		-		

### 6.5.4. Equipment

Category	Model/type	Manufacturer
Caprobox	310 and 350 nm	caprotec bioanalytics GmbH, Berlin, DE
Centrifuge	Micro star 17R	VWR International GmbH, Darmstadt, DE
Centrifuge	5702 R	Eppendorf AG, Hamburg, DE
Centrifuge	Micro centrifuge AL	Carl Roth GmbH, Karlsruhe, DE
Centrifuge	Mini centrifuge MCF-2360	LMS Consult GmbH, Brigachtal, DE
Electrophoresis	Blotting system EBX-700	C.B.S. Scientific, San Diego, CA, USA
Electrophoresis	Novex Mini-Cell	Life Technologies, Thermo Fischer Scientific GmbH, Dreieich, DE
Electrophoresis	Power Supply 300V	VWR International GmbH, Darmstadt, DE
Ice Machine	ZNE125	Ziegra Eismaschinen GmbH, Isernhagen, DE
Imaging System	Syngene G:BOX XT4	Integrated Scientific Solutions Inc., San Diego, CA, USA
Incubator	Hera Cell 150	Thermo Fischer Scientific GmbH, Dreieich, DE
Magnetic Stirrer	RCT basic	IKA-Werke GmbH, Staufen, DE
Mass Spectrometer	LTQ Velos	Thermo Fischer Scientific GmbH, Dreieich, DE
Mass Spectrometer	LTQ XL	Thermo Fischer Scientific GmbH, Dreieich, DE
Mass Spectrometer	amaZon speed	Bruker Corporation, Billerica, MA, USA
Microscope	Inverted Microscope DM IL	Leica Mikrosysteme Vertrieb GmbH, Wetzlar, DE
nHPLC	Ultimate 3000	Dionex, Thermo Fischer Scientific GmbH, Dreieich, DE
pH meter	SevenEasy S20	Mettler Toledo GmbH, Gießen, DE
Pipetting	Finnpipette Novus i MCP8	Thermo Fischer Scientific GmbH, Dreieich, DE
Pipetting	Manual Research	Eppendorf AG, Hamburg, DE
Rotator	Multimix 115V	VWR International GmbH, Darmstadt, DE
Shaker	Rocking Shaker Rocky	Labortechnik Fröbel GmbH, Lindau, DE
Shaker	Orbital Shaker OS-10	BioSan, Riga, LV
Sonicator	Sonorex	Bandelin, Berlin, DE
Spectrophotometer	Micro plate reader Anthos 2010	anthos Mikrosysteme GmbH, Krefeld, DE
Spectrophotometer	Varian Cary 50 Bio	Agilent Technologies, Inc., Santa Clara, CA, USA
SpeedVac	EZ-2plus	GeneVac Inc, Stone Ridge, NY, USA
Thermocycler	T Gradient	Biometra GmbH, Göttingen, Germany
Thermo-Shaker	TS-100	BioSan, Riga, LV
Vortex	Genie 2	Scientific Industries, Inc., Bohemia, NY, USA
Weighing scales	SI-234A	Denver Instrument, Bohemia, NY, USA
Weighing scales	XP105 Delta Range	Mettler Toledo GmbH, Gießen, DE

# References

---

1. Paul, S. M. *et al.* How to improve R&D productivity: the pharmaceutical industry's grand challenge. *Nat. Rev. Drug Discov.* **9**, 203–214 (2010).
2. Hay, M., Thomas, D. W., Craighead, J. L., Economides, C. & Rosenthal, J. Clinical development success rates for investigational drugs. *Nat. Biotechnol.* **32**, 40–51 (2014).
3. Raida, M. Drug target deconvolution by chemical proteomics. *Curr. Opin. Chem. Biol.* **15**, 570–5 (2011).
4. Lee, J. & Bogoy, M. Target deconvolution techniques in modern phenotypic profiling. *Curr. Opin. Chem. Biol.* **17**, 118–126 (2013).
5. Bantscheff, M., Scholten, A. & Heck, A. J. R. Revealing promiscuous drug-target interactions by chemical proteomics. *Drug Discov. Today* **14**, 1021–1029 (2009).
6. Lenz, T., Fischer, J. J. & Dreger, M. Probing small molecule-protein interactions: A new perspective for functional proteomics. *J. Proteomics* **75**, 100–15 (2011).
7. Ruddigkeit, L., Blum, L. C. & Reymond, J. L. Visualization and virtual screening of the chemical universe database GDB-17. *J. Chem. Inf. Model.* **53**, 56–65 (2013).
8. Médard, G. *et al.* Optimized Chemical Proteomics Assay for Kinase Inhibitor Profiling. *J. Proteome Res.* **14**, 1574–1586 (2015).
9. Daub, H. *et al.* Kinase-Selective Enrichment Enables Quantitative Phosphoproteomics of the Kinome across the Cell Cycle. *Mol. Cell* **31**, 438–448 (2008).
10. Medvedev, A., Kopylov, A., Buneeva, O., Zgoda, V. & Archakov, A. Affinity-based proteomic profiling: Problems and achievements. *Proteomics* **12**, 621–637 (2012).
11. Koster, H. *et al.* Capture compound mass spectrometry: a technology for the investigation of small molecule protein interactions. *Assay Drug Dev Technol* **5**, 381–390 (2007).
12. Luo, Y. *et al.* The cAMP capture compound mass spectrometry as a novel tool for targeting cAMP-binding proteins: from protein kinase A to potassium/sodium hyperpolarization-activated cyclic nucleotide-gated channels. *Mol. Cell. Proteomics* **8**, 2843–56 (2009).
13. Fischer, J. J. *et al.* Dasatinib, imatinib and staurosporine capture compounds - Complementary tools for the profiling of kinases by Capture Compound Mass Spectrometry (CCMS). *J. Proteomics* **75**, 160–8 (2011).
14. Fischer, J. J. *et al.* Comprehensive identification of staurosporine-binding kinases in the hepatocyte cell line HepG2 using Capture Compound Mass Spectrometry (CCMS). *J. Proteome Res.* **9**, 806–17 (2010).
15. Luo, Y. *et al.* GDP-capture compound--a novel tool for the profiling of GTPases in pro- and eukaryotes

- by capture compound mass spectrometry (CCMS). *J. Proteomics* **73**, 815–9 (2010).
16. Lenz, T. *et al.* Profiling of methyltransferases and other S-adenosyl-L-homocysteine-binding Proteins by Capture Compound Mass Spectrometry (CCMS). *J. Vis. Exp.* (2010). doi:10.3791/2264
  17. Dalhoff, C. *et al.* Synthesis of S-adenosyl-L-homocysteine capture compounds for selective photoinduced isolation of methyltransferases. *Chembiochem* **11**, 256–65 (2010).
  18. Rotili, D. *et al.* A photoreactive small-molecule probe for 2-oxoglutarate oxygenases. *Chem. Biol.* **18**, 642–654 (2011).
  19. Rix, U. *et al.* Chemical proteomic profiles of the BCR-ABL inhibitors imatinib, nilotinib, and dasatinib reveal novel kinase and nonkinase targets. *Blood* **110**, 4055–4063 (2007).
  20. Liu, Y., Patricelli, M. P. & Cravatt, B. F. Activity-based protein profiling: the serine hydrolases. *Proc. Natl. Acad. Sci. U. S. A.* **96**, 14694–14699 (1999).
  21. Bantscheff, M. *et al.* Quantitative chemical proteomics reveals mechanisms of action of clinical ABL kinase inhibitors. *Nat. Biotechnol.* **25**, 1035–1044 (2007).
  22. Ovaa, H. *et al.* Chemistry in living cells: Detection of active proteasomes by a two-step labeling strategy. *Angew. Chemie - Int. Ed.* **42**, 3626–3629 (2003).
  23. Speers, A. E., Adam, G. C. & Cravatt, B. F. Activity-based protein profiling in vivo using a copper(i)-catalyzed azide-alkyne [3 + 2] cycloaddition. *J. Am. Chem. Soc.* **125**, 4686–4687 (2003).
  24. Salisbury, C. M. & Cravatt, B. F. Optimization of activity-based probes for proteomic profiling of histone deacetylase complexes. *J. Am. Chem. Soc.* **130**, 2184–2194 (2008).
  25. McKay, C. S. & Finn, M. G. Click Chemistry in Complex Mixtures: Bioorthogonal Bioconjugation. *Chem. Biol.* **21**, 1075–1101 (2014).
  26. Sletten, E. M. & Bertozzi, C. R. Bioorthogonal chemistry: Fishing for selectivity in a sea of functionality. *Angew. Chemie - Int. Ed.* **48**, 6974–6998 (2009).
  27. Sletten, E. M. & Bertozzi, C. R. From mechanism to mouse: a tale of two bioorthogonal reactions. *Acc. Chem. Res.* **44**, 666–76 (2011).
  28. Jewett, J. & Bertozzi, C. Cu-free click cycloaddition reactions in chemical biology. *Chem. Soc. Rev.* **39**, 1272–1279 (2010).
  29. Patterson, D. M., Nazarova, L. a & Prescher, J. a. Finding the right (bioorthogonal) chemistry. *ACS Chem. Biol.* **9**, 592–605 (2014).
  30. Kolb, H. C., Finn, M. G. & Sharpless, K. B. Click Chemistry: Diverse Chemical Function from a Few Good Reactions. *Angew. Chem. Int. Ed. Engl.* **40**, 2004–2021 (2001).

31. Kolb, H. C. & Sharpless, K. B. The growing impact of click chemistry on drug discovery. *Drug Discov. Today* **8**, 1128–37 (2003).
32. Wu, P. *et al.* Efficiency and fidelity in a click-chemistry route to triazole dendrimers by the copper(I)-catalyzed ligation of azides and alkynes. *Angew. Chemie - Int. Ed.* **43**, 3928–3932 (2004).
33. Saxon, E. & Bertozzi, C. R. Cell surface engineering by a modified Staudinger reaction. *Science* **287**, 2007–2010 (2000).
34. Lin, F. L., Hoyt, H. M., van Halbeek, H., Bergman, R. G. & Bertozzi, C. R. Mechanistic investigation of the staudinger ligation. *J. Am. Chem. Soc.* **127**, 2686–2695 (2005).
35. Tam, A., Soellner, M. B. & Raines, R. T. Electronic and steric effects on the rate of the traceless Staudinger ligation. *Org. Biomol. Chem.* **6**, 1173–1175 (2008).
36. Tam, A. & Raines, R. T. Coulombic effects on the traceless Staudinger ligation in water. *Bioorg. Med. Chem.* **17**, 1055–1063 (2009).
37. Best, M. D. Click chemistry and bioorthogonal reactions: unprecedented selectivity in the labeling of biological molecules. *Biochemistry* **48**, 6571–84 (2009).
38. Michael, A. Ueber die Einwirkung von Diazobenzolimid auf Acetylendicarbonsauremethylester. *J. fur Prakt. Chemie* **48**, 94–95 (1893).
39. Huisgen, R. Kinetics and Mechanism of 1,3-Dipolar Cycloadditions. *Angew. Chemie Int. Ed. English* **2**, 633–645 (1963).
40. Finn, M. G. & Fokin, V. V. Click chemistry: function follows form. *Chem. Soc. Rev.* **39**, 1231–2 (2010).
41. Himo, F. *et al.* Copper(I)-catalyzed synthesis of azoles. DFT study predicts unprecedented reactivity and intermediates. *J. Am. Chem. Soc.* **127**, 210–216 (2005).
42. Worrell, B. T., Malik, J. a. & Fokin, V. V. Direct evidence of a dinuclear copper intermediate in Cu(I)-catalyzed azide-alkyne cycloadditions. *Science (80-. )*. **340**, 457–460 (2013).
43. Hein, J. E. & Fokin, V. V. Copper-catalyzed azide-alkyne cycloaddition (CuAAC) and beyond: new reactivity of copper(I) acetylides. *Chem. Soc. Rev.* **39**, 1302–15 (2010).
44. Zhang, L. *et al.* Ruthenium-catalyzed cycloaddition of alkynes and organic azides. *J. Am. Chem. Soc.* **127**, 15998–9 (2005).
45. Meldal, M. & Tornøe, C. W. Cu-catalyzed azide-alkyne cycloaddition. *Chem. Rev.* **108**, 2952–3015 (2008).
46. Rostovtsev, V. V., Green, L. G., Fokin, V. V. & Sharpless, K. B. A stepwise huisgen cycloaddition process: Copper(I)-catalyzed regioselective 'ligation' of azides and terminal alkynes. *Angew. Chemie - Int. Ed.* **41**, 2596–2599 (2002).

47. Chan, T. R., Hilgraf, R., Sharpless, K. B. & Fokin, V. V. Polytriazoles as copper(I)-stabilizing ligands in catalysis. *Org. Lett.* **6**, 2853–5 (2004).
48. Wang, Q. *et al.* Bioconjugation by copper(I)-catalyzed azide-alkyne [3 + 2] cycloaddition. *J. Am. Chem. Soc.* **125**, 3192–3 (2003).
49. Hong, V., Steinmetz, N. F., Manchester, M. & Finn, M. G. Labeling live cells by copper-catalyzed alkyne-azide click chemistry. *Bioconjug. Chem.* **21**, 1912–6 (2010).
50. Soriano Del Amo, D. *et al.* Biocompatible copper(I) catalysts for in vivo imaging of glycans. *J. Am. Chem. Soc.* **132**, 16893–9 (2010).
51. Agard, N. J., Prescher, J. a & Bertozzi, C. R. A strain-promoted [3 + 2] azide-alkyne cycloaddition for covalent modification of biomolecules in living systems. *J. Am. Chem. Soc.* **126**, 15046–15047 (2004).
52. Gaetke, L. M., Chow-Johnson, H. S. & Chow, C. K. Copper: toxicological relevance and mechanisms. *Arch. Toxicol.* **88**, 1929–38 (2014).
53. Sletten, E. M. & Bertozzi, C. R. A hydrophilic azacyclooctyne for cu-free click chemistry. *Org. Lett.* **10**, 3097–3099 (2008).
54. Ning, X., Guo, J., Wolfert, M. a. & Boons, G. J. Visualizing metabolically labeled glycoconjugates of living cells by copper-free and fast huisgen cycloadditions. *Angew. Chemie - Int. Ed.* **47**, 2253–2255 (2008).
55. Chang, P. V *et al.* Copper-free click chemistry in living animals. *Proc. Natl. Acad. Sci. U. S. A.* **107**, 1821–6 (2010).
56. Jewett, J. C., Sletten, E. M. & Bertozzi, C. R. Rapid Cu-free click chemistry with readily synthesized biarylazacyclooctynones. *J. Am. Chem. Soc.* **132**, 3688–90 (2010).
57. Koo, H. *et al.* Bioorthogonal copper-free click chemistry inVivo for tumor-targeted delivery of nanoparticles. *Angew. Chemie - Int. Ed.* **51**, 11836–11840 (2012).
58. Evans, H. L. *et al.* Copper-free click—a promising tool for pre-targeted PET imaging. *Chem. Commun.* **48**, 991 (2012).
59. Van Berkel, S. S. *et al.* Metal-free triazole formation as a tool for bioconjugation. *ChemBioChem* **8**, 1504–1508 (2007).
60. Blackman, M. L., Royzen, M. & Fox, J. M. Tetrazine ligation: fast bioconjugation based on inverse-electron-demand Diels-Alder reactivity. *J. Am. Chem. Soc.* **130**, 13518–9 (2008).
61. Devaraj, N. K., Weissleder, R. & Hilderbrand, S. a. Tetrazine-based cycloadditions: application to pretargeted live cell imaging. *Bioconjug. Chem.* **19**, 2297–9 (2008).
62. Kim, C. H., Axup, J. Y. & Schultz, P. G. Protein conjugation with genetically encoded unnatural amino

- acids. *Curr. Opin. Chem. Biol.* **17**, 412–419 (2013).
63. Shih, H. W., Kamber, D. N. & Prescher, J. a. Building better bioorthogonal reactions. *Curr. Opin. Chem. Biol.* **21**, 103–111 (2014).
64. Versteegen, R. M., Rossin, R., Ten Hoeve, W., Janssen, H. M. & Robillard, M. S. Click to release: Instantaneous doxorubicin elimination upon tetrazine ligation. *Angew. Chemie - Int. Ed.* **52**, 14112–14116 (2013).
65. Matikonda, S. S. *et al.* Bioorthogonal prodrug activation driven by a strain-promoted 1,3-dipolar cycloaddition. *Chem. Sci.* **6**, 1212–1218 (2015).
66. Kolodych, S. *et al.* Discovery of chemoselective and biocompatible reactions using a high-throughput immunoassay screening. *Angew. Chemie - Int. Ed.* **52**, 12056–12060 (2013).
67. Nikolaev, V. O. & Lohse, M. J. Monitoring of cAMP synthesis and degradation in living cells. *Physiology (Bethesda)*. **21**, 86–92 (2006).
68. Rall, T. W., Sutherland, E. W. & Berthet, J. The relationship of epinephrine and glucagon to liver phosphorylase. I. Liver phosphorylase; preparation and properties. *J. Biol. Chem.* **218**, 459–468 (1956).
69. Sutherland, E. W. & Rall, T. W. Fractionation and characterization of a cyclic adenine ribonucleotide formed by tissue particles. *J. Biol. Chem.* **232**, 1077–1091 (1958).
70. Rall, T. & Sutherland, E. Formation of a cyclic adenine ribonucleotide by tissue particles. *J. Biol. Chem.* **232**, 1065–1076 (1958).
71. Cook, W. H., Lipkin, D. & Markham, R. The formation of a cyclic dianhydrodiadenylic acid (I) by the alkaline degradation of adenosine-5'-triphosphoric acid (II). *J. Am. Chem. Soc.* **79**, 3607–3608 (1957).
72. Godinho, R. O., Duarte, T. & Pacini, E. S. a. New perspectives in signaling mediated by receptors coupled to stimulatory G protein: the emerging significance of cAMP efflux and extracellular cAMP-adenosine pathway. *Front. Pharmacol.* **06**, 1–9 (2015).
73. Kamenetsky, M. *et al.* Molecular Details of cAMP Generation in Mammalian Cells: A Tale of Two Systems. *J. Mol. Biol.* **362**, 623–639 (2006).
74. Jaiswal, B. S. & Conti, M. Calcium regulation of the soluble adenylyl cyclase expressed in mammalian spermatozoa. *Proc. Natl. Acad. Sci. U. S. A.* **100**, 10676–10681 (2003).
75. Litvin, T. N., Kamenetsky, M., Zarifyan, A., Buck, J. & Levin, L. R. Kinetic properties of 'soluble' adenylyl cyclase: Synergism between calcium and bicarbonate. *J. Biol. Chem.* **278**, 15922–15926 (2003).
76. Antoni, F. a. New paradigms in cAMP signalling. *Mol. Cell. Endocrinol.* **353**, 3–9 (2012).
77. Steegborn, C. Structure, mechanism, and regulation of soluble adenylyl cyclases — similarities and differences to transmembrane adenylyl cyclases. *Biochim. Biophys. Acta - Mol. Basis Dis.* **1842**, 2535–

- 2547 (2014).
78. Desman, G., Waintraub, C. & Zipin, J. H. Investigation of cAMP microdomains as a path to novel cancer diagnostics. *Biochim. Biophys. Acta - Mol. Basis Dis.* **1842**, 2636–2645 (2014).
  79. Cheepala, S. *et al.* Cyclic Nucleotide Compartmentalization: Contributions of Phosphodiesterases and ATP-Binding Cassette Transporters. *Annu. Rev. Pharmacol. Toxicol.* **53**, 231–253 (2012).
  80. Walsh, D. A., Perkins, J. P. & Krebs, E. G. An adenosine 3',5'-monophosphate-dependant protein kinase from rabbit skeletal muscle. *J. Biol. Chem.* **243**, 3763–3765 (1968).
  81. Taskén, K. & Aandahl, E. M. Localized effects of cAMP mediated by distinct routes of protein kinase A. *Physiol. Rev.* **84**, 137–167 (2004).
  82. Taylor, S. S. *et al.* Signaling through cAMP and cAMP-dependent protein kinase: Diverse strategies for drug design. *Biochim. Biophys. Acta - Proteins Proteomics* **1784**, 16–26 (2008).
  83. Edwards, A. S. & Scott, J. D. A-kinase anchoring proteins: Protein kinase A and beyond. *Curr. Opin. Cell Biol.* **12**, 217–221 (2000).
  84. Burke, D., Howells, J. & Tomlinson, S. E. Hcn channels: Function and clinical implications. *Neurology* **81**, 513–514 (2013).
  85. Podda, M. V. & Grassi, C. New perspectives in cyclic nucleotide-mediated functions in the CNS: The emerging role of cyclic nucleotide-gated (CNG) channels. *Pflugers Arch. Eur. J. Physiol.* **466**, 1241–1257 (2014).
  86. Almahariq, M., Mei, F. C. & Cheng, X. Cyclic AMP sensor EPAC proteins and energy homeostasis. *Trends Endocrinol. Metab.* **25**, 60–71 (2014).
  87. Bos, J. L. Epac proteins: multi-purpose cAMP targets. *Trends Biochem. Sci.* **31**, 680–686 (2006).
  88. Scholten, A. *et al.* Analysis of the cGMP/cAMP interactome using a chemical proteomics approach in mammalian heart tissue validates sphingosine kinase type 1-interacting protein as a genuine and highly abundant AKAP. *J. Proteome Res.* **5**, 1435–1447 (2006).
  89. Aye, T. T. *et al.* Selectivity in enrichment of cAMP-dependent protein kinase regulatory subunits type I and type II and their interactors using modified cAMP affinity resins. *Mol. Cell. Proteomics* **8**, 1016–1028 (2009).
  90. Scholten, A., Van Veen, T. a B., Vos, M. a. & Heck, A. J. R. Diversity of cAMP-dependent protein kinase isoforms and their anchoring proteins in mouse ventricular tissue. *J. Proteome Res.* **6**, 1705–1717 (2007).
  91. Kovanich, D. *et al.* Sphingosine kinase interacting protein is an A-kinase anchoring protein specific for type I cAMP-dependent protein kinase. *ChemBioChem* **11**, 963–971 (2010).

92. Shi, H., Zhang, C.-J., Chen, G. Y. J. & Yao, S. Q. Cell-based proteome profiling of potential dasatinib targets by use of affinity-based probes. *J. Am. Chem. Soc.* **134**, 3001–14 (2012).
93. Shah, N. P. *et al.* Overriding imatinib resistance with a novel ABL kinase inhibitor. *Science* **305**, 399–401 (2004).
94. Apperley, J. F. Chronic myeloid leukaemia. *Lancet* **385**, 1447–1459 (2014).
95. Greuber, E. K., Smith-Pearson, P., Wang, J. & Pendergast, A. M. Role of ABL family kinases in cancer: from leukaemia to solid tumours. *Nat. Rev. Cancer* **13**, 559–71 (2013).
96. Wang, J. Y. J. The capable ABL: what is its biological function? *Mol. Cell. Biol.* **34**, 1188–97 (2014).
97. Shaul, Y. & Ben-Yehoyada, M. Role of c-Abl in the DNA damage stress response. *Cell Res.* **15**, 33–35 (2005).
98. Wen, S. T. & Van Etten, R. a. The PAG gene product, a stress-induced protein with antioxidant properties, is an Abl SH3-binding protein and a physiological inhibitor of c- Abl tyrosine kinase activity. *Genes Dev.* **11**, 2456–2467 (1997).
99. Lin, J. *et al.* Oncogenic activation of c-Abl in non-small cell lung cancer cells lacking FUS1 expression: inhibition of c-Abl by the tumor suppressor gene product Fus1. *Oncogene* **26**, 6989–6996 (2007).
100. Cong, F. *et al.* Cytoskeletal protein PSTPIP1 directs the PEST-type protein tyrosine phosphatase to the c-Abl kinase to mediate Abl dephosphorylation. *Mol. Cell* **6**, 1413–1423 (2000).
101. Das, J. *et al.* 2-Aminothiazole as a novel kinase inhibitor template. Structure-activity relationship studies toward the discovery of N-(2-chloro-6-methylphenyl)-2-[[6- [4-(2-hydroxyethyl)-1-piperazinyl]-2-methyl-4-pyrimidinyl]amino]-1, 3-thiazole-5-carboxamide (Dasatini. *J. Med. Chem.* **49**, 6819–6832 (2006).
102. Golas, J. M. *et al.* SKI-606, a 4-anilino-3-quinolinecarbonitrile dual inhibitor of Src and Abl kinases, is a potent antiproliferative agent against chronic myelogenous leukemia cells in culture and causes regression of K562 xenografts in nude mice. *Cancer Res.* **63**, 375–381 (2003).
103. Buchdunger, E. *et al.* Inhibition of the Abl protein-tyrosine kinase in vitro and in vivo by a 2-phenylaminopyrimidine derivative. *Cancer Res.* **56**, 100–104 (1996).
104. Weisberg, E. *et al.* Characterization of AMN107, a selective inhibitor of native and mutant Bcr-Abl. *Cancer Cell* **7**, 129–141 (2005).
105. O’Hare, T. *et al.* AP24534, a Pan-BCR-ABL Inhibitor for Chronic Myeloid Leukemia, Potently Inhibits the T315I Mutant and Overcomes Mutation-Based Resistance. *Cancer Cell* **16**, 401–412 (2009).
106. Adrián, F. J. *et al.* Allosteric inhibitors of Bcr-abl-dependent cell proliferation. *Nat. Chem. Biol.* **2**, 95–102 (2006).

107. Zhang, J. *et al.* Targeting Bcr-Abl by combining allosteric with ATP-binding-site inhibitors. *Nature* **463**, 501–506 (2010).
108. Davis, M. I. *et al.* Comprehensive analysis of kinase inhibitor selectivity. *Nat. Biotechnol.* **29**, 1046–51 (2011).
109. Lombardo, L. J. *et al.* Discovery of N-(2-chloro-6-methylphenyl)-2-(6-(4-(2-hydroxyethyl)-piperazin-1-yl)-2-methylpyrimidin-4-ylamino)thiazole-5-carboxamide (BMS-354825), a dual Src/Abl kinase inhibitor with potent antitumor activity in preclinical assays. *J. Med. Chem.* **47**, 6658–6661 (2004).
110. Harrington, E. *et al.* VX-680, a potent and selective small-molecule inhibitor of the Aurora kinases, suppresses tumor growth in vivo. *Nat. Med.* **10**, 262–267 (2004).
111. Moasser, M. M., Srethapakdi, M., Sachar, K. S., Kraker, A. J. & Rosen, N. Inhibition of Src kinases by a selective tyrosine kinase inhibitor causes mitotic arrest. *Cancer Res.* **59**, 6145–6152 (1999).
112. Akeno-Stuart, N. *et al.* The RET kinase inhibitor NVP-AST487 blocks growth and calcitonin gene expression through distinct mechanisms in medullary thyroid cancer cells. *Cancer Res.* **67**, 6956–6964 (2007).
113. Vandyke, K., Fitter, S. & Zannettino, C. W. The tyrosine kinase inhibitor dasatinib (SPRYCEL) inhibits chondrocyte activity and proliferation. *Blood Cancer J.* **1**, e2 (2011).
114. Chen, B.-A. & Chen, R. The role of dasatinib in the management of chronic myeloid leukemia. *Drug Des. Devel. Ther.* **9**, 773–779 (2015).
115. Fabarius, A. *et al.* Centrosome aberrations and G1 phase arrest after in vitro and in vivo treatment with the SRC/ABL inhibitor dasatinib. *Haematologica* **93**, 1145–1154 (2008).
116. Bevilacqua, V. *et al.* Copper-chelating azides for efficient click conjugation reactions in complex media. *Angew. Chemie - Int. Ed.* **53**, 5872–5876 (2014).
117. Li, J. *et al.* A chemical and phosphoproteomic characterization of dasatinib action in lung cancer. *Nat. Chem. Biol.* **6**, 291–299 (2010).
118. Kitagawa, D. *et al.* Activity-based kinase profiling of approved tyrosine kinase inhibitors. *Genes to Cells* **18**, 110–122 (2013).
119. Szklarczyk, D. *et al.* STRING v10: protein-protein interaction networks, integrated over the tree of life. *Nucleic Acids Res.* **43**, D447–52 (2015).
120. Cox, J. *et al.* MaxLFQ allows accurate proteome-wide label-free quantification by delayed normalization and maximal peptide ratio extraction. (2014).
121. Chong, Y.-P., Mulhern, T. D. & Cheng, H.-C. C-terminal Src kinase (CSK) and CSK-homologous kinase (CHK)--endogenous negative regulators of Src-family protein kinases. *Growth Factors* **23**, 233–244 (2005).

122. Kim, D.-J., Yi, Y.-W. & Kim, J. H. In situ monitoring of bindings between dasatinib and its target protein kinases using magnetic nanoparticles in live cells. *J. Am. Chem. Soc.* **130**, 16466–16467 (2008).
123. Kisselev, L. L. Mammalian tryptophanyl-tRNA synthetases. *Biochimie* **75**, 1027–1039 (1993).
124. Tzima, E. & Schimmel, P. Inhibition of tumor angiogenesis by a natural fragment of a tRNA synthetase. *Trends Biochem. Sci.* **31**, 7–10 (2006).
125. Corkery, B. M. Tyrosine Kinase Inhibitors in Triple Negative Breast Cancer. (2010).
126. Trinka, E., Höfler, J., Leitinger, M. & Brigo, F. Pharmacotherapy for Status Epilepticus. *Drugs* (2015). doi:10.1007/s40265-015-0454-2
127. Whysner, J., Ross, P. M. & Williams, G. M. Phenobarbital mechanistic data and risk assessment: enzyme induction, enhanced cell proliferation, and tumor promotion. *Pharmacol. Ther.* **71**, 153–91 (1996).
128. Larsen, M. & Jefcoate, C. Phenobarbital Induction of CYP2B1, CYP2B2, and CYP3A1 in Rat Liver: Genetic Differences in a Common Regulatory Mechanism. *Arch. Biochem. Biophys.* **321**, 467–476 (1995).
129. Waxman, D. J. & Azaroff, L. Phenobarbital induction of cytochrome P-450 gene expression. *Biochem. J.* **281**, 577–592 (1992).
130. Gerets, H. H. J. *et al.* Characterization of primary human hepatocytes, HepG2 cells, and HepaRG cells at the mRNA level and CYP activity in response to inducers and their predictivity for the detection of human hepatotoxins. *Cell Biol. Toxicol.* **28**, 69–87 (2012).
131. Lee, G. H. Paradoxical effects of phenobarbital on mouse hepatocarcinogenesis. *Toxicol. Pathol.* **28**, 215–225 (2000).
132. Kawamoto, T. *et al.* Phenobarbital-responsive nuclear translocation of the receptor CAR in induction of the CYP2B gene. *Mol. Cell. Biol.* **19**, 6318–22 (1999).
133. Marc, N. *et al.* Regulation of phenobarbital induction of the cytochrome P450 269/10 genes in primary mouse hepatocyte culture: Involvement of calcium- and cAMP- dependent pathways. *Eur. J. Biochem.* **267**, 963–970 (2000).
134. Galisteo, M. *et al.* Involvement of cyclic nucleotide- and calcium-regulated pathways in phenobarbital-induced cytochrome P-450 3A expression in mouse primary hepatocytes. *J. Pharmacol. Exp. Ther.* **290**, 1270–1277 (1999).
135. Rencurel, F. *et al.* AMP-activated protein kinase mediates phenobarbital induction of CYP2B gene expression in hepatocytes and a newly derived human hepatoma cell line. *J. Biol. Chem.* **280**, 4367–4373 (2005).
136. Rencurel, F. *et al.* Stimulation of AMP-activated protein kinase is essential for the induction of drug metabolizing enzymes by phenobarbital in human and mouse liver. *Mol. Pharmacol.* **70**, 1925–1934

- (2006).
137. Harach, T. Crossroads between drug and energy metabolism : Role of constitutive androstane receptor and AMP-activated kinase. (2010).
  138. Blättler, S. M., Rencurel, F., Kaufmann, M. R. & Meyer, U. a. In the regulation of cytochrome P450 genes, phenobarbital targets LKB1 for necessary activation of AMP-activated protein kinase. *Proc. Natl. Acad. Sci. U. S. A.* **104**, 1045–1050 (2007).
  139. Joannard, F., Galisteo, M., Corcos, L., Guillouzo, a & Lagadic-Gossmann, D. Regulation of phenobarbital-induction of CYP2B and CYP3A genes in rat cultured hepatocytes: involvement of several serine/threonine protein kinases and phosphatases. *Cell Biol. Toxicol.* **16**, 325–37 (2000).
  140. Kobayashi, K., Hashimoto, M., Honkakoski, P. & Negishi, M. Regulation of gene expression by CAR: an update. *Arch. Toxicol.* **89**, 1045–1055 (2015).
  141. Shindo, S., Numazawa, S. & Yoshida, T. A physiological role of AMP-activated protein kinase in phenobarbital-mediated constitutive androstane receptor activation and CYP2B induction. *Biochem. J.* **401**, 735–741 (2007).
  142. Mutoh, S. *et al.* Phenobarbital indirectly activates the constitutive active androstane receptor (CAR) by inhibition of epidermal growth factor receptor signaling. *Sci. Signal.* **6**, ra31 (2013).
  143. Meyer, S. a, Gibbs, T. A. & Jirtle, R. L. Independent mechanisms for tumor promoters phenobarbital and 12-O-tetradecanoylphorbol-13-acetate in reduction of epidermal growth factor binding by rat hepatocytes. *Cancer Res.* **49**, 5907–5912 (1989).
  144. Meyer, S. a & Jirtle, R. L. Old dance with a new partner: EGF receptor as the phenobarbital receptor mediating Cyp2B expression. *Sci. Signal.* **6**, pe16 (2013).
  145. Joseph, B. K. *et al.* Inhibition of AMP Kinase by the Protein Phosphatase 2A Heterotrimer, PP2A<sup>pp2r2d</sup>. *J. Biol. Chem.* **290**, 10588–98 (2015).
  146. Ferro, M. & Bassi, A. Induction of cytochrome(s) P450-dependent drug metabolism in cultured MH1C1 hepatoma cells. *Cell Biochem. Funct.* **2**, 263–268 (1984).
  147. Donato, M. T. *et al.* Evaluation of the xenobiotic biotransformation capability of six rodent hepatoma cell lines in comparison with rat hepatocytes. *In Vitro Cell. Dev. Biol. Anim.* **30A**, 574–80 (1994).
  148. Lempiäinen, H. *et al.* Phenobarbital mediates an epigenetic switch at the constitutive androstane receptor (CAR) target gene Cyp2b10 in the liver of B6C3F1 mice. *PLoS One* **6**, e18216 (2011).
  149. Phillips, J. M. & Goodman, J. I. Multiple Genes Exhibit Phenobarbital-Induced Constitutive Active/Androstane Receptor–Mediated DNA Methylation Changes during Liver Tumorigenesis and in Liver Tumors. *Toxicol. Sci. an Off. J. Soc. Toxicol.* **108**, 273–289 (2009).
  150. Swales, K. & Negishi, M. CAR, driving into the future. *Mol. Endocrinol.* **18**, 1589–1598 (2004).

151. Han, Y., Wang, Q., Song, P., Zhu, Y. & Zou, M.-H. Redox regulation of the AMP-activated protein kinase. *PLoS One* **5**, e15420 (2010).
152. Ching, J. K., Rajguru, P., Marupudi, N., Banerjee, S. & Fisher, J. S. A role for AMPK in increased insulin action after serum starvation. *Am. J. Physiol. Cell Physiol.* **299**, C1171–9 (2010).
153. Conney, a H. Pharmacological implications of microsomal enzyme induction. *Pharmacol. Rev.* **19**, 317–366 (1967).
154. Okey, A. B. Enzyme induction in the cytochrome P-450 system. *Pharmacol. Ther.* **45**, 241–298 (1990).
155. Giuditta, A. & Casola, L. Mechanism of barbiturate inhibition on purified flavoenzymes. *Biochim. Biophys. Acta (BBA)-Enzymology ...* **110**, 17–31 (1965).
156. Li, D. & Roberts, R. Human Genome and Diseases: WD-repeat proteins: structure characteristics, biological function, and their involvement in human diseases. *Cell. Mol. life Sci.* **58**, 2085–2097 (2001).
157. Kim, J., Min, G. & Kemper, B. Chromatin Assembly Enhances Binding to the CYP2B1 Phenobarbital-responsive Unit (PBRU) of Nuclear Factor-1, which Binds Simultaneously with Constitutive Androstane Receptor (CAR)/Retinoid X Receptor (RXR) and Enhances CAR/RXR-mediated Activation of the PB. *J. Biol. Chem.* **276**, 7559–7567 (2001).
158. Luc, P. V, Adesnik, M., Ganguly, S. & Shaw, P. M. Transcriptional regulation of the CYP2B1 and CYP2B2 genes by C/EBP-related proteins. *Biochem Pharmacol* **51**, 345–356 (1996).
159. Honkakoski, P. & Negishi, M. Characterization of a phenobarbital-responsive enhancer module in mouse P450 Cyp2b10 gene. *J. Biol. Chem.* **272**, 14943–9 (1997).
160. Dolfini, D. & Mantovani, R. Targeting the Y/CCAAT box in cancer: YB-1 (YBX1) or NF-Y? *Cell Death Differ.* **20**, 676–85 (2013).
161. Eliseeva, I. a, Kim, E. R., Guryanov, S. G., Ovchinnikov, L. P. & Lyabin, D. N. Y-Box-Binding Protein 1 and Its Functions. *Biochemistry* **76**, 1402–1433 (2011).
162. Wu, J. Disruption of the Y-Box Binding Protein-1 Results in Suppression of the Epidermal Growth Factor Receptor and HER-2. *Cancer Res.* **66**, 4872–4879 (2006).
163. Ren, H. *et al.* Evidence for the involvement of xenobiotic-responsive nuclear receptors in transcriptional effects upon perfluoroalkyl acid exposure in diverse species. *Reprod. Toxicol.* **27**, 266–277 (2009).
164. Phillips, J. M., Burgoon, L. D. & Goodman, J. I. The constitutive active/androstane receptor facilitates unique phenobarbital-induced expression changes of genes involved in key pathways in precancerous liver and liver tumors. *Toxicol. Sci.* **110**, 319–333 (2009).
165. Phillips, J. M., Burgoon, L. D. & Goodman, J. I. Phenobarbital elicits unique, early changes in the expression of hepatic genes that affect critical pathways in tumor-prone B6C3F1 mice. *Toxicol. Sci.* **109**,

- 193–205 (2009).
166. Zhou, S., Sun, X., Liu, L., Wang, X. & Liu, K. Increased expression of aquaporin-1 in the anterior temporal neocortex of patients with intractable epilepsy. *Neurol. Res.* **30**, 400–405 (2008).
167. Binder, D. K., Nagelhus, E. A. & Ottersen, O. P. Aquaporin-4 and epilepsy. *Glia* **60**, 1203–1214 (2012).
168. Dudek, F. E. & Rogawski, M. A. Regulation of Brain Water: Is There a Role for Aquaporins in Epilepsy? *Epilepsy Curr.* **5**, 104–106 (2005).
169. Higgins, L. G. & Hayes, J. D. Mechanisms of induction of cytosolic and microsomal glutathione transferase (GST) genes by xenobiotics and pro-inflammatory agents. *Drug Metab. Rev.* **43**, 92–137 (2011).
170. Foerster, S. *et al.* Characterization of the EGFR interactome reveals associated protein complex networks and intracellular receptor dynamics. *Proteomics* **13**, 3131–3144 (2013).
171. Wei, B., Guo, C., Liu, S. & Sun, M.-Z. Annexin A4 and cancer. *Clin. Chim. Acta.* **447**, 72–78 (2015).
172. Wos, M. & Bandorowicz-Pikula, J. [Participation of annexins in endocytosis and EGFR-mediated signal transduction]. *Postepy Biochem.* **60**, 55–61 (2014).
173. Grewal, T. & Enrich, C. Annexins--modulators of EGF receptor signalling and trafficking. *Cell. Signal.* **21**, 847–858 (2009).
174. Kahn, R. A. *et al.* Arf family GTPases: roles in membrane traffic and microtubule dynamics. *Biochem. Soc. Trans.* **33**, 1269–1272 (2005).
175. Sukhanova, A. *et al.* Targeting C4-demethylating genes in the cholesterol pathway sensitizes cancer cells to EGF receptor inhibitors via increased EGF receptor degradation. *Cancer Discov.* **3**, 96–111 (2013).
176. Cao, H., Chen, J., Krueger, E. W. & McNiven, M. A. SRC-mediated phosphorylation of dynamin and cortactin regulates the 'constitutive' endocytosis of transferrin. *Mol. Cell. Biol.* **30**, 781–792 (2010).
177. Sousa, L. P. *et al.* Suppression of EGFR endocytosis by dynamin depletion reveals that EGFR signaling occurs primarily at the plasma membrane. *Proc. Natl. Acad. Sci.* **109**, 4419–4424 (2012).
178. Tong, J., Taylor, P. & Moran, M. F. Proteomic Analysis of the Epidermal Growth Factor Receptor (EGFR) Interactome and Post-translational Modifications Associated with Receptor Endocytosis in Response to EGF and Stress. *Mol. Cell. Proteomics* **13**, 1644–1658 (2014).
179. Uhlen, M. *et al.* Proteomics. Tissue-based map of the human proteome. *Science* **347**, 1260419 (2015).
180. Abou-Zeid, N. *et al.* MICAL-like1 mediates epidermal growth factor receptor endocytosis. *Mol. Biol. Cell* **22**, 3431–3441 (2011).

181. Zhang, L., Gjoerup, O. & Roberts, T. M. The serine/threonine kinase cyclin G-associated kinase regulates epidermal growth factor receptor signaling. *Proc. Natl. Acad. Sci. U. S. A.* **101**, 10296–301 (2004).
182. Culi, J., Springer, T. A. & Mann, R. S. Boca-dependent maturation of beta-propeller/EGF modules in low-density lipoprotein receptor proteins. *EMBO J.* **23**, 1372–1380 (2004).
183. Cobb, B. D. & Clarkson, J. M. A simple procedure for optimising the polymerase chain reaction (PCR) using modified Taguchi methods. *Nucleic Acids Res.* **22**, 3801–3805 (1994).
184. Smith, P. K. *et al.* Measurement of protein using bicinchoninic acid. *Anal. Biochem.* **150**, 76–85 (1985).
185. Maizel, J. V. Evidence for multiple components in the structural protein of type 1 poliovirus. *Biochem. Biophys. Res. Commun.* **13**, 483–489 (1963).
186. Raymond, S. & Weintraub, L. Acrylamide gel as a supporting medium for zone electrophoresis. *Science* **130**, 711 (1959).
187. Laemmli, U. K. Cleavage of structural proteins during the assembly of the head of bacteriophage T4. *Nature* **227**, 680–5 (1970).
188. Maizel, Jr, J. V. SDS polyacrylamide gel electrophoresis. *Trends Biochem. Sci.* **25**, 590–592 (2000).
189. Towbin, H., Staehelin, T. & Gordon, J. Electrophoretic transfer of proteins from polyacrylamide gels to nitrocellulose sheets: procedure and some applications. *Proc. Natl. Acad. Sci. U. S. A.* **76**, 4350–4 (1979).
190. Burnette, W. N. 'Western blotting': electrophoretic transfer of proteins from sodium dodecyl sulfate--polyacrylamide gels to unmodified nitrocellulose and radiographic detection with antibody and radioiodinated protein A. *Anal. Biochem.* **112**, 195–203 (1981).

# Curriculum vitae

---

For reasons of data protection, the Curriculum vitae is not published in the online version.

For reasons of data protection, the Curriculum vitae is not published in the online version.